ACOUSTIC CONDITION MONITORING & FAULT DIAGNOSTICS FOR INDUSTRIAL SYSTEMS

Jarek Grebenik

PhD Thesis

Submitted in partial fulfilment of the
requirements for Doctor of Philosophy in
Electrical Engineering

UNIVERSITY OF
LINCOLN

The University of Lincoln School of Engineering
Brayford Pool, Lincoln, LN6 7TS, United Kingdom

2020-06-04

Preface

The thesis provides an account of the research work undertaken by Mr Jarek Grebenik into acoustic condition monitoring and fault diagnosis for industrial systems across a period of study from February 2016 to February 2020, as partial fulfilment of a PhD in Electrical Engineering from The University of Lincoln. The research was supervised by Dr Saket Srivastava, Prof Chris Bingham and Dr Yu Zhang.

The research was carried out in accordance with the requirements of The University of Lincoln research regulations and codes of practice and it has not been submitted for any other academic award. Except where indicated by reference, the work is that of the author. Work done in collaboration or with assistance of others is indicated. Any views expressed are those of the author.

ACOUSTIC CONDITION MONITORING & FAULT DIAGNOSTICS FOR INDUSTRIAL SYSTEMS

Jarek Grebenik

PhD Thesis

Submitted in partial fulfilment of the
requirements for Doctor of Philosophy in
Electrical Engineering

UNIVERSITY OF
LINCOLN

The University of Lincoln School of Engineering
Brayford Pool, Lincoln, LN6 7TS, United Kingdom

2020-06-04

Preface

The thesis provides an account of the research work undertaken by Mr Jarek Grebenik into acoustic condition monitoring and fault diagnosis for industrial systems across a period of study from February 2016 to February 2020, as partial fulfilment of a PhD in Electrical Engineering from The University of Lincoln. The research was supervised by Dr Saket Srivastava, Prof Chris Bingham and Dr Yu Zhang.

The research was carried out in accordance with the requirements of The University of Lincoln research regulations and codes of practice and it has not been submitted for any other academic award. Except where indicated by reference, the work is that of the author. Work done in collaboration or with assistance of others is indicated. Any views expressed are those of the author.

Statement of Ethics

The ethical principles and values published by the Engineering Council (2014) have been upheld throughout and are at the forefront of the rationale behind this research. There are increasing demands for industrial systems to operate continuously with maximum availability and minimum costs, combined with improving standards in personnel health and safety and care for the natural environment. To these ends, advancements of the cutting edge of acoustic condition monitoring and fault diagnosis technology and methods is ethically justified.

Statement of Ethics

The ethical principles and values published by the Engineering Council (2014) have been upheld throughout and are at the forefront of the rationale behind this research. There are increasing demands for industrial systems to operate continuously with maximum availability and minimum costs, combined with improving standards in personnel health and safety and care for the natural environment. To these ends, advancements of the cutting edge of acoustic condition monitoring and fault diagnosis technology and methods is ethically justified.

Acknowledgements

My thanks go to Dr. Saket Srivastava, who provided guidance but also pushed me to go further.

Thanks also to Prof. Chris Bingham, who gave me a great deal of advice, and helped me develop my academic writing skills.

I am extremely grateful to Mr. Peter Hobden, his technical expertise and assistance proved invaluable throughout the last phase of this project. I owe him a huge debt of gratitude.

My gratitude also extends to Mr. Jacob Corr, his help with some technical aspects was critical to completing this project.

I would like to thank Miss Shannon Cherry. Her love and support kept me going through some difficult times. Despite many difficulties she remained supportive until the end.

Finally, I thank my parents, Michael and Lynne Grebenik, for their help and support throughout, and in particular my mother. In 2013, when I graduated in Mechanical Engineering, she saw the potential for me to go further and join the floppy-hat brigade. Her support was invaluable throughout the final stages of the project and I would have been unable to continue without her. My achievement here is very much a reflection of her support and love.

Publications Stemming from Research Undertaken

The following publications [1]–[3] have resulted from the research documented in this thesis. Each is included as an addendum at the end of the thesis for completeness.

[1] J. Grebenik, Y. Zhang, C. Bingham, and S. Srivastava, "Roller element bearing acoustic fault detection using smartphone and consumer microphones - comparing with vibration techniques," in *Proceedings of the 17th International Conference on Mechatronics - Mechatronika (ME)*, IEEE, Prague, Czech Republic: IEEE, 2016, pp. 1–7.

[2] J. Grebenik, C. Bingham, and S. Srivastava, "Continuous acoustic monitoring of electrical machines; processing signals from USB microphone & mobile smartphone sensors detecting DC motor controller fault," in *Proceedings of the 5th International Conference on Control, Decision & Information Technologies (CoDIT)*, IEEE, Thessaloniki, Greece: IEEE, 2018, pp. 677–682.

[3] J. Grebenik, C. Bingham, and S. Srivastava, "Acoustic diagnostics of electrical origin fault modes with readily available consumer-grade sensors," *IET Electric Power Applications*, 2019. [Online]. Available: https://doi.org/10.1049/iet-epa.2019.0232.

Abstract

Condition monitoring and fault diagnostics for industrial systems is required for cost reduction, maintenance scheduling, and reducing system failures. Catastrophic failure usually causes significant damage and may cause injury or fatality, making early and accurate fault diagnostics of paramount importance. Existing diagnostics can be improved by augmenting or replacing with acoustic measurements, which have proven advantages over more traditional vibration measurements including, earlier detection of emerging faults, increased diagnostic accuracy, remote sensors and easier setup and operation. However, industry adoption of acoustics remains in relative infancy due to vested confidence and reliance on existing measurement and, perceived difficulties with noise contamination and diagnostic accuracy. Researched acoustic monitoring examples typically employ specialist surface-mount transducers, signal amplification, and complex feature extraction and machine learning algorithms, focusing on noise rejection and fault classification. Usually, techniques are fine-tuned to maximise diagnostic performance for the given problem. The majority investigate mechanical fault modes, particularly Roller Element Bearings (REBs), owing to the mechanical impacts producing detectable acoustic waves. The first contribution of this project is a suitability study into the use of low-cost consumer-grade acoustic sensors for fault diagnostics of six different REB health conditions, comparing against vibration measurements. Experimental results demonstrate superior acoustic performance throughout but particularly at lower rotational speed and axial load. Additionally, inaccuracies caused by dynamic operational parameters (speed in this case), are minimised by novel multi-Support Vector Machine training. The project then expands on existing work to encompass diagnostics for a previously unreported electrical fault mode present on a BrushLess Direct Current motor drive system. Commonly studied electrical faults, such as a broken rotor bar or squirrel cage, result from mechanical component damage artificially seeded and not spontaneous. Here, electrical fault modes are differentiated as faults caused by issues with the power supply, control system or software (not requiring mechanical damage or triggering intervention). An example studied here is a transient current instability, generated by

non-linear interaction of the motor electrical parameters, parasitic components and digital controller realisation. Experimental trials successfully demonstrate real-time feature extraction and further validate consumer-grade sensors for industrial system diagnostics. Moreover, this marks the first known diagnosis of an electrically-seeded fault mode as defined in this work. Finally, approaching an industry-ready diagnostic system, the newly released PYNQ-Z2 Field Programmable Gate Array is used to implement the first known instance of multiple feature extraction algorithms that operate concurrently in continuous real-time. A proposed deep-learning algorithm can analyse the features to determine the optimum feature extraction combination for ongoing continuous monitoring. The proposed black-box, all-in-one solution, is capable of accurate unsupervised diagnostics on almost any application, maintaining excellent diagnostic performance. This marks a major leap forward from fine-tuned feature extraction performed offline for artificially seeded mechanical defects to multiple real-time feature extraction demonstrated on a spontaneous electrical fault mode with a versatile and adaptable system that is low-cost, readily available, with simple setup and operation. The presented concept represents an industry-ready all-in-one acoustic diagnostic solution, that is hoped to increase adoption of acoustic methods, greatly improving diagnostics and minimising catastrophic failures.

Contents

List of Figures

List of Tables

Nomenclature

The lists below define all the abbreviations, characters and symbols used throughout this document. For ease of reference all abbreviations, characters, symbols, citations, figures, tables and equations within the text are linked.

Abbreviations

ACTMS	Acoustic Combustion Turbine Monitoring System
ADC	Analogue to Digital Converter
AE	Acoustic Emission
AI	Artificial Intelligence
ANN	Artificial Neural Network
ASIC	Application Specific Integrated Circuit
BLDC	BrushLess Direct Current
BRAM	Block Random Access Memory
BUFG	Global Clock Buffer
CNN	Convolutional Neural Network
CPU	Central Processing Unit
CWT	Continuous Wavelet Transform
DAC	Digital to Analogue Converter
DFT	Discrete Fourier Transform
DSP	Digital Signal Processing
DWT	Discrete Wavelet Transform
EDM	Electrical Discharge Machining
EEMD	Ensemble Empirical Mode Decomposition
EMD	Empirical Mode Decomposition
EMI	Electromagnetic Interference
FDA	Fisher Discriminant Analysis
FF	Flip-Flop
FFT	Fast Fourier Transform
FIFO	First In, First Out
FIR	Finite Impulse Response
FPGA	Field-Programmable Gate Array
FTF	Fundamental Train Frequency
GPP	General Purpose Processor
GPU	Graphics Processing Unit
HDL	Hardware Description Language
HFRT	High-Frequency Resonance Technique
HHT	Hilbert-Huang Transform
HSA	Hilbert Spectral Analysis
IC	Integrated Circuit
ICA	Independent Component Analysis

IDE	Integrated Development Environment
ILA	Integrated Logic Analyzer
IMF	Intrinsic Mode Function
IO	Input/Output
IP	Intellectual Property
k-NN	k-Nearest Neighbours
LUT	Look-Up Table
MCSA	Motor Current Signature Analysis
MUSIC	Multiple Signal Classification
PCA	Principal Component Analysis
PCB	Printed Circuit Board
PSO	Particle Swarm Optimisation
PWM	Pulse Width Modulation
REB	Roller Element Bearing
RFI	Radio Frequency Interference
RMS	Root Mean Square
RPFI	Roller Pass Frequency Inner-Race
RPFO	Roller Pass Frequency Outer-Race
RSF	Roller Spin Frequency
RVM	Relevance Vector Machine
SDSoC	Software Defined System on Chip
SoC	System on Chip
STFT	Short-Time Fourier Transform
SURE	Stein's Unbiased Risk Estimate
SVM	Support Vector Machine
SysGen	Xilinx System Generator for Simulink
VHDL	VHSIC Hardware Description Language
VHSIC	Very High Speed Integrated Circuit
VLSI	Very Large Scale Integration
WPD	Wavelet Packet Decomposition
WPT	Wavelet Packet Transform

Characters & Symbols

b	Dyadic Translation
c	Speed of Sound
E	Effective Elastic Modulus
g	High-Pass Filter (Wavelet Transform)
h	Low-Pass Filter (Wavelet Transform)
K_s	Bulk Modulus
m	Mass
M	Molecular Mass
P	Pressure
CPV	Cauchy Principle Value
v	Velocity
V	Volume
$W_{(\alpha,b)}$	Wavelet Coefficients
α	Dyadic Dilation
γ	Heat Capacity Ratio
θ	Angle
λ	Wavelength
ρ	Density
φ	Phase
φ	Dyadic Dilation Function
ψ	Analysing Wavelet / Mother Wavelet
ω	Angular Frequency

Chapter 1

Introduction & Background

The continuing development of industrial systems combined with requirements for cost reductions resulting from; reduced maintenance, improved maintenance scheduling and reduction in catastrophic machine failures, necessitates further advancement of current fault diagnostic technology. Catastrophic failures have the potential to cause serious injury or fatality to surrounding people, and will often cause extreme damage to adjacent components or systems, exponentially increasing the amount of downtime experienced and the cost of repair. The early detection of emerging faults can dramatically decrease the chance of catastrophic failure and allow for fault growth monitoring and improved maintenance scheduling. Existing diagnostic systems for industrial monitoring and fault diagnostics are typically reliant on vibration measurements. However, the use of measurements from acoustic sensors has, more recently, become a prevalent method owing to its advantages over its more established counterpart. [1], [2], [83], [84] refer to earlier works and show that acoustic sensors can offer earlier and more accurate detection of emerging changes in system characteristics, improved cost-benefit trade-off, readily accessible transducers, ease of setup and operation, and no detrimental impact on nominal system integrity by employing remote acoustic sensors. Despite these advantages, industry uptake of acoustic sensing techniques has been hindered by two main factors. Firstly, the vested confidence and reliance on traditional measurements such as vibration based techniques, and secondly, the poor reputation of acoustics for reliability and difficulties with the intrusions of unwanted noise.

Owing to advancements in computational hardware and Digital Signal Processing (DSP) capabilities, acoustic techniques are now becoming more widely available with improved performance and reliability. In turn, there is renewed research and industry interest into the potential performance benefits and the novel application of acoustic measurements. This research project

addresses these issues and provides techniques to facilitate the industrial adoption of acoustic measurements for fault diagnostic and monitoring purposes.

Currently reported research into the use of acoustic measurements for fault diagnostics and condition monitoring focuses predominantly on mechanical fault modes e.g. acoustic waves generated through physical impact of a roller on a protruding defect on the raceway within a Roller Element Bearing (REB) supporting a rotating shaft [1]. Often, the acoustic waves generated by the fault are measured using specialist high-frequency sensors that are surface mounted to the component under test, such as in [82]. These frequencies, known as Acoustic Emission (AE), typically include ultrasonic frequencies in the range of 100 to 1000 kHz. There are relatively few examples that employ consumer-grade acoustic sensors for diagnostics of audible frequency acoustic waves within the range of 20 Hz to 20 kHz. Moreover, there is little to no literature available on their use for the detection of electrically seeded fault modes.

1.1 Problem Definition

The literature review in Chapter 2 identifies a number of problems hindering the mainstream adoption of acoustic methods for industrial fault diagnostics and condition monitoring. It also highlights areas for potential advancements. These problems and development areas are summarised below:

1. The vast majority of investigations into acoustic fault diagnostics and condition monitoring employ specialist research-grade piezoelectric transducers that are surface mounted to the component under test and monitor AE frequencies. Whilst laudable and of interest, in many cases consumer-grade sensors would be capable of providing comparable diagnostic performance. Further, these consumer-grade systems do not require complex pre-amplification, specialist cabling and Analogue to Digital Converter (ADC) equipment, and they provide a significantly improved cost to benefit ratio. Although some examples using consumer-grade sensors are available, there is still much development to prove the suitability of these sensors for a wide variety of monitoring applications.

2. In nearly all reported experiments into acoustic fault diagnostics, the

fault is artificially created through human intervention as a research exercise. The fault is nearly always created by intentionally causing physical damage to the mechanical integrity of the component. This provides data sets in 'book-end' states of either being very healthy or badly damaged, with no data for natural fault emergence or propagation. It also has the added disadvantage of preventing continuous real-time diagnostics as the system must be shutdown, disassembled and reassembled with the damaged component. The delay and reassembly of the system may induce unintended changes within the data that could unintentionally skew the results.

3. There have been very few examples of continuous real-time processing for acoustic condition monitoring and this is a critical success factor for an industry-ready system.

4. Continuous real-time processing of more complex feature extraction and machine learning algorithms is difficult and extremely costly to achieve on General Purpose Processor (GPP). The costs of implementing a continuous processing system on GPP not only include very high specification and costly components but also high operational costs from high power consumption and cooling requirements.

5. Achieving excellent diagnostic performance for most applications requires expert setup with appropriate selection and configuration of feature extraction and decision making algorithms. A diagnostic system is typically designed for a specific application with performance demonstrated in a single environment.

6. The adoption of Field-Programmable Gate Array (FPGA) to implement the complex feature extraction and machine learning algorithms is very small. Although there are some examples where a single feature extraction algorithm has been implemented, there is very little in the field of acoustic condition monitoring and nothing regarding multiple concurrent algorithms.

7. There remains much debate over the 'best' feature extraction and machine learning algorithms suitable for acoustic condition monitoring and fault diagnostics. Investigations into algorithm performance should be based on simulated data, and those based on experimental data (particularly where the data set is not publicly available) should not

be given too much credence. In addition, the choice of the analysing domain, inherent algorithm and algorithm configuration should be tailored to the application.

8. To date, there is little to no literature addressing fault diagnostics for electrical fault modes, particularly when considering the use of acoustic measurements. Further, the majority of the electrically-based diagnostic techniques require specialist expertise to setup, are difficult to retrofit on established systems, and the results can be difficult to interpret without expert knowledge.

These problems and areas for further development form the base requirements for this research project.

1.2 Research Objectives

The outstanding research objectives identified and addressed in this project are:

1. Investigate the potential simplicity of an acoustic diagnostic system for a mechanical fault mode - with a focus on the suitability of consumer-grade sensors for industrial adoption in the field.
2. Investigate the application of acoustic diagnostic methods to electrically-seeded fault modes.
3. Demonstrate real-time fault diagnostics for a naturally occurring fault that does not require human intervention to trigger or for the system to be shutdown.
4. Investigate the potential scope of reprogrammable hardware for use in the field of acoustic diagnostics and condition monitoring.

After a comprehensive literature review, the following chapters aim to address these problems and fulfil the objectives as outlined in the next section.

1.3 Project Outline

The next chapter continues with an account of background theory and a literature survey relating to research activity reported in this thesis. It is focused on three key areas:

- the theory behind fault diagnostic systems including real-time considerations in Section 2.1,
- mechanical fault mode diagnostics in Section 2.2,
- and electrical fault mode diagnostics in Section 2.3.

Chapter 3, Consumer-Grade Acoustic Sensor Diagnostics for Roller Element Bearings, demonstrates simple diagnostics of six different REB fault conditions, comparing the performance of two consumer-grade acoustic sensors (a USB microphone and a smartphone) and a vibration accelerometer. REBs are responsible for around half of all machine failures and are the most commonly scrutinised component in the literature, making them a suitable case study in this work. A summary of the contributions of this chapter:

1. Introduces and presents a novel technique employing multiple machine learning algorithms to account for dynamic operational parameters.
2. The suitability of consumer grade acoustic sensors and simple feature extraction is proven experimentally for application to mechanical fault modes.
3. The superior performance of the consumer-grade microphone and Wavelet Packet Transform (WPT) feature extraction over the smartphone and Empirical Mode Decomposition (EMD) is demonstrated experimentally.

Chapter 4, Continuous Real-Time Diagnostics of an Electrical Fault Mode, explores the application of acoustics to electrical fault modes; a significantly understudied field. In contrast to mechanical fault modes, there is little to no literature available on this topic. This chapter demonstrates real-time acoustic detection of transient, unpredictable commutation-event current instabilities stemming from a Pulse Width Modulation (PWM)-controller powering a BrushLess Direct Current (BLDC) motor drive system under test. A summary of the contributions of this chapter:

1. The first known case of acoustic diagnostics of an electrical origin fault, as defined in this work, is demonstrated experimentally.
2. Continuous real-time monitoring is implemented, an essential aspect for an industry-ready diagnostic system.
3. The suitability of consumer-grade sensors and the WPT and EMD algorithms for real-time implementations is presented.

Chapter 5, Acoustic Diagnostic System Programmable Hardware Implementation, elaborates the need for continuous real-time DSP for real world industrial monitoring systems. Implementation of feature extraction algorithms on FPGA devices provides a substantial increase in processing efficiency owing to the hardware-based parallel programmability. The practical implementation of an acoustic monitoring system is achieved by programming a low-cost FPGA development board to detect electrically-based faults, as in Chapter 4. This chapter also lays the foundation for the development of highly advanced 'all-in-one' diagnostic solution, equipped with multiple feature extraction tools and advanced machine learning and control. A summary of the contributions of this chapter:

1. FPGA implementations of the WPT & EMD feature extraction algorithms are detailed.
2. Real-time processing of multiple feature extraction algorithms operating simultaneously is demonstrated.
3. The concept for an industry-ready 'all-in-one' solution is presented and partially developed.
4. The FPGA implementations utilise the newly released PYNQ-Z2 FPGA development board.

Chapter 6 summarises the project, with the project contributions and main findings given in Section 6.1, followed by a full evaluation of the research problem and objectives in Section 6.2. Recommendations and areas for further investigation are proposed in Section 6.3.

Chapter 2

Literature Review

This chapter provides the relevant background theory and a literature survey relating to research activity reported in this thesis. It is focused on three key areas:

- the theory behind fault diagnostic systems including real-time considerations in Section 2.1,
- mechanical fault mode diagnostics in Section 2.2,
- and electrical fault mode diagnostics in Section 2.3.

2.1 Diagnostic System Considerations

Diagnostic and monitoring systems are designed to provide information on the health condition of specific components or systems. This information is used by control systems or technical staff to prevent further damage and schedule appropriate maintenance. These systems are found in the majority of fields and industry types, from chemical production to biological engineering. Generic performance indicators for an effective diagnostic system are:

- detection at an early stage of fault evolution
- accurate and precise diagnostics
- robust performance i.e. minimal false alarms and not influenced by external factors
- continuous real-time monitoring with minimal delay
- minimal power consumption and computational overhead
- simplicity and ease of installation and operation
- low capital cost outlay
- maximum reliability with backup available for critical applications.

Designing a system to meet all these requirements is extremely challenging

Figure 2.1: Diagram of a diagnostic/monitoring system.

and an appropriate balance must be found for a given application. A typical diagnostic system is comprised of the functional elements shown in Figure 2.1. It is important to note that the majority of systems convert analogue sensor signals to a digital format to allow computation and use of a wide variety of feature extraction and machine learning algorithms. However, some systems (a minority) employ only analogue signal processing.

This section considers the different components and requirements of a diagnostic system and provides an overview of the supporting theory. Although much of the theory can be employed in other diagnostic fields, for brevity this section focuses primarily on acoustic measurements and techniques.

2.1.1 Acoustic Sensor Technology

Acoustic waves are typically longitudinal or transverse. Both are transient elastic waves generated by the rapid release of strain energy. A longitudinal wave is an oscillation of internal pressure, formed of compression and rarefaction. It is the most common type of acoustic wave and exhibits much higher energy transfer than an equivalent transverse wave [4]. A microphone is a device that converts an acoustic wave into an electrical signal. They can be remote devices in air or liquid, or be mounted directly to solid components. There are four main methods to convert an acoustic signal to one appropriate for processing, viz. capacitive techniques, inductive techniques, piezoelectric and optical.

Capacitive microphones are based on detecting changes in capacitance. In microphones, the capacitor is typically comprised of a fixed and rigid backplate and a flexible diaphragm. The acoustic wave energy is transferred to the diaphragm, thus changing the distance between the two capacitive plates, resulting in capacitance fluctuations proportional to the acoustic wave energy. Low frequency capacitive microphones use a high impedance circuit to maintain a fixed charge on the capacitor. As the distance between the plates varies, the amount of charge the capacitor can hold changes accordingly. These

variations in current are amplified and measured. High frequency capacitive microphones employ low impedance circuits, and use the capacitance as a tuning component of a radio frequency circuit (usually around 8 MHz). Changes in the capacitance modulates the tuning of the radio frequency oscillator in proportion to the incident sound waves. A demodulator circuit then converts the signal back to a conventional audio signal [5]. Capacitive microphones typically have higher bandwidths than dynamic counterparts (induction based), because their diaphragms can be made very thin and do not need to move the mass of a coil. Diaphragms are usually only a few microns thick, made from mylar with a thin gold coating to make it electrically conductive. The back plate of the capacitor is fixed with perforated holes to allow air to pass through; this prevents the internal pressure of the capacitor from damping the movement of the diaphragm. The back plate will also have holes drilled part way through, to compensate for the natural frequency of the diaphragm [6]. A diagram of a typical capacitive microphone circuit is given in Figure 2.2. More advanced capacitive microphones, operating in the ultrasonic range are available in [7]. This work gives a comprehensive explanation on the operation and manufacture of micro-machined ultrasonic transducers.

Induction microphones, also known as dynamic microphones, use a small movable induction coil attached to diaphragm that is sensitive to the movement caused by the acoustic waves. The coil is placed in the magnetic field of a permanent magnet, producing a varying current in the coil via

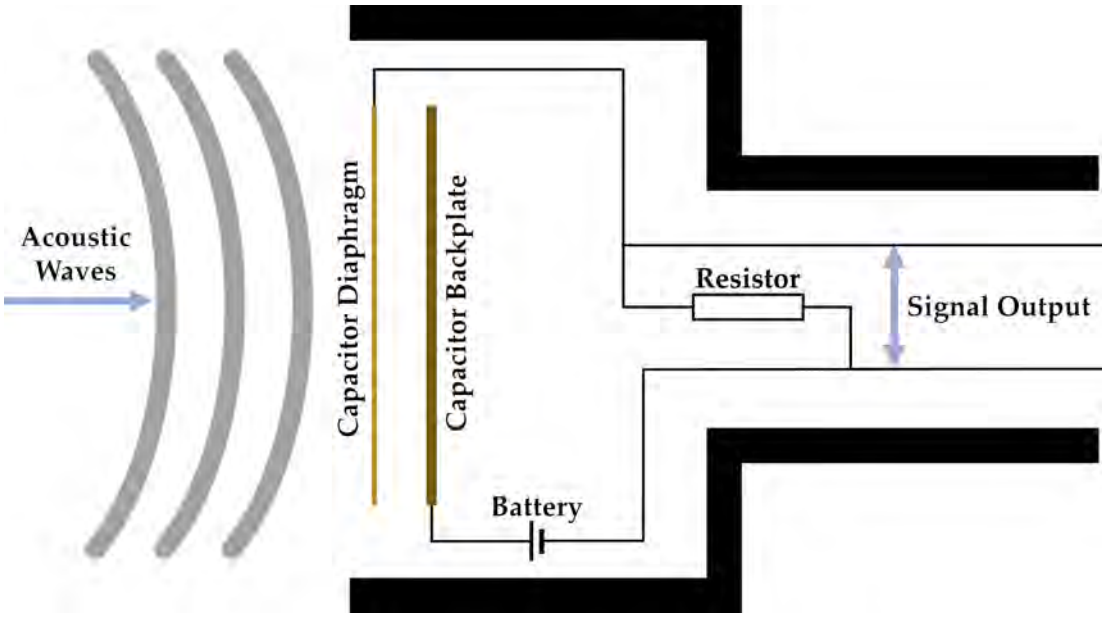

Figure 2.2: Diagram of a capacitive microphone circuit.

electromagnetic induction. These microphones are cheap to manufacture, rugged and do not require a phantom power source, which makes them suitable for on-stage musical performances, for example. However, typically capacitive or induction ribbon microphones are preferred for recording in a studio setting due to their superior sound reproduction. The performance of induction coil microphones deteriorates at higher frequencies due to the mass of the coil, thus making them unsuitable for high-frequency applications.

Capacitive and induction microphones are typically airborne and can pickup acoustic waves with some degree of directional sensitivity. A polar pattern indicates how sensitive a microphone is to acoustic waves arriving from different angles about its central axis. Figure 2.3, shows four main types of polar pattern; omnidirectional, cardioid, supercardioid and bidirectional.

Omnidirectional microphones are equally sensitive to sound from any direction (in reality this is not achievable as the build of the microphone housing slightly flattens the polar pattern). Cardioid, supercardioid and a number of other variations are categorised under unidirectional microphones as they are sensitive to sound from the front with reduced pickup from the side and rear of the microphone [8]–[10]. This makes cardioid microphones the best suited for condition monitoring applications as they are less sensitive to noise from other sources.

Not all microphones exhibit directional sensitivity however. Those that are surface mounted are only sensitive in one direction; perpendicular to the mount surface (aside from some specialist sensors capable of measuring shear waves when surface mounted). The most common form of surface mounted microphones use the piezoelectric effect. These contain a piezoelectric crystal or ceramic that produces a voltage when under strain. Single crystal materials have long term stability when handled correctly but are generally less sensitive than their ceramic counterparts. Ceramic materials can be easily manufactured using a sintering process and their piezo-effect is trained during formation. They have very good sensitivity but degrade over time, especially with increased temperature. Piezoelectric sensors possess a very high impedance characteristic which gives good noise rejection. Displacement sensors are a common variety, designed to measure sound from within a solid body. They are surface mounted onto the body, thus becoming insensitive to waves in the surrounding environment and are often capable of sensing very high frequencies [11], [12]. The S9208 produced by Mistras Physical Acoustics is an

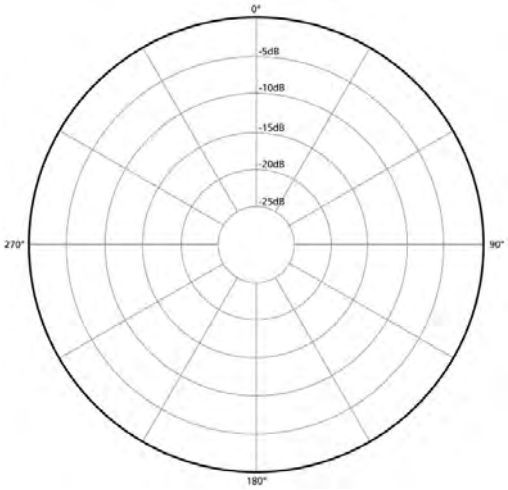

(a) Omnidirectional Graph

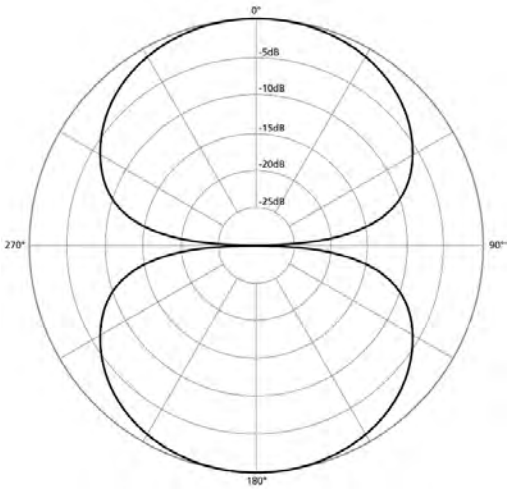

(b) Bidirectional Graph

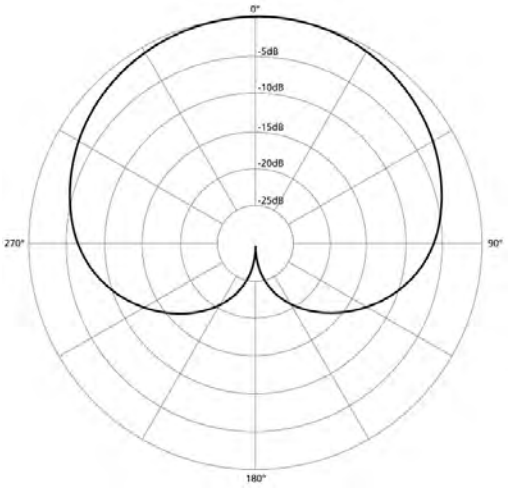

(c) Cardioid Graph

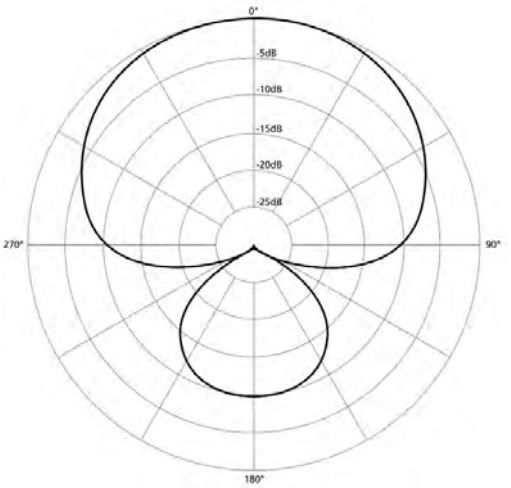

(d) Supercardioid Graph

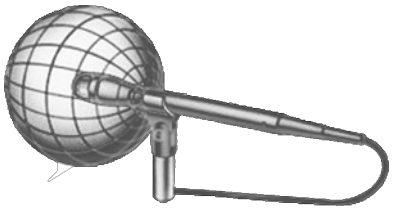

(e) Omnidirectional Image

(f) Bidirectional Image

(g) Cardioid Image

(h) Supercardioid Image

Figure 2.3: The four main types of polar pattern [8].

example, with a piezoelectric crystal sensor, designed to give a flat frequency response from 20 to 1000 kHz for surface acoustic displacements [13].

Optical microphones or fibre optic microphones use a laser light source to project light via an optical fibre onto a reflective diaphragm. Reflected light travels to a photo sensitive detector via another optical fibre. The acoustic wave causes the diaphragm to move, changing the direction of the reflected light. Positioning of the diaphragm determines the intensity of the light measured [14]–[16]. By design they are immune to Electromagnetic Interference (EMI) and Radio Frequency Interference (RFI), meaning noise from those sources is not present, as with other conventional microphones. Unfortunately, they are prone to self-noise, generated primarily in the photo detector due to the design of the photodiode. Typical self-noise values are around 60 dB, which is high compared with conventional designs [14]. However, this noise is random and from a known source; noise from conventional microphones would have induced noise from undesirable sources including EMI and RFI which would be unknown.

In summary, capacitive microphones are generally best suited to applications where fault information is contained within the audible frequency range, whereas piezoelectric sensors perform best where greater sensitivity to ultrasonic frequencies and noise rejection is required. Although optical microphones would be more desirable, their specialist nature, high costs and limited availability make their practical use problematic for the majority of systems. There are a wide range of fault mechanisms that produce audible frequencies, readily measurable with consumer-grade capacitive cardioid microphones.

2.1.2 Data Acquisition

Sensor measurements are normally output in an analogue format. Although some systems employ analogue filtering and processing techniques, these are relatively uncommon. In nearly all cases, analogue signals require digitisation through analogue to digital sampling. An ADC measures the voltage at discrete time intervals (forming the sampling rate), normally measured in Hertz. Sampling theory dictates that the sampling frequency must be at least double the highest signal frequency, e.g. in the case of audible frequency microphones, the highest sensitive frequency is usually 24 kHz, which is why

digital microphones commonly provide a 48 kHz digitised signal. Audio frequencies can be categorised into audible, ultrasonic and infrasonic. Audible frequency for humans is defined as 20 to 20 000 Hz with higher frequencies being ultrasonic and lower frequencies being infrasonic. Infrasonic frequencies are generated by sources such as volcanoes, earthquakes and avalanches. They are generally less used in the field of condition monitoring. Another important definition is AE which is typically defined as ultrasonic in the range of 100 to 1000 kHz. Therefore, appropriate sampling for AE frequencies requires sampling rates of at least 2 MHz. [17] reports that higher ultrasonic frequencies often provide better signal to noise ratio, as typical background noise frequencies tend to be lower than those of AE. Hence peak AE sensor responses are designed to fall within the AE range, and are insensitive to lower frequencies.

The electrical signals produced by most sensors are typically low level and require amplification to be transmitted and measured accurately. Most microphones use an integrated preamplifier to boost the signal for transmission along a cable. Secondary amplification can then further boost the signal for long distance transmission or provide a greater amplitude range for measurement. To accurately sample the microphone output voltage, the ADC resolution must be sufficient to give the required precision. For instance, most microphones produce a bi-polar signal in the low millivolts range, where most amplifiers output a 0 to 10 V signal.

2.1.3 Fault Feature Extraction Techniques

The raw signal from almost any sensor will invariably contain unwanted noise which can originate from the surrounding environment at the point of sensor capture, or from a wide variety of electrical and electromagnetic sources. Noise contamination when combined with signal attenuation and degradation, sensor imperfections, and analogue to digital conversion, normally results in the desired fault information becoming buried, hidden and difficult to identify. Separating relevant acoustic fault signatures from unwanted noise can prove challenging in a real-world environment. The goal of feature extraction is to isolate as much fault information as possible with minimal computational overhead.

2.1.3.1 Overview

Mathematically, there are three primary domains in which signals are traditionally analysed. Firstly, the time domain, with a plethora of mathematical techniques and algorithms available, ranging in complexity, from basic mathematical operations such as multiplication, through to composite sequential operations forming algorithmic analysis. Secondly, the Fourier transform, or variations thereof, converts a time or spatial domain signal to the frequency domain by representing the signal as a superposition of sine and cosine functions. There is usually a real part representing the amount of frequency from the original signal and a complex part representing the phase offset at that frequency [18]. The Fast Fourier Transform (FFT) is commonly utilised to calculate the Discrete Fourier Transform (DFT) of a uniformly sampled signal by factorising the DFT matrix into the product of a few sparse matrices, with the resulting factors being applied to a vector. This reduces the arithmetic complexity from n^2 operations to $n \log n$ where n is the data size. Frequency analysis has been used to identify particular frequencies that are representative of a fault, for example in [1], [19] for REBs, or in [20] where it is applied to Intrinsic Mode Functions (IMFs) generated through Hilbert-Huang Transform (HHT) to better extract the characteristics of REB fault frequencies.

The third domain, known as the time-frequency domain, allows the study of both time and frequency information simultaneously. However, there is a trade-off in resolution between the two domains. Figure 2.4 illustrates the concept of how the different domains map resolution in time and frequency. Techniques such as Short-Time Fourier Transform (STFT) can achieve a required resolution in both time and frequency. However, this comes with the expense of significantly disproportionate computation requirements, unfortunately making it currently unsuitable for low-cost real-time continuous processing and for large datasets. The advantage of so-called wavelet transforms is in the configuration of the domain resolutions, making the algorithm significantly more efficient whilst still achieving the resolutions required.

Fault detection algorithms can be broadly categorised into those that can detect continuous or transient faults. Continuous faults often stem from, for example, a mechanically worn component or a pressurised leak, whereas a transient fault example could be a mechanical impact, for example, damage

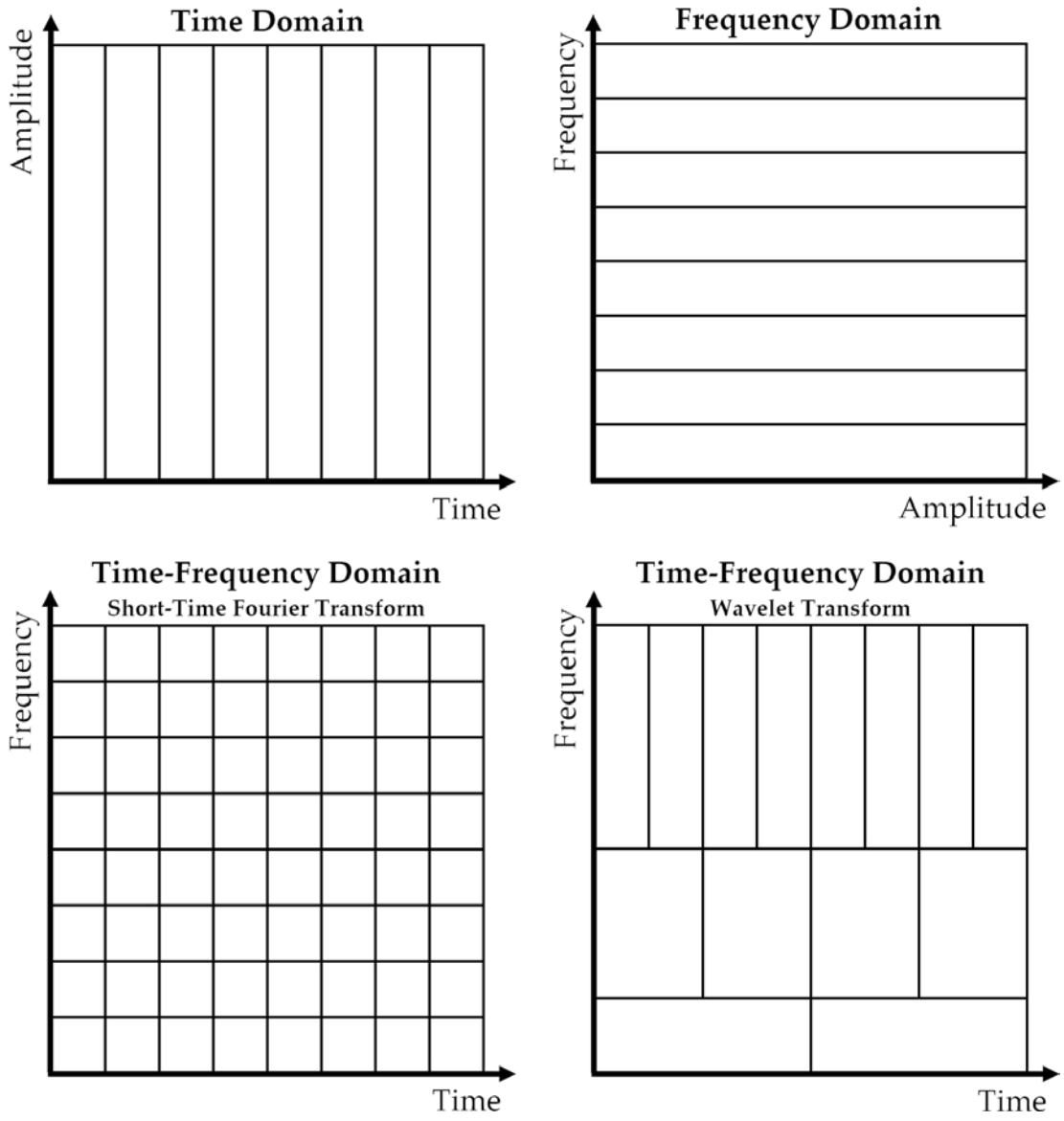

Figure 2.4: Diagram illustrating resolution mapping of time, frequency, and time-frequency domains.

to the race of a roller bearing. Identifying a continuous fault is relatively straightforward as marked differences between healthy and unhealthy states would usually be evident in the frequency spectrum. Equally, in the time domain a change from a healthy to an unhealthy state may also be evident. However, transient fault types can prove more challenging as the fault signature is often hidden in the time domain and may only result in very low-level changes in the frequency domain. A time-frequency algorithm can then be used to better identify such conditions. When considering different feature extraction methods, it is crucial that the nature of the fault features are well-understood. In this case, as is common with transient fault detection, the signature is of high frequency and short time duration. Therefore, an optimal

detection algorithm would seek to reveal frequency changes with respect to time, as corroborated in [21]–[34].

There are many well-known time-frequency techniques, such as the STFT, spectrogram analysis, wavelet transform, Wigner distribution, Wigner-Ville, Choi-Williams, and HHT, from which many variations are derived. For this work, two feature extraction algorithms, WPT and EMD, are chosen for comparative purposes. These techniques are prominent in the field with proven suitability and excellent performance [31].

2.1.3.2 Wavelet Theory

The wavelet transform can be considered a dynamic extension to the classical Fourier transform which uses the sum of complex exponentials; but instead employs a dyadic dilation of a scaling function, and translation of a mother wavelet function (example given in Figure 2.5) [18], [35]. The Continuous Wavelet Transform (CWT) of a finite energy signal $x(t)$ is the result of convolving that signal with a dyadic scaling and translation of a mother wavelet $\Psi(t)$ of the form:

$$W_{(\alpha,b)} = \alpha^{\frac{1}{2}} \int_{-\infty}^{\infty} x(t)\Psi * \left(\frac{t-b}{\alpha}\right) dt \tag{2.1}$$

where $W_{(\alpha,b)}$ is the wavelet coefficient, α is the dyadic scaling, b is the dyadic translation and Ψ is the mother wavelet.

A true CWT requires an infinite number of functions that generate an infinite number of coefficients, which is impossible to realise practically. Letting $\alpha = 2^m$ and $b = n2^m$ (where m and n are integers), the CWT becomes discrete and forms an orthonormal basis set;

$$\Psi_{(m,n)}(t) = 2^{-\frac{m}{2}}\Psi(2^{-m}t - n) \tag{2.2}$$

allowing a realisable calculation overhead. The base scale is usually a fractional power of two in the form $2^{j/v}$, where j represents the number of scales and v represents the fidelity of each scale (sometimes known as the number of 'voices per octave'). The resulting number of coefficients remains

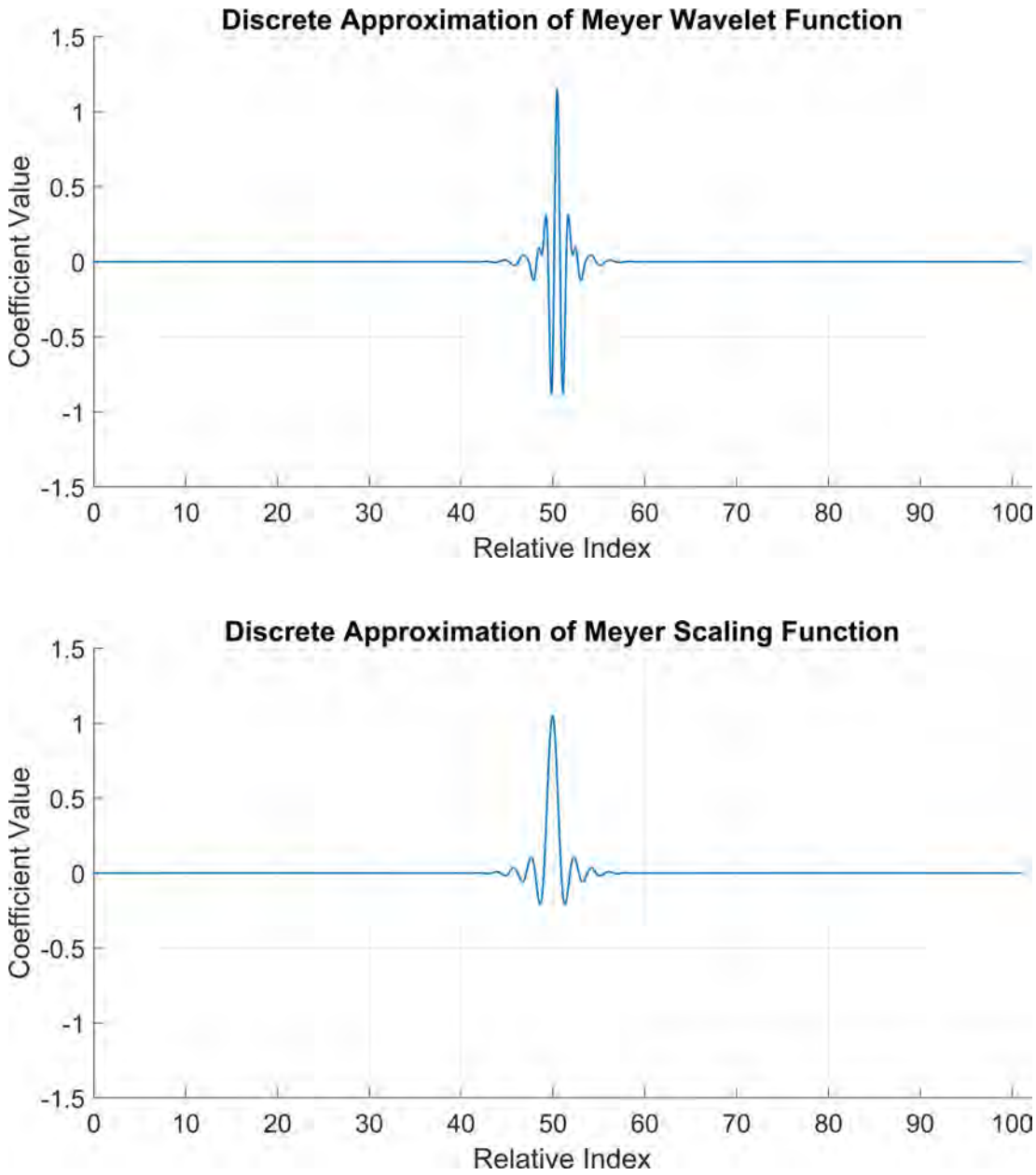

Figure 2.5: Plot of an example dmey wavelet and scaling function. Axis units not relevant.

very high - an M by N matrix, where N is the input signal length and M is the number of scales.

The Discrete Wavelet Transform (DWT) discretises the scale to $2^{j/1}$ with only a single 'voice per octave' and base scale of two. This results in the number of coefficients being equal to an $L+1$ by N matrix, where L is the decomposition level. The DWT convolves the original signal with a low pass filter $h(n)$ and high pass filter $g(n)$, and downsamples by a factor of two. $h(n)$ and $g(n)$, Figure 2.6, are a coarse discretisation of the dyadic scaling and wavelet

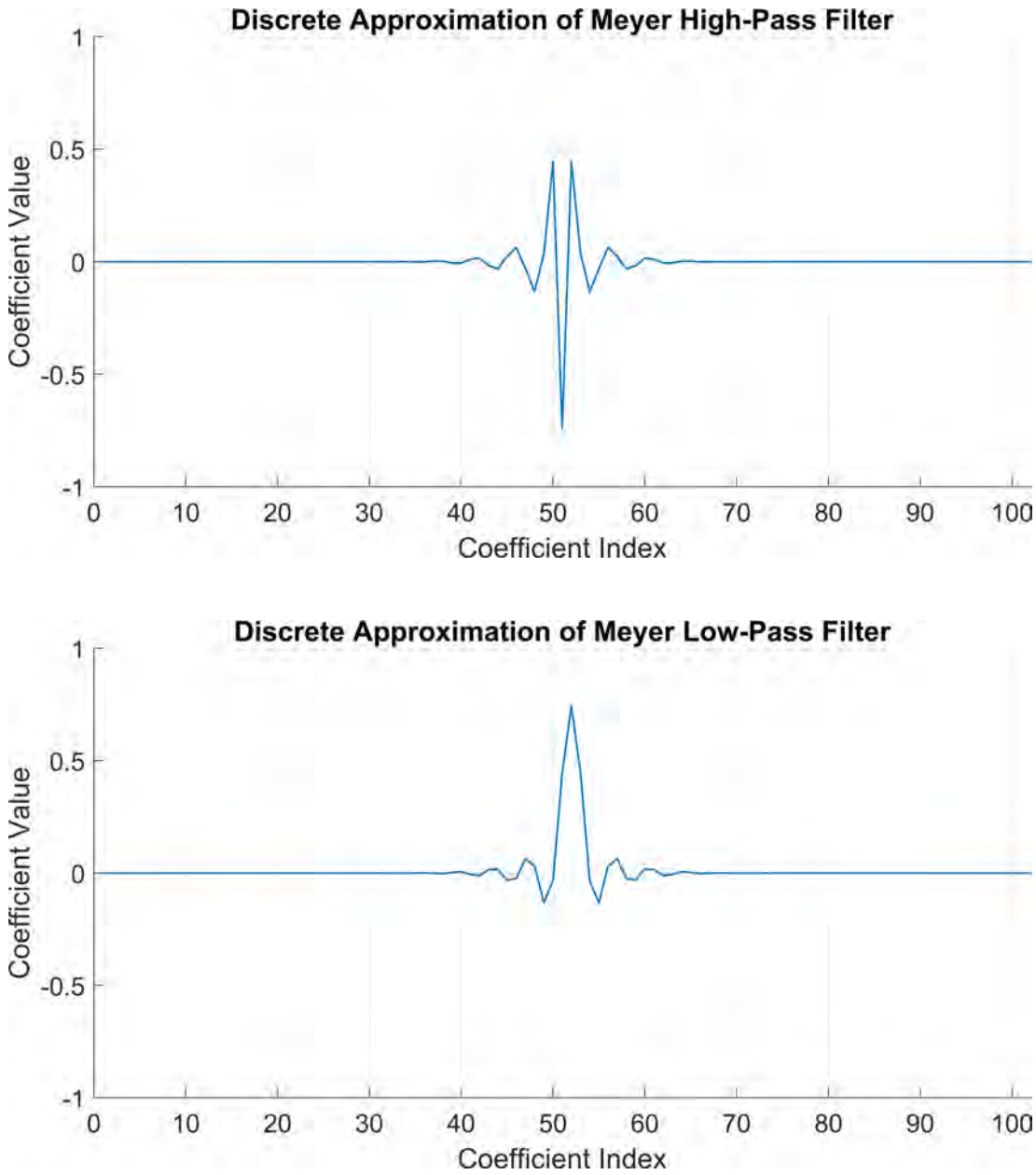

Figure 2.6: Plot of the discrete approximation of Meyer high and low pass filter coefficients.

function, and take the form:

$$h(n) = \frac{1}{\sqrt{2}} \langle \varphi(t), \varphi(2t - n) \rangle \tag{2.3}$$

$$g(n) = \frac{1}{\sqrt{2}} \langle \Psi(t), \Psi(2t - n) \rangle = (-1^n) h(1 - n) \tag{2.4}$$

where $\varphi(t)$ is the dyadic scaling function.

This results in approximate coefficients cA_1 and detail coefficients cD_1. The process can be repeated on the approximation coefficients to give a multi-level decomposition, as depicted in Figure 2.7. Reconstruction of the signal involves upsampling by two and convolving the approximation and detail coefficients with low and high pass reconstruction filters, respectively, giving the real approximation and detail that are then summed [21], [31], [35].

The WPT follows the same principle but additionally decomposes the 'detail path' and the 'approximation path' at each level. This results in an even wavelet packet tree shown in Figure 2.8. Frequency folding, which occurs with WPT, results in low pass filtered signals containing information on the high frequency content. Consequently, the reconstruction order is aligned to the frequency order by inverting the position of each right-hand branch. For example, at the third level the natural order is 0, 1, 2, 3, 4, 5, 6, 7 but the frequency order becomes 0, 1, 3, 2, 7, 6, 4, 5 [21], [31], [35].

Although the CWT offers high-fidelity, it is excessive for the majority of fault diagnostic purposes and the computational resources required are generally too large for low-cost, continuous real-time processing. The DWT or WPT offers a sparse representation of the signal providing compression, but also reconstruction of the original signal from the approximation and detail coefficients. The additional terminal nodes of WPT over DWT allows deeper analysis of the different frequencies and the complex reconstruction can use

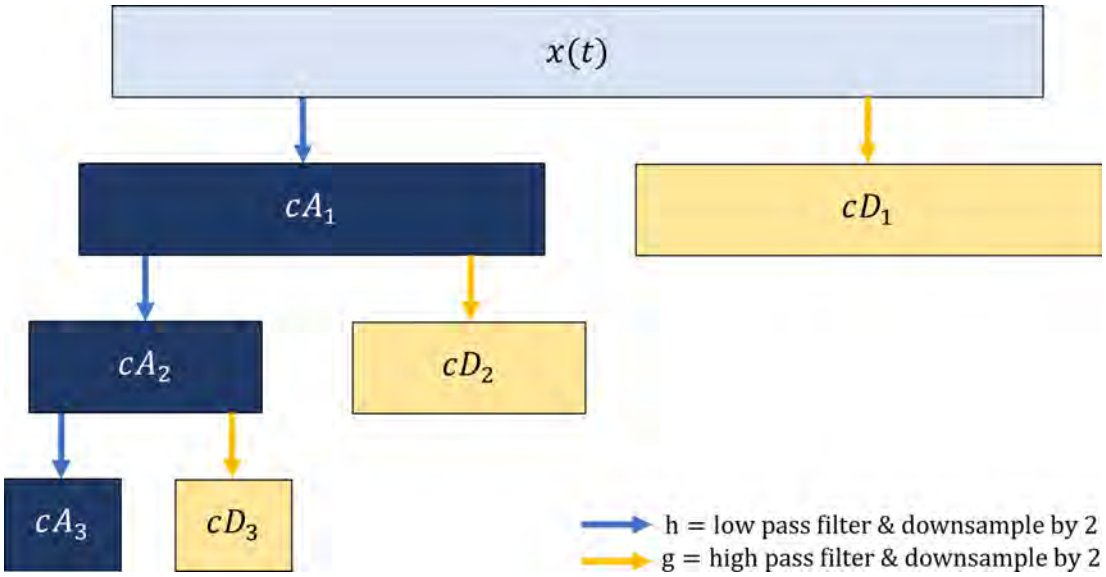

Figure 2.7: Example three-level DWT. The original time domain signal, $x\,(t)$, is decomposed into approximation coefficients cA_1 and detail coefficients cD_1, and so on. Signal reconstruction uses cA_3 and cD_1 to cD_3.

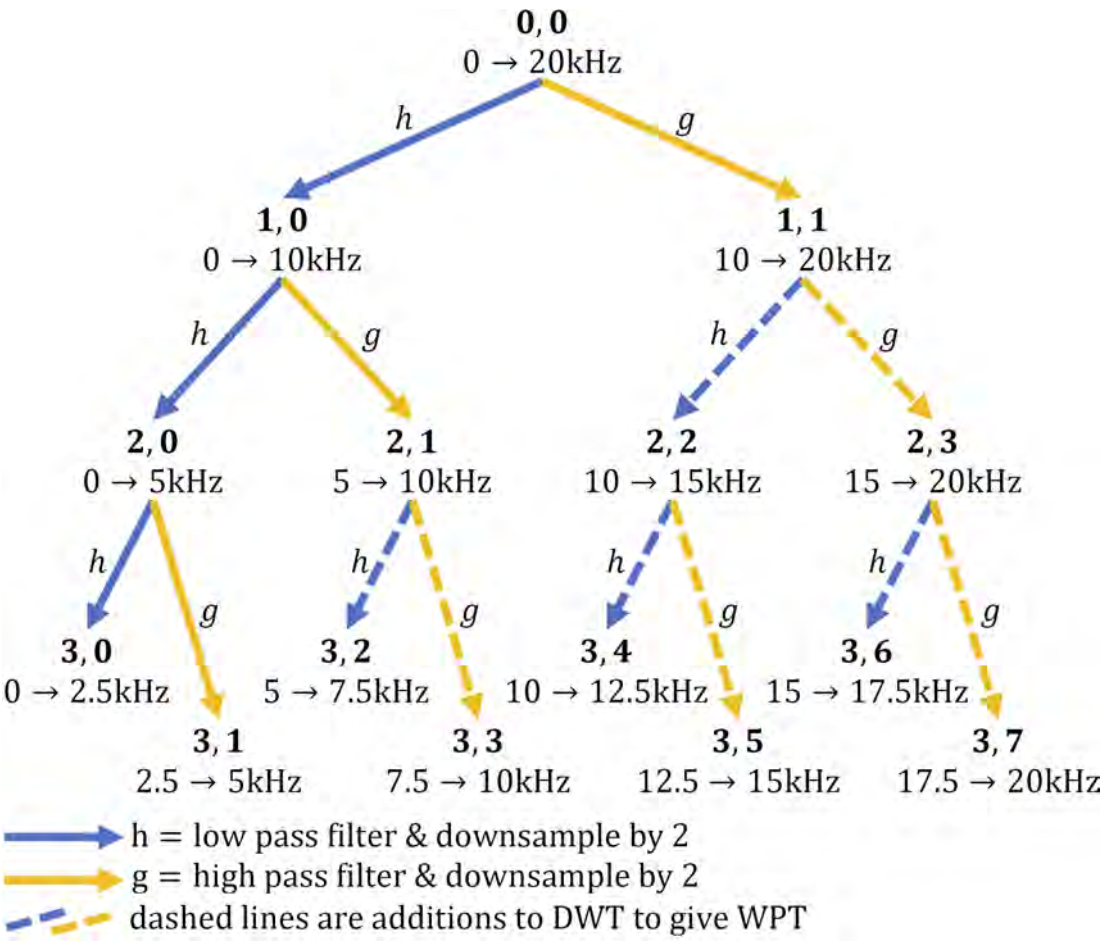

Figure 2.8: Example three-level WPT tree showing the frequency range corresponding to each node coordinate. Dashed lines show the additional branches of WPT compared to DWT.

specific terminal nodes facilitating unparalleled isolation of fault information, revealing the abrupt changes in hidden frequencies [21], [27], [31], [34], [35]. Based on the above, it is concluded that the WPT algorithm is best suited for fault diagnosis and is therefore selected for use going forward.

To achieve good performance, the configuration of the WPT requires detailed consideration. Optimal selection of the mother wavelet is the most critical parameter and is dictated by the similarity of the wavelet shape to the signal or signature through dilation and translation. There is no defined method to determine this, although researchers have devised various quantitative measures, all fundamentally based on experimentation and *a posteriori* knowledge of relevant signatures. Typically, a selection of different wavelets are tested for various quantitative performance factors such as maximum energy, minimum entropy and minimum reconstruction, among others. In [36], five attributes; energy, Shannon-entropy, signal power to noise power

ratio, mean square error, and maximum absolute squared deviation, are evaluated across twenty-six different wavelets. Three separate weighting schemes are applied to the attributes using the analytic hierarchy process (based on pairwise comparison matrix of the attributes). Each weighting scheme revealed a performance ranking order of the wavelets analysed, where the highest-ranking wavelet is deemed to deliver the best performance for the given application. A simpler approach is given in [37], where the maximum energy to Shannon-entropy ratio is used as a measure of wavelet performance. This method is particularly suited to transient acoustic fault signatures buried within normal operational characteristics.

The required number of decomposition levels can be visually determined through inspection of the terminal node coefficients using the Matlab wavelet analyser, aiming to maximise the isolation of the fault signature from unwanted noise. Additional decomposition levels increases the number of terminal nodes that can be analysed. However, this also increases the computational load.

2.1.3.3 Empirical Mode Decomposition Theory

EMD forms the first part of the HHT [38] and is a time domain signal decomposition method particularly suited to analysing non-linear and non-stationary systems and signals. Each decomposition level begins with a sifting operation, where smooth upper and lower envelopes of the signal are generated using cubic spline interpolation between local maxima and minima, shown in Figure 2.9. The mean of the two envelopes m_1 is then subtracted from the original signal to give the first sifted component, $h_1 = x(t) - m_1$. The second sifting iteration treats h_1 as the input and m_{11} as the mean of the new input upper and lower envelopes giving $h_{11} = h_1 - m_{11}$. This process is repeated k times, $h_{1k} = h_{1(k-1)} - m_{1k}$ until a termination criterion is reached. This forms the first IMF, $c_1 = h_{1k}$, which is subtracted from the original signal to give the first residue $r_1 = x(t) - c_1$. The residue is then treated as the input and the sifting process repeats j times until the stoppage criterion, $r_j = r_{(j-1)} - c_j$ is reached. Various stoppage criteria can be used, such as a standard deviation match, a predefined threshold, energy difference tracking or S-number (the number of consecutive sifting iterations where the number of zero crossings and extrema are the same or differ by one). The IMFs are oscillatory functions with higher IMF decomposition levels revealing

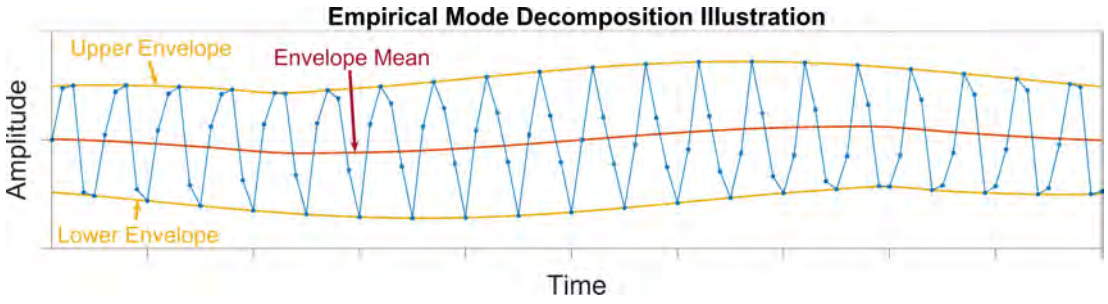

Figure 2.9: Illustration of the sifting operation.

subsequently lower frequencies. All the IMFs are the same length as the original signal and they must satisfy the two criteria below, such that their superposition will reconstruct the original signal:

- the number of IMF extrema (the sum of the maxima and minima) and the number of zero crossings must either be equal or differ at most by one,
- at any point of an IMF the mean value of the envelope defined by the local maxima and the envelope defined by the local minima shall be zero.

It is well known that EMD is prone to mode mixing and aliasing issues with more intermittent signals [39], resulting in IMFs that are devoid of physical meaning. EMD also degrades when multiple concurrent data points form a flat or non-oscillatory part of the signal, a square wave for example. To counter these disadvantages Ensemble Empirical Mode Decomposition (EEMD) [39], adds white noise to the input signal and then takes the ensemble mean of multiple outputs to form a single IMF. Accuracy is increased by using more ensembles, cancelling the white noise. However, this is computationally intensive and makes EEMD unsuitable for low-cost real-time processing. Further, since acoustic signals are highly-oscillatory EEMD would not provide any significant advantage over conventional EMD. Although EMD remains a time domain algorithm, it does provide an analysis of pseudo-time-frequency information, albeit, with the result devoid of physical meaning and the IMFs not precisely orthogonal. For the acoustic signals analysed here, EMD can imprecisely reveal the short-time transient frequency changes with excellent detection accuracy providing isolation of an empirically-derived fault signature.

Unlike the WPT algorithm, configuration of EMD does not require such detailed consideration. The way EMD works is highly adaptable to the input

signal, and the choices made when configuring will not have much impact on the algorithm performance, unless given very specific circumstances. The main consideration is the required number of decomposition levels, which can be determined experimentally. The resultant IMFs can then be analysed using further algorithms, statistical analysis, or visual means. [39] provides additional information on the EMD algorithm and a brief overview of its use for rotating machinery health monitoring.

2.1.3.4 Hilbert-Huang Transform

As previously mentioned, HHT [38] is formed of EMD combined with Hilbert spectral analysis to give the instantaneous frequency information [40]. Each IMF is transformed with the Hilbert transform which can be described as the convolution of the signal $x(t)$ with the function $h(t) = \frac{1}{(\pi t)}$. However, because the integrals do not converge the Cauchy Principle Value (CPV) applies:

$$H(x)(t) = CPV \int_{-\infty}^{\infty} x(\tau)\, h(t-\tau)\, d\tau = \frac{1}{\pi} PV \int_{-\infty}^{\infty} \frac{x(\tau)}{t-\tau} d\tau \tag{2.5}$$

Following this, the original data can be expressed as:

$$X(t) = \mathbf{R} \sum_{j=1}^{n} a_j(t)\, e^{i \int \omega_j(t) dt} \tag{2.6}$$

This gives both amplitude and frequency components as a function of time. This instantaneous frequency information allows for detailed analysis of non-stationary and non-linear systems.

2.1.3.5 Feature Analysis

The final step to achieve automated fault diagnostics is to analyse the extracted features against healthy system operation to determine the presence of faults or additional information. Techniques vary according to the complexity of the problem and application specific requirements. At the most fundamental level, this could be a binary problem, classifying between healthy and unhealthy states. Problems at this level are often solved using threshold-based detection methods. Statistical features such as maximum peak amplitude, peak to peak distance, crest factor, energy, entropy, kurtosis, skewness and Root Mean Square (RMS) provide a numerical representation that can be directly compared or become an input observation for machine learning.

2.1.4 Machine Learning Techniques

Machine learning in this context refers to the classification and decision making algorithms that can be used to automatically analyse data and provide useful information, thus Artificial Intelligence (AI) is often used synonymously (although in many contexts this refers to more complex systems). There are a wide range of 'traditional' machine learning algorithms available, some of the more well known include Artificial Neural Network (ANN), Support Vector Machine (SVM) and k-Nearest Neighbours (k-NN) [41]. These techniques are capable of excellent performance in terms of diagnostic accuracy and computational efficiency, and they can solve complex and chaotic problem types. However, they often require supervised training, and their performance can degrade with extreme complexity or large datasets. A selection of algorithms and techniques widely used in the field of fault diagnostics are now discussed.

2.1.4.1 Artificial Neural Network

ANNs are formed as a large collection of weighted neurons, linked together by axons, shown in Figure 2.10. Each neural unit is connected with many others. These links can be enforcing or inhibitory in their effect on the activation state of connected neural units. Each individual neural unit may have a summation function which combines the values of all its inputs together. There may be a threshold function or limiting function on each connection and on the unit itself: such that the signal must surpass the limit before propagating to other neurons. These systems are self-learning and trained, rather than explicitly programmed. They excel in areas where the solution or feature detection is difficult to express in a traditional computer program.

ANNs typically consist of multiple layers or a cube design, where the signal path traverses from front to back. Back propagation is where the forward stimulation is used to reset weights on the 'front' neural units and this is sometimes done in combination with training where the correct result is known. More ANNs are freer flowing in terms of stimulation and inhibition, with connections interacting in a much more chaotic and complex fashion. Dynamic neural networks are the most advanced, based on rules, they can form new connections and even new neural units dynamically, while disabling others.

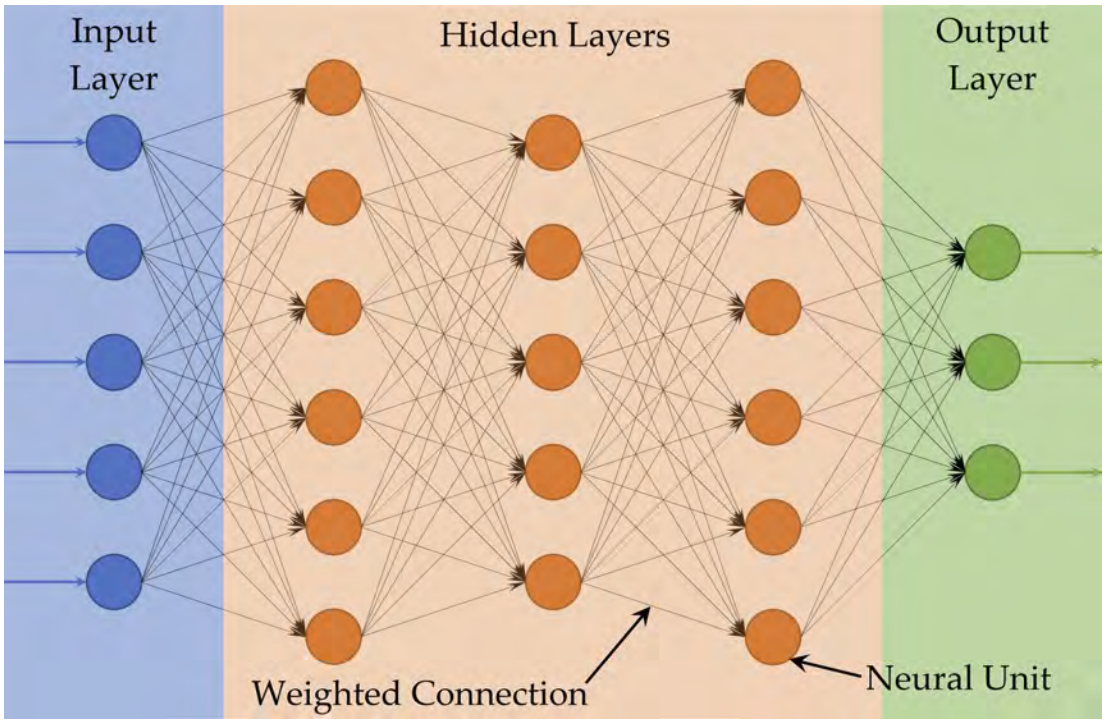

Figure 2.10: Illustration of a simple ANN.

The goal of the ANN is to solve problems in the same way as the human brain. Modern ANN projects typically work with a few thousand to a few million neural units and millions of connections, which is still several orders of magnitude less complex than the human brain (closer to that of an earthworm). ANNs can take extended periods to train and be very computationally demanding. However, they are well suited to more complex problems and still perform well with large datasets.

2.1.4.2 Support Vector Machine

A SVM is a supervised machine learning algorithm for classification and regression, originally proposed by Vapnik in 1963 [42]. It uses labelled training data to define a separating linear hyperplane, maximising the space between different classes i.e. the biggest margin. The nearest data points to the margin are known as support vectors and are used to define the hyperplane. New data points can then be assigned to one category or another according to their relative location to the defined hyperplane. To illustrate, as in Figure 2.11, consider a training dataset of n points: $(\vec{x}_1, y_1), \ldots, (\vec{x}_n, y_n)$, where y_i is either 1 or -1 indicating the class to which x_i belongs, and x_i is a p-dimensional real vector. The hyperplane can be expressed as:

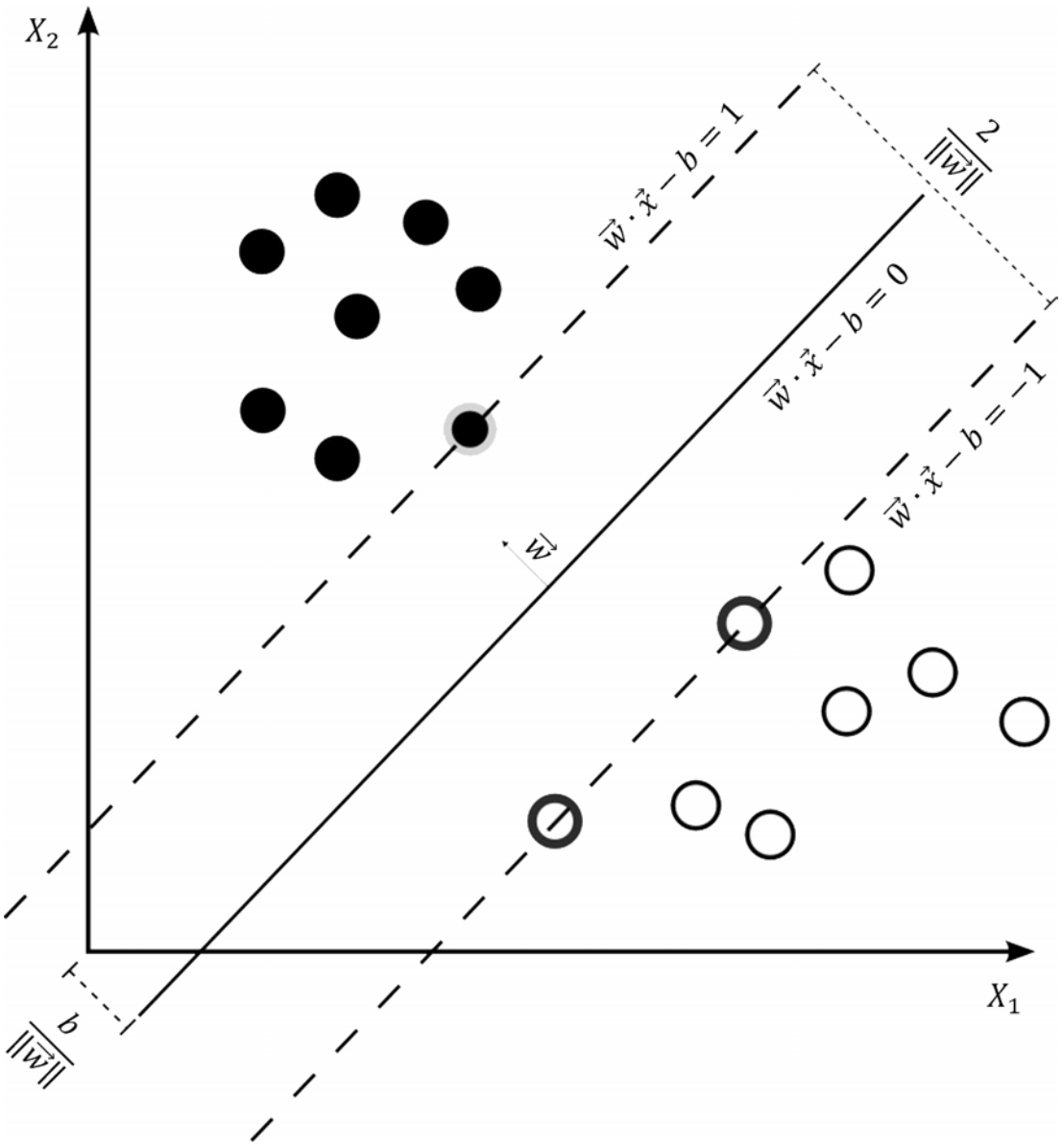

Figure 2.11: Illustration of a SVM, showing the linear hyperplane and margins for a simple classification problem.

$$\vec{w}\cdot\vec{x}-b=0 \tag{2.7}$$

where $\vec{w}$ defines the boundary, $\vec{x}$ is the input data and b is a scalar threshold.

With training data that is linearly separable, the two class margins are defined as $\vec{w}\cdot\vec{x}-b=1$ and $\vec{w}\cdot\vec{x}-b=-1$. The algorithm wants to maximise the separation distance between classes given by $\frac{2}{\|\vec{w}\|}$ and ensure no data points fall within the margin giving;

$$min\ \|\vec{w}\|\ subject\ to\ y_i\ (\vec{w}\cdot\vec{x}-b)\geq 1, for\ i=1,\ \ldots,\ n \tag{2.8}$$

This is known as a hard margin as data points of a particular class fall exclusively on one side; a soft margin is where some data points for a particular class may fall on the incorrect side. Here, the hinge loss function λ is introduced to account for the trade-off between the distance away from the margin and moving the margin, expanding the problem to:

$$min\ \left[\frac{1}{n}\sum_{i=1}^{n} max\ (0,\ 1-y_i\ (\vec{w}\cdot\vec{x}_i-b))\right]+\lambda\|\vec{w}\|^2 \tag{2.9}$$

Clusters cannot usually be separated using a linear classifier unless the problem is quite simple. Therefore, for more complex cases, a SVM can employ the kernel trick; mapping the inputs to high-dimensional feature spaces. The high dimensionality of the feature space allows for a linear solution in that space. This becomes more computationally intensive but by using a specified kernel the dot product and transformation to the high dimensional feature space can be in a single operation. There are many different types of kernel including polynomial, sigmoid and radial basis function [42].

SVMs perform well in terms of accuracy, training time and computational efficiency compared with other machine learning techniques. However, it should be noted that by comparison, they are suited for smaller datasets and dimensionality [1].

2.1.4.3 Principle Component Analysis

Principal Component Analysis (PCA) [43] is a statistical analysis method that converts a series of variables with a number of observations into orthogonal linearly uncorrelated principal components. Each principal component must contain the largest possible variance and be orthogonal to the previous one. The resulting component vectors can then be used for dimensionality reduction and analysis of contributing variables. By definition there must be fewer principal components than original variables. PCA can be undertaken by finding the eigenvalues of the covariance matrix after normalisation of each variable.

If x is a vector of p random variables and the variances are of interest, then unless p is small, analysing the variances will often prove ineffective. PCA

looks for principal components α_k; the first step is to find a linear function ${\alpha_1}'x$ of the elements of x having maximum variance, where α_1 is a vector of p constants:

$$ {\alpha_1}'x = \alpha_{11}x_1 + \alpha_{12}x_2 + \ldots + \alpha_{1p}x_p = \sum_{j=1}^{p} \alpha_{1j}x_j \tag{2.10} $$

The next linear function ${\alpha_2}'x$, uncorrelated to ${\alpha_1}'x$ having maximum variance, and so on up to the ${\alpha_k}'x$, where at the kth level ${\alpha_k}'x$ has maximum variance and is uncorrelated with all the previous components. It is possible for k to go up to p components but it is hoped that the majority of the of the variation in x will be accounted for by m principal components where $m \ll p$. When PCA is applied for machine learning, it is an unsupervised algorithm that aids in the identification of the features that contain the largest amount of fault signature information. This allows less useful features to be disregarded.

2.1.4.4 Deep Learning

Deep learning refers to a subset of machine learning techniques that have developed due to advancements in computational hardware, algorithm development and the availability of 'big data'. These algorithms are more complex and operate by attempting to solve the problem by developing a hierarchy of concepts or rules, each defined by its relations to simpler concepts or rules [41], [44]. The nature of the operation allows for more complex problems to be solved, and moreover, performance is adaptable and robust allowing algorithms to be trained in widely varying contexts. These algorithms can often solve the same problems as the aforementioned traditional algorithms without prior feature extraction, i.e. analysing the the raw data. They are also suited to analysing larger datasets, albeit with an extended and computationally intensive training period. Examples of deep learning algorithms include the Convolutional Neural Network (CNN), Deep Belief Network, Recurrent Neural Network and Generative Adversarial Network [41], [44].

2.1.4.5 Comparison & Summary

The performance of any classification algorithm is highly dependent on the differentiating features presented for training. Several studies have compared the performance of SVMs and ANNs for REB fault classification and concluded that SVMs outperform their counterpart with regard to accuracy, training time

and computational efficiency. This is shown in [42] which compares SVMs with ANNs, optimising their parameters using genetic algorithms and finding the ANN to require significantly more training time. Both systems were capable of 100% accuracy, but the SVM was significantly quicker in training and operation. In [27] results from two classification methods are compared; a radial basis kernel SVM optimised for the cost and gamma parameters to use the minimum number of support vectors, and a three-layer feed-forward ANN trained using supervised back propagation. Results indicated that the SVM is more readily implemented, and gave better results. SVMs tends to perform better than ANNs for this application, but only for smaller datasets [45]. Note that implementation on real industrial machines would require a much larger and more sophisticated data set in which case ANNs would likely give better performance.

The use of deep learning algorithms would likely yield the best overall performance for most real-world applications, where large datasets and complex decision making are necessary. Careful consideration must be given to the dataset size and the problem complexity before employing deep learning methods, as more traditional techniques will deliver superior cost to benefit performance for simpler application requirements.

2.1.5 Continuous Processing & Specialist Hardware

Industry requires continuous real-time fault diagnostics and condition monitoring to prevent catastrophic failure and unscheduled maintenance. The application will determine how timely the information must be. In the case of a REB defect developing, it is likely that the REB will continue to function normally for a reasonable amount of time after first detection, allowing maintenance to be planned and the REB replaced at the least cost. However, in the case of a critical fault developing on an electrical machine, it may be necessary to stop the motor immediately to prevent further damage. Both these examples rely on the fault information being received at the earliest possible time. The problem is that the complex algorithms required for feature extraction and decision making are difficult to compute in real-time using GPP. The relevant background and theory of computer hardware for continuous processing is now discussed.

Computing hardware can be categorised into GPPs, programmable DSPs, reconfigurable hardware and Application Specific Integrated Circuits (ASICs) [46]. The degree of programmability against specialisation is shown in Figure 2.12.

GPP refer to the type of computational Integrated Circuits (ICs) typically found in computers, such as CPUs and GPUs. They are capable of performing a wide variety of processing tasks with ease and can cater for nearly all requirements. They incur relatively high power consumption and generate significant heat which requires specialist cooling to dissipate. Although there are many different technologies used, at a fundamental level these processors execute one operation at a time in a sequential manner. This makes them comparatively slow and energy intensive for more specialised processing requirements.

At the other end of the spectrum, ASICs are specially designed for computational efficiency for a limited processing task. These highly specialised processors deliver extreme performance i.e. super fast computation with low power consumption and heat generation. However, they can only perform within their design parameters and cannot be modified or adapted for changing operational requirements or data. Their high performance comes with extremely high development costs, therefore they are typically only developed for mass production so the development costs can be recouped. The high development costs usually make ASICs cost prohibitive where only a relatively small number of units are be required.

Programmable DSP have three development drivers; data parallelism, application specific specialisation, and functional flexibility. These types of processors are ideal for working on signals in real time. However, they are not designed to run complex classification or decision making

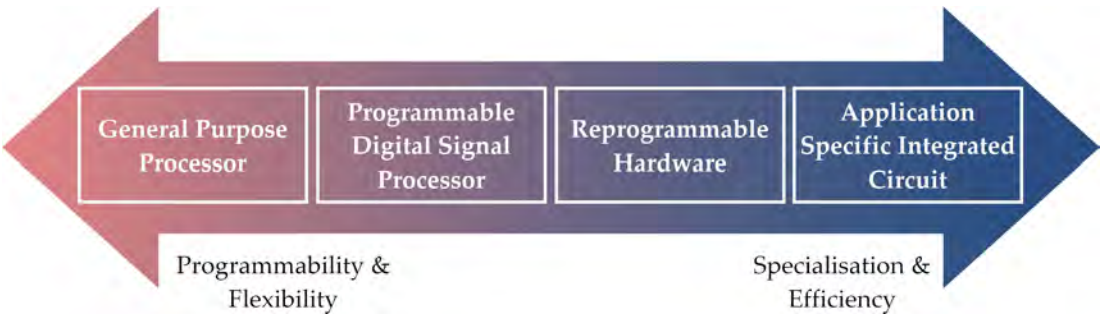

Figure 2.12: Diagram showing different processing implementations.

algorithms, and interfacing with data storage and other components can prove challenging. There are many different models and types, with some customisation available, but they are often designed to perform specific tasks.

Specialist equipment from National Instruments or similar companies can often provide a solution for rapid data acquisition and processing. However, in this case, the algorithms are required to operate concurrently in real-time, which is not currently available with this type of equipment.

This leaves reconfigurable hardware, which typically refers to FPGA ICs [46]–[48]. Modern FPGAs are a collection of fine-grained programmable logic blocks interconnected by wires and programmable multiplexing switches. The lookup table (a small programmable memory) defines the logic for each block. Each block can also contain a number of Flip-Flops (FFs) for fine-grained storage. The user can program and reprogram the hardware to perform complex combinational and parallel functions. Currently, FPGAs typically have around 10 million logic blocks and can operate at clock speeds of around 500 MHz. The primary advantage of FPGAs is that they can be programmed and reprogrammed to meet changing, user specific requirements [46]. Although FPGAs are supposedly less programmable than GPP and programmable DSPs, this is mainly due to the constraints on the nature of their processing. FPGAs can be programmed to execute the feature extraction and classification algorithms extremely quickly and efficiently by programming them to execute functional blocks in parallel. FPGAs offer so much parallelism that even low-cost and readily-available FPGAs can implement multiple feature extraction algorithms and use advanced machine learning without compromising on speed or power consumption.

The following investigations have recognised the need for faster FPGA processing and offer insight into its practical implementation. References [49], [50] investigate faults on induction motors - focussing on broken rotor bars, both use a Xilinx Spartan-3 FPGA platform. The former implements DWT whereas the latter implements EMD with full spline-cubic function, an adaptive linear neural network frequency estimator and ANN classification.

[51] approaches an FPGA implementation of high-frequency resonance analysis to identify the characteristic frequencies of an inner and outer race

seeded defect in a roller element bearing. They use Matlab/Simulink compiler (DSP Builder) to convert their model to VHSIC Hardware Description Language (VHDL) and program an Altera Cyclone II.

In [52], a powerful FPGA board is used to implement real-time diagnostics on roller element bearings by processing AE signals with WPT feature extraction and SVM classification. The board used is a Xilinx Virtex-7 development kit, processing 2.5 s of audio from a Physical Acoustics WSα 100 to 900 kHz AE sensor. The SVM classified processed signals based on 78 training samples of 2.5 s for each of the four bearing classes; these being healthy, or with a defect on the outer race, inner race or roller element.

Work reported in [53] samples high-frequency AE signals at 5 MHz and 16 bit resolution. These are processed in real-time through DWT feature extraction using a ZedBoard development kit equipped with the Zynq-7000 FPGA. In this instance, the output signal is used to increase productivity of pulsed laser ablation in liquids through optimised control of the working distance between the laser and liquid.

[54] employs a Xilinx Virtex-5 FPGA in an attempt to implement ultrasonic non-destructive evaluation for critical structures. The FPGA board interfaces with ADC and Digital to Analogue Converter (DAC) daughter boards and a touchscreen controller is developed on the embedded Microblaze in C, interfacing through the RS232 serial port. The implementation gives a reasonable reconstruction of the split spectrum processing algorithm compared against results from Matlab.

Removing power disturbances is a common problem in many electrical measurements. [55], [56] investigate FPGA-based solutions. In [55] the DWT is implemented on two Xilinx XC4010XL FPGAs to improve power quality. Whereas [56] removes power-line interference on electrocardiogram signals using similar DWT filtering and reconstruction, realised on an XUP Virtex-II Pro development board.

Similarly, real-time processing of electrocardiogram signals to remove noise is explored by [57]–[59]. In [57] computationally intensive parts of the HHT algorithm, such as cubic spline interpolation and the stop sifting criteria, are implemented in FPGA on a ZebBoard using Xilinx Software Defined System on Chip (SDSoC). Synthesised electrocardiogram signals are processed comparing between a software (Matlab) only process and a hardware assisted

process. Although processing times are reduced with hardware assistance, the implementation could be significantly improved by coding directly in Hardware Description Language (HDL) rather than using a C to HDL compiler.

Work reported in [58] uses DWT processing implemented using Xilinx Virtex-5 FPGA comparing a conventional multiplier architecture with a distributed arithmetic architecture. Results showed that the former could be implemented in a single clock cycle giving significantly more throughput, $\approx$1000 Mbit/s, compared to 8 clock cycles and $\approx$300 Mbit/s for the latter architecture.

A comprehensive monitoring system is presented in [59] including the design and implementation of an electrocardiogram measurement module, an ADC module, a data flow management system, an EMD processor, and a DAC module that outputs the processed signal. Although the EMD algorithm is implemented on a TMS320C6713 DSP, the data flow management system is implemented on an Altera Cyclone 2C20 FPGA by VHDL coding using Quartus II, where the timing and memory allocation is of particular interest. The authors note that a complete FPGA solution to be the next step of their work.

Another application reported in [60] and [61] investigates wheeze detection from audio using Mel-frequency cepstral coefficients feature extraction and either SVM or feed-forward multilayer perceptron ANN classification. A low-cost Nexys-4 development board that uses the Xilinx Artix-7 FPGA is programmed using the Xilinx System Generator. The default SVM configuration and prior ANN implementation are optimised to deliver significant improvements in output latency, and resource and power consumption.

The work presented in [62] employs FPGA processing for directional localisation of sound. A Virtex-5 FPGA performs filtering and calculates sound localisation through computation of the azimuth angle. This example offers some insight to the practical implementation of the Block Random Access Memory (BRAM) for real-time streaming.

The system described in [63] is a remote environment monitoring station that is solar/battery powered using an Artix-7 FPGA equipped with a microphone array and wireless communication. The system is designed to detect, identify and localise acoustic sources in national parks. It can detect gunshots,

and airborne and ground vehicle traffic for example. This is achieved by implementing substantial filtering techniques with sparse coefficient state tracking for detection and classification, and geometric wideband Capon angle of arrival estimation for localisation. The FPGA system is used here for its low-power consumption, high computational efficiency and low-latency real-time processing, a marked improvement over the pre-existing systems which either required excessive resources making them unsuitable for remote deployment or were overly simplistic thus unable to achieve the required performance for real-world applications.

The work reported [64]–[67] investigates the implementation of various digital signal processing algorithms onto an FPGA architecture. They all identify the inherent parallelism of the FPGA as providing a substantial advantage over conventional processing architecture. [65] in particular, demonstrates a FPGA implementation of real-time EMD.

In [68] a Xilinx Zynq-7000 FPGA is compared against Tegra K1 GPU and a high performance computation server (equipped with multiple Nvidia Tesla P100 GPUs) for an ultrasonic fault detection system based on a SVM. Experimental results showed that the FPGA outperformed the GPU's execution time by a factor of 10. Although the server was almost 3 times faster, it costs around 20 times more and requires significantly more power. Furthermore, FPGA performance could be drastically improved by implementing the algorithm directly using Verilog or VHDL instead of the Xilinx System Generator (a high-level abstraction tool).

[69] discusses the use of FPGAs for large data acquisition and real-time processing from the perspective of experimental physics and industrial control systems. The authors employ a National Instruments FlexRIO PXIe 7966R card, equipped with a Xilinx Virtex 5 FPGA, to expedite data acquisition for large data sets at rapid sampling rates.

FPGAs have traditionally been used by specialists to prototype designs for ASIC processors. However, improved design tools like the Xilinx System Generator and SDSoC Development Environment, have made FPGA programming more accessible for both industry and for research. FPGAs are now being used for their customisability to deliver efficient and fast processing without the design requirements and costs associated with ASICs.

2.2 Mechanical Fault Modes

The mechanisms that cause acoustic waves are commonplace in mechanical systems, for example, as a result of physical impact/contact or internal material cracking. The literature available on the benefits of acoustic measurements for diagnostics with mechanical fault modes is substantial. This section discusses the most relevant published material categorised by component.

2.2.1 Roller Element Bearings

The REB is widely used in rotating machinery, its numerous failure modes make it responsible for over half of all rotating machine failures [33]. REB failure will likely result in; extreme damage to other machine components, prolonged downtime and heavy repair costs, additional health and safety risks, and environmental damage. Fault detection for REBs is therefore of significant importance, particularly when identifying incipient defects before they cause notable damage and allowing for preventative maintenance. Continuous real-time monitoring is necessary for critical systems and allows emerging changes to system characteristics to be monitored and for appropriately scheduling maintenance [70], [71].

REB damage such as galling, spalling, brinelling, peeling, wear, fatigue, overloading, and particle ingress, have been traditionally identified using vibration measurements [23], [71]–[75]. Defects are typically categorised by their location where characteristic fault frequencies are excited respective to the Roller Pass Frequency Outer-Race (RPFO), Roller Pass Frequency Inner-Race (RPFI), Roller Spin Frequency (RSF) and Fundamental Train Frequency (FTF), or a combination thereof [23], [33], [73]. The characteristic frequencies are dependent on the REB geometry and rotational speed according to Equations 2.11 to 2.14.

$$RPFO = \frac{nf_r}{2}\left[1 - \frac{d}{D}\cos\Phi\right] \tag{2.11}$$

$$RPFI = \frac{nf_r}{2}\left[1 + \frac{d}{D}\cos\Phi\right] \tag{2.12}$$

$$RSF = f_r\frac{D}{2d}\left[1 - \left(\frac{d}{D}\cos\Phi\right)^2\right] \tag{2.13}$$

$$FTF = \frac{f_r}{2}\left[1 - \frac{d}{D}\cos\Phi\right] \tag{2.14}$$

where n is the number of rollers, f_r is the shaft speed, Φ is the angle of load from the radial plane, d is the roller diameter, and D is the pitch diameter. No slippage is assumed.

2.2.1.1 Vibration Measurements

There are many examples where frequency spectrum analysis or, more commonly, time-frequency analysis is used to identify related fault signatures. [76] presents a comparison of two wavelet de-noising techniques for REB prognostics; filter-based and decomposition-based for vibration measurements. Vibrations are measured from four running REBs at 2000 rpm under high radial load (approx. 2.7 t) until failure, providing the natural development of the defect. REB failure is determined by debris analysis captured by a magnetic plug in the lubrication oil cycle. The results show that wavelet filtering is superior for de-noising signals to reveal impulse-like features. These features result in a greater spread of the wavelet coefficients. The authors found that by optimising the wavelet shape factor using the minimal Shannon-entropy criterion, and optimising the wavelet scale through Singular Value Decomposition to maximise the periodicity, the resultant de-noising can reveal extremely weak impulsive signals, provided they are periodic. The natural degradation of REBs over a long period is a novel approach in contrast to the many treatments of artificially seeded defects.

In [77], WPT combined with an adaptive network-based fuzzy interference system is employed for multiple band-pass filtering of vibration signals from low-speed REBs at 20, 60 and 120 rpm. The adaptive network-based fuzzy interference system is a type of expert system that operates similarly to an ANN, where logical rules are applied to a knowledge base to deduce new information. In this case, the interference engine is optimised through ANN training. It is used to determine which wavelet packets contain REB fault information thereby becoming an automatic feature extractor. The selected packets are used to reconstruct a signal which is now filtered and contains the REB fault information. Peak indexing is then used to determine fault severity on the outer race, inner race and roller element. This approach provides better

signal to noise ratio compared to standard high-pass filtering, with improved extraction of the high-frequency transients reminiscent of the faults.

[23] proposes using Morlet wavelet band-pass filter to remove the frequency ranges not containing fault information. The filter properties are optimised using differential evolution by kurtosis maximisation. The authors then use sparse code shrinkage to minimise the noise that remains. The power spectrum of the envelope then reveals the characteristic fault frequencies of the repetitive vibration impulses generated by defects on a REB inner and outer race.

Similarly, [24] replicates this work but uses antisymmetric real Laplace wavelet filtering instead of the Morlet wavelet. Initially both methods in [23], [24] are tested on artificially simulated fault signals with added Gaussian noise. However, the results of this were unrevealing. Subsequent experimental trials tested two N205 REBs with a respective inner and outer race defects, artificially machined using Electrical Discharge Machining (EDM) to $0.2\,\mathrm{mm}$. Radial vibration is measured at $\approx 20\,\mathrm{kHz}$ for $0.5\,\mathrm{s}$ with the REB rotating at $25\,\mathrm{Hz}$ and $30\,\mathrm{Hz}$, respectively. Additional Gaussian noise is added to the measured vibration signals in [24], these are then processed as above. Both denoising techniques perform well and isolate the characteristic fault frequencies and their harmonics.

[78] utilises synchronous averaging reassigned wavelet scalogram to detect weak REB fault information from vibration measurements. The signal processing comprises of the CWT to provide the wavelet scalogram, each is then reassigned for multiple scales, with multiple cycles then averaged together. This aids amplification of the weaker fault information and helps remove noise, albeit computationally demanding.

A different approach to wavelets is presented in [27] where, rather than utilising DWT filtering as above, the authors opt to employ the less common CWT in an effort to improve performance. Two mother wavelets, Morlet and Daubechies10, decompose the vibration measurements, sampled at only $7.68\,\mathrm{kHz}$. In this case, the data is measured from a motor fault simulator rig at no-load, half-load and full-load, only differentiating between a healthy motor system and a motor system with faulty REBs (the precise nature of the fault is not specified). The authors process the signals using CWT and then compare the performance of an SVM and ANN classifier. From 150 data samples, 120 are used for training the classifier, leaving 30 for experimental

testing. Results favoured the SVM classifier which outperformed the ANN in accuracy and ease of implementation and optimisation. Interestingly, the differences in performance between the two mother wavelets are only present in the ANN classification, where the Morlet wavelet delivers marginally better classification. However, no differences are observed in the SVM results. Initial results with the wavelet scale $1-15$ are improved with a reduced scale of $1-8$. In this case the SVM delivered $100\,\%$ accuracy.

[79], [80] analyse vibration signals by EMD feature extraction that feeds into an ANN for REB diagnostics. Statistical features (including energy entropy, kurtosis, peak to peak and skewness) from the IMFs are analysed by an ANN to differentiate between a healthy REB and three different defect types (inner and outer race and roller), each with a degraded and failed condition. [80] uses data from an independent experiment, where three experimental trials run four Rexnord ZA-2115 double-row REBs evenly spaced on a shaft, with the two centre REBs loaded with $\approx 2.7\,\mathrm{t}$. The shaft is rotated by an AC motor at $\approx 33\,\mathrm{Hz}$ for $35\,\mathrm{days}$ causing four different REBs to fail. Vibration measurements of $1\,\mathrm{s}$ duration are recorded every $10\,\mathrm{min}$ at a $20\,\mathrm{kHz}$ sampling rate. This method's diagnostic performance is reasonable and comparable to other works, however, fault detection only occurs when the REB condition deteriorates, noted as the degraded condition. In this condition the REB is producing much more vibration owing to a major defect and at this stage the REB performance is compromised. The formation of the defect and its development occurs considerably earlier and remains undetected by these vibration techniques.

The investigation in [20] demonstrates hybrid EMD-FFT feature extraction on vibration measurements. The pseudo-time-frequency analysis of the EMD provides the IMFs that would then normally be analysed using Hilbert Spectral Analysis (HSA). However, in this work the authors analyse the IMFs using FFT to better capture the characteristic fault frequencies in the frequency domain. The vibration data is measured from a test rotor supported by an artificially damaged deep-groove 6203 REB under no-load, with the shaft driven at $30\,\mathrm{Hz}$ by an AC motor. Experimental results clearly show the characteristic fault frequencies and subsequent harmonics.

[28] proposes hybrid WPT and EMD feature extraction for early fault diagnostic from vibration measurements on rotating machinery. The paper provides good background for the algorithms, and tests the performance of

its hybrid feature extraction on simulated signals. A motor drive system is setup that can simulate different fault types, mostly related to REBs but also relating to shaft and gearbox problems. Vibration measurements are processed initially by WPT, primarily for denoising, then by EMD. The resultant IMFs are analysed for statistical features which are input to a backward propagation ANN to determine the condition. The results presented show promise for this hybrid processing, although significant uncertainties remain.

An investigation in [71] employs complex data processing on simulated and experimental data. The method begins with a new wavelet based on kernel local Fisher Discriminant Analysis (FDA), in which the parameters of the wavelet are optimised for performance of the FDA using Particle Swarm Optimisation (PSO). However, this alone does not produce satisfactory classification results. Therefore both the one-against-one and one-against-all techniques are utilised. These map the multi-classification problem to a series of binary problems, each then classified by a SVM. A decision fusion mechanism then merges the SVMs results to finally identify the REB condition. This study analyses an independent experimental data set. The REB faults include 7, 14 and $21\,\mathrm{mm}$ point defects on the inner and outer race and the roller independently. Combined with a healthy bearing condition, this gives ten conditions to classify. Although the classification accuracy of the method is good, very little information on the actual results is reported.

In [81] spectrum images of vibration signals are generated through FFT and processed using two-dimensional PCA to extract the eigen images. Euclid distance discriminance is then used to measure the similarity between known training images and unseen test images. This technique is applied to REB faul diagnostics across a range of operating conditions with two fault sizes on the usual components. Overall, the method achieved classification accuracy of $95.65\,\%$ for the smaller fault size and $99.90\,\%$ for the larger fault size. Although excellent classification is achieved, the method is computationally intensive and relies on accurate training images.

2.2.1.2 Comparisons of Vibration & Acoustic Measurements

There are several studies that compare the performance of measurements from vibration sensors with those of acoustic sensors. Most often, AE transducers that can probe the 0.1 to $\approx 1\,\mathrm{MHz}$ frequency range normally associated with AE. Analysis of fault information in this higher frequency range allows easy

filtering of unwanted mechanical noise that is usually in a much lower audible frequency range, thereby providing improved diagnostic performance.

[82] utilise a Wilcoxan 736T high-frequency accelerometer and a Mistras Physical Acoustics R15 AE transducer to acquire vibration and acoustic measurements from Timken LM490209 cup and LM490238 cone REBs with damaged races (2.54 mm long scratches of varying thickness). The measurements are processed using the High-Frequency Resonance Technique (HFRT) consisting of band-pass filtering of resonance frequencies, demodulation, then low-pass filtering. The signal is then resampled and envelope processed through an adaptive line enhancer. Results revealed that peak ratio was a good indicator of defect presence for both measurements, and provided some correlation with varying defect thicknesses. In contrast to most investigations, the authors found performance of the vibration and acoustic measurements to be comparable. However, little information on the acoustic data acquisition is presented and it is likely that the acoustic data performance could be improved with minor modifications.

A major advantage of acoustic techniques over vibration measurement is shown in [83], where experimental results from REB outer race protrusions are analysed to estimate the defect size. The authors employ a Mistras Physical Acoustics WD piezoelectric transducer (100 to 1000 kHz) and an Endevco Dynamic Instrument Division Model 236 Isobase resonant accelerometer (flat frequency response 0.01 to 8 kHz). Even with no feature extraction processing, the acoustic measurements are able to accurately estimate the defect sizes. The outer race defects include four with fixed width and increasing length, correlating to the measured impact duration of the defects, and three with a fixed length and increasing width, correlating to the measured impact amplitude. However, the vibration results are unable to detect the smaller defects or discern any size information.

[84] continues this investigation with Cooper 01B40MEX split REBs seeded with incrementing defects on the inner and outer race. A Mistras Physical Acoustics WD AE transducer with a frequency response of 100 to 1000 kHz is mounted on the bearing housing and sampled at 8 MHz with 40 dB amplification. The shaft is rotated at 25 and 50 Hz with four different radial loads. Observations of the raw signal are revealing - the relationship between defect size and signal energy is clearly observable, the maximum amplitude for the outer race defects also shows proportionality with defect size. However,

due to the acoustic transmission path, this is not the case for the inner race defects. Although the theoretical results were calculated, the experimental results were quite different mainly due to observable slippage. Overall, the relationship between defect size and the acoustic signal is very strong and acoustic measurements can be used to estimate defect size and track propagation.

[85] compares results from spectral kurtosis analysis of both AE and vibration signals for REB diagnostics. A single thrust SKF51210 REB modified to have a flat race, for accelerated degradation due to increased surface pressure, is rotated at 1500 rpm. The rear of the flat race is equipped with four Mistras Physical Acoustics 100 to 750 kHz AE transducers with 40 dB pre-amplification, sampled at 2 MHz periodically every 3 min. The bearing is axially loaded at 50 kN to accelerate degradation. Both AE and vibration signals are processing using spectral kurtosis and kurtogram, primarily for denoising. Experimental results demonstrated that the acoustic signals were significantly more sensitive to incipient damage, with the vibration signals unable to discern information at this early stage.

2.2.1.3 Low-Speed Bearing Considerations

It is generally agreed that when REBs are operated at low rotational speeds, vibration assessment breaks down, and acoustic methods retain their excellent performance. This is shown in [75] where both vibration and acoustic techniques are compared on a cylindrical SKF NF307 REB, with a separable inner and outer race. The REB inner and outer races are artificially seeded with either spalling or hairline scratching (simulating a crack). The roller is damaged to represent either a small or medium spall. A low speed machinery fault simulation test rig rotates the shaft at either 20 or 80 rpm with a radial load of 5 kN. A Mistras Physical Acoustics R3a AE sensor, with a frequency range of 25 to 530 kHz, and an unspecified accelerometer are sampled by a micro-DSP system at 500 kHz with 18 bit resolution for 10 s recording duration. The authors compare SVM with Relevance Vector Machine (RVM) classification, with various input features attempted. The difficulties with processing larger data sets with frequency domain and time-frequency domain techniques is highlighted causing the authors to employ several variations of component analysis in an effort to improve performance. Unfortunately, the difficulties with selection and configuration of an appropriate kernel led to

poor performance in most cases. However, the results still highlight superior accuracy from the acoustic measurements over those from the vibration sensor.

Similarly in [70] vibration and acoustic measurements are sampled from a large-size REB akin to those used in turn-tables, elevators and cranes. An integrated test rig rotates the bearing at 8 rpm, with the REB equipped with four AE sensors (Valpey-Fisher VP-1093 pinducers) and four accelerometers (three single-axis Kistler8002 and one three-axis Brüel & Kjaer 4504A) sampling at 40 kHz. The authors take care to replicate early stage wear defects by cutting a small groove across the inner race. Feature extraction is by use of EEMD and multi-scale PCA, differing from typical multi-scale PCA which traditionally uses the wavelet transform. The non-stationary and non-linear nature of signals led the authors to think EEMD would perform better. However, with EEMD being extremely computationally intensive, it is unsuitable for any type of continuous real-time monitoring system. Furthermore, it is unlikely that the ensembles would reveal any additional information compared with a regular EMD. There is little comparison made between the acoustic and vibration measurements. These results, and those of previous studies identify a detrimental characteristic of acoustic measurements: the high sampling rates required for AE data combined with the long recording durations required by slow speed REBs, make data acquisition, storage and processing problematic. Consequently, AE data is often analysed in the hit-based or continuous time domain and relatively rarely in the frequency domain.

[86] investigates detection of natural fault formation and propagation in slow-speed REBs. An SKF 51210 thrust REB is modified, replacing its original grooved race with a flat race from an SKF 92320TN of the same size. This allows for accelerated natural crack formation and propagation. A purpose-built test rig rotates the text REB at 72 rpm in a specially designed housing allowing four Mistras Physical Acoustics PICO AE transducers (200 to 750 kHz with 2 MHz sampling) to be mounted directly to the race. The authors employ several feature extraction techniques, namely information entropy, shape factor, envelope analysis, FFT, and CWT amongst others. The CWT proved extremely adept at detecting the defect in its earlier stages of formation. Additionally, the acoustic wave velocity in the REB material allow the four AE sensors to provide accurate and pronounced radial localisation of the

defect. Further, the size of the naturally formed defect is accurately estimated from the duration of the AE impact feature given the known rotational speed. Overall, this investigation provides an excellent demonstration of AE techniques and the additional information that can be extracted from the acoustic signals.

In [87] low-speed 6205-2RS REBs rotating at speeds below 10 Hz are monitored by AE transducers with a frequency response of 125 to 1000 kHz. This method uses heterodyne frequency reduction to reduce the AE sampling rate to that comparable with vibration techniques, around 8 kHz. The reduced sample rate decreases the computational load for feature extraction and further processing. Spectral averaging of the signals is performed and various features based on Shannon entropy are used to distinguish between fault conditions. In this investigation, inner race, outer race, roller element, and cage faults are artificially seeded on the REB for testing. Experimental results show good separation between the different defects for several features, and at lower rotational speeds.

[88] compares vibration and acoustic techniques for low-speed REB fault diagnostics. The authors provide a brief overview of both techniques and a comparative study of published research. They conclude the superior performance of acoustic methods, particularly for low-speed applications, owing to the additional sensitivity and range of AE sensors.

2.2.1.4 Acoustic Measurements

There are numerous investigations into acoustic measurements and the surrounding processing algorithms for feature extraction and classification. [89] supports the earlier detection capabilities of acoustic over vibration measurements even with relatively standard feature extraction in the form of the HFRT. The investigation uses a Mistras Physical Acoustics D9201A AE transducer with band-pass filtering allowing the 20 to 90 kHz range, sampled at 200 kHz. The signal is processed using a short-time overlapping energy and zero-crossing rate, combined with peak finding and frequency comparison. A linear discriminant, gradient-search classifier is used to determine the fault condition. This method was more accurate than the equivalent HFRT and it was realised for continuous real-time monitoring through microprocessor hardware.

The authors of [90] employ an energy indexing technique, where the RMS of a signal segment is compared to the RMS of a larger segment. This ratio is extremely sensitive to the windowing parameters, in this case, the segment ratio is $1\,\%$ with $100\,\%$ representing a single revolution of the shaft. Naturally, smaller segmenting makes the technique more sensitive to local changes, potentially causing false alarms. Coarser segmenting provides more data reduction, but the faults potentially go undetected. A Cooper 01B40MEX separable REB is seeded with an outer race defect 0.85 by $0.85\,\mathrm{mm}$ and data is recorded for different rotational speeds. The energy index ratio is raised to the power 10 for amplification of the fault features. Although reasonable detection results and limited time localisation are achieved, this method is susceptible to many external variables that could easily degrade its performance. Results may also be improved by comparing ratios of other time domain statistical values such as kurtosis.

[91] presents REB diagnostics through analysis of AE signals for cyclostationarity. This occurs when statistical features of the signal exhibit periodicity. An experimental test uses two split Copper 01B40MEX REBs rotated at $25\,\mathrm{Hz}$. AE signals are acquired from Mistras Physical Acoustics WD transducer, with a 100 to $1000\,\mathrm{kHz}$ frequency response, fitted to the top of the REB housing. The raw signal is amplified at $40\,\mathrm{dB}$ and sampled at $8\,\mathrm{MHz}$. Envelope analysis is compared with spectral correlation and integrated spectral correlation, with the latter delivering the best diagnostic performance on outer race defects. In contrast, diagnostics of the inner race proved challenging for this method, especially for smaller sizes.

[92] investigates a single-row deep-groove SKF 6205 REB exhibiting a spall on the outer race, inner race, roller and a combination of these. Three AE transducers are sampled at $5\,\mathrm{kHz}$ for $5\,\mathrm{s}$ duration using an OROS 3 acoustic analyser with NVGATE software. The HHT is used for feature extraction with a series of statistical parameters including crest factor, kurtosis, shape factor, ringdown count and signal energy, are input into a k-NN classifier. The authors used the Waikato Environment for Knowledge Analysis to determine k-NN as the best performing classifier. Classification accuracy of $\approx 96\,\%$ is achieved across a substantial data set.

In [34] a Mistras Physical Acoustics Nano-30 AE transducer, with a frequency response of 125 to $750\,\mathrm{kHz}$, is sampled at 0.5 or $2\,\mathrm{MHz}$ for a duration of $3\,\mathrm{s}$. The sensor collects data from a Timken 09074 tapered REB with the separable

outer race engraved to represent a typical defect. Ten repeated trials at shaft speeds of either 5 or ≈18 Hz with and without a radial 100 N load are averaged for each operating case. The authors initially use the CWT, testing a series of different mother wavelets. The wavelet with the highest kurtosis to Shannon-entropy ratio is deemed to give the best performance. The WPT with the corresponding mother wavelet is used to decompose the AE signals into three frequency bands. The Hilbert transform calculates the envelope and the band with the highest kurtosis to Shannon-entropy ratio is selected as an optimal band-pass filter. The passed frequencies are then denoised with adaptive thresholding. The envelope spectrum (Hilbert transform and FFT, multi-scaled for better frequency resolution), can then diagnose the characteristic fault frequencies. The kurtosis to Shannon-entropy is established as the optimal quantitative performance measure based on early comparative testing of various statistical and information features using Plackett-Burman Experimental Design. Experimental results demonstrate that the amplitude of the fault signature increases in relation to the higher radial load and that the shaft speed relates to the frequency band in which the fault signature is present, with higher speeds increasing the fault frequency. The lower sampling rate and shorter duration data is used to establish the excellent performance of the method. The remaining faster sampled data is used to investigate whether the defect size can be estimated accurately. Two different defect sizes are tested; scratches across the outer race with a fixed depth of 0.5 mm and widths of 1 or 2 mm. The results revealed that the defect size estimation is not sensitive to changes in load or shaft speed, and the method performed well with a 10 % error between the theoretical and experimentally derived values, mostly attributable to the assumption of no slippage.

Worthy of note, [19] investigates the feasibility for acoustic detection of early stage REB faults on trains as they pass measurement equipment. This involves minimising the Doppler effect using an array of microphones to create a targeted listening beam. Envelope analysis via the Hilbert transform identifies impact events and FFT reveals the characteristic fault frequencies. Initial laboratory experiments use a test rig and a FAG 801023AB automotive tapered REB with incremental stages of spalling on the outer race and roller. Results demonstrate that smaller defects require faster rotation speeds to achieve better detection. A real-world implementation on a railway track monitors a train equipped with a 10 to 12 kHz sine wave generator. The authors

found that a linear microphone array reduced background noise compared to a spiral array. The test signal is successfully detected and further work is needed to investigate whether real REB defects can be detected in a real-world environment.

2.2.2 Electrical Machines

Induction motors are widely used in many industrial systems, often providing system critical services. Although most devices are robust and provide excellent performance, failures still occur primarily due to damage of the REB, stator or rotor. Diagnostic techniques for induction motors still include vibration and acoustic measurements, but Motor Current Signature Analysis (MCSA) is also commonly used. MCSA can be used to diagnose REB defects as discussed above, where the REB typically supports a shaft. In this section, most considered cases are referring to the REBs that are internal to the motor. Continuing from the previous work on REBs, the following investigations discussed typically include diagnostics of REB faults and additional fault mechanisms associated with induction motors, most commonly broken rotor bars and shorted windings.

[93] compares stator current, vibration and acoustic diagnostic techniques on broken rotor bars and various REB defects under varied operating conditions. A smoothed pseudo Vigner-Ville distribution is employed for time-frequency analysis with comparable resolutions to wavelet techniques. A two-pole three-phase $2.24\,\mathrm{kW}$ induction motor is monitored by a Hall effect current transducer, two single-axis accelerometers (radial and axial), and a microphone (that is remote from the system $\approx 15\,\mathrm{cm}$ away). Data is sampled at $1\,\mathrm{kHz}$ for $20\,\mathrm{s}$ duration with ten repeated trials for different combinations of speed and load operating conditions. The results showed that the acoustic measurements performed better in the lower-frequency band for detection of the REB faults. The current analysis provided more accurate diagnosis of the broken rotor bar. However, the acoustic method could be improved through better experimental setup and signal processing.

[94] realises oscilloscope-based, real-time acoustic signature processing of a chemical plant motor using contact-mounted acoustic sensors, similar in principle to traditional vibration monitoring. The results show good detection properties, albeit with the research predicated on sensor positioning rather

than real-time remote detection of faults.

[95] investigates diagnostics for broken rotor bars in 0.5 kW induction motors and shorted rotor coils in 13 kW DC motors using acoustic measurements from an Olympus WS 200S consumer-grade voice recorder. The digital sensor samples single-channel 16 bit audio at 44.1 kHz. The Multiple Signal Classification (MUSIC) algorithm estimates the frequency content of the signals using an eigenspace method. Additionally, the authors employ further processing in the form of a combination of linear predictive coding, reflection coefficients and log area ratio coefficients. The processed features along with those from the MUSIC method are input into two different classifiers, Bayes and nearest neighbour. Results showed the nearest neighbour classifier to have slightly better efficiency for the same training and test data, and that good diagnostic performance is achieved with the consumer-grade acoustic microphones.

[96] diagnoses shorted stator coils on a synchronous motor using measurements from an Olympus TP7 consumer-grade microphone at 44.1 kHz. In this case, the line spectral frequency technique is used to create ten feature vectors which are input into a k-NN classifier that clusters them according to their Minkowski distance. The motor is operated at 25 Hz rotational speed in open-loop control i.e. with no feedback loop. Diagnostic accuracy of 100 % is achieved for three coefficients from the line spectral frequency technique, and more coefficients caused the diagnostic performance to degrade.

[97] diagnoses stator inter-turn faults, dynamic eccentricity problems and a hybrid combination of these. The experimental setup employs a BLDC motor drive system, monitored in real-time using an oscilloscope FFT of the input current. The frequency analysis is compared against simulation results from a finite element model, showing excellent agreement of the fundamental fault frequencies. Combinations of different speed and load configurations are tested to ensure robust performance of the method. This investigation demonstrates the commercial requirement for real-time fault detection, delivering near instant operator feedback.

In [98], [99] differential diagnoses between several REB defects is investigated. Specifically, shorted coils of auxiliary and main windings, broken rotor bars, and broken squirrel-cage ring on a single-phase induction motor using acoustic measurements from a consumer-grade Zalman ZM-MIC1

microphone. Feature extraction is based on frequency vectors that help form a feature vector of between 1 and 22 frequency components. Training data allows a nearest neighbour, nearest mean and Gaussian mixture classifiers to then match new data to known values. The results showed the nearest mean classifier to perform best in this case. Although the diagnostic performance is satisfactory, the techniques are sensitive to external noise resulting in false alarms.

[100] presents an interesting method to estimate three-phase induction motor torque from acoustic measurements. The authors utilise a six-level relational-dilation wavelet transform to preserve frequency resolution in the lower bands. This algorithm performs greater sampling in the time-frequency space than the more traditional wavelet transform and this can be advantageous for transient fault diagnostics. Through analysis of REB cage faults, broken rotor bars and single phasing faults, the estimated torque from the acoustic signals is shown to be very close to the measured torque. This investigation marks another example where useful additional information is derived from acoustic measurements that other sensors cannot provide.

A different approach to detect imbalance and bearing damage on an induction motor is presented in [101] where triple-axis vibration measurements are analysed using a quaternion-based algorithm. This method is very computationally efficient using basic mathematical operations, and not requiring the common space transformations associated with other techniques. The accuracy of this technique is impressive and increases with more samples; with 100 or more samples giving $\approx$100 % accuracy.

In addition to the above, there are a number of reviews in [102]–[107], that discuss diagnostic techniques relating to induction motors. [102] focuses on stator faults, these account for around 37 % of failures. Unfortunately, there is little comparison between different techniques but the authors did identify that machine learning and classification algorithms are key to the future development of smarter diagnostic systems.

In [103] fairly comprehensive information on different fault modes associated with electric motors is provided. The authors show that MCSA is the dominant diagnostic technique used for most fault types and that automated fault detection using expert systems, neural network and fuzzy-logic are growing in the field.

[104] compares induction motor diagnostic methods, categorised into time domain, frequency domain, time-frequency domain and AI-based, and focusing on four fault types viz. REB faults, air-gap eccentricity, broken rotor bar and stator short winding faults. This investigation presents excellent information on fault types, their formation and a clear comparison of different methods in the aforementioned categories. There is little mention of acoustic or vibration methods, and the focus is on electrical measurements of current, voltage and flux. Nevertheless, the authors conclude that easy, low-cost, non-intrusive techniques, able to monitor through non-stationary conditions, is the direction for further development. This very much describes acoustic-based methods.

The review of techniques in [105] concentrates entirely on broken rotor bar faults for induction motors and a brief overview of different processing algorithms is provided for a variety of measurements. The authors identify that acoustic analysis performs well, independent of load variation and supply imbalances, with noise contamination from the surroundings being the only significant drawback. However, time-frequency analysis such as HHT and DWT makes acoustic methods much more robust and one of the strongest candidates for early detection of emergent faults.

[106] discusses the use of the wavelet transform on start-up currents for squirrel-cage motors. Four main approaches, viz. scalogram, analysis of wavelet ridges, analysis of DWT coefficients and wavelet decomposition, can be used to detect broken rotor bars. The analysis of the start-up current eliminates many steady-state issues such as varying loads. Further, the harmonics generated during start-up are more easily detected than those in steady state operation.

[107] provides a brief review of various fault diagnostics for traction induction motors, deducing the popularity and effectiveness of MCSA and highlighting future direction of time-frequency feature extraction and AI decision making.

2.2.3 Gearboxes

The gearbox is typically purely mechanical and a critical component for most rotating machinery, and makes an ideal subject for acoustic diagnostic techniques. Similarly to induction motors, gearboxes nearly always contain

REBs which account for around two thirds of gearbox failures, the remaining third is almost entirely made up of gear failures. This section concentrates on gear fault diagnostics since REB diagnostics have been discussed above in Section 2.2.1 Roller Element Bearings. Many types of gearbox are used in industry but the majority of the causes and failures are common across all types; including tooth wear, fatigue, corrosion, cracking, pitting, particle ingress and improper or lack of lubrication. Early diagnostic techniques were typically vibration-based, analysing averaged changes over time. Whilst good detection rates are achievable, very little additional information such as locality or severity is obtainable. Therefore, commensurate with other diagnostic systems, time-frequency analysis is now emerging as the preferred choice.

[108] compares the effectiveness of acoustic and vibration signals for gear fault diagnostics through Wigner-Ville distribution. The study uses a Brüel & Kjaer microphone system and an accelerometer synchronised at 6.4 kHz from a two stage helical gearbox with the pinion gear exhibiting various stages of gear cracking, tooth wear and finally a broken tooth. Using a smoothed pseudo-Wigner-Ville distribution to minimise interference terms and reduce noise, vibration and acoustic detection of tooth wear and broken tooth are comparable, but the acoustic signal is able to detect gear cracking at a much earlier stage in its development. In this case, the faults are artificially seeded, resulting in a lack of data for fault formation. Continuous real-time acoustic monitoring would likely be able to detect tooth cracks as they form. This study also highlights the advantages of the wavelet transform, which is believed to outperform the smoothed pseudo-Wigner-Ville distribution in detecting small transient events, although it was not adopted in this case.

Continuing this study, [109] compared Morlet, Mexican-hat and the Gabor-based wavelet transforms to attain better time-frequency localisation, finding that this feature extraction method provides detection at earlier stages of fault development compared with the Wigner-Ville distribution and instantaneous power spectrum. The variable window sizes of wavelets also makes this technique more computationally efficient. However, to achieve satisfactory performance the optimal selection of the mother wavelet is essential. In this case, the Gabor-based wavelet proved most effective with good results also being achieved by the Morlet wavelet. Further, when analysing airborne acoustic measurements the distance of the microphone

from the source is shown to be critical to good performance. In the reported case, the optimum distance was 5 cm with the microphone likely being saturated when placed too close, and with external noise becoming more prominent and valuable fault information being attenuated at greater distances. Despite adding additional environmental noise to the experimental setup, it is demonstrated that with appropriate processing, the fault information can still be extracted and good diagnostic performance achieved. The authors also highlight the advantages of acoustic sensors over those of vibration; primarily being remote from the workpiece gives freedom of positioning with small changes to the microphone not affecting the performance, where small changes to the accelerometer positions has a large detrimental impact on the information attained.

In [110] AE and vibration measurements are compared for diagnostic performance on seeded damage to helical gears. The helical gears are rotated at 690 rpm with a Mistras Physical Acoustics differential AE sensor attached. The sensor has a flat frequency response of 100 to 1000 kHz sampled at 10 MHz, connected via slip ring. An Endevco Isobase 236 accelerometer, with 10 to 8000 Hz frequency response, is mounted to the bearing pedestal. Results show a clear relationship between AE RMS and the volume of removed material from the gear tooth. The acoustic measurements are also more sensitive to the defects than the vibration measurements.

Similarly, [111] compares AE and vibration signals for crack detection in gear teeth. The vibration sensors comprise of two Brüel & Kjaer accelerometers mounted on two axes of the casing and sampled at 50 kHz for 1 s. The acoustic sensors are three wide-band Mistras Physical Acoustics AE transducers (100 to 800 kHz frequency response) sampled at 2 MHz for 100 ms, one mounted on the output shaft, the second on output shaft bearing casing, and the third in friction contact with the input rotating gear using a specially designed mount. The test rig is a single-stage with two gears (25 and 53 teeth) exhibiting artificial tooth cracking over a relatively long-term trial allowing the fault propagation to be observed. The trial duration revealed the feature changes due to rising oil temperature which reduces the oil film thickness between the meshing gears, resulting in increasing vibration and acoustic features. The authors compare a wide range of time, frequency and time-frequency features, with DWT detail features proving extremely effective. Results show that the acoustic performance was far superior to the vibration. The AE features exhibit

regionally linear behaviour with gradient changes indicating propagation of the crack. The vibration measurements were unable to identify the early and middle stage fault conditions.

The authors of [112] employ two wide-band AE transducers sampled at 500 kHz (frequency chosen based on pencil lead break test - giving best signal to noise ratio) to measure AE from a split-torque gearbox. EMD decomposes the AE signal into IMFs and a threshold-based denoising technique is applied to each one. The IMFs are then added to form a new signal and six parameters are extracted as the fault features, viz. ring-down count, duration, peak amplitude, rise time, RMS, and crest factor. These are compressed into a single feature by comparing the Mahalanobis distance between healthy and unhealthy states, with unhealthy states exhibiting a larger value. A statistical method based on Chebyshev's inequality is used to calculate a detection threshold. This technique is shown to be highly effective with better sensitivity than previously reported EMD methods.

2.2.4 Additional Applications

Acoustic measurements have been used for diagnostics and condition assessment in many different applications. This section discusses the other mechanical fault modes that have been investigated by researchers. The use of gearboxes in offshore wind turbines accounts for a lot of research interest into their remote monitoring. In [113] an alternative use of acoustic measurements for wind turbines is presented. This investigation is to determine whether additional weight on a wind turbine blade can be detected. A blade of a small test turbine is loaded with four incremental weights to represent issues such as blade icing. A pressure sensitive Brüel & Kjaer 40AF free-field microphone is placed $\approx$1.1 m upwind of the turbine and is sampled at 48 kHz, 16 bit resolution for $\approx$10 s durations. Two features are extracted from the data viz. the spectral magnitude of the rotation speed and the frequency variation of the rotation speed are input into a fuzzy-logic interference classifier, trained on two thirds of the data and tested with the remaining third. Results accurately predict the weight added to the turbine blade, although significant erroneous results are present which is damaging to the integrity of this method. The experimental setup could be significantly improved with better positioning of the acoustic sensor and more precise testing. Nevertheless, it demonstrates an excellent potential application for acoustic monitoring.

[114] analyses the effectiveness of using AE to detect tool and workpiece malfunctions in milling operations. A Kistler 8152A (50 to 400 kHz) AE transducer is fixed directly on the workpiece, sampled at 800 kHz. The AE measurements clearly identify when the cutting edges are in contact with the workpiece, evident by the saw-tooth like waveform. A STFT of the signals reveals the target frequency band and the amplitudes are compared for different known states of tool wear. It is demonstrated that the amplitude can be used to provide an accurate estimation of the tool wear.

Further wear detection and monitoring is investigated in [115], where AE signals from two martensitic plates in friction contact are measured. A STFT, signal energy and CWT combination, performs feature extraction, revealing changing frequency components relating to the wear amount. Three wear states are identified from the results; run-in, permanent-wear, and wear-out (prior to failure). The data is acquired using an FPGA board, although it is unclear whether this is used to implement the signal processing.

To date, consumer-grade sensors have been used largely for urban noise mapping and voice monitoring for medical and speech recognition purposes, although extensions to system monitoring have been previously reported by [116]–[118]. In such investigations, the consumer-grade sensors found in smartphones and tablets, are combined with purpose built diagnostic applications on various platforms, to record and process all in a single device, providing diagnostics for a reciprocating air compressor by detecting leakage from either the inlet or outlet valves. The compressor is driven by a 1.5 kW motor and has a pressure range up to 10 bar. These investigations provide a good description of the application development but the information on the exact signal processing is unclear. The applications record data and perform some basic filtering for de-noising. A large number of features (286) are then extracted in the time and frequency domains using wavelet transforms. These features are then analysed using PCA or statistical analysis to determine which are most appropriate for use. The selected features are then input to a SVM or z-score measure for classification. Significant supervised training is required in all cases, and issues where the entire data set is corrupt or provides erroneous results are discussed. These therefore mark some of the early investigations into using smartphone type devices for condition assessment of industrial machines. However, the focus on the application and operating systems leaves significant areas for further research and development.

For a similar application to that discussed previously, [119] uses AE measurements to detect leaking from plastic water pipes. In this investigation, long-term data is analysed using STFT to determine an optimum mother wavelet for real-time leak detection using the wavelet transform. The authors use visual analysis to determine the optimum mother wavelet. In this case, detection of a leak might be better served using a comparison in the frequency domain, as a leak would represent a continuous fault mode rather than a transient, making resolution in the time domain of minor importance.

[120] presents vibration signal denoising for a jet engine compressor using a variety of DWT and thresholding denoising combinations evaluated for the best signal to noise ratio, percentage RMS difference, cross-correlation and mean square error. It was demonstrated that the dmey mother wavelet and the Rigorous Stein's Unbiased Risk Estimate (SURE) thresholding delivered the best performance out of those tested. However, it should be noted that this experiment was undertaken with a real world noisy signal and so the actual denoising performance of the algorithm is better proven on simulated signals. Furthermore, the work focuses on the denoising performance rather than fault detection accuracy.

[121] demonstrates the use of AE to detect natural crack formation and propagation in slow speed shafts whilst in operation. The test rig uses two Physical Acoustics WD AE transducers (200 to 750 kHz) mounted to an overhanging REB housing which is used to apply load to the shaft. Results showed that a higher load caused crack formation earlier but its propagation causing failure was of a similar time to the low-loaded shaft. There is a clear observable correlation between the AE energy, crack propagation and formation of shaft defects. In a similar effort to detect crack formation, Mistras Physical Acoustics, the manufacturer of many AE transducers used in research, developed the Acoustic Combustion Turbine Monitoring System (ACTMS) Figure 2.13. This commercial product is an AE monitoring system designed to detect crack formation in stator blades of large General Electrical utility gas turbines. The system uses a conical array of microphones magnetically mounted to the compressor casing at the early stages to provide localisation information. By recognising multiple AE events in a localised area, the ACTMS generates warnings and alarms to notify turbine operators of the potentially damaged blade location [122].

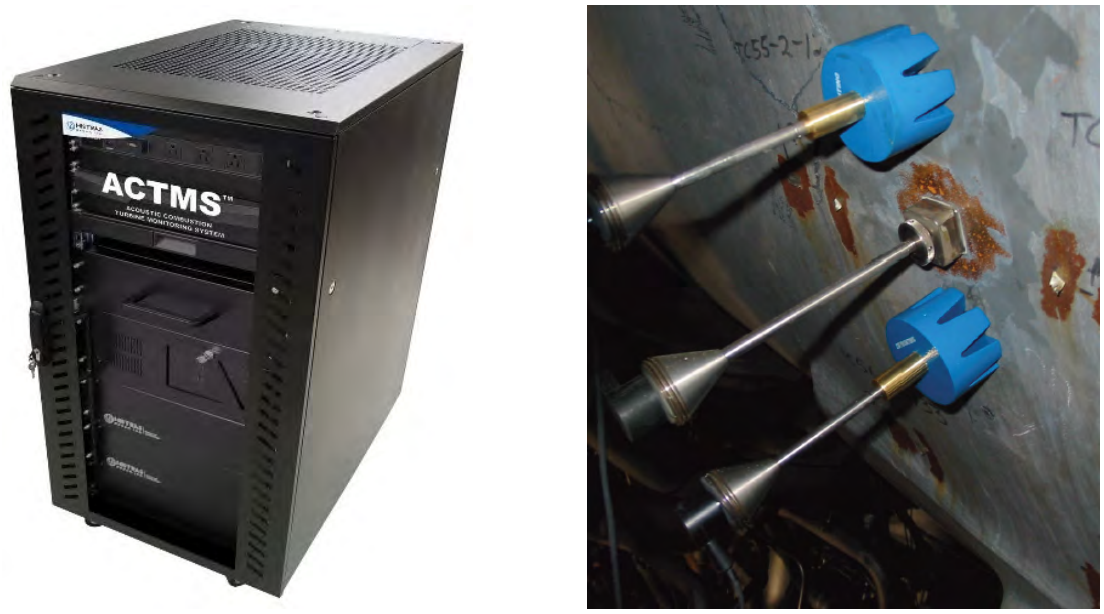

(a) Mistras ACTMS Processing Unit (b) ACTMS Acoustic Sensors

Figure 2.13: The Mistras ACTMS [122].

Another investigation in [123] examines the use of AE and vibration measurements to detect damage in aluminium plates. This work is of particular interest due to the use of a smartphone for data analysis. The experiment uses two aluminium plates (150 mm by 400 mm by 2 mm), with one of plates fatigued to introduce a 73 mm crack near the centre. The plate is excited using an ultrasonic transducer at 40 kHz and the response signal is demodulated for analysis. Additional excitation is provided by the smartphone as a square audio wave at 230 and 327 Hz, driving the generating transducer. Frequency analysis of the response signals show clear frequency differences between the healthy and cracked plates. In this experiment, the smartphone is used to provide a control interface, capture and store data from the data acquisition module and analyse the data providing plate condition information. The acoustic microphone built into the smartphone is not used and a separate data acquisition system is employed for sampling specialist sensors and wirelessly transmitting the data to the smartphone.

[124] reviews condition monitoring for industrial systems specifically; rotating machinery, cutting tools and robots, and also machine learning techniques and embedded monitoring systems. Acoustic and vibration measurements feature heavily, and the paper provides a good overview of these areas.

2.2.5 Summary

The previously described research, provides a comprehensive overview of current acoustic fault detection and monitoring methods for mechanical fault modes. Several key trends and important themes can be identified:

1. Acoustic sensors, that are setup correctly, will typically provide signals that contain more extractable information than vibration measurements. Notably, the ability to; detect a defect at an earlier stage in its formation, estimate the size of a defect, and extract localisation information.

2. Acoustic sensors are either consumer-grade and record in the audible frequency range (20 to 20 000 Hz), or are classed as AE transducers, recording a much higher frequency range, typically between 100 to 1000 kHz. The AE sensors provide a better signal as they are surface mounted to the component. Therefore, the acoustic waves generated by faults are not attenuated by surrounding air and do not suffer the noise contamination from their environment as remote consumer sensors. The high frequency signal allows tiny acoustic features, such as crack formation and small mechanical impacts, to be readily detected, but at the expense of being remote from the workpiece. Acoustic sensors, unlike vibration accelerometers, are not dependent on their positioning relative to the axis of vibration, and multiple sensors are not required.

3. The vast majority of research into acoustic monitoring has used specialist, research-grade AE transducers that require pre-amplification, specialist cabling and ADC equipment. These sensor systems are costly and can yield poor results if not setup correctly. Although limited use of consumer-grade sensors is reported, this area remains underdeveloped.

4. Most of the investigations do not demonstrate an industry-ready system with real-time continuous monitoring.

5. Continuing from Item 4, in almost all cases, the defect studied is created artificially through human intervention as part of the research investigation. This has the disadvantage of only providing data in the extreme healthy and unhealthy states. Moreover, to create the defect, the system must be shutdown and disassembled, preventing continuous real-time monitoring and also introducing differences in the reassembly and operational conditions that may effect the results.

6. A plethora of feature extraction techniques and algorithms are available but the literature has clearly identified that analysis in the time-frequency domain will produce the best diagnostic performance for periodic transient, impulse-like events. Wavelet analysis is particularly well-suited and is employed in many of the reported investigations with clear advantages over many other techniques. However, optimal selection of the mother wavelet is critical to achieving good performance with this method.

7. The final trend is the ever increasing use of AI decision making and machine learning classification algorithms. These intelligent systems can greatly increase the accuracy and scope of the diagnostic system when provided with good features and known states for training. The main disadvantage with these algorithms is the requirement for training data with known physical conditions, which is often difficult to attain. A key area for development is for novelty detection algorithms where new features can be identified and trained into the model during operation, which in the long-term would provide a more stable system for a given situation.

2.3 Electrical Fault Modes

Research into the use of acoustic measurements for fault diagnostics is naturally heavily biased towards mechanical fault modes as the generation of the acoustic waveforms is generally well understood. However, there has been little to no research into the suitability of acoustic techniques for electrical fault mode diagnostics. Despite several investigations into faults, such as broken rotor bars and shorted windings in induction motors, under the pretext of an electrical fault mode, the failure mechanism is still physical damage to the component, i.e. mechanical in nature. This is almost always artificially created through human intervention, when the system is shutdown and disassembled, as part of the research exercise. Thus, only data in the extreme healthy and unhealthy conditions can be gathered, and continuous real-time monitoring of fault formation and propagation is prevented. This section provides additional detail and examples of electrical measurements for diagnostic purposes, and discusses the nature of electrical fault modes and best diagnostic practices.

2.3.1 Electrical Diagnostic Techniques

Section 2.2.2 provides some insight into induction motor fault diagnostics by way of acoustic and vibration measurements, briefly touching on MCSA. Further information on fault diagnostic techniques is provided in [125] which examines many approaches categorised by rotor, stator, mechanical faults, permanent magnet synchronous machines, and power components and converters. MCSA is one of the most widely used electrical diagnostic techniques but there are many others. This subsection will discuss these techniques in more detail before continuing with the discussion of other electrical fault modes.

MCSA is a well-established technique that can be used to detect a wide-range of motor faults. In its simplest form, MCSA involves frequency spectrum analysis of the motor drive currents through FFT. Faults such as REB defects become detectable as the damage results in changes to the air gap eccentricity, thus becoming visible in the current spectrum. In this form, MCSA is not suited for diagnostics of transient events or fault signatures that do not produce obvious changes in the frequency spectrum. To address this issue, many authors employ time-frequency analysis in place of FFT, most commonly a variation of the wavelet transform. [126] compares the DWT and CWT to analyse motor stator currents measured using Hall effect current transducers. An initial FFT spectrogram shows the formation of frequency side bands, characteristic of outer race REB faults. Results from the CWT also show REB damage through wavelet scalogram, which outperformed the DWT owing to the additional scale fidelity.

Similarly in [106] a broken rotor bar is detected through transient MCSA realised through CWT and DWT of the start-up motor currents for a squirrel-cage induction motor. Typically, a FFT enables detection of side-band harmonics. However spectral leakage, low-load and low-slip conditions, and erroneous diagnostics can cause similar side-bands. To address these issues, the stator current can be analysed over rapidly changing conditions, such as during start-up. This is typically referred to as transient MCSA, not to be confused with MCSA during steady-state operation utilising time-frequency feature extraction. Analysis of the start-up current provides larger side-band harmonics, regardless of loading conditions, making the broken bar fault more evident. As the slip changes, the side-band harmonics change proportionally, providing a pattern over time which allows the broken bar fault to be

distinguished from other faults. Discussion of the CWT and DWT reveals that the CWT provides better resolution of the side-band harmonics evolution. However, it does incur significant computational resources and time. The DWT proves to be a more efficient technique in this case, providing sufficient resolution with far less computational overhead.

Another example is given in [127] where stator currents are analysed using a four-band Finite Impulse Response (FIR) filtering via WPT to detect broken rotor bar fault. The four-band analysis reduces the number of required multiplications by almost half compared against traditional half-band WPT. A three-phase $\approx$750 W four-pole motor is rotated at 29 Hz at full-load. Broken rotor bars are simulated by drilling holes at both ends of the bar. Testing is performed on a single broken bar and then with two broken bars. The stator phase current is decomposed into 15 Hz frequency bands using four-band FIR filtering. The resulting node of interest, exhibits substantial increases in overall energy relating to the broken rotor bars, commensurate with the theoretical side-band frequencies. However, the accuracy of this method deteriorates under light or no-load conditions.

In [128] air gap eccentricity is simulated in a fractional-slot concentrated winding permanent magnet synchronous machine. The air gap, between one tooth and stator yoke, is modelled using both the finite element and permanence network methods. Back electromotive force measurements at no load are measured from an 18 slot, 16 pole machine, modified to simulate the fault. Results show that this type of fault can cause poor performance for many diagnostic techniques, specifically those based on second order harmonics tracking. Therefore modelling requires the tolerance deviations to be included.

High-frequency injection operates on the same principle as sensorless motor control, where the saliency is used to estimate rotor position by superimposing a low-magnitude, high-frequency sinusoidal signal on the excitation voltage and measuring the high-frequency modulation changes. By profiling these healthy and unhealthy states, such signatures can be used to detect faults in the windings or elsewhere in the electromagnetic circuit [129]–[131]. This technique has many advantages over traditional MCSA for detecting emerging faults in the stator windings which do not produce significant changes in the frequency spectrum for MCSA to detect. Moreover, changes to the harmonic components caused by these faults are often hidden, because changes in

loading conditions can produce the same result. An example case is given in [129] where a six-pole 3.82 kW permanent magnet machine is powered through PWM at 10 kHz. The injection voltage amplitude is 10 V at 1 kHz frequency. The saliency results validate the accuracy of this technique with clearly marked differences between healthy and faulty states. Faults in the stator windings such as short-circuits and incipient short-circuits are readily distinguished within a single turn. This method has the added advantage that it does not require any additional transducers.

2.3.2 Electrical Fault Mode Examples

The above literature shows that these diagnostic techniques are primarily designed to detect faults present due to a physical degradation in the component integrity. Whilst this damage may result in electrical disruption, ultimately the failure mechanism remains mechanical in nature. Faults of a pure electrical origin are extremely difficult to classify, and there is little to no literature defining or addressing faults of this type. Therefore, this work refers to electrical faults as: those which do not result from physical changes to the component, typically caused by problems with power conversion, supply, or the control system, and possibly arising from sensor, software or design issues.

2.3.3 Summary

The previous sections have provided a comprehensive overview of various electrically-biased diagnostic techniques, primarily designed for induction machines and generators. Discussion on the nature of mechanical and electrical fault modes is provided, and the main findings are as follows:

1. Electrical fault modes in this work are differentiated from mechanical fault modes. Mechanical fault modes are to include faults that are caused by physical changes to component integrity, even if these are the cause of electrical disruption, for example broken rotor bars or short circuits in induction motors. Electrical fault modes are to include faults that result from problems with power conversion or supply or the control system and software, for example a current instability caused by non-linear interaction with a PWM-controller.

2. To date, there is little to no literature that address fault diagnostics for

electrical fault modes, particularly when considering the use of acoustic measurements.

3. The electrically-based diagnostic techniques are effective and have been adopted for use in industry. However, they require specialist expertise to setup and interpret the results. They would also be difficult to retro-fit to already established systems.

4. The electrical diagnostic techniques are not susceptible to noise contamination in the same way as acoustic measurements. However, electrical measurements may be compromised by electrical noise from erroneous sources, which may cause misinterpretation. Diagnostic performance and result interpretation can also be hindered by varying operational conditions, in particular, changes in the driven load.

5. The requirement for advanced classification and machine learning techniques is not as prevalent as with other measurements. The reason behind this is two-fold; the investigation of a singular fault, and the lack of noise contamination from other sources.

Chapter 3

Consumer-Grade Acoustic Sensor Diagnostics for Roller Element Bearings

Summary: The use of acoustic measurements for fault diagnostics remains in its relative infancy in terms of industry adoption. Acoustic fault diagnostics is traditionally associated with mechanical fault modes and has the potential to vastly outperform or augment more established measurements such as vibration. Roller Element Bearings (REBs) are a crucial component in nearly all rotating machinery, their failure is responsible for around half of all rotating machine failures making early fault identification a priority. Very often, acoustic diagnostic systems employ a specialist research-grade acoustic transducer, surface-mounted to the component under test. This chapter presents a suitability investigation, comparing measurements from two consumer-grade acoustic sensors and a vibration accelerometer, for diagnostic performance on REBs. Six REBs are tested, each exhibiting a different condition; healthy, heavily worn, or with a number of specific point defects on different components within the REB. A simple diagnostic method is employed, extracting signatures from the frequency spectrum for each REB by training a Support Vector Machine (SVM) classifier for each motor operating condition. Results from experimental trials are commensurate with the literature already discussed. The acoustic sensors deliver superior classification performance over the vibration, particularly at slower speed and lower radial load. These consumer-grade sensors are easy to setup and operate, and can be easily transferred to other applications. They could be readily adopted by industry and quickly implemented to solve a wide range of audible fault diagnostic and monitoring applications.

3.1 Introduction

REBs are critical components for nearly all rotating machinery. Early stage defects emerge and propagate into more serious faults, eventually causing catastrophic failure without maintenance. REBs are responsible for around half of all rotating machine failures [33], making early diagnosis of paramount importance. Conventionally, REBs are monitored by analysis of vibration measurements, requiring multiple accelerometers mounted to the REB housing to detect each axis of movement. It is now widely accepted that acoustic methods have a number of advantages over vibration and typically achieve better performance [83], [84]. Comparisons between both methods and additional research into acoustic methods for REB diagnostics is discussed in Section 2.2.1. In most cases, specialist research-grade piezoelectric Acoustic Emission (AE) transducers are employed to monitor ultrasonic acoustic frequencies allowing the acoustic waves, generated by impact of the roller elements with a defect, to be detected. These AE sensors require surface mounting to the REB housing, specialist low-noise cabling, pre-amplification, high sampling rates achieved through research-grade Analogue to Digital Converter (ADC) and expertise to correctly analyse and interpret the signals.

This chapter aims to address the above issue through an investigation into the suitability of readily available consumer-grade acoustic sensors for accurate REB fault diagnostics. These sensors have the following advantages:

- only sensitive to the audible frequency range and can be sampled at much lower sampling rates,
- do not require additional specialist equipment for setup or operation,
- can be positioned independent and remote from the component under test, thereby having no detrimental impact on nominal system integrity and allowing the sensor to be easily maintained with no impact on the system under test,
- and significantly improved cost to benefit ratio.

In addition to publication [1], this suitability investigation is comprised of the literature review presented in Section 2.2 and the following experiment; where six common faults in a REB are diagnosed with comparison between two consumer-grade acoustic sensors and a traditional vibration accelerometer.

A summary of the contributions of this chapter:

1. Introduces and presents a novel technique employing multiple machine learning algorithms to account for dynamic operational parameters.
2. The suitability of consumer grade acoustic sensors and simple feature extraction is proven experimentally for application to mechanical fault modes.
3. The superior performance of the consumer-grade microphone and Wavelet Packet Transform (WPT) feature extraction over the smartphone and Empirical Mode Decomposition (EMD) is demonstrated experimentally.

3.2 Experimental Setup

A Gunt PT501 REB fault simulator is setup; it consists of an electric drive motor, shaft with laser tachometer and REB housing with variable radial load in the horizontal axis via micrometer readout winding screw connected through a rubber shock-absorbing mount. The housing allows for six FAG X-life NU204ETVP2 REBs to be easily interchanged. The six REBs are provided by the manufacturer as teaching & research aids in the following conditions:

A. new healthy condition
B. defect on outer race
C. defect on inner race
D. defect on roller element
E. defect on outer race, inner race and roller element
F. old worn condition

Where possible the defects are shown in Figure 3.1. All the bearings are suitably and uniformly lubricated prior to use.

A single-axis accelerometer, sensitive to frequencies up to 10 kHz, is mounted radially and vertically on the bearing housing. This vibration sensor is sampled at 25 kHz and 8 bit resolution by an OWON VDS3102 USB oscilloscope connected to a laptop running the proprietary software of the oscilloscope. The first consumer-grade acoustic sensor is Samsung Galaxy S7 Edge running Android Voice Recorder allowing mp3 file saves at $160\,\mathrm{kB\,s^{-1}}$.

The smartphone inbuilt microphone is sampled at 44.1 kHz and 8 bit resolution. The smartphone is positioned ≈20 cm away from the REB housing with the sensitive plane aimed directly towards the bearing. However, in order to provide real-world experimental data the smartphone was handheld throughout experimental trials resulting in some variation in positioning, in keeping with practical operation. The second consumer-grade acoustic sensor is an Audio-Technica AT2020 USB+ condenser cardioid microphone. Two microphones are setup equidistant from the REB with their sensitive plane aimed towards the REB. A photograph of the experimental setup is shown in Figure 3.2, note that the smartphone is not present in this image.

Experimental trials are conducted for 24 different operating conditions consisting of combinations of 6 rotational speeds and 4 radial load variations.

Figure 3.1: Photographs of damaged REBs used for experimental trials in this work. From left to right; REB C showing the inner race defect, REB E showing the roller defect and REB F showing wear. Note there was only a single defect on the inner race of REB E compared to the two defects seen above on REB C.

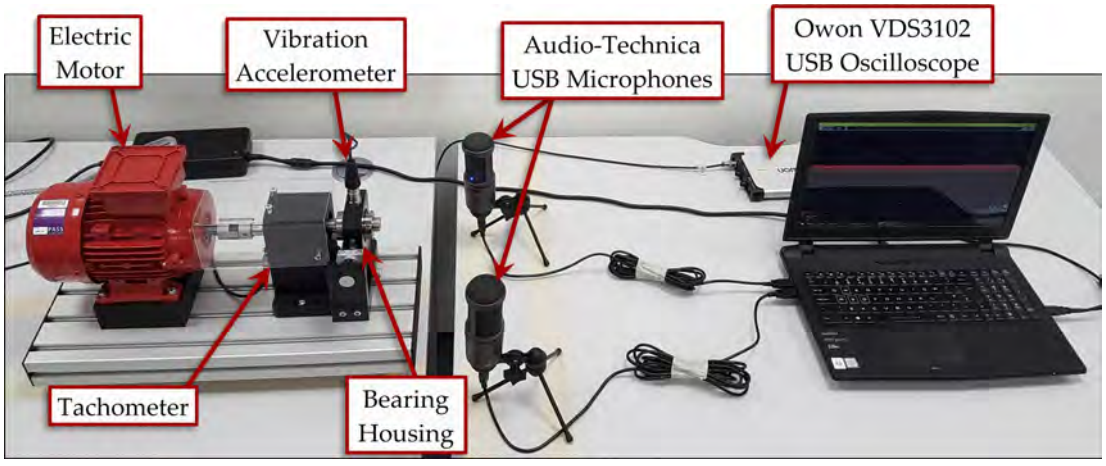

Figure 3.2: Photograph of the REB experimental setup showing; the Gunt PT501, two USB microphones, OWON oscilloscope, and laptop. The smartphone position varied approximately between the two microphones at about the same height as the bearing.

Table 3.1: REB experiment operational parameters.

	Setting	Effective Value
Speed	0	298 rpm
	2	829 rpm
	4	1341 rpm
	6	1865 rpm
	8	2428 rpm
	10	3050 rpm
Load	3 mm	0 N
	4 mm	5 N
	5 mm	18 N
	6 mm	32 N

The speed and load settings and effective values are given in Table 3.1. Note that the given rotation speed is reduced by ≈1 to 2 rpm per increase in load. For each setup configuration, five 10 s data blocks are saved from each of the sensors for analysis.

3.3 Signal Processing

The signal processing consists of a feature extraction algorithm that feeds into a classification algorithm in order to investigate the suitability of consumer-grade sensors and demonstrate a simple and easy to use setup. For this case, only Fast Fourier Transform (FFT) is used to convert the time domain signals into the frequency domain. A SVM is trained to distinguish between the six different REBs. An overview of the signal processing is shown in Figure 3.3.

Before the raw signals can be processed some minor modifications are required. An unfortunate high-amplitude artefact of the signals saved from the smartphone is found at the very start and end of the signal saves, this is likely caused internally by the smartphone software and is only noticeable upon close inspection in Matlab. To ensure these do not affect the results and for uniform data processing, all sensor signals are clipped to a length of 8 s, removing 1 s data from the start and end. The next step is to separate the remaining data into training and testing data sets; from the five experimental

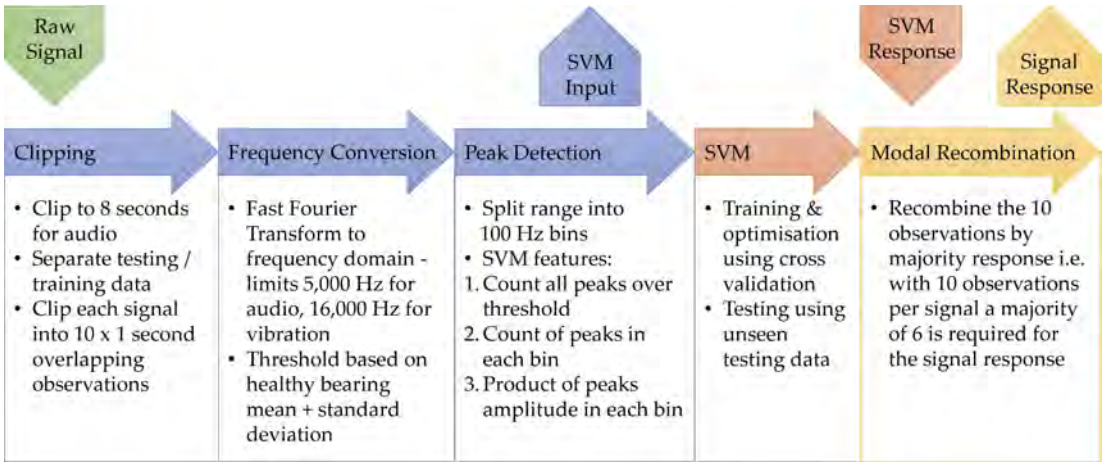

Figure 3.3: Flow diagram of the REB case study signal processing.

trials, the first is used for training and the remaining four are used for testing. Additional observations are generated to facilitate smoother training and operation of the SVM, these are created by clipping each signal into 10 overlapping 1 s observations.

The feature extraction in this case, is intended to demonstrate the potential simplicity of acoustic monitoring, the additional information contained in the acoustic signal over the vibration, and the performance and importance of the machine learning algorithm. Initially, the data is a time domain signal as shown in Figure 3.4. A FFT is employed to convert to the frequency domain with the frequency spectrum shown in Figure 3.5. The frequency spectrum revealed that nearly all the energy was contained below 5 kHz for the acoustic signals and below 16 kHz for the vibration signals. It should be noted that although the vibration sensor is only rated up to 10 kHz some additional frequencies may still be picked up by the sensor. Traditionally when using vibration monitoring, the characteristic fault frequencies become increasingly apparent (visible/detectable) as the defect increases in severity. However, to provide a comparison between the vibration and acoustic signals, a SVM is used to find the signature for each bearing without any *a priori* input using very simple features. The input features for the SVM are developed by separating the frequency spectrum into 100 Hz frequency bins. Considering the frequency content of the signals is expected to be greater for a damaged REB over a healthy REB, a threshold is calculated for each operating condition based on the signals for REB A (the new and healthy bearing). The threshold is set as the frequency mean plus the standard deviation (1σ being optimal). One set of input features for the SVM are the count of the number of peaks

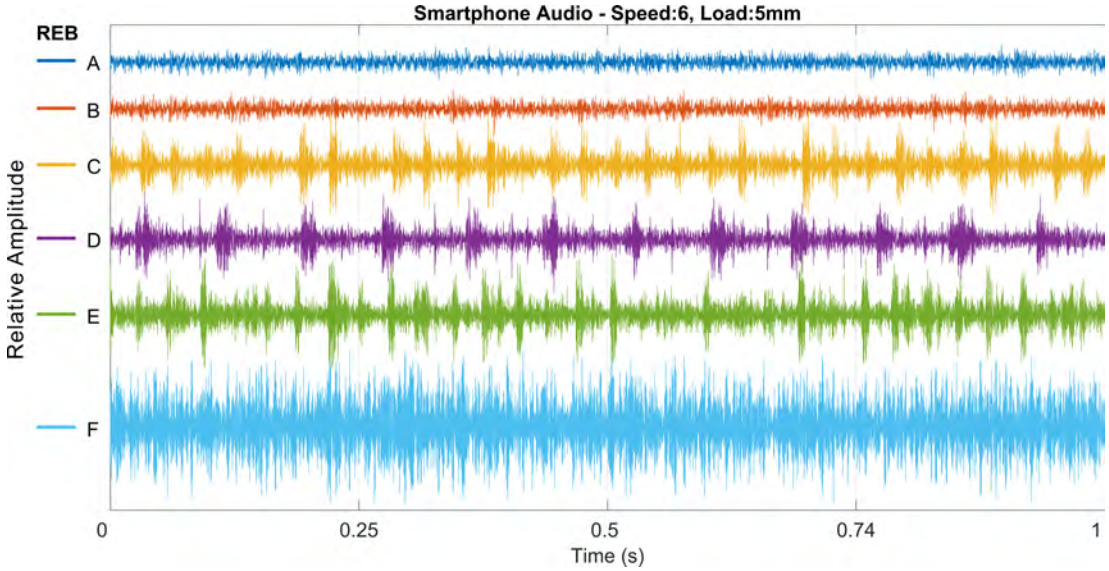

Figure 3.4: Smartphone audio one second time plot for all bearings at speed 6 and load 5. The defect impacts are visible as periodic amplitude spikes, particularly for D, the roller defect.

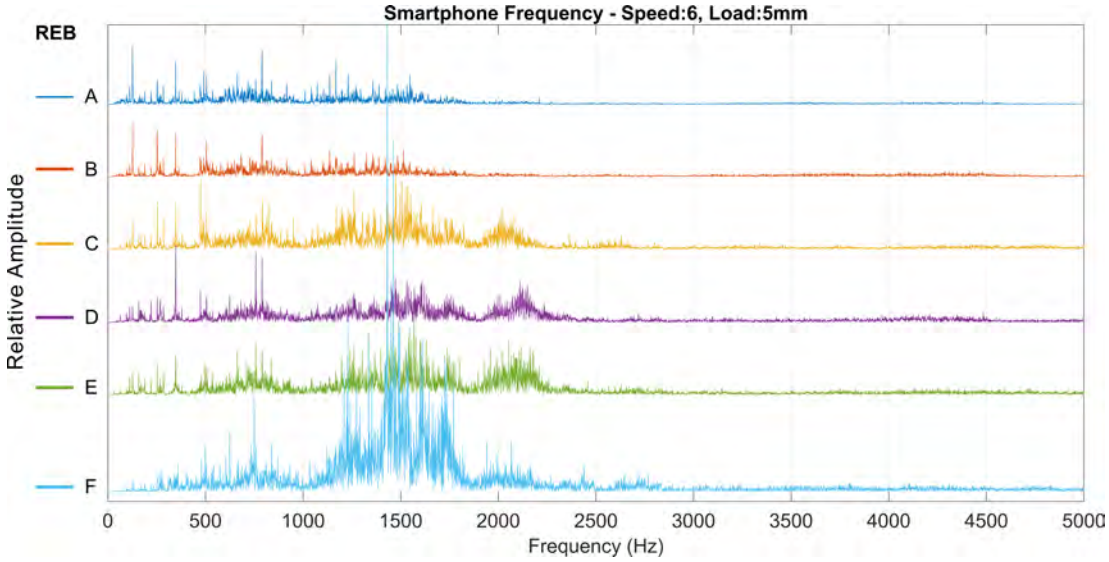

Figure 3.5: Smartphone frequency plot for all bearings. Note the differences from that of bearing A are primarily related to the defects present and characterise the fault frequencies in the audio frequency spectrum. However, there will also be small differences caused by tiny changes in operating conditions, setup, etc.

above the threshold for each bin and also over the whole frequency spectrum. Another input feature is the product of the amplitudes of all the peaks over the threshold for each bin. The dividing bins, the mean of the frequency content, and the peaks above the threshold are shown in Figure 3.6.

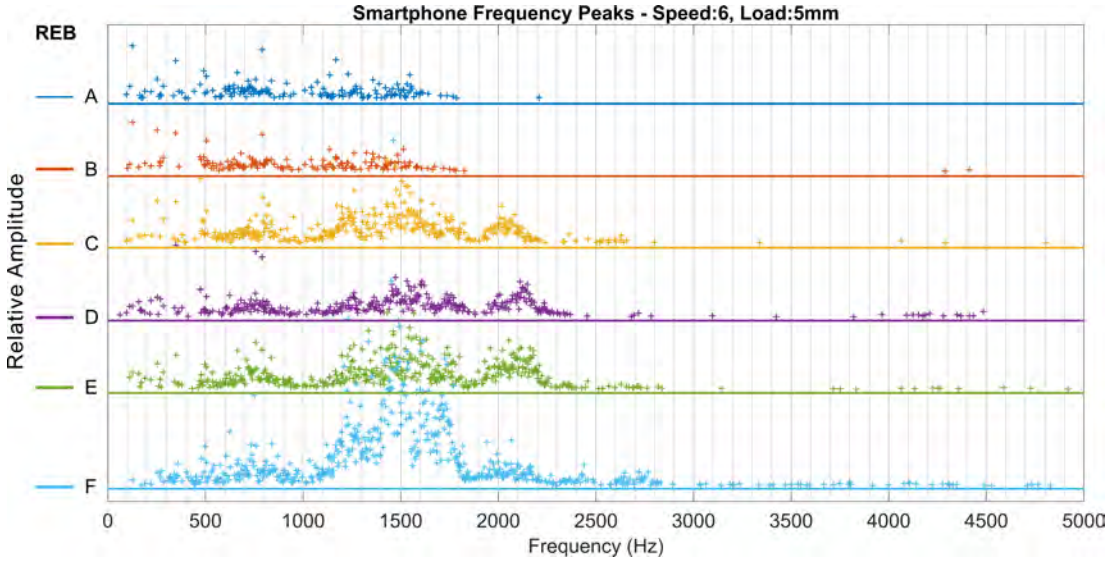

Figure 3.6: Smartphone peaks plot for all bearings at speed 6 and load 5. Vertical lines spaced every 100 Hz show the bin frequency boundaries. The horizontal lines show the mean of each signal. The plot only shows frequency peaks above the cut off threshold (the mean plus one standard deviation). These are the data points used by the SVM.

It is a common misconception that diagnostic systems must be able to cope and deliver good performance for varying operating conditions, without any additional input or *a priori* knowledge. However, in nearly all rotating machine applications a monitoring system would have access to additional information. In the case of rotating machinery, it is likely that the rotational speed and load would be known values measured independently.

These known values are exploited to improve diagnostic accuracy in this case study. To remove the inaccuracy caused by variations in operating conditions, a new SVM is trained for each variation in speed and load. In this case, a quadratic SVM employing a second order polynomial kernel is trained and tested for each operating condition. This achieved using Matlab to split the data by operating condition and then train a new SVM for each set. All the SVMs have the same training parameters, it is only the training data that differs between each one. This results in each SVM having a different set of support vectors. When evaluating new data, the appropriate SVM is used for the given operating parameter.

The multi-SVM accuracy is evaluated by k-fold cross-validation using 5 non-overlapping folds. This splits the observations into folds, training is performed with the out-of-fold observations, and validation uses the in-fold observations, the average overall error across all the folds is then calculated.

The cross-validation is only performed on the training dataset to prevent under and over fitting. Modal recombination is used to consolidate the results from each observation of the SVM. Given 10 overlapping observations per signal a majority of 6 identical results is taken as the actual result for the given input signal.

3.4 Experimental Results

The accuracy results of the trained SVMs from the cross-validation testing are presented in Table 3.2. These results demonstrate that the classifier is performing well for the given input data. It is therefore reasonable that the results from the previously unseen test data are an accurate reflection of the system performance. Table 3.3 presents the classification accuracy of the unseen test data. The processing for this data follows the same methodology but it is not used for training the classification algorithm. The percentage classification accuracies are shown between the six different bearings across all operating conditions. Further, the percentage REB classification accuracies are presented grouped by the speed and load settings. The classification results clearly demonstrate the superior performance of the acoustic signals over those of the vibration. This is commensurate with the literature discussed in Section 2.2, where works including [83]–[85] also agree on the superior performance of acoustic methods over vibration. Note, that although better diagnostic accuracy can be achieved through more complex feature extraction, the purpose of this experiment is to demonstrate a simple and easy to use setup. Figure 3.7 shows a graphical representation of the classification performance. It is clear to see that both acoustic sensors performed better than the vibration accelerometer. The slightly better performance of the microphone over the smartphone is attributed to its larger and more open diaphragm. Examination of the errors reveals that REBs A and B (healthy and outer race defect) were most often misclassified by the vibration method, particularly at low loads. This is likely attributed to the defect producing

Table 3.2: Multi-SVM Training Data Cross Validation Accuracy

	Smartphone	**Microphone**	**Vibration**
Mean Accuracy (%)	99.97	99.97	99.75
Standard Deviation	0.02	0.03	0.01

Table 3.3: Experiment classification results (%).

		Smartphone	Microphone	Vibration
REB	**A**	96.25	95.83	63.75
	B	95.83	96.25	57.08
	C	87.50	95.83	82.08
	D	97.08	93.75	72.50
	E	90.83	95.00	68.33
	F	95.42	99.58	85.83
Speed Setting	**0**	90.42	90.83	50.42
	2	93.75	97.08	75.00
	4	93.75	97.08	72.92
	6	97.92	95.42	81.25
	8	91.67	97.08	75.42
	10	95.42	98.75	74.58
Load Setting (mm)	**3**	86.67	92.78	65.00
	4	94.17	95.28	68.89
	5	97.22	97.78	69.72
	6	97.22	98.33	82.78
Overall Accuracy		**93.82**	**96.04**	**71.60**

insufficient vibrations at lower radial loads preventing the defect frequencies separating from the normal operation signature. In this situation, the vibration measurements misclassified 7 unhealthy states as healthy and 9 healthy states as unhealthy from 144 total inputs. Clearly, differentiating between these two conditions is one of the most essential functions of any diagnostic system. The acoustic signals did not exhibit any error in this regard. It is REB E (exhibiting the combination of defects) that was also most misclassified. Interestingly in all cases, the error is for one of REBs B, C or D; i.e. one of the other individual faults.

Grouping the results by speed, presented in Figure 3.8 reveals that the classification accuracy increases with rotational speed. However, there is a slight fall in classification accuracy at higher speeds (at speed settings 8 and 10), possibly due to saturation of the acoustic sensors. It is notable that the sound level indicator of the smartphone does saturate for very brief periods whilst recording data for the higher speed settings under load. This might

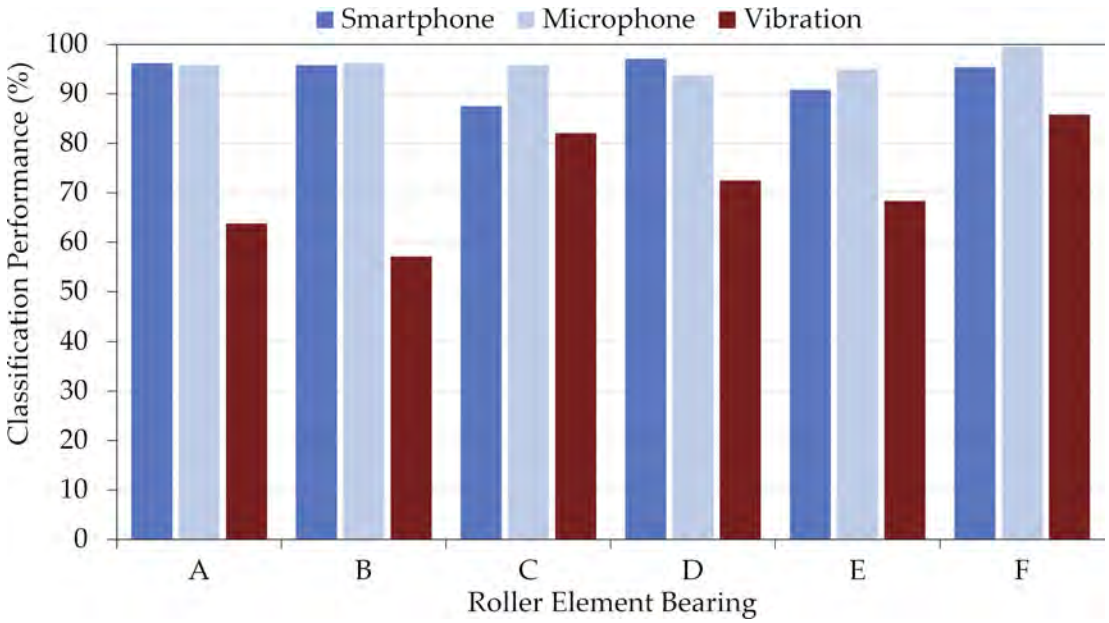

Figure 3.7: REB experiment classification performance categorised by REB. Data from Table 3.3.

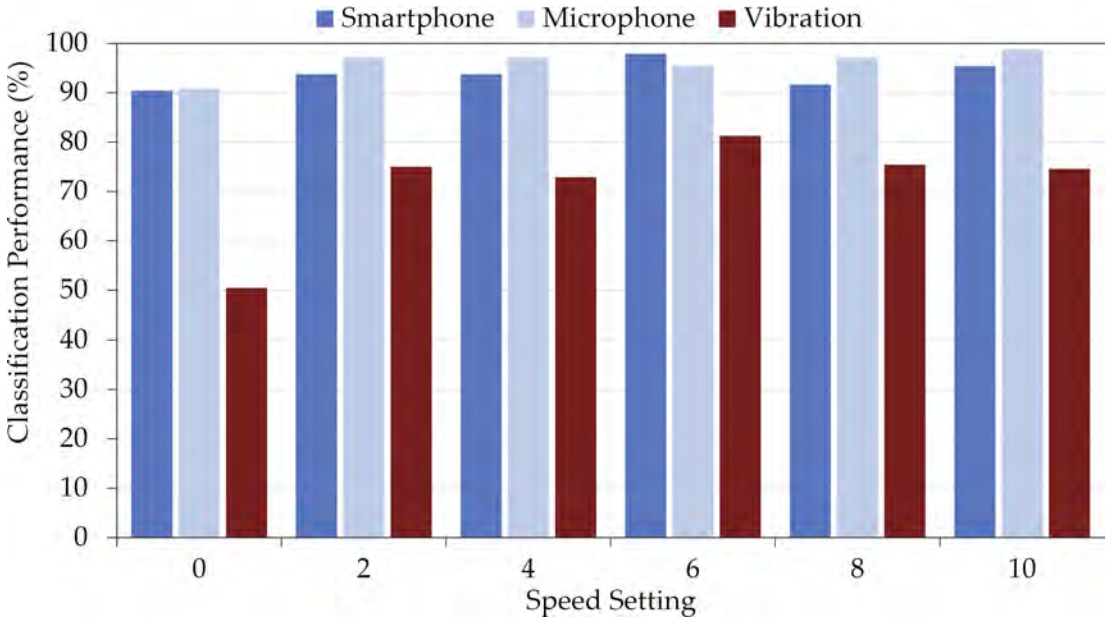

Figure 3.8: REB experiment classification performance categorised by motor speed setting. Data from Table 3.3.

be the cause for the observed degradation in accuracy for the smartphone results compared to the microphone, and if so could be rectified by positioning the smartphone further away reducing the sound pressure to within its most sensitive range.

Grouping the results by load setting in Figure 3.9 reveals greater classification accuracy as the load increases. This is to be expected as the additional load will

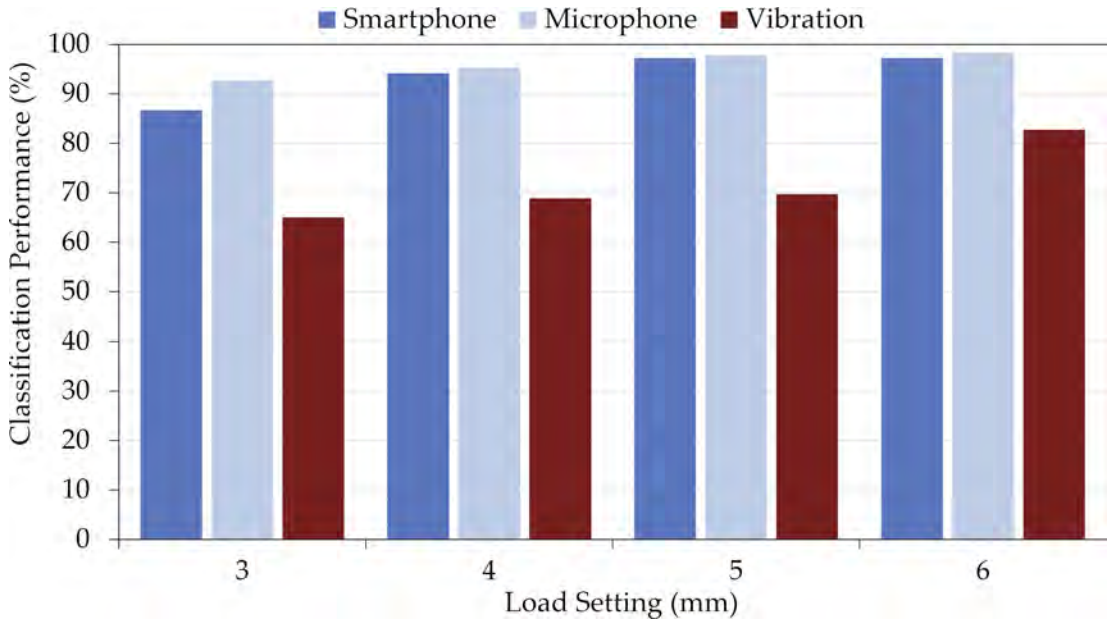

Figure 3.9: REB experiment classification performance categorised by load setting. Data from Table 3.3.

cause result in a greater impact on the defect creating stronger acoustic waves and increasing the vibration.

Overall, the acoustic sensors far outperformed their vibration counterpart, with the performance gap evident for slower speeds and low loads. The vibration performance drops markedly for low speed and loads, where both acoustic sensors only suffer a slight decrease in performance. Unfortunately, the vibration method misclassified $\approx 5\,\%$ of the input data as healthy when a fault was present. Considering the acoustic sensors, the microphone delivered slightly better performance than the smartphone in almost all cases. The smartphone sensor is housed within a very small orifice at the base of the device and the diaphragm is extremely small, which is likely to be the reason for the reduced performance. Conversely, the microphone has a much larger diaphragm visible behind a protective mesh, undoubtedly allowing for better transmission of the acoustic waves to the diaphragm. Analysis between the signals from both microphones revealed no differences in performance. Empirical investigation into the distance of the microphone from the bearing housing revealed a distance of approximately $10\,\mathrm{cm}$ is optimal, with the microphone likely being saturated when placed closer, and with external noise becoming more prominent and valuable fault information being attenuated at greater distances.

3.5 Conclusions

This chapter has considered the diagnostic performance of two consumer-grade acoustic sensors (a USB microphone and a smartphone), along with a vibration accelerometer, when applied to the diagnosis between six different REB conditions. Training a multi-SVM classification system involves extracting signatures for each REB from the frequency spectrum. A new SVM is trained for each variation in operating conditions. The multi-SVM approach developed in this chapter demonstrates a simple solution to address dynamic and non-stationary operating conditions. This technique could be readily scaled to include interpolation between known points allowing the entire operating range to be diagnosed. This marks a different and novel approach to solving the problems of diminished diagnostic accuracy when including dynamic operating conditions.

Results from experimental trials reveal that the signatures from the acoustic signals provided superior diagnostic performance to the vibration sensors across all operating conditions. The performance difference increased for lower rotational speeds and radial loads as the vibration performance markedly decreases. The vibration measurements achieved overall accuracy of $75\,\%$. The microphone also outperformed the smartphone achieving $100\,\%$ diagnostic accuracy compared to $95\,\%$ of the smartphone. The ability of the smartphone and microphone to outperform the vibration signal not only demonstrates the efficacy of acoustics measurements but also the suitability of consumer-grade sensors for fault diagnostics of REBs and other mechanical fault modes. The processing and memory capabilities of the smartphone remain restrictive for complex signal processing and large training databases; nevertheless the method presented in this chapter could be implemented entirely on a smartphone device enabling on-site diagnostics given a suitable acoustic environment. As a minimum these highly accessible devices can be used for data acquisition and transmission. These devices are particularly suited to fault diagnostics where the fault mode produces acoustic waves in the audible frequency range. Further work into other types of fault modes is therefore warranted.

3.6 Extension to Electrical Fault Modes

An addendum to this chapter is the extension of this method to diagnose an electrical fault mode. Unstable current dynamics in Pulse Width Modulation (PWM) BrushLess Direct Current (BLDC) machines, for instance, is a relatively common issue under widely varying operational conditions or during controller commissioning. In the most severe circumstances, inappropriately controlled currents can lead to permanent demagnetisation of the motor as well as damage to the power electronics [3].

In this initial investigation, a BLDC motor is setup, controlled using a digital PWM current controller that produces a 10 kHz frequency. The current controller is known to exhibit transient current instabilities under some operating conditions creating high frequency torque transients in the motor. An oscilloscope plot in Figure 3.10 shows one phase of the motor input current with one of the current instabilities present.

The acoustic setup is easily transferred to a different machine for this investigation, in contrast the vibration probe could not be transferred without considerable work and high risk of damage. The consumer-grade microphone and smartphone are used to sample audio under two operating conditions of the motor; normal healthy operation and unhealthy operating conditions

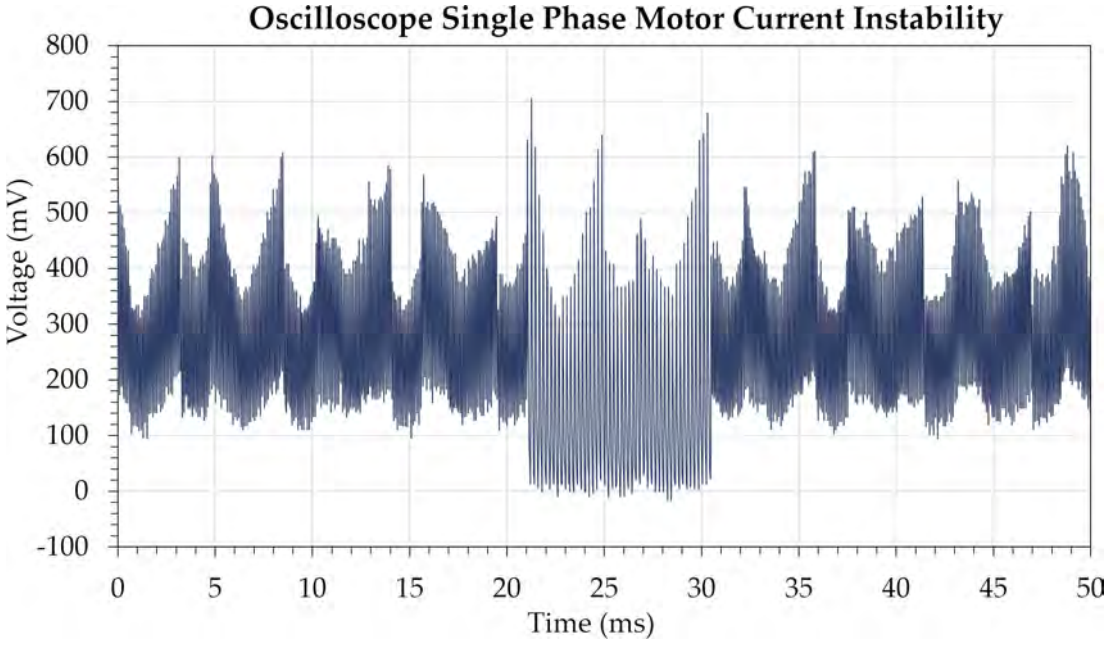

Figure 3.10: Oscilloscope save of a single phase of motor current. The instability is visible between 21 and 31 milliseconds.

Table 3.4: Motor current instability classification results.

	Smartphone	**Microphone**
Overall Accuracy (%)	97.50	100

producing the current instabilities. Both sensors record samples of the motor sounds which are processed according to the method described in (Section 3.3), i.e. no changes from REB experiment are made. Results from experimental trials are presented in Table 3.4.

The results show that this method can accurately distinguish between the healthy and unhealthy operation of the motor. This is the first known instance that a fault of this nature has been diagnosed using acoustic techniques and further investigation into the fault and more accurate diagnostics is required. This initial investigation is further evidence of the suitability of consumer-grade acoustic sensors with simple signal processing for accurate diagnostics on industrial systems.

Chapter 4

Continuous Real-Time Diagnostics of an Electrical Fault Mode

Summary: Acoustic diagnostics, traditionally associated with mechanical fault modes, can potentially be used for a wider range of monitoring applications. Typically, fault modes are induced purposefully by the researchers through physical component damage whilst the system is shutdown. This chapter presents low-cost real-time fault diagnostics of a previously unreported acute electrical-origin fault that manifests sporadically during system operation without a purposefully triggered intervention. A suitability study into acoustic measurements from readily available consumer-grade sensors for low-cost real-time diagnostics of audible faults, and a brief overview of the theory and configuration of the wavelet packet transform (including optimal wavelet selection methods) and empirical mode decomposition processing algorithms, is also included. The example electrical-origin fault studied here is an unpredictable motor current instability arising from the interaction of the parasitic components of the motor leads and phase impedance, and the Pulse Width Modulation (PWM)-controller of a BrushLess Direct Current (BLDC) motor. Experimental trials positively detect $99.9\,\%$ of the 1160 resultant high-bandwidth torque transients using acoustic measurements from a USB microphone and a smartphone. Whilst the use of acoustic techniques for detecting emerging electrically originating faults remains largely unexplored, the techniques demonstrated here can be readily adopted for the prevention of catastrophic failure of drive and power electronic components.

4.1 Introduction

The use of acoustic techniques for fault diagnostics and monitoring of mechanical fault modes has been well documented in Section 2.2 and experimentally in Chapter 3. The advantages of acoustic methods are well proven to include earlier and more accurate detection of emerging changes in system characteristics, improved cost-benefit trade-off, readily accessible transducers, ease of setup and operation, and no detrimental impact on nominal system integrity by virtue of employing remote sensors. The majority of research work to date has employed specialist research-grade Acoustic Emission (AE) transducers to detect the initial acoustic front generated by impact-based mechanical fault modes. By contrast, there is little to no research into acoustic diagnostics for electrical fault modes. Although some electrical diagnostic techniques (discussed in Section 2.3) can be used, these require specialist knowledge and can be difficult to implement on established systems. There are few examples that demonstrate continuous real-time diagnostics - an essential quality for an industry-ready diagnostic monitoring system. In the majority of cases, the component under test is monitored in a healthy condition and then the fault is purposefully created artificially through human intervention whilst the system is shutdown. This introduces error into the investigation and only provides data in the 'book-end' healthy and unhealthy conditions.

Continuing from Chapter 3, this chapter builds on this previous investigation, continuing research into acoustic diagnostics of electrical fault modes, demonstrating continuous real-time diagnostics of a fault that manifests spontaneously without human intervention. Specifically, as an example case study, a permanent magnet BLDC motor drive system that exhibits sporadic current instabilities which only occur during well-bounded operating regimes (at relatively high rotor speeds under light load conditions) is considered. It is notable that a $25\,\%$ change in the proportional gain element of the current controller negates the unstable operation thereby indicating that the instability is controller induced, and a result of the non-linear interaction of the motor electrical parameters, parasitic components and digital controller realisation. By way of example, Figure 4.1 shows each phase current supplied to the BLDC motor under no-load operation (hence the voltage overhead is insufficient to produce classical 'flat-topped' current waveforms). In this case, four discrete periods of unstable controller induced current oscillations that remain

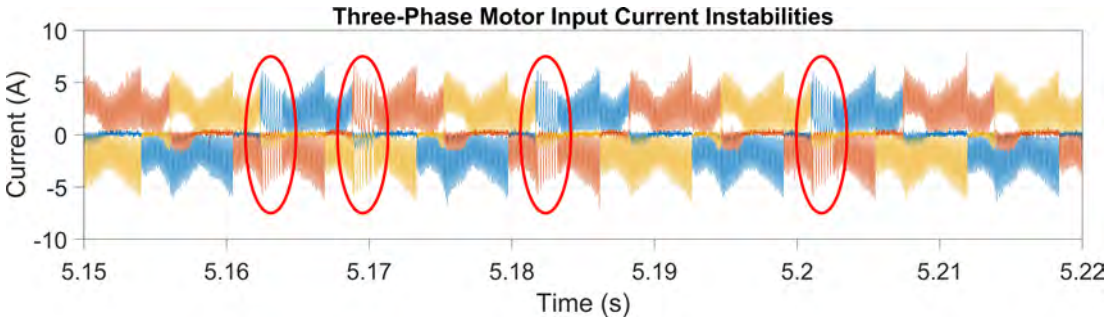

Figure 4.1: Three-phase BLDC motor currents with four distinct current instabilities circled.

for the commutation period can be seen. These unstable events have the potential to propagate to drive system failure, poor performance or possible demagnetisation of the motor (if the commutation sequence is disrupted) [3], [125]. Although a single significant event could initiate these failure modes, a more likely scenario is that multiple minor events would occur over a prolonged period, causing long-term damage that would otherwise remain undetected. The current instabilities induce an audible, mechanical torque transient within the motor, producing an acoustic signature in the audible range (20 Hz to 20 kHz) commensurate with typical PWM frequencies and AC sources, and making consumer-grade acoustic transducers appropriate. This differs from prior investigations that typically employ vibration sensors or specialised piezoelectric transducers, surface mounted for higher-frequency pickup (typically 100 kHz to 1 MHz), [83] for example. Such sensor systems are of comparatively high-cost, require complex specialist setup and operation (low-noise transmission and amplification, and fast data acquisition), are more susceptible to operational damage, and are intrusive to the system under test. Electrical origin fault modes are traditionally diagnosed electrically with techniques such as Motor Current Signature Analysis (MCSA) [125]. Furthermore, to date, research has focused on detecting faults caused by mechanical changes to the system. The method presented here is widely applicable to both mechanical and electrically-seeded faults that result in an audible signature. The particular case considered in this chapter represents one practical example.

The key contributions of this chapter are:

- the diagnosis of electrical origin faults where the failure mode is unseeded (i.e. not by human intervention) and manifests sporadically during continuous system operation,
- the proposed use of consumer-grade acoustic sensors that are readily available for low-cost continuous real-time monitoring,
- a brief comparison of methods for optimal selection of the mother wavelet when using wavelet transformations.

In addition to the publication [2], this investigation is comprised of the literature review presented previously in Chapter 1 and the following experiment; where an unpredictable electrical transient current instability is detected within a BLDC motor using consumer-grade acoustic measurements in real-time. The audio measurements are processed in real-time using Wavelet Packet Transform (WPT) and Empirical Mode Decomposition (EMD) feature extraction algorithms. In this case, the fault signature is so well isolated that further decision making or classification algorithms are not required for accurate diagnostics.

4.2 Experimental Setup

A three-phase BLDC 36 V 1600 W Unite MY1020 motor is powered through a bespoke digital current controller. Internal Hall-effect sensors are used to facilitate commutation. Consumer-grade acoustic transducers, specifically an Audio-Technica AT2020 USB+ microphone and a Samsung Galaxy S7 smartphone using the WO Mic application, are both positioned ≈10 cm from the motor with their sensitive planes directed toward the motor. A setup diagram is given in Figure 4.2. Both acoustic sensors have their own inbuilt analogue to digital converter and connect digitally via USB for continuous real-time sampling at 48 kHz with 16-*bit* resolution using Matlab. In parallel with the sampling, Matlab discretises the data into packets and processes each one using the feature extraction techniques, delivering real-time analysis every 0.2 s. *A posteriori* knowledge of the instability duration (approximately 1.5 ms) is used to define the system refresh rate of 5 Hz; sufficiently long to capture entire instability periods but fast enough to prevent damage to the

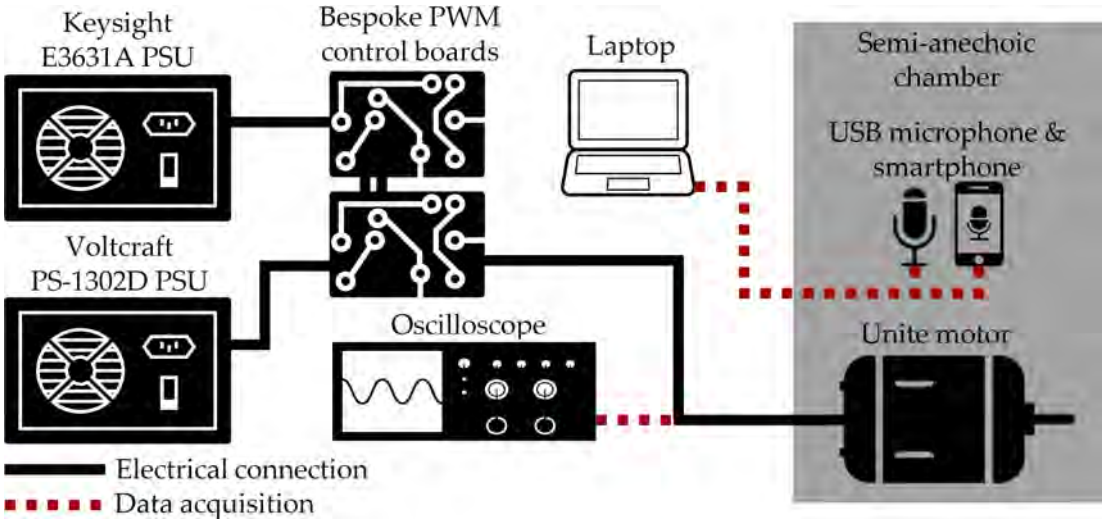

Figure 4.2: Diagram of the experimental setup.

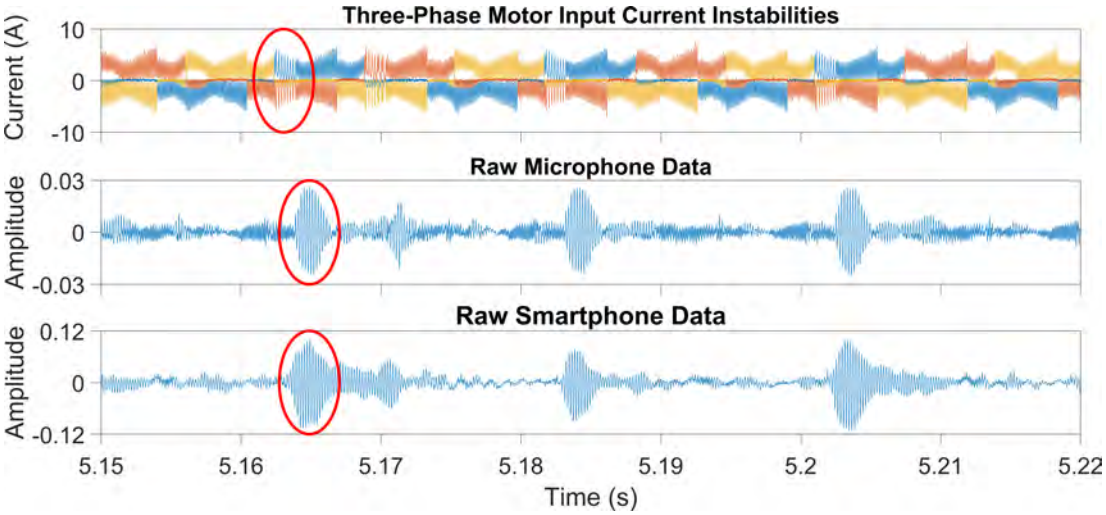

Figure 4.3: Raw unprocessed data showing the same four current instabilities from Figure 4.1 with the microphone and smartphone acoustic signals. The first instability is circled for each signal.

motor drive. The three motor phase currents are measured using three isolated high-bandwidth Hall-effect current sensors, sampled at 250 kHz with 16-*bit* resolution on an oscilloscope. The high sampling rate allows inter-PWM current characteristics to be captured. The motor and acoustic sensors are sited in a semi-anechoic chamber, ensuring minimal background noise. Nevertheless, signal processing is still required to adequately separate the fault information from unwanted motor noise. The unprocessed signals are shown in Figure 4.3.

4.3 Wavelet Packet Transform Configuration

Optimal selection of the mother wavelet is critical to the performance of the WPT and is dictated by the similarity of the wavelet shape to the signal or signature through dilation and translation, i.e. through dilation and translation how well can the wavelet match the signal or signature. There is no definitive methodology for determining this, although researchers have devised various quantitative measures as aids, all fundamentally based on experimentation and *a posteriori* knowledge of relevant signatures. Typically, a selection of different wavelets are tested for various quantitative performance factors such as maximum energy, minimum entropy, minimum reconstruction error, cross-correlation to name a few. In [36], five attributes (energy, Shannon-entropy, signal power to noise power ratio, mean square error, and maximum absolute squared deviation) are evaluated for twenty-six different wavelets. Three separate weighting schemes are applied to the attributes using the analytic hierarchy process (based on pairwise comparison matrix of the attributes). Each weighting scheme revealed a performance ranking order of the wavelets analysed where the highest-ranking wavelet is deemed to deliver the best performance for the given application. A slightly simpler approach is given in [37], where the maximum energy to Shannon-entropy ratio is used as a measure of wavelet performance. This method is undertaken for the investigation in this chapter, as the acoustic fault signature is known to be of a transient nature within the normal operational characteristics of the motor. Although for certain applications it may be necessary to undertake a further comparative study of information measures (joint entropy, conditional entropy, mutual informal, relative entropy and comparative information entropy for example), it is unnecessary in this case due to the transient nature of the fault signature. Therefore, the best maximum energy to Shannon-entropy ratio is used here to select the wavelet. Sixty different wavelet types from the Haar, Daubechies, Symlets, Coiflets, Biorthogonal, Reverse-Biorthogonal, Discrete approximation of Meyer (dmey) and Fejer-Korovkin families are analysed for their maximum signal energy (Equation 4.1) and Shannon-entropy (Equation 4.2). The summarised results in Table 4.1 reveal the dmey wavelet (from Figure 2.5) to be most suitable for these signals.

Table 4.1: Summarised results showing the maximum extracted energy to Shannon-entropy ratio for a selection of different wavelets analysed. Note that the DMey wavelet has the highest ratio.

Wavelet	**Ratio**	**Wavelet**	**Ratio**
Haar	11.4	Sym4	11.7
Db2	7.3	Sym6	12.0
Db4	9.6	Bior2.6	13.9
Db6	13.2	Bior4.4	14.8
Coif1	7.7	Fk4	8.4
Coif2	11.3	Fk8	9.6
Coif4	9.5	Mey	19.7
Sym2	11.3	DMey	24.5

$$E_{energy} = \int \int |W(s,t)|^2 \, dsdt \tag{4.1}$$

where $W(s,t)$ are the wavelet coefficients.

$$E_{entropy}(s) = -\sum_{i=1}^{N} p_i \cdot \log_2 p_i \tag{4.2}$$

where p_i is the energy probability distribution of the wavelet coefficients, defined in [37].

The number of decomposition levels required is determined visually by inspecting the terminal node coefficients in the Matlab wavelet analyser; aiming to maximise isolation of the fault signature from unwanted noise. This analysis, Figure 4.4 shows excellent fault signature isolation into terminal node $[3,1]$ or 8. The original signal is reconstructed from these coefficients, thus excluding most of the unwanted noise and delivering the fault information signature. Reconstruction is realised through upsampling by two and convolving the approximation and detail coefficients with low and high pass reconstruction filters, respectively, which gives the real approximation and detail that are summed together.

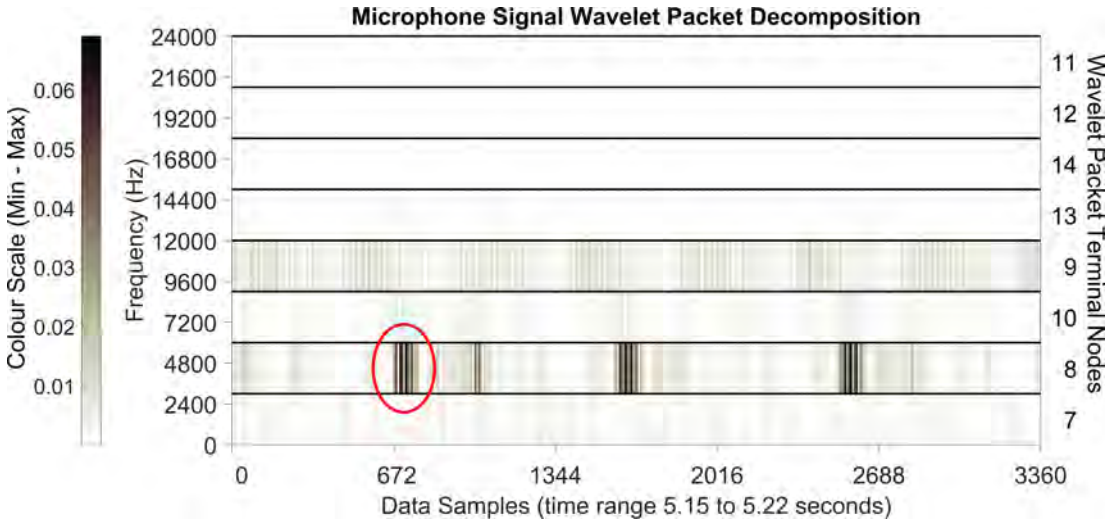

Figure 4.4: Colour mapping of terminal node coefficients from three-level dmey WPT of microphone data. The instability information from Figure 4.1 can be seen as dark patches in terminal node [3,1] or 8. First one circled for clarity.

4.4 Empirical Mode Decomposition Configuration

An empirical approach is used to establish the required number of decomposition levels. Both microphone and smartphone measurements are initially decomposed into four levels giving the four Intrinsic Mode Functions (IMFs) shown in Figure 4.5. As the fault information is expected to be high-frequency it would likely be contained in the early IMFs. The default stopping criterion is based on standard deviation matching, and a maximum of 2000 sifting iterations to allow normal operation of the sifting process.

Results in Figure 4.5 show the majority of the fault information preserved in IMF 1. Fault information is not apparent in the subsequent IMFs, indicating a high frequency fault signature. A single decomposition is therefore sufficient, providing IMF 1 for analysis and the residue containing unwanted noise.

4.5 Fault Diagnostic Method

In summary, acoustic measurements from the USB microphone and smartphone are pre-processed using the WPT and EMD algorithms, thereby delivering four sensor / algorithm combinations, Figure 4.6.

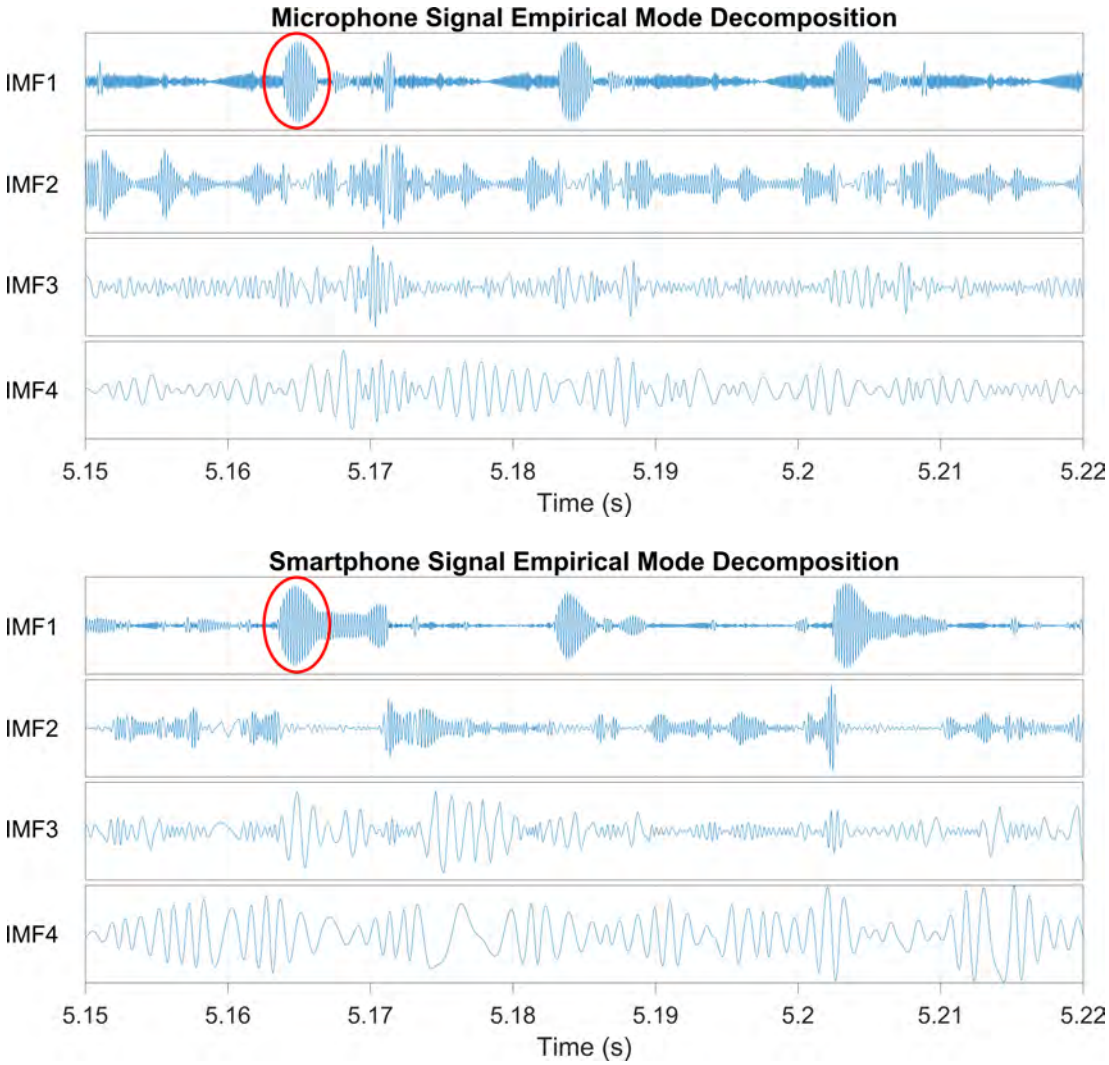

Figure 4.5: Four-level EMD of both microphone and smartphone data. The four instabilities are visible in the first IMF, first one circled. Note that only relative amplitude is significant.

Finally, standard peak finding is used to detect fault events in each pre-processed signal. Detection is qualified using an amplitude threshold based on standard deviation derived from preliminary test data. Windowing discretises individual instabilities using a lower limit separation of 0.02 s (sufficiently long to distinguish between events, but short enough to not class two events together). Figure 4.7 shows the detection threshold with the identified event start and end points.

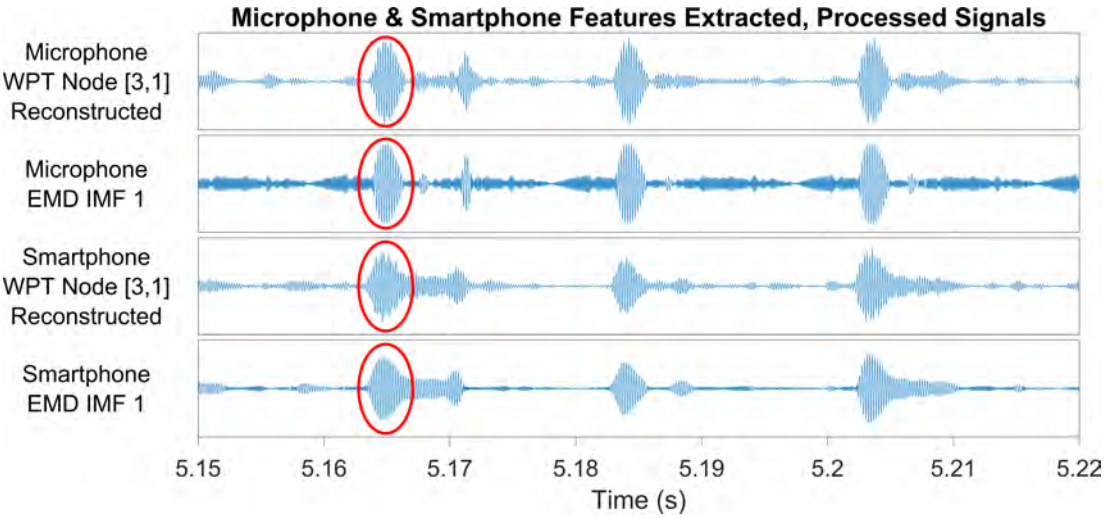

Figure 4.6: Processed microphone and smartphone signals ready for fault diagnostic analysis. Note that only relative amplitude is significant.

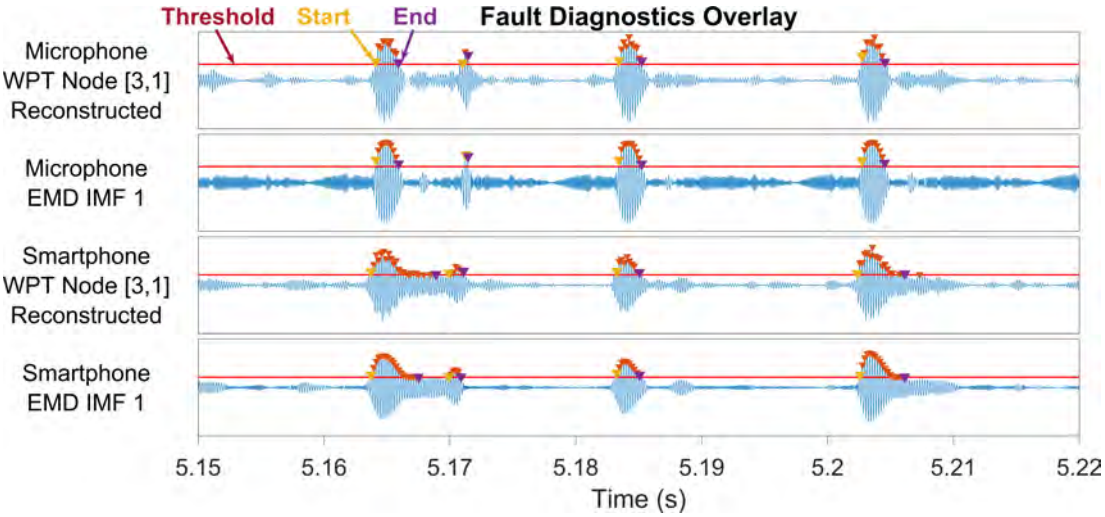

Figure 4.7: Processed signals showing almost exclusively fault information. The peak detection threshold is shown by the horizontal red line with detected peaks marked in red, and the start and end of each discrete instability in yellow and purple respectively.

4.6 Experimental Results

The results from three experimental trials are now presented with analysis of the sensor and feature extraction algorithm relative performance, and detection rates of the electrically-seeded instabilities.

4.6.1 Consumer Transducer Performance

Firstly, the number of unstable periods for each trial are counted from the motor phase current measurements, and are compared in Table 4.2 against the

Table 4.2: The total number of unstable features found for each trial using the phase current measurements as a reference for the acoustically detected faults. Blue indicates some unstable periods were missed, orange indicates false positive detections (which also result in percentages over 100 %), and green indicates best performance.

Trial	Instability Periods During Trial	Diagnostic Performance			
		Microphone		Smartphone	
		WPT	EMD	WPT	EMD
1	327	327	326	309	290
		100.0%	99.7%	94.5%	88.7%
2	690	690	658	685	668
		100.0%	95.4%	99.3%	96.8%
3	143	142	142	147	145
		99.3%	99.3%	102.8%	101.4%
TOTAL	1160	1159	1126	1141	1103
		99.9%	97.1%	98.4%	95.1%

four sensor and algorithm combinations (top row of each trial). The bottom row of each trial is a percentage of the sensor/algorithm detection rate against the actual occurrences. The green values show that the microphone/WPT combination provided 100 % accuracy in detecting the fault periods during trials 1 and 2, with only a single missed instability period during trial 3. This excellent performance is further highlighted in Table 4.3, where the mean percentage of correct detection across all three trials reveals the performance of the sensors, algorithms and combinations. The USB microphone marginally outperforms the smartphone by 1.7 %, achieving an overall detection rate of 99.9 %. This is attributable to its larger, open diaphragm, compared to the smartphone which has a water-resistant microphone within a small aperture. Nevertheless, the smartphone performance remains impressive considering the relative disadvantages. The semi-anechoic environment minimises background noise and is partially responsible for the high detection rates achieved. Nevertheless, the results do demonstrate the potential benefits of the proposed methodology.

Table 4.3: Correct detection percentage across all three trials. Green indicates best performance and overlap.

	WPT	EMD	Mean
Microphone	99.9%	97.1%	98.5%
Smartphone	98.4%	95.1%	96.1%
Mean	99.1%	96.1%	

Table 4.4: Mean processing times across all trials normalised to the system refresh rate. Green and orange indicate the fastest and slowest processing time respectively.

Trial	**WPT**	**EMD**
1	-0.31	1.69
2	-0.55	-2.37
3	-0.52	-0.18
Mean	-0.46	-0.28

4.6.2 Fault Signature Extraction Algorithm Performance

Results in Tables 4.2 and 4.3 show that the WPT algorithm outperforms EMD in detection performance by isolating the fault signature entirely into one terminal node. In some cases, EMD failed to separate events that occurred in close proximity, resulting in multiple instabilities being classed as one by the detection algorithm.

Regarding real-time processing, the mean data packet processing times provide an indication of computational efficiency for the feature extraction algorithms as given in Table 4.4. The times are normalised to the system refresh rate (0.2 s) for clarity. Processing times are seen to be very close to the system refresh rate. A slower processing rate is not suitable for real-time systems as the time lag will continue to increase and the system will ultimately exceed the memory capacity of the computational unit. Both feature extraction algorithms performed well overall, with EMD exhibiting the slowest and fastest processing. However, WPT proved to be consistently faster, delivering the fastest mean processing time.

4.7 Conclusions

This chapter has introduced the use of acoustic measurements for low-cost real-time detection of an acute electrical origin fault mode that manifests sporadically under well-bound operating conditions on a BLDC motor drive system. The example fault mechanism investigated is a transient current instability that arises in the motor supply from the controller due to the non-linear interaction of the PWM-controller parameters, parasitic components and digital controller realisation. This case study verifies that acoustic measurements are capable of detecting electrical origin faults. Low-cost continuous real-time acoustic monitoring is realised through the readily available consumer-grade sensors employed, specifically a USB microphone and portable smartphone. These sensor types can be readily adopted to solve a wide variety of real-world condition monitoring and fault detection requirements in both mechanical and electrical systems and of both mechanical and electrical origin fault modes. Across the three experimental trials undertaken, 1160 discrete unstable controller induced current oscillations were present. An investigation into the suitability of consumer-grade sensors and feature extraction algorithm performance, (specifically combinations of a USB microphone and smartphone acoustic transducers with WPT or EMD feature extraction) revealed that all combinations delivered excellent performance. However, it was the USB microphone and WPT feature extraction that performed best - correctly identifying 1159 (99.9 %) of the instabilities. This is attributed to the larger diaphragm of the USB microphone and optimal selection of the analysing wavelet by the highest energy to Shannon-entropy ratio method. Although the USB microphone performed marginally better, the smartphone offers the potential to become an all-in-one future diagnostic tool given the obvious advantages of being established, easily accessible, relative low-cost, self-powering, remote from the system, and with internet and other communication built in. This research may provide the stimulus for the widespread adoption of consumer-grade sensors and smartphone technology for fault detection and monitoring of both mechanical and electrical systems and fault modes.

Despite achieving continuous real-time processing for this investigation, the monitoring time of the system remains relatively short at only 30 s of continuous monitoring. Although the laptop used is capable of longer monitoring times, long-term use would eventually result in the processing

lagging the data recording. Furthermore, the laptop requires significant power to run and is unsuitable for a continuous monitoring application. Therefore, further research into programmable hardware is necessary.

Chapter 5

Acoustic Diagnostic System Implementation on Field Programmable Hardware

Summary: The goal of an 'all-in-one' acoustic diagnostic system has long been out of reach primarily due to differing application requirements, specialised matching and tuning of feature extraction and decision algorithms to the problem, and comparatively high capital costs and power consumption for continuous real-time monitoring systems. Presented is the design of a proposed all-in-one concept solution. A Field-Programmable Gate Array (FPGA) development board delivering continuous real-time processing with multiple feature extraction algorithms simultaneously. This example, implements three variations of the Wavelet Packet Decomposition (WPD) and Empirical Mode Decomposition (EMD) algorithms on a PYNQ-Z2 FPGA, tested by identifying electrical faults on a BrushLess Direct Current (BLDC) motor drive system in a similar setup to Chapter 4. Prior systems focus on matching and tuning a specific feature extraction/decision making algorithm to the application. The novel approach proposed here equips the FPGA with a variety of feature extraction 'tools', and utilises advanced machine learning to determine the best tool or tool combination for the application whilst operating in training mode. In monitoring mode, only the optimum combination of feature extraction algorithms are active, and their parameters are fine-tuned by machine learning during operation to ensure diagnostic performance is maximised, despite potentially changing variables and conditions. Ultimately, this chapter delivers a sophisticated multi-algorithm, low cost and power system, and lays the foundation for automatic training and adaptability through machine learning development that would undoubtedly improve diagnostic performance beyond current achievements.

5.1 Introduction

The drive for continuous improvement of fault diagnostic and condition monitoring systems has led to a resurgence of research and development of acoustic measurements for this purpose. Literature reviewed in Chapter 1 combined with research investigations in Chapters 3 and 4 shows conclusively that acoustic measurements are ideally suited to solve a wide range of fault diagnostic and monitoring applications, with a wide scope for quick deployment of consumer-grade sensors for audible monitoring applications.

Separation of the fault signatures from additive noise has been the focus of much research. Often referred to as 'feature extraction', a plethora of processing algorithms and techniques are capable of isolating fault signatures. Selecting an appropriate processing method requires understanding of the unwanted noise characteristics (which are always present) and the hidden fault signature therein. To give a brief overview, signals can be analysed in either the time domain, the frequency domain or the time-frequency domain. For acoustic signals, time domain analysis is usually not revealing, unless the fault signature has a consistently higher amplitude than the signal noise. Analysis of the frequency spectrum by Fast Fourier Transform (FFT), or variation thereof, is well-suited to differentiating between known healthy and unhealthy states of a continuous nature (such as a pressurised gas leak). However, pure frequency analysis breaks down when the fault signature energy is reduced, as with a transient fault mode for example. For instance, particle ingress on the race of a Roller Element Bearing (REB), produces a periodic impact, but does not have substantial impact on the frequency spectrum since the fault is only present for comparatively short periods of time throughout the whole signal. This problem is compounded as the ratio of unhealthy to healthy state time becomes lower, i.e. a very short time fault that does not often occur is usually more difficult to detect than one of a longer time duration with higher occurrence. The time-frequency domain allows the analysis of both the time and frequency information simultaneously, albeit with a resolution trade-off. The Short-Time Fourier Transform (STFT) is the most well-known time-frequency algorithm, as it maps the domains with excellent resolution in both time and frequency, as shown in Figure 2.4. However, this algorithm is computationally intensive and requires a disproportionate time to compute. More efficient time-frequency

analysis can be realised through wavelet transform, Hilbert-Huang Transform (HHT), or Wigner-Ville distribution as examples, and there are also pseudo-time-frequency techniques such as EMD available. Nevertheless, these algorithms are still complex and require significant computation, leading to a few researchers implementing them using FPGA hardware. By exploiting the massive parallel processing, FPGA devices offer significant improvements in processing time and efficiency [132].

Literature previously discussed in Section 2.1.5 clearly indicates that FPGAs can be used to implement complex time-frequency analysis for real-time processing requirements through efficient parallel processing, with low capital and operational costs and low power consumption. These examples also show that matching the algorithm to the problem, and further tuning the algorithm parameters, is crucial to achieving reasonable diagnostic performance. For example, the performance of the Wavelet Packet Transform (WPT) is highly dependent on appropriate selection of the analysing mother wavelet or reconstruction nodes when filtering.

Acoustic fault diagnostics, despite many proven advantages, retains the following issues that continue to hinder widespread industry adoption:

- Delivery of continuous real-time processing through complex feature extraction and decision algorithms is challenging, and typically requires high capital cost for high specification General Purpose Processors (GPPs) and associated equipment.
- A high specification GPP will undoubtedly exhibit high power consumption, and thus require cooling to prevent overheating. This increases operational costs, and can make the equipment unsuitable for hot environments. Further, this equipment is often delicate and difficult to protect without due consideration of cooling requirements.
- Specialist expert development is usually required to match and tailor feature extraction and decision algorithms to the problem in an effort to achieve reasonable diagnostic performance.
- System algorithms are often finely-tuned, susceptible to performance degradation from changing operational and environmental variables. Further, it is likely that the system will only be capable of monitoring a single fault for a specific setup and acoustic environment.

This chapter explores the use of FPGA devices for the implementation of multiple feature extraction algorithms to operate simultaneously in continuous real-time. The PYNQ-Z2 FPGA System on Chip (SoC) development board Figure 5.1 (newly released at the time of writing), is used as an example FPGA for system development, testing and proof of concept. FPGA software is employed to implement WPD and EMD feature extraction in Hardware Description Language (HDL) to allow programming of the FPGA device. The algorithms are designed to operate in continuous real-time, with several variations of the WPD operating in parallel simultaneously. To verify performance and validate the implementation, acoustic signals from a consumer-grade microphone are processed on the FPGA, delivering real-time fault diagnostics for an electrically-based fault mode. In this case, an acute current instability manifesting in the Pulse Width Modulation (PWM) controller of a BLDC motor drive system, producing an audible torque transient. This fault mode and experiment are described in detail in Chapter 4 and [2], [3].

In addition, this chapter proposes the implementation of advanced machine learning algorithms that perform the following functions:

1. Analysis of the incoming signal and the extracted feature signals to determine an optimal feature extraction method. This could be a single

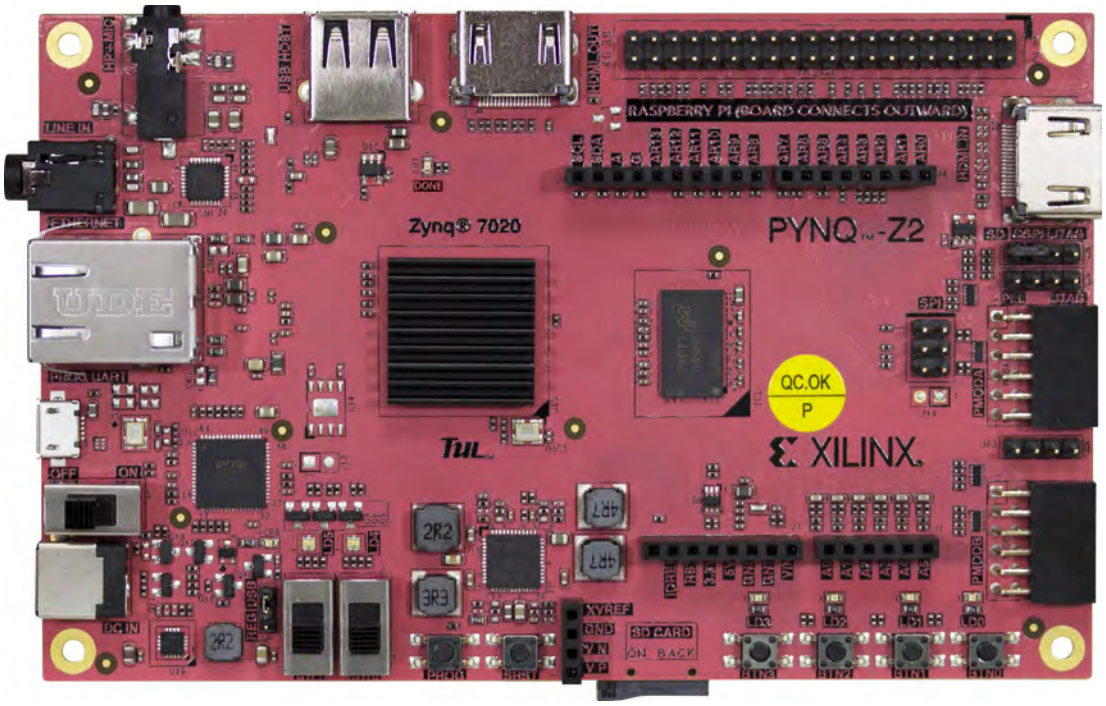

Figure 5.1: Image of the PYNQ-Z2 development board.

algorithm or a combination of multiple different algorithms or their variations. Whilst performing this function, the system is referred to as operating in training mode.

2. Possess the ability to control the feature extraction algorithms in terms of adjusting their configuration parameters and whether they are operational or not.
3. Operate in monitoring mode, where only the optimal feature extraction method is actively processing, and the machine learning is periodically fine-tuning its configuration parameters as more data is analysed. This ensures the system is continuously updating to maximise diagnostic accuracy.

This system has numerous benefits and advantages over those currently in operation, namely; reduced capital expenditure and operational costs, low power consumption and thermal dissipation, no requirement for expert algorithm matching and tailoring, adaptive to new problems and changing system and environmental characteristics. The chapter continues by providing a detailed design of the diagnostic system, examining the hardware required, the overall system development, the FPGA implementation of the feature extraction algorithms, and finally the programming of the FPGA. An overview of the experimental setup is provided, and the results are analysed with discussion on system validation and performance. The main findings of the work are then presented in the conclusions.

A summary of the contributions of this chapter:

1. FPGA implementations of the WPT & EMD feature extraction algorithms are detailed.
2. Real-time processing of multiple feature extraction algorithms operating simultaneously is demonstrated.
3. The concept for an industry-ready 'all-in-one' solution is presented and partially developed.
4. The FPGA implementations utilise the newly released PYNQ-Z2 FPGA development board.

5.2 Hardware Abstraction

The PYNQ-Z2 FPGA development board produced by TUL (Technology Unlimited), is a relatively recent addition to the FPGA family at the time of writing. It is equipped with a Xilinx Zynq 7020 SoC containing a 650MHz dual-core Cortex-A9 processor and an Artix-7 equivalent FPGA. The full specifications and schematic are available in [133]. This particular model is chosen for the Xilinx Zynq 7020 SoC, the connectors available, and the inherent design for audio processing. Analysis of the PYNQ-Z2 schematic, reveals details of the ADAU1761BCPZ Digital Signal Processing (DSP) Integrated Circuit (IC), which provides integrated filtering of the PYNQ-Z2 line-in port. Although this filtering may be beneficial in noise removal, for the purposes of obtaining an unfiltered raw signal, the line-in port must be bypassed. Furthermore, routing the signal from the line-in to the programmable logic of the FPGA creates additional difficulties for sampling and DSP. The programmable logic can easily access the integrated Analogue to Digital Converter (ADC) of the PYNQ-Z2, which samples directly from Arduino headers present on the board up to $1\,\mathrm{Mbit}$. Therefore, this port is used to sample the input signal.

The acoustic input signal is generated by an Audio-Technica AT2020 USB+ microphone audio output port (a $3.5\,\mathrm{mm}$ audio jack), that provides a $\pm 5\,\mathrm{V}$ bipolar signal. However, the PYNQ-Z2 ADC requires a unipolar signal between 0 and $3.3\,\mathrm{V}$ in order to prevent damage. Therefore, analogue signal modification is necessary. A bespoke Printed Circuit Board (PCB) Arduino Microphone Shield is designed for this purpose, using National Instruments Multisim and Ultiboard versions 14.2. It is based on the dimensions and connectors of the Arduino Uno, allowing a direct connection to the Arduino headers present on the PYNQ-Z2. The schematic, silk layer and a 3D render of the PCB are given in Figures 5.2 and 5.3. The PCB is produced on 2-layer FR4 with the surface-mount components soldered and the op-amps added.

In summary, the acoustic diagnostic monitoring systems consists of the low-cost and readily available consumer-grade microphone, the bespoke PCB Arduino Microphone Shield and PYNQ-Z2 development board. The Audio-Technica AT2020 USB+ microphone outputs a $\pm 5\,\mathrm{V}$ bipolar acoustic signal from the $3.5\,\mathrm{mm}$ audio jack, connected to the signal input of the PCB. This converts the signal to unipolar between 0 and $3.3\,\mathrm{V}$, which is then

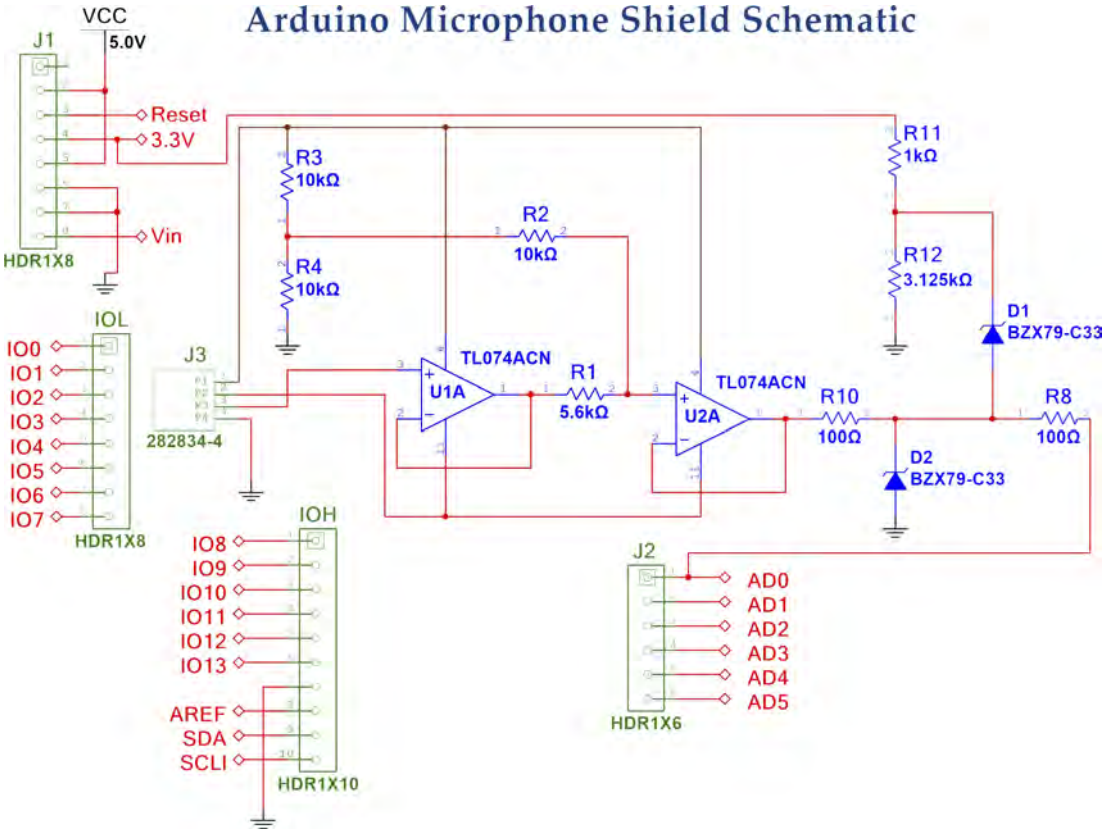

Figure 5.2: Multisim schematic of the Arduino Microphone Shield.

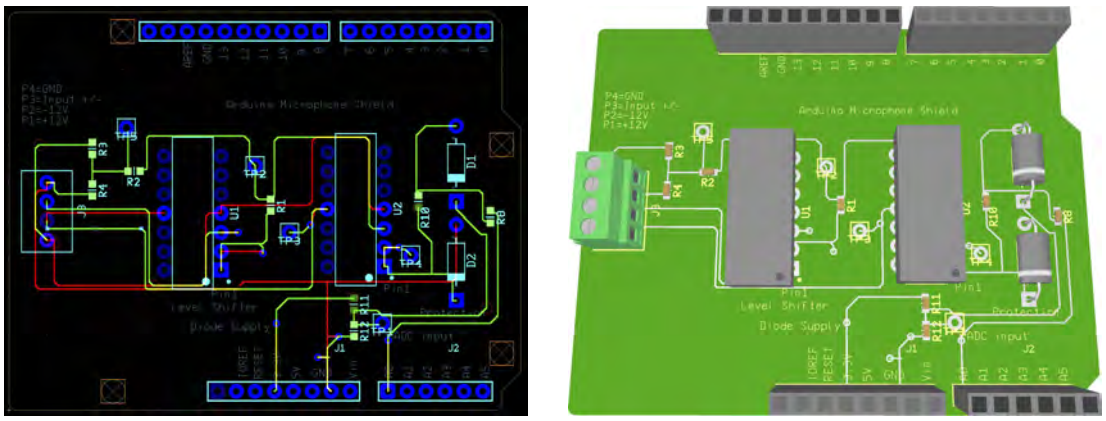

Figure 5.3: Image of the Ultiboard silk layer (left) three-dimensional model (right) of the Arduino Microphone Shield.

sampled by the PYNQ-Z2 ADC. The ADC samples the signal at 100 kHz and 16 bit resolution, to be processed in the programmable logic system detailed below.

The PYNQ-Z2 is connected by USB to a laptop, powering the board and allowing a serial connection. The PYNQ-Z2 Arduino headers provide 3.3 V to the diode protection circuit on the PCB. The PCB op-amp circuit is powered independently with a ±12 V DC supply. The microphone is USB

powered.

5.3 System Development

A plethora of different options and methods can be utilised for development of an FPGA system, from coding directly in HDL, to utilising high-level abstraction tools such as Xilinx Vivado and Xilinx System Generator for Simulink (SysGen). The method presented here is chosen for a combination of speed of development, simplicity of design, and software functionality. To understand how the system is developed, it is important to explain the system from the top level down. At the highest level, the FPGA is programmed with a system wrapper in the form of a bitstream. This wrapper contains all of the functional elements of the system as Intellectual Property (IP) blocks, each with their own inputs and outputs. Some of these blocks are generated automatically, representing aspects of the physical FPGA hardware. For example, the ZYNQ7 Processing System which critically provides the system clock wire. Other IP blocks are configured for specific functions, the ADC block for example, and some are completely bespoke - designed to implement the signal processing algorithms in the programmable logic. The full system wrapper diagram is shown in Figure 5.4 and the key component blocks are as follows:

- **ADC**
  This block is generated using the XADC Wizard and represents the physical ADC present on the hardware of the PYNQ-Z2. The block allows the ADC to be programmed for Dynamic Reconfiguration Port sampling of the signal at 100 kHz and 16 bit resolution.
- **Block Memory Generator (ROM_Signal)**
  The Block Memory Generator is used to store a segment of real data recorded from the microphone. The data is stored in COE format in read only memory, allowing data samples to be streamed in synchronisation with an enable signal. The enable signal acts as a flag that a data sample is present - this is critical to the operation of the system as the data stream rate is significantly slower than the system clock. This block replicates the function of the ADC block for system testing. The sample data streams in a continuous loop.

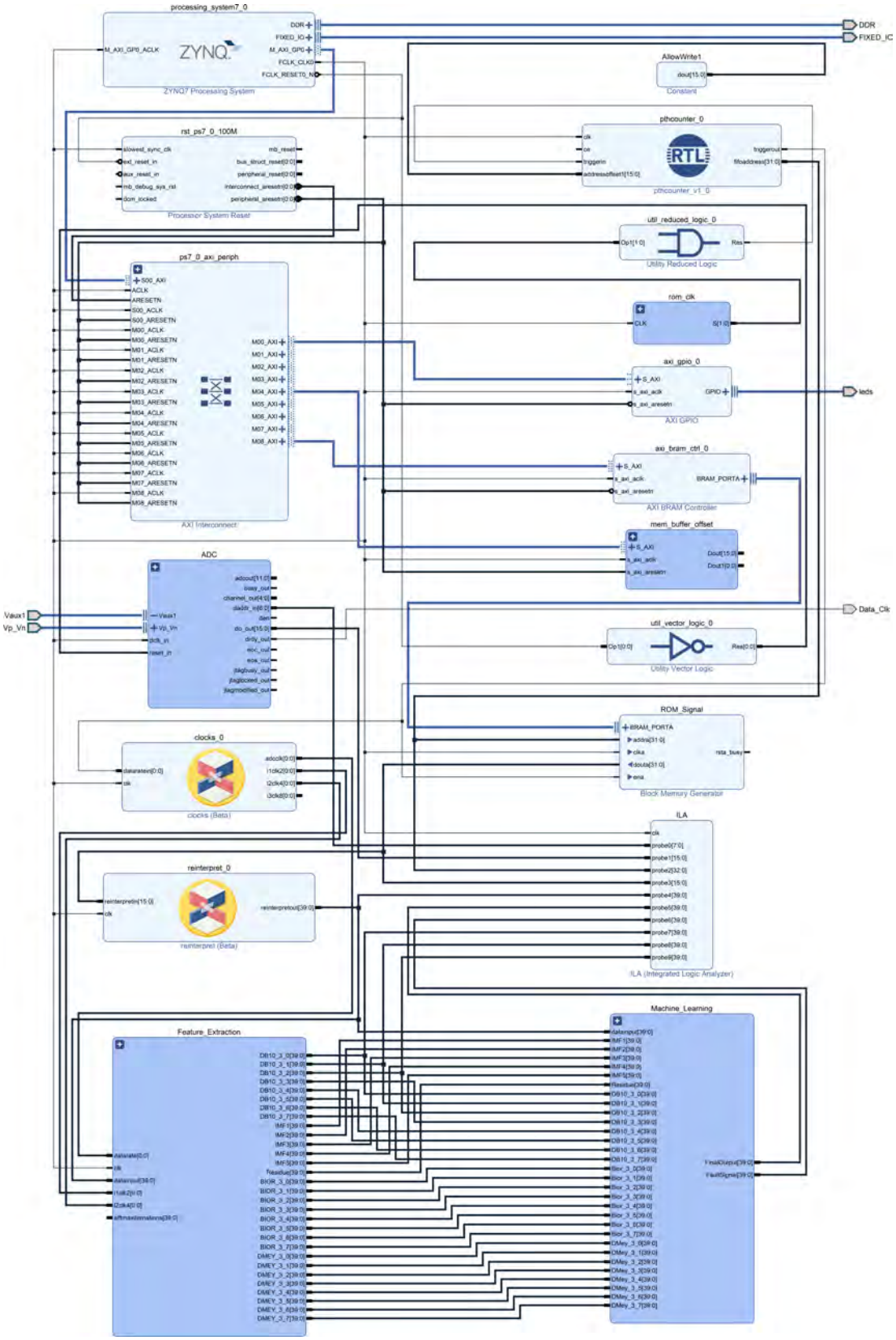

Figure 5.4: Vivado Block Design showing the system wrapper made up of different functional blocks.

- **Feature_Extraction**
  This block contains the different feature extraction algorithms with various input parameters that connect the Machine_Learning block (explained below). In this case, the block contains SysGen implementations of three-level bior3.5, db4 and dmey WPD and five-level EMD. A detailed explanation of these sub-blocks is provided in the next subsection.
- **Machine_Learning**
  This block, shown here for illustration of the concept, would contain complex machine learning, likely based on Convolutional Neural Network (CNN), to analyse the processed features and determine the most optimal feature extraction method. This system would also contain a control block to differentiate between a learning and optimisation mode and an operation mode. When the system is setup to analyse a given problem, the data is streamed through multiple feature extraction algorithms, the parameters of which can be adjusted in combination with optimisation algorithms. After a training period, the CNN would determine an optimised method for feature extraction and switch the system into operation mode. In this mode, only the chosen feature extraction streams would remain active, streaming real-time and continuous diagnostic information directly to the safety systems of the component under test, or to trained operational staff. The development of the machine learning system is complex and beyond the scope of this project. The block is included here to demonstrate the idea and show how the system would likely appear.
- **Integrated Logic Analyzer (ILA)**
  The ILA provides an interface with Xilinx Vivado, allowing data sampling from pins in the system. The ILA requires significant resources, therefore configuration of the sampling rate, resolution and number of pins requires careful consideration. The ILA interface is used to save the processed data from the feature extraction algorithms for the purposes of providing research data. Fault diagnostic information can be readily streamed to other connection ports on the PYNQ-Z2 to facilitate either real-time diagnostics or system shutdown or fail-safe procedures in the event of positive detection.

The Feature_Extraction block is a top level hierarchy of sub-blocks containing the FPGA implementations of the various feature extraction algorithms. A full subsystem diagram is given in Figure 5.5. The implementation of multiple feature extraction algorithms that operate simultaneously in real-time through the use of FPGA parallel processing is one of the major contributions of this research. To demonstrate the concept, wavelets from three different families are used to deliver three-level WPD, alongside a five-level EMD.

5.3.1 Wavelet Packet Decomposition Implementation

The input data stream and data rate is sourced from either the ADC or the Block Memory Generator (ROM_Signal). It is critical to understand that the FPGA runs on a fixed system clock of 125 MHz, but the data stream (either from the ROM or the ADC) is sampled at 48 kHz. Therefore, the data rate is significantly (orders of magnitude) slower than the system clock. Both the ADC and the Block Memory Generator provide an enable signal which matches the data rate, i.e. each time the sample is updated the enable signal flags positive for one system clock cycle.

The data stream input for the feature extraction algorithm is an unsigned 16 bit number, i.e. between zero and $2^{16} = 65536$, meaning the vertical centre is halfway at 32768. The first SysGen IP block (the reinterpret_0 block) centres the signal around zero and adjusts the output stream to a signed 40 bit number with 23 bit binary point inclusive. This is shown in Figure 5.6. The output of this block then streams to the input of the various wavelet blocks. For brevity and simplicity, the design of the wavelet blocks is demonstrated using the db4 and bior3.5 wavelet, as these have a small number of coefficients (16 and 24 respectively). The bior3.5 coefficients are plotted in Figure 5.7. Figures 5.8 and 5.9 show the bior3.5 SysGen model. The signal from the prior reinterpret block is streamed in at the DataInput gateway in. The data stream splits to pass through the high pass filter, $g(n)$ above, and the low pass filter, $h(n)$ below. The filters are implemented by convolving the input data with the high and low pass wavelet coefficients (constants labelled HiD001 to HiD012 and LoD001 to LoD012 respectively). The timing of the data stream is controlled using the DataRateIn gateway in, representing the enable signal from the ADC or memory block, shown in blue. The enable signal allows the registers to update according to the data rate, with the multiplication and addition operating on the system clock.

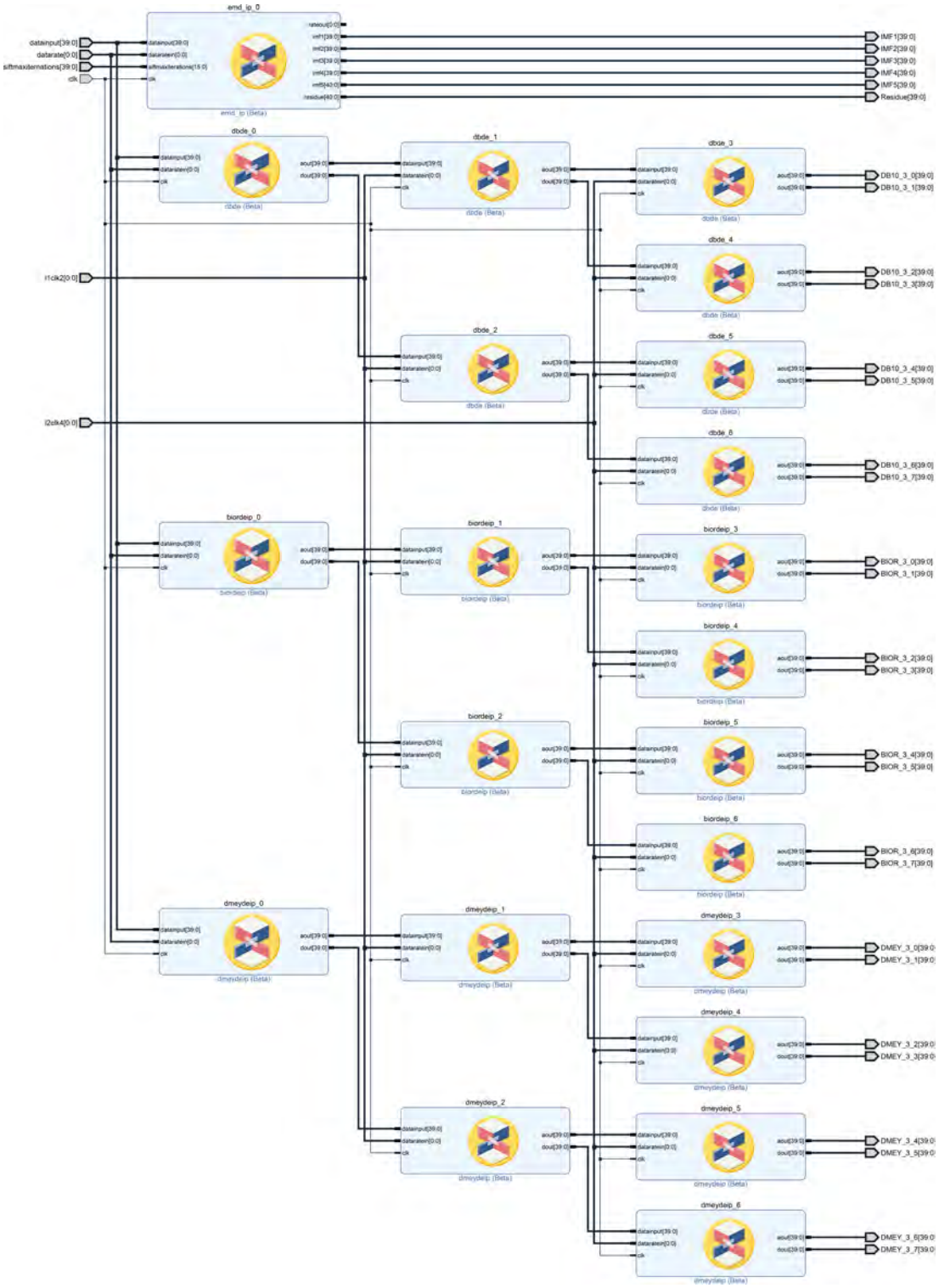

Figure 5.5: Vivado Block Design of the Feature_Extraction hierarchy.

There were numerous technical challenges and difficulties whilst implementing the wavelet architecture. Initially, the SysGen multiply blocks were implemented using DSP slices, meaning one slice is used for each wavelet coefficient. With the PYNQ-Z2 FPGA having only 220 DSP

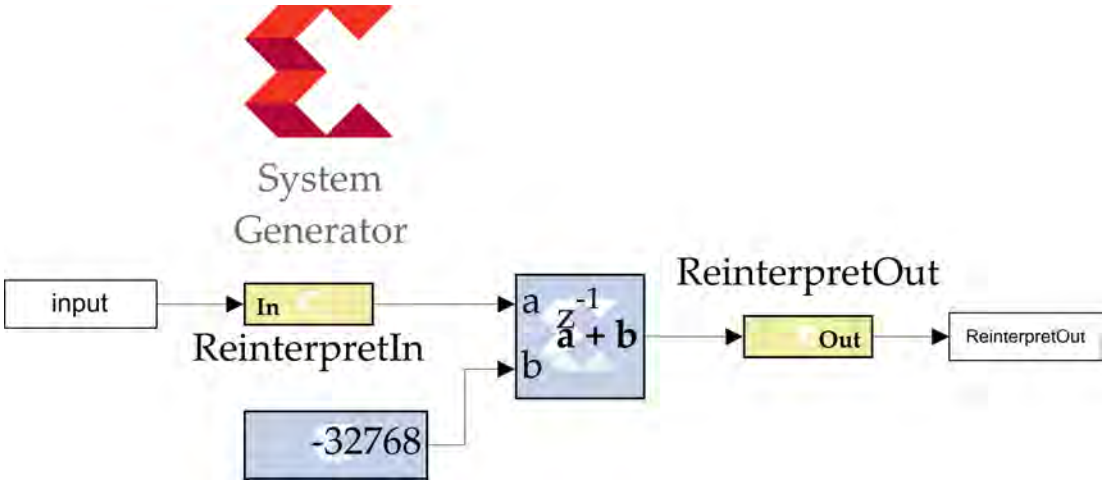

Figure 5.6: SysGen design of the reinterpret block.

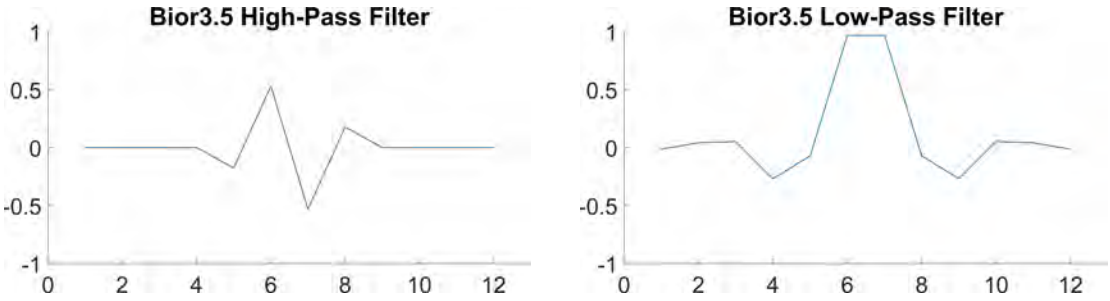

Figure 5.7: Plots of the bior3.5 high and low pass filter coefficients.

slices, it quickly becomes impossible to implement multiple wavelets and levels of decomposition. Therefore, the multiplication was implemented on the programmable logic fabric. Another problem is to be able to query data from the FPGA, as once within the programmable logic, it becomes extremely challenging to query. This is where the ILA implementation is invaluable as it allows data to be passed to configurable probes for viewing and export. Further conflicts between the different programs (Matlab, Simulink, SysGen

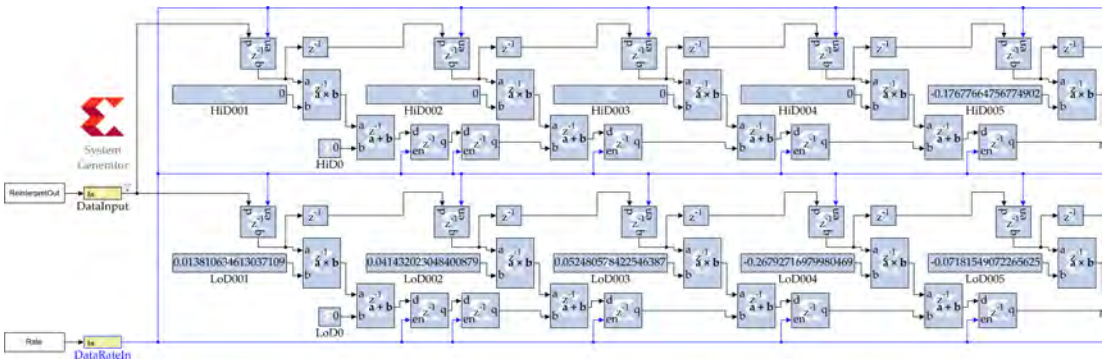

Figure 5.8: Beginning of the bior3.5 wavelet SysGen model. The data enable signal is shown in blue.

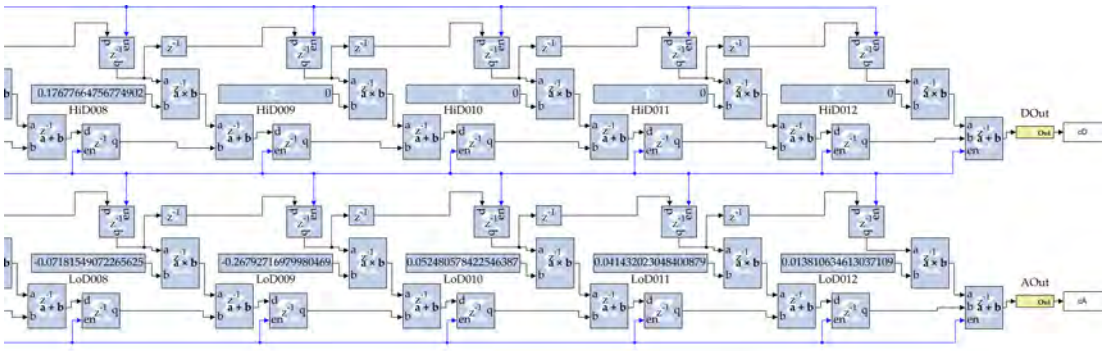

Figure 5.9: End of the bior3.5 wavelet SysGen model. The data enable signal is shown in blue.

and Vivado), such as versions, number systems and implementation methods, made system development and testing difficult.

5.3.2 Empirical Mode Decomposition Implementation

The implementation of the EMD algorithm is substantially more complex due to the different timings and processes required. A diagram of the full system is shown in Figure 5.10. The IP block receives the same data input and enable signal as the wavelet design, however, in this system 16 bit resolution is maintained throughout the processing stream. The system presented performs five levels of decomposition, i.e. producing five Intrinsic Mode Functions (IMFs). For the purposes of this research, no more than five IMF are required, however, further development would seek to add additional IMF calculations, potentially delivering ten to twelve IMFs (comparable with Matlab). Furthermore, the option to control the number of decompositions performed would prevent unnecessary processing for many cases.

The following numbered list is mapped to numbers annotated on Figures 5.10 to 5.23, further annotations are provided where appropriate. The data flow and algorithm process is summarised as follows:

1. **Input Data Buffer**

   The EMD algorithm requires a reasonable amount of consecutive data samples for normal operation. Therefore, the Input FIFO memory buffer near the top of the diagram stores consecutive data samples as they are received. Once the buffer has sufficient samples, they are emptied at the system clock rate into the Extrema Detection system.

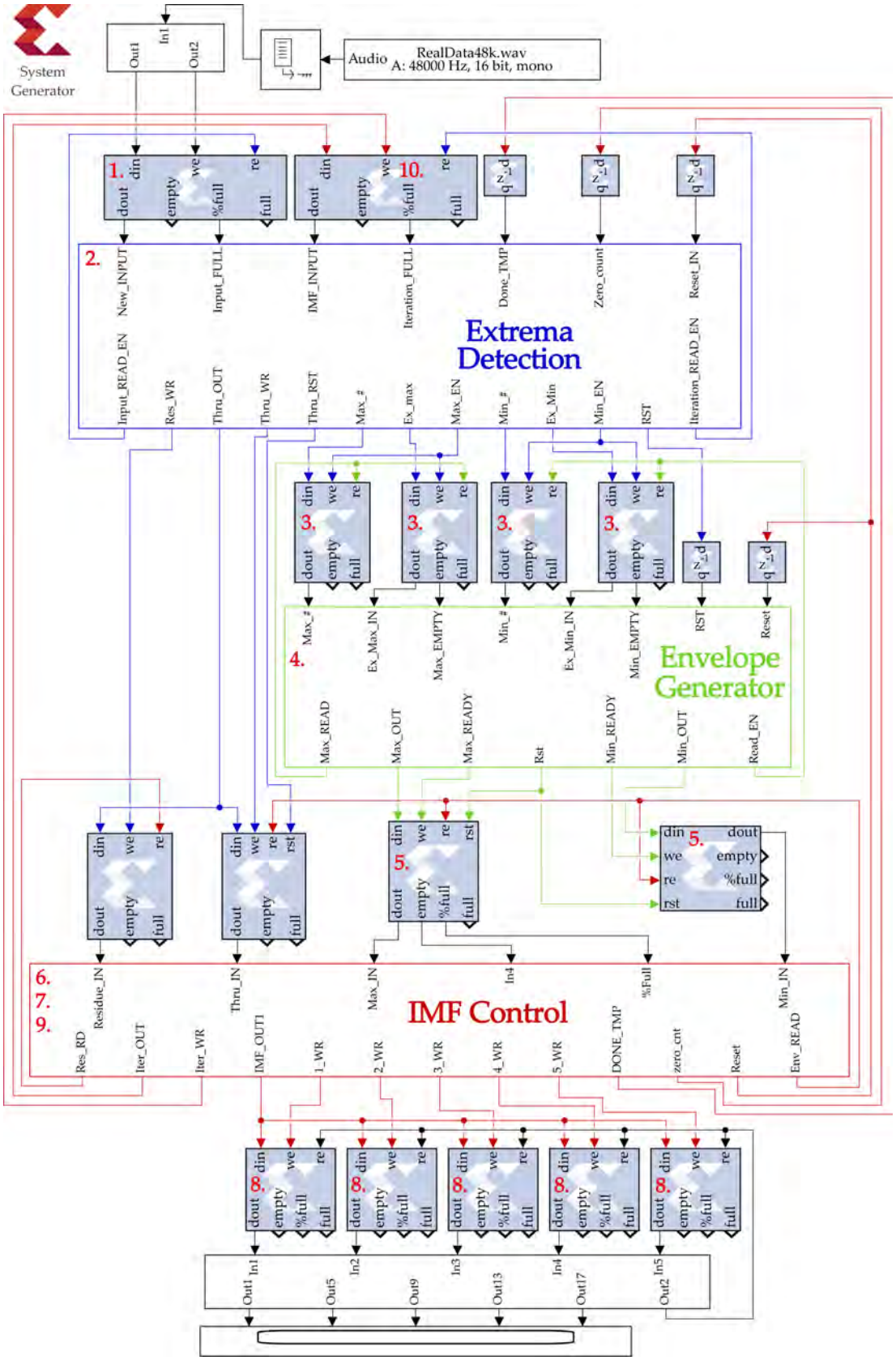

Figure 5.10: Implementation of EMD in SysGen.

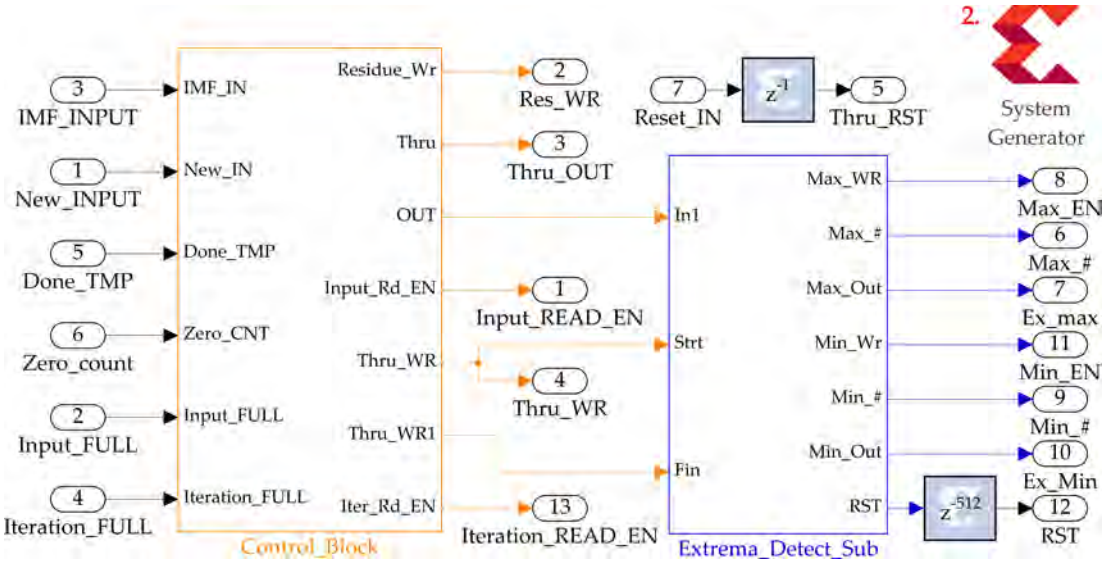

Figure 5.11: The Extrema Detection subsystem.

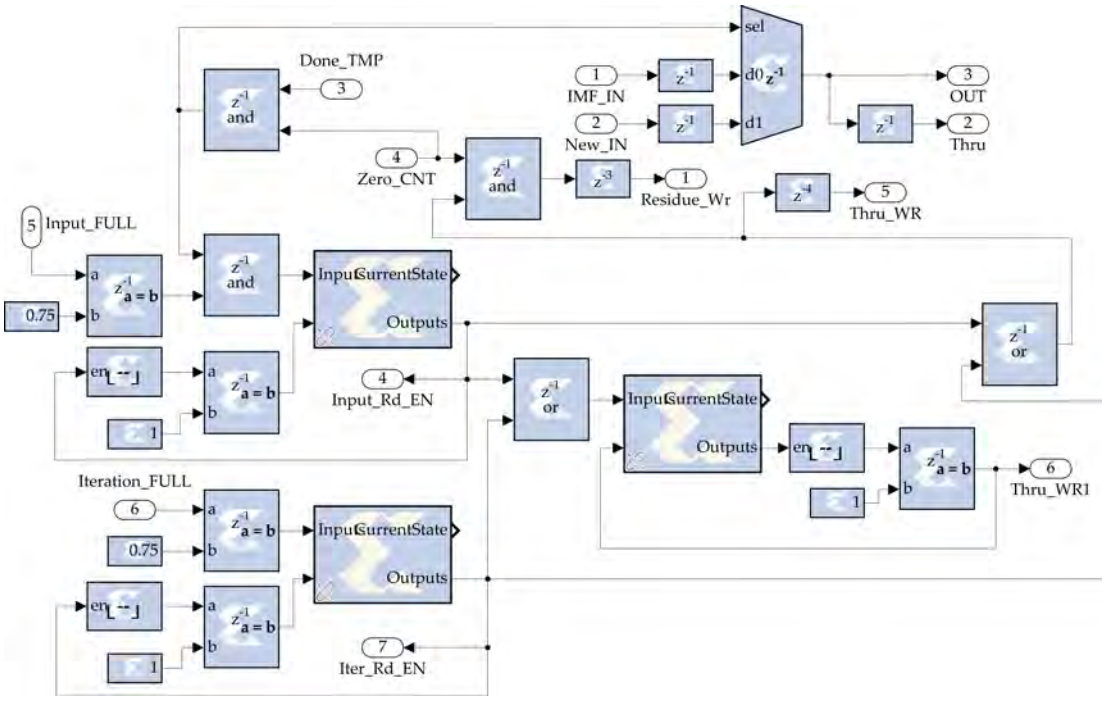

Figure 5.12: The Control Block sub-subsystem.

2. **Extrema Detection Process**

   This process runs at the system clock, examining each sample against the one in front and behind to determine whether it is an extrema; a local minima or maxima.

3. **Extrema Buffer**

   The local maxima and local minima are output into the Extrema Buffer FIFO memory, each stored as a separate signal whilst maintaining their

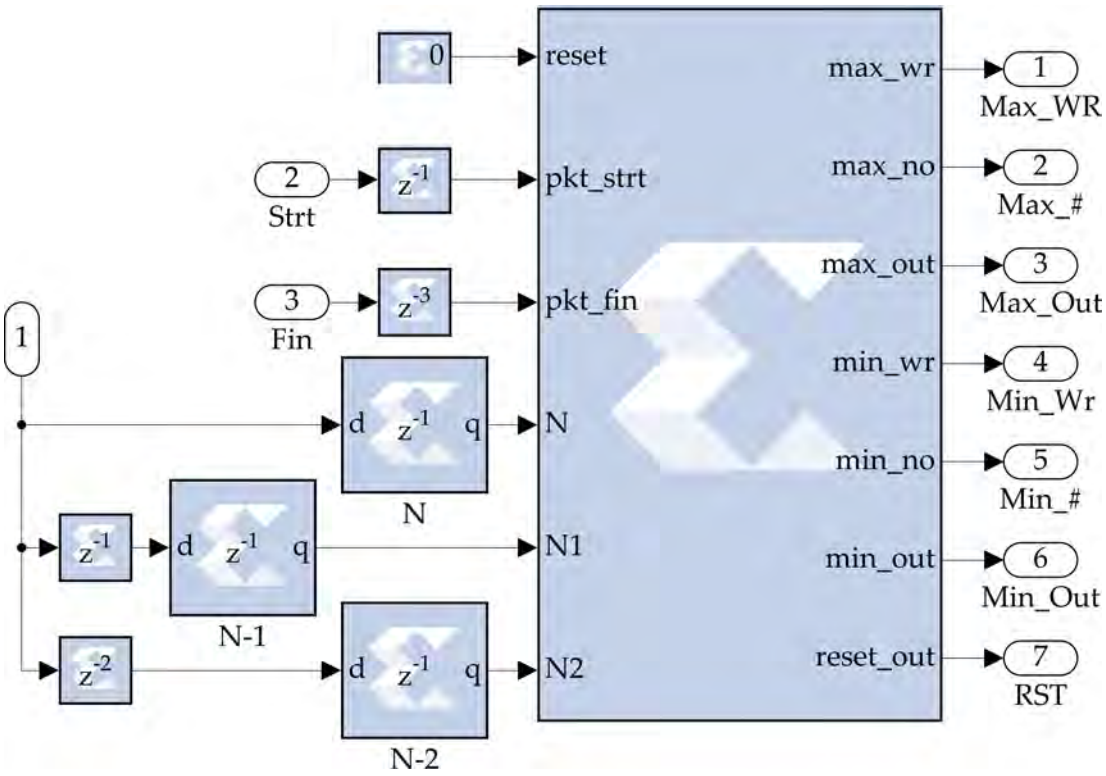

Figure 5.13: The Extrema Detect Sub sub-subsystem.

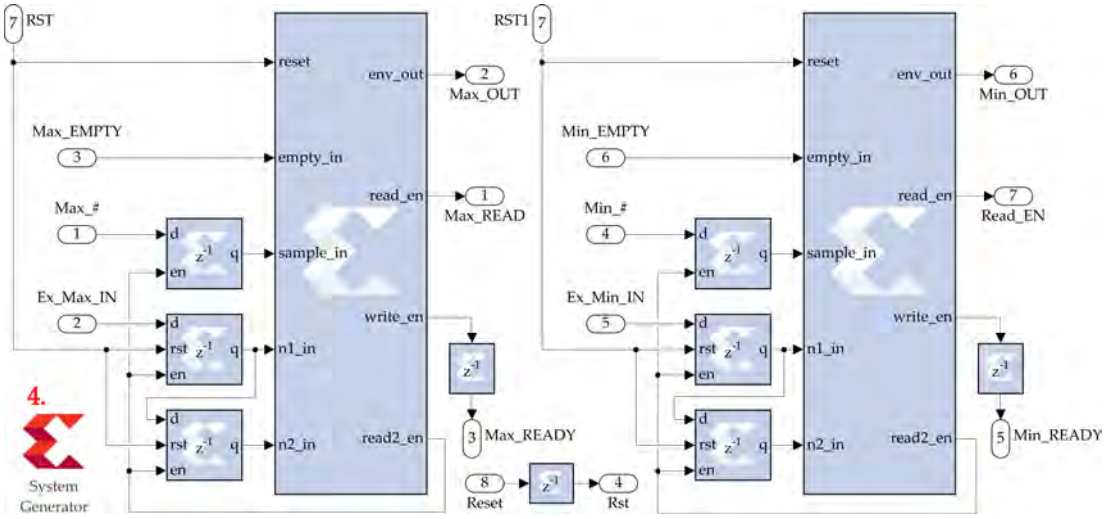

Figure 5.14: The Envelope Generator subsystem.

sample number within the original data. Once the extrema signals for the input signal are complete, they are sent to the Envelope Generator.

4. **Envelope Generation Process**

   The maxima and minima envelopes are generated using linear interpolation. For example, between each local maxima linear interpolation provides data values for the number of samples that are between.

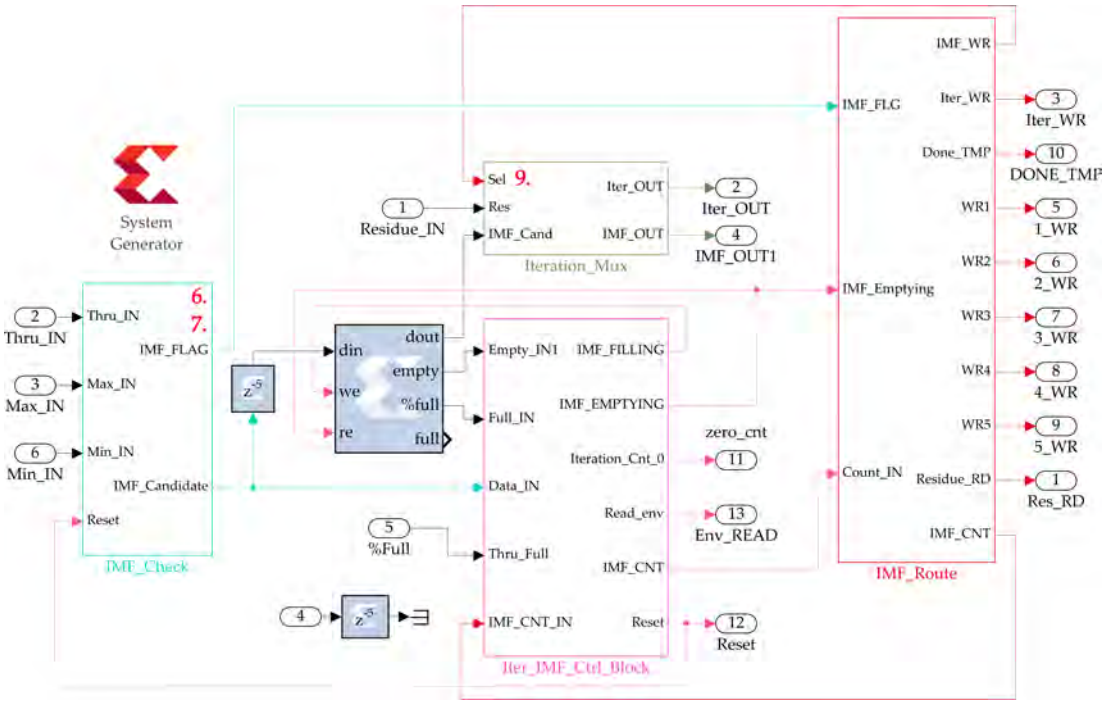

Figure 5.15: The IMF Control subsystem.

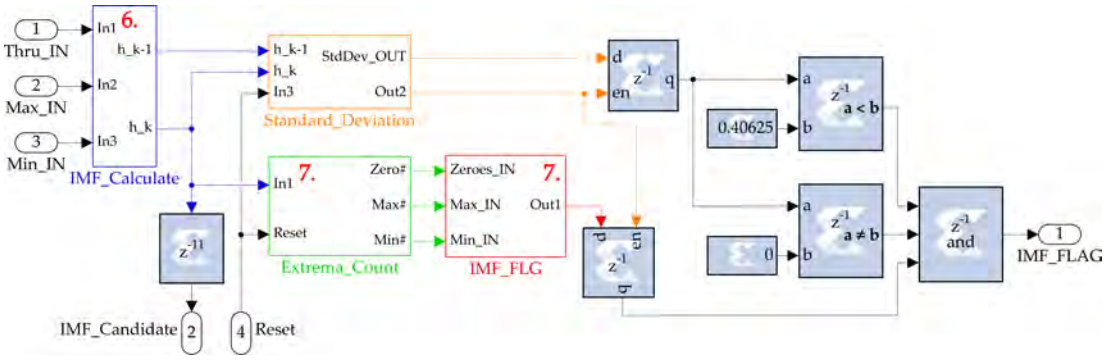

Figure 5.16: The IMF Check sub-subsystem.

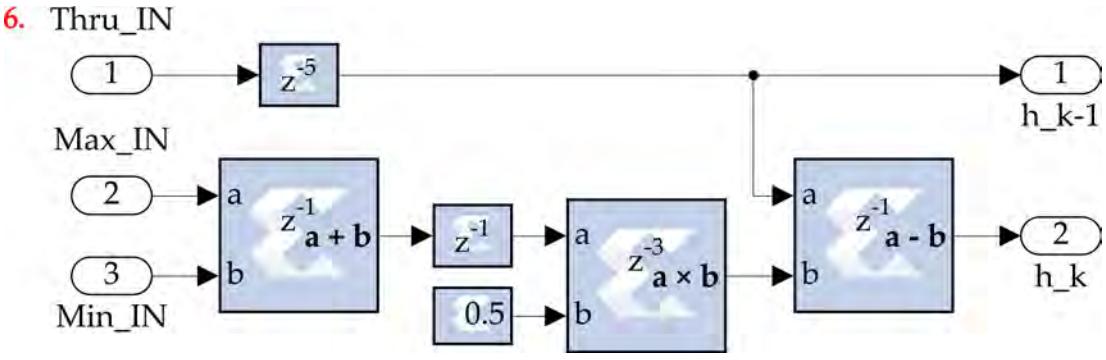

Figure 5.17: The IMF Calculate sub-sub-subsystem.

5. Envelope Buffer

The Envelope Buffer stores the full upper and lower envelopes for the given input signal. Once both envelopes are complete, the signals are

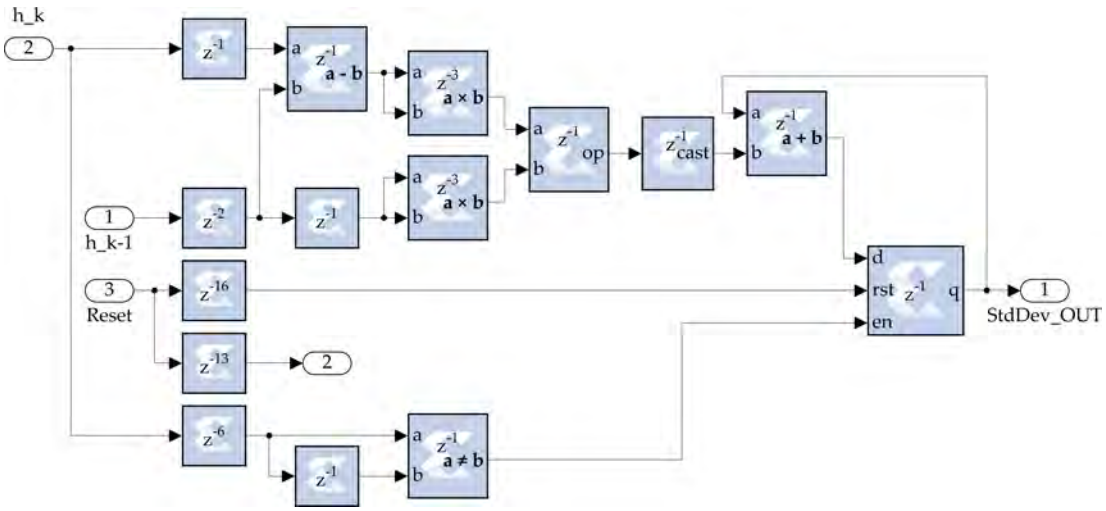

Figure 5.18: The Standard Deviation sub-sub-subsystem.

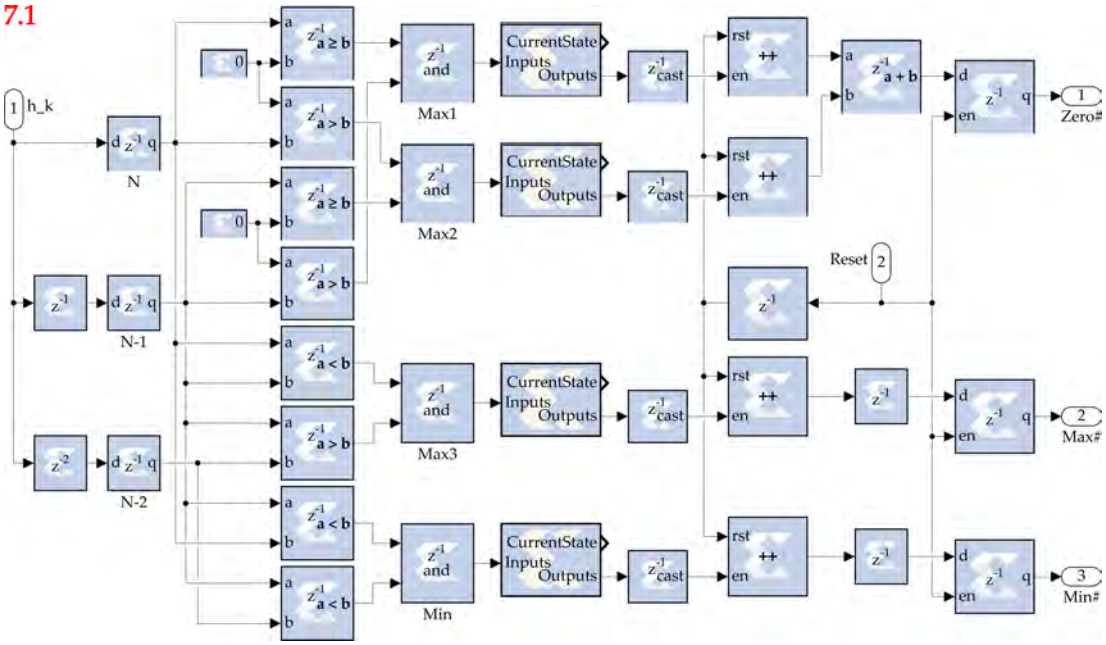

Figure 5.19: The Extrema Count sub-sub-subsystem.

sent to the IMF Calculation Process.

6. **IMF Calculation Process**
   The upper and lower envelopes are averaged to find the mean envelope which is then subtracted from the original input signal.

7. **IMF Check Process**
   The potential IMF is then checked against the criteria for the number of extrema and zero crossings. This is made up by two sub-processes:

   7.1. Counting the number of local maxima, local minima and zero crossings in the potential IMF.

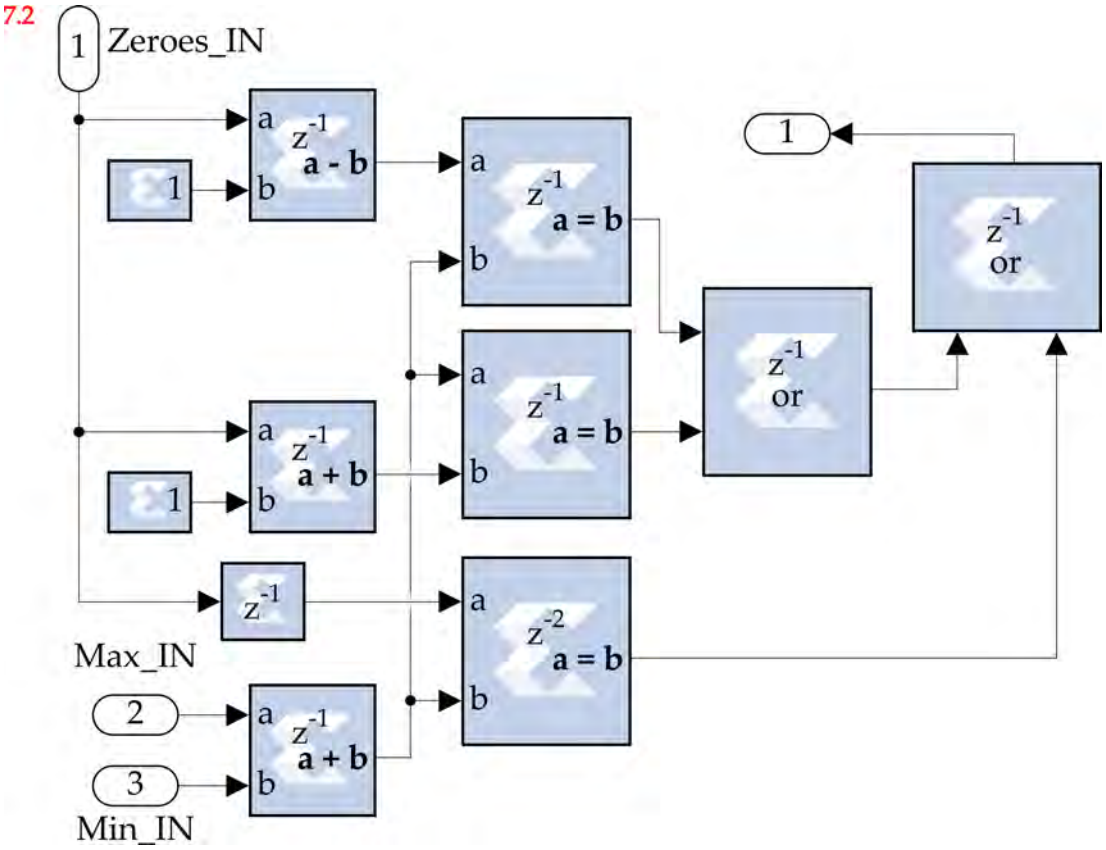

Figure 5.20: The IMF FLG sub-sub-subsystem.

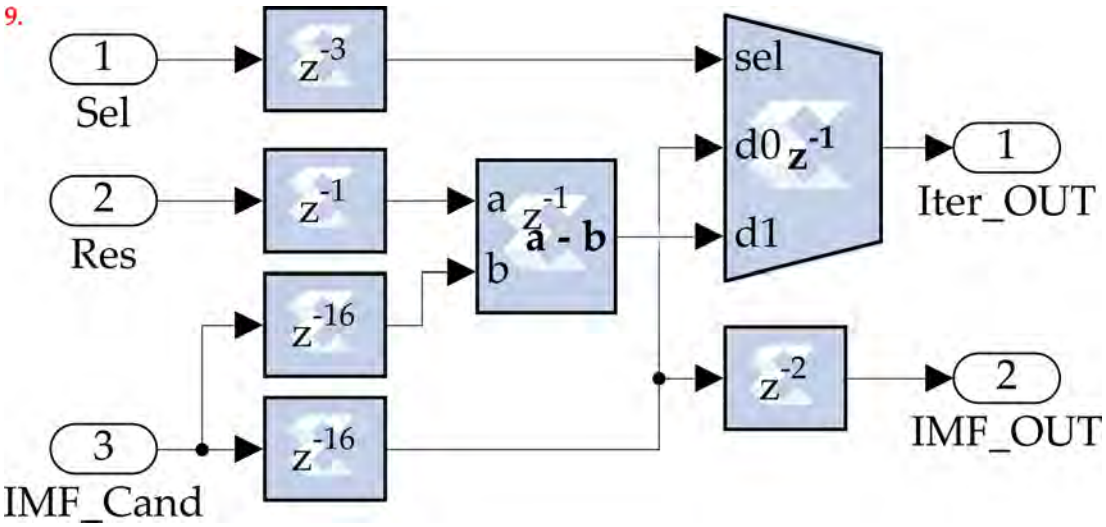

Figure 5.21: The Iteration Mux sub-subsystem.

7.2. Comparing the extrema to the number of zero crossings.

Should a potential IMF fail the criteria, the sifting operation restarts. However, if it satisfies, then it is output into FIFO memory.

8. **IMF Output**
   The confirmed IMF is stored in FIFO memory buffer for output. This system is capable of calculating up to five IMFs.

9. **IMF Subtraction**
   The confirmed IMF is subtracted from the original input signal to provide the input signal for the next iteration (referred to as the residue).

10. **Residue Input Buffer & Subsequent Iterations**
    The residue signal is stored in the Residue Input Buffer and is taken as the input signal for the next iteration. The iteration repeats until either the signal is completely decomposed or five IMFs have been extracted.

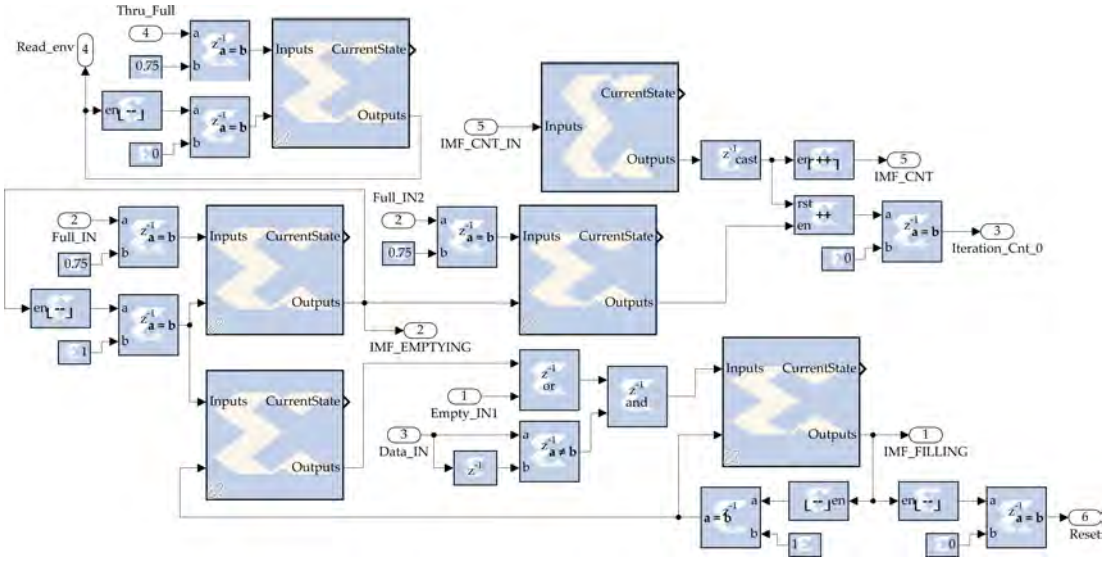

Figure 5.22: The Iter IMF Ctrl sub-subsystem.

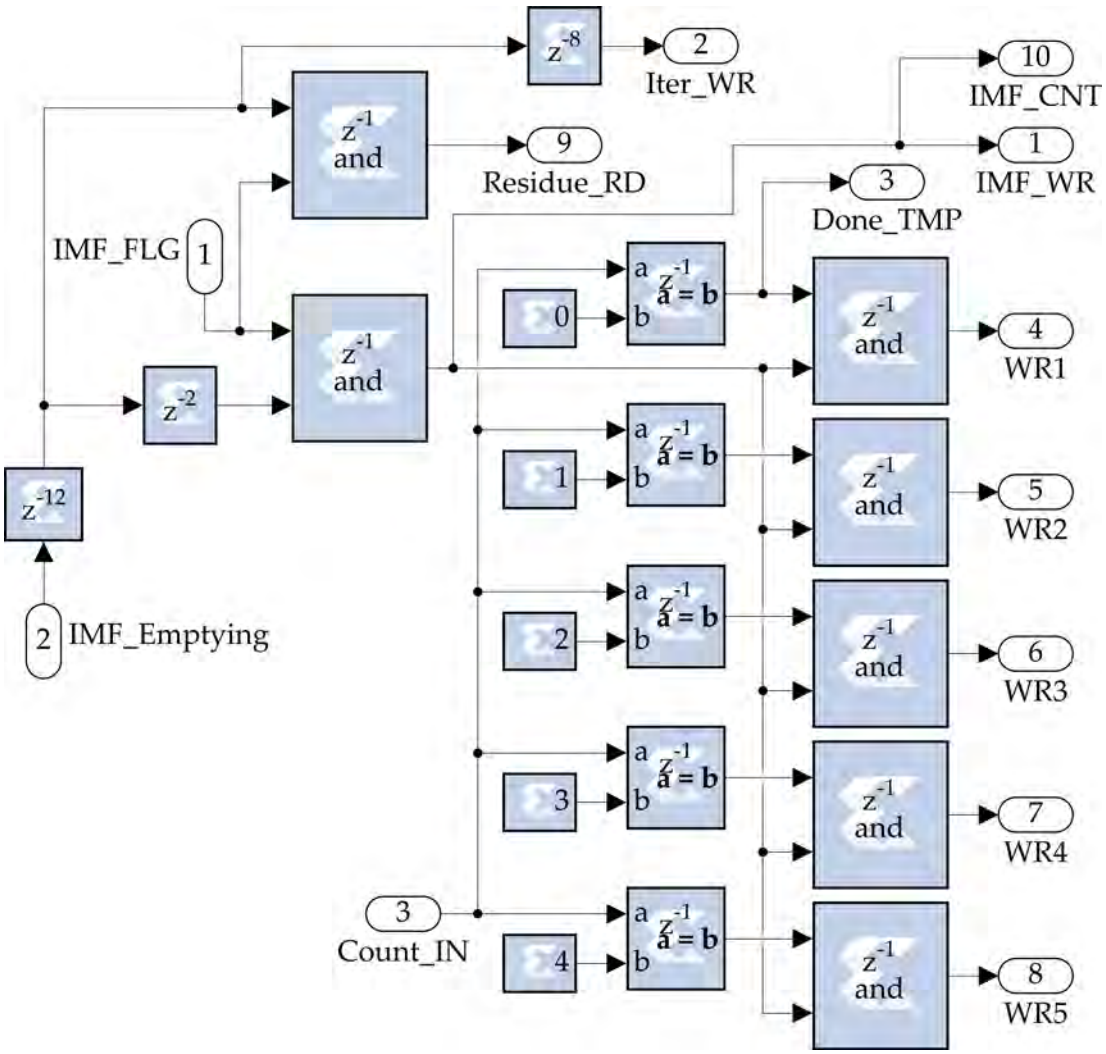

Figure 5.23: The IMF Route sub-subsystem.

5.3.3 System Implementation

The SysGen designs for the WPD and EMD algorithms are generated into an IP block using the Xilinx System Generator token present on the SysGen design. This packages the design into a single HDL system. Xilinx Vivado is then configured to refresh internal IP repositories to enable the IP block to be added into the Vivado Block Design. Each IP block only shows the Xilinx gateways in and out, with incoming and outgoing signals on the left and right of the block respectively. Once the block design is complete, the whole system design is generated in Vivado. This allows the design to be synthesised. In a nutshell, synthesis refers to simulating the design as on the hardware, a necessary step before the system can be implemented. In this context, implementation refers to Vivado programming the synthesised design for operation on the hardware. If successful, the implemented design can be generated into a programmable bitstream to be programmed onto the actual FPGA IC. At this stage the ILA can be utilised to query data from system block ports.

The implementation of the db4 wavelet for a single level of decomposition is successful, the results are presented in Section 5.4. However, the implementation of all three chosen wavelets, and to perform three levels of decomposition, requires more slice Look-Up Tables (LUTs) than are available from the PYNQ-Z2 programmable logic. Approximately, 1 million slice LUTs would be required, available on an FPGA such as the Xilinx Virtex-7 series or similar, but excessive compared to the $13,300$ available on the PYNQ-Z2. An image of a programmable logic cell from the PYNQ-Z2 is given in Figure 5.24. The large number required is a result of the way FPGAs implement high-precision mathematical operations i.e. those with a larger number of binary bits. The implementation splits the bits into manageable sets, performs the operation on each set and then joins the resultant sets back together. The nature of the $40\,\text{bit}$ operations, required to maintain precision between the signed $16\,\text{bit}$ incoming signal and the $25\,\text{bit}$ wavelet coefficients, results in an excessive requirement for CARRY4 cells. Potential solutions include reducing the precision of the wavelet coefficients, or scaling to comply with $16\,\text{bit}$ operations.

For proof of concept, the whole system is built for implementation on a larger VC707 series board. The successful build demonstrates that the system can be readily generated into a bitstream to program the board. For the purposes of IP block testing and real-world experimentation, the system is reconfigured

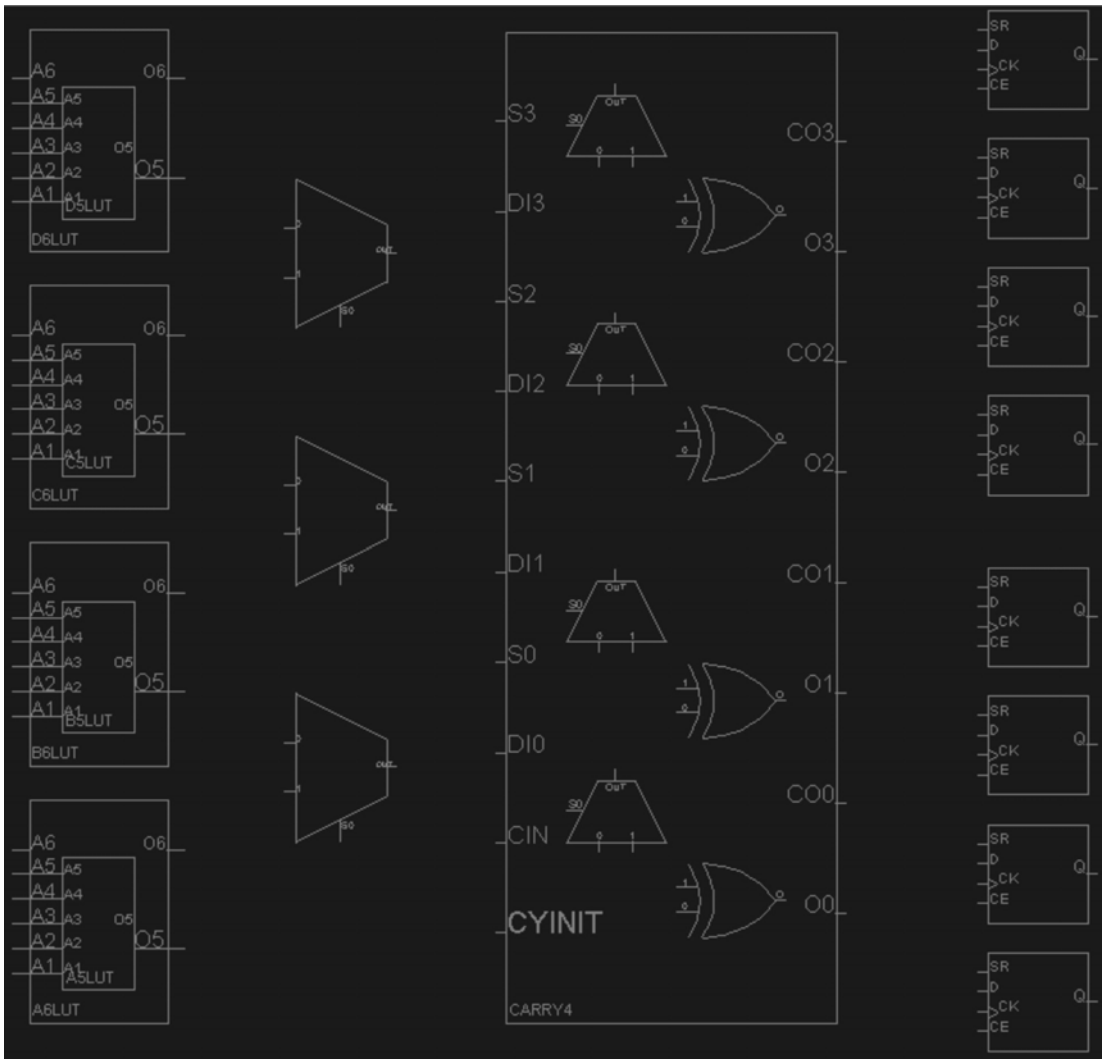

Figure 5.24: Diagram representing typical programmable logic on the Zynq 7020. Note, the different LUTs and the CARRY4 cell.

to test each individual feature extraction algorithm in turn. For brevity, the db4 WPD is used as an example test. Figure 5.25 shows the db4 WPD system design implemented on the PYNQ-Z2 IC Input/Output (IO) pins. Note the microphone input voltage on VP_0. It is important to note, that although it appears that both positive and negative voltage pins are available, the negative pin can still only accept positive voltages (to prevent damage to the IC), the negative aspect is assigned in software only. Figure 5.26 shows the implemented design on the IC programmable logic. The ILA remains a resource intensive IP block, it can be reduced in implementation size on the IC by reducing the sampling rate and the number of probes, however, this would make data extraction problematic. The ILA is superfluous to the operation of the feature extraction and further development would remove the ILA, freeing up space for additional algorithm implementation.

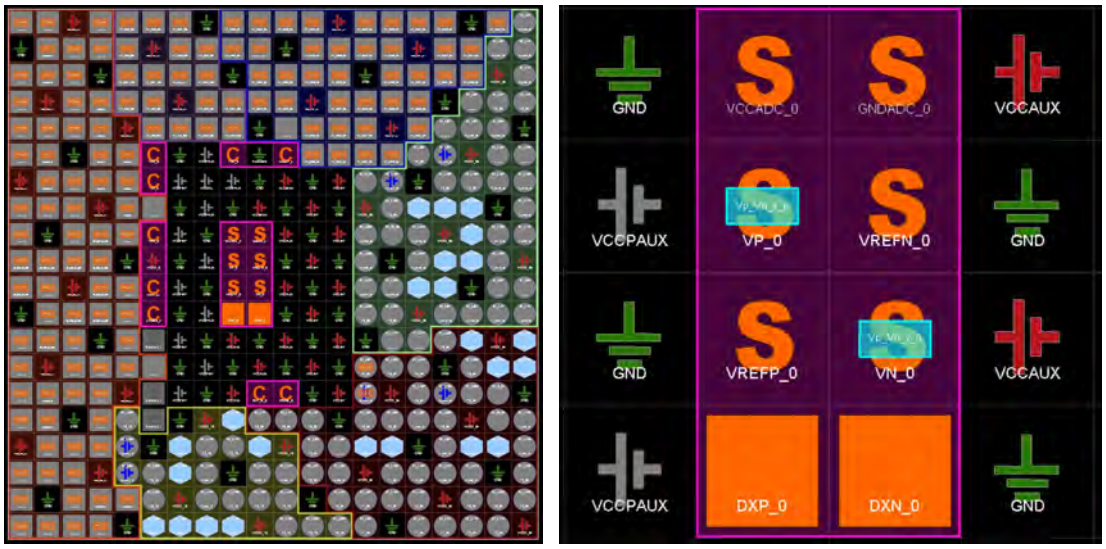

Figure 5.25: IO pins of the implemented Zynq 7020. Left: view of the whole IC. Right: closer view of the central pins, showing pin VP_0 which is the microphone input voltage.

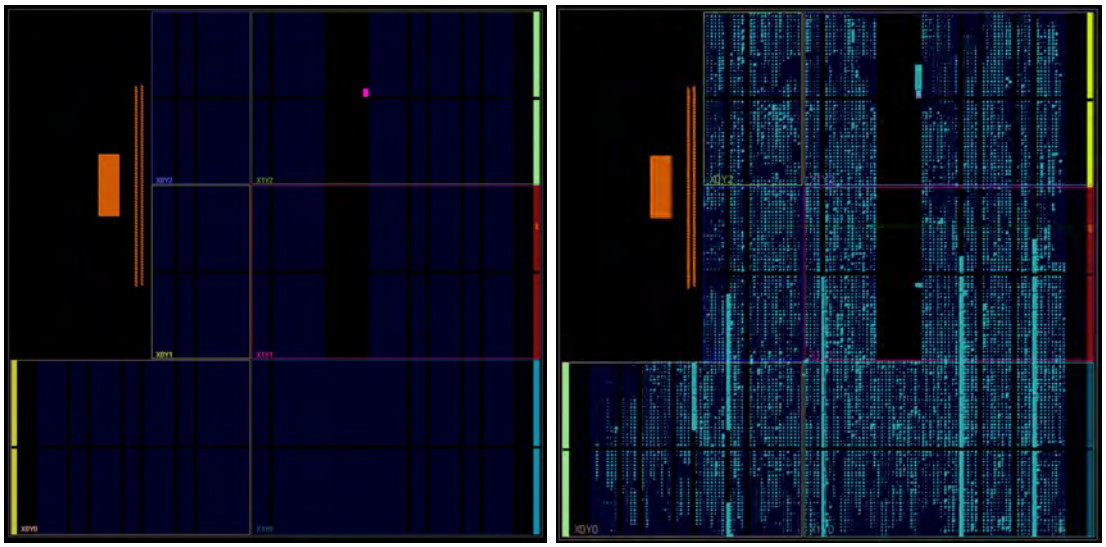

Figure 5.26: The Zynq 7020 device view. Left: the blank device. Right: the device now programmed with the db4 & bior3.5 experiment system.

The aforementioned issues with available resources, preventing three levels of decomposition for three different wavelets, still allows the two smaller wavelets (db4 and bior3.5) to be implemented for parallel simultaneous operation on the PYNQ-Z2, albeit only for a single decomposition. This demonstrates the concept of running two DSP feature extraction algorithms concurrently on a single device in continuous real-time. The results are presented in the next section.

5.4 Experimental Setup

The experimental setup from Section 4.2 is repeated with the following changes. Only the Audio-Technica AT2020 USB+ microphone is setup for acoustic measurements from the three-phase BLDC 36 V 1600 W Unite MY1020 motor. The microphone audio output is connected to the bespoke Arduino microphone shield which is mounted directly onto the Arduino headers present on the PYNQ-Z2 FPGA. The PYNQ-Z2 ADC samples the 0 to 3.3 V signal from the shield and processes it in hardware as per the system previously described. The setup diagram is given in Figure 5.27. Figure 5.28 shows a top down photograph of the PYNQ-Z2 with the bespoke PCB Arduino Microphone Shield attached and connected during the experiment. Additional setup information is provided in Section 5.2 and is summarised here for completeness.

Regarding electrical power connections, the PYNQ-Z2 is connected by USB to a laptop, powering the board and providing a serial data connection. The PCB op-amp circuit is powered independently using an ELC ALF1502D symmetric DC power supply, set to provide a ±12 V DC supply. The PYNQ-Z2 Arduino headers provide 3.3 V power to the diode protection circuit on the PCB. The microphone is powered by USB from the laptop.

The Unite MY1020 BLDC motor has three-phase supply currents measured using isolated high-bandwidth Hall-effect sensors sampled at 250 kHz at 16 bit resolution on an oscilloscope. The motor supply current is delivered by a bespoke Arduino-based PWM control unit. Under certain operating

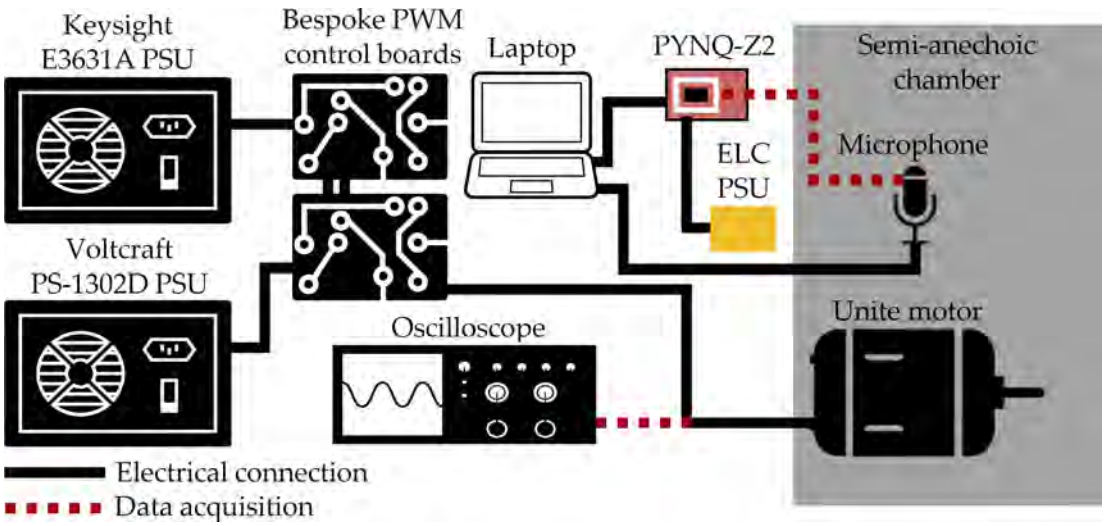

Figure 5.27: Diagram of the experimental setup.

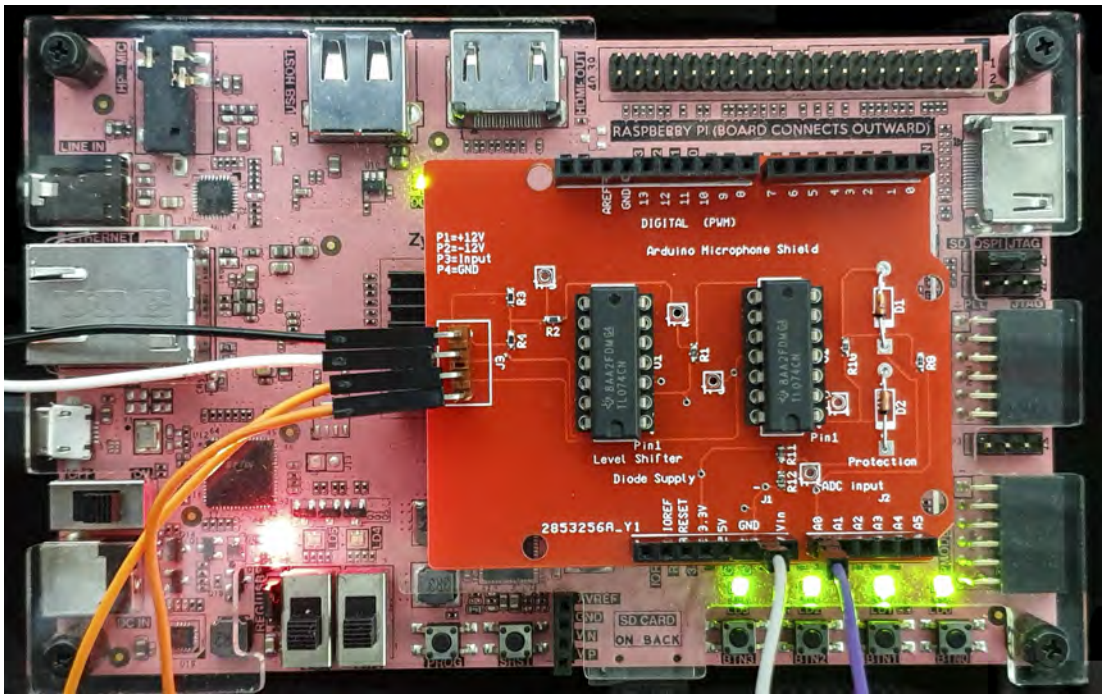

Figure 5.28: Photograph of the PYNQ-Z2 with the bespoke PCB Arduino Microphone Shield taken during the experiment.

conditions, the PWM sequence can become unstable for a whole commutation cycle. A representative example of the supply current instabilities is given in Figure 4.1 from Section 4.1. This case is ideal for real-time diagnostics as the fault occurs during continuous operation of the system, and, does not need to be shutdown to have the mechanical structure modified with a seeded defect. Furthermore, with the fault being erratic and unpredictable, continuous real-time monitoring is necessary.

Two experimental trials are undertaken, with the PYNQ-Z2 programmed with different builds. The first build contains netlist (implemented design) for both db4 and bior3.5 WPD algorithms. The second build only contains the db4 wavelet. Results are presented below for both trials. In addition, the dmey wavelet build is tested, but results cannot be extracted due to insufficient resources for the ILA to function properly. This is due to the dmey wavelet having 102 coefficients for both the high and low pass filters, (204 in total), compared to the db4 wavelet only having 16 in total.

5.5 Results & Discussion

Figures 5.29 and 5.30 present a single-level WPD of the raw microphone signal. Figure 5.29 shows the raw current and microphone signals, followed by the approximation and detail signals which are calculated in Matlab. Figure 5.30 also shows the raw microphone signal, followed by the approximation and detail signals which are calculated in through hardware simulation. Note the excellent similarity between both the approximation signals. The difference between the detail signals is attributable to minor discrepancies stemming from resolution, quantisation and clock timing. Closer analysis of between the two signals reveals that the spectral barrier is slightly different, i.e. the hardware simulation results in a difference in where the frequencies are separated between the high and low pass filters. Nevertheless, these results validate the hardware implementation of the WPD algorithm.

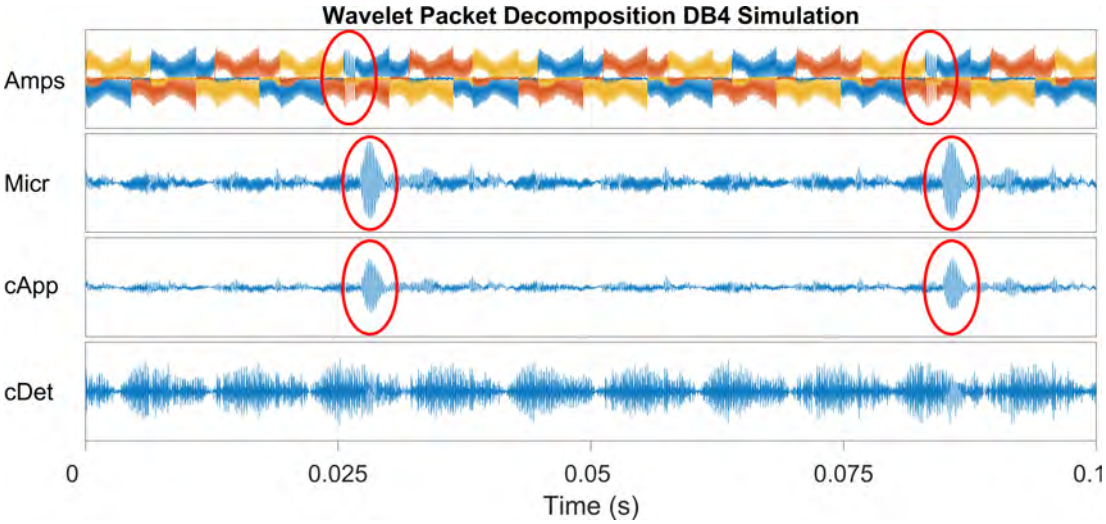

Figure 5.29: db4 WPD of the microphone data. Amps: motor input current plot (−10 to 10 A). Micr: raw microphone signal. cApp & cDet: respective plots of the approximation and detail signals calculated in Matlab. Circles indicate current instability faults.

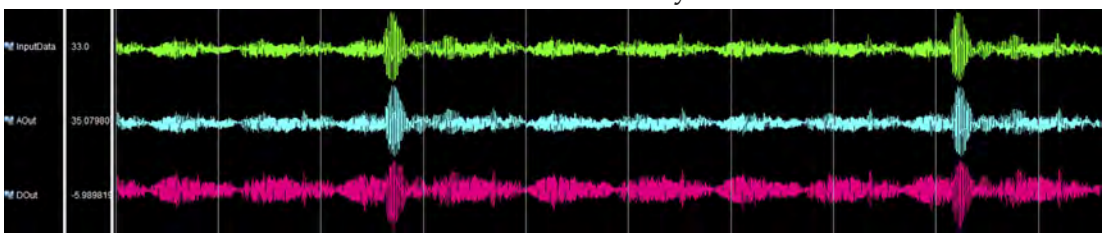

Figure 5.30: Hardware simulation of db4 wavelet IP block performed on the same input data as Figure 5.29. From top down: raw microphone signal, approximation signal, detail signal. Note, the faults are clearly visible, particularly in the approximation signal.

Figure 5.31 presents an EMD of the raw microphone signal, showing five IMFs and the residue calculated in Matlab. By default, Matlab uses cubic spline interpolation to generate the upper and lower envelopes. These are used to calculate the mean, which is subsequently subtracted from input signal. Cubic spline interpolation is substantially more accurate than the linear interpolation implemented in this design. However, this will only be evident given close inspection between the extrema. To give comparable results, Figure 5.32, the design of the EMD implementation required adjustment for the algorithm to operate on the entire test signal. This prevents the signal being separated into the FIFO memory sets required for real-time operation. The performance of the hardware simulation is excellent, delivering a very close match to Matlab. On closer inspection, the signal is substantially less smooth than the Matlab output, i.e. with clear steps visible as the signal is buffered through the sifting process. The implementation of the EMD algorithm onto FPGA requires additional development before the IP block can run on the hardware.

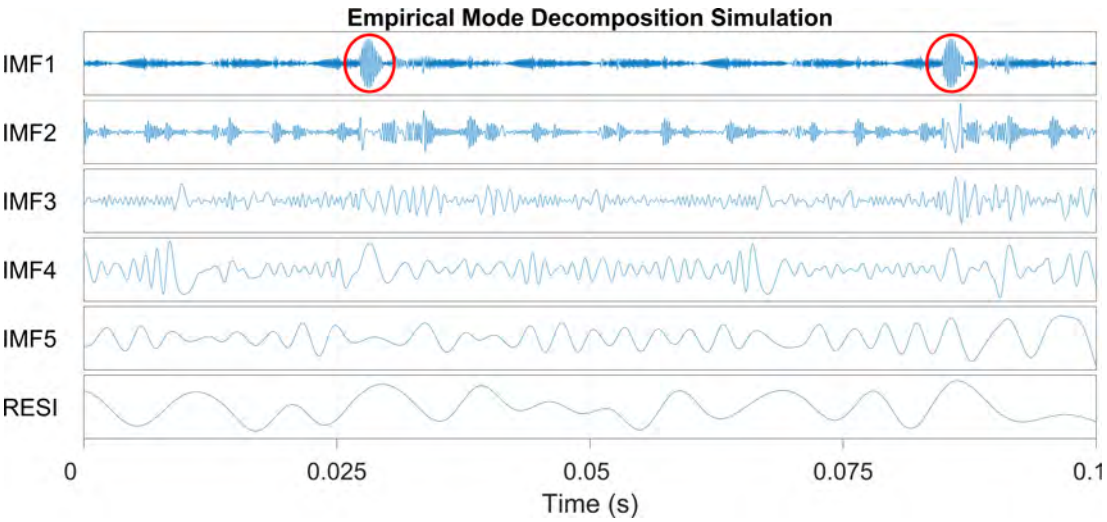

Figure 5.31: EMD of the raw microphone signal performed in Matlab.

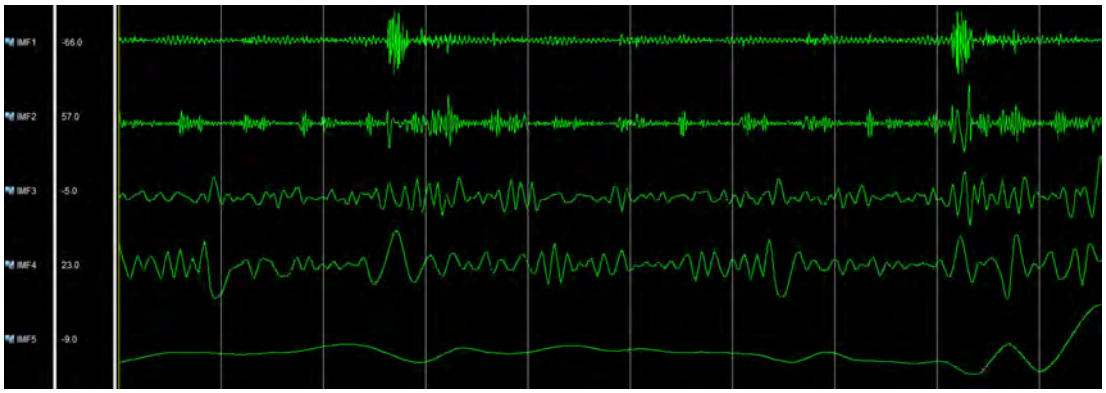

Figure 5.32: Hardware simulation of EMD of the raw microphone signal.

The ILA is used to capture data during the experiment. This involves triggering the ILA manually until a suitable fault feature is present. Figure 5.33 shows an ILA capture, where a current instability has occurred. Describing the image from the top down, the microphone signal from the PYNQ-Z2 ADC (modified by the PCB microphone shield, sampled at 100 kHz 16 bit unsigned), the output of the Reinterpret IP block (signal adjusted to signed 40 bit with 23 bit binary point), the db4 WPD approximation and detail signals, and the bior3.5 WPD approximation and detail signals. This result validates the WPD implementation operates correctly on the PYNQ-Z2 FPGA. Similar results are obtained for the dmey wavelet block. Thus, it can be inferred that the overall system from Figure 5.5, would operate correctly if implemented on an FPGA with additional programmable logic resources. This is also the first known instance of multiple feature extraction algorithms of this nature operating concurrently and continuously in real-time.

Once the design has successfully been implemented in Vivado, it can be analysed for resource utilisation and power consumption. The available programmable logic of the FPGA and the required usage for the db4 & bior3.5 WPD experiment system is presented in Table 5.1. The resources are primarily used by the ILA and the feature extraction block. The ILA specifically requires 62 Block Random Access Memory (BRAM) tiles, ≈44 % of those available. Interestingly the db4 IP block requires 9836 slice LUTs used as logic (≈19 %

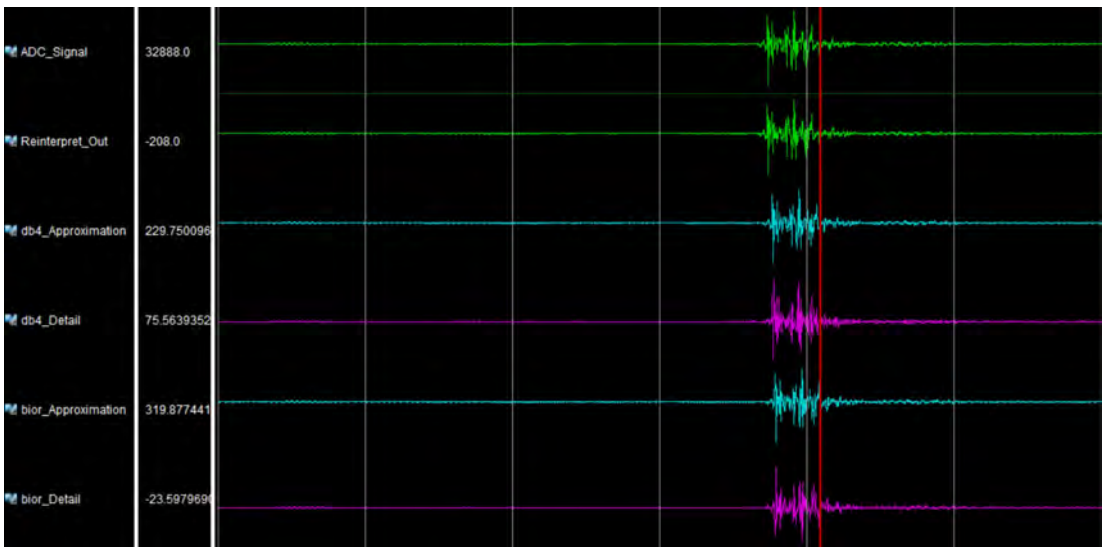

Figure 5.33: Capture from the ILA during the motor experiment. From top down: ADC output signal, Reinterpret block output signal, db4 approximation signal, db4 detail signal, bior3.5 approximation signal, bior3.5 detail signal.

Table 5.1: Utilisation report of the db4 & bior3.5 WPD build (whole), and the db4 only build.

Build	Resource	Utilisation	Available	Utilisation (%)
whole	LUT	29,894	53,200	46.79
	LUTRAM	508	17,400	2.92
	FF	13,009	10,6400	12.23
	BRAM	62	140	44.29
	IO	2	125	1.60
	BUFG	2	32	6.25
db4 only	LUT	13,383	53,200	25.16
	LUTRAM	422	17,400	2.43
	FF	8,164	10,6400	7.67
	BRAM	44.50	140	31.79
	IO	2	125	1.60
	BUFG	2	32	6.25

of those available), but also 4553 slices (≈34 % of those available). Whereas the bior IP block requires 11,311 slice LUTs used as logic (≈21 % of those available), but also 5736 slices (≈43 % of those available). Further breakdown reveals that the slices in most demand (77 % used) are required by the multiply SysGen blocks. This is likely due to them executing within a single system clock cycle, thus adjusting the timings to allow the multiply operation to have 3 system clock cycles, would likely significantly reduce the required number of slices.

Analysis of the power consumption estimates the total on-chip draw to be ≈1.8 W for the db4 only build, and ≈1.9 W for the db4 & bior3.5 build. There will be additional power requirements for the PCB microphone shield and other devices on the board, however, the overall power consumption will remain relatively small (≤≈15 W). The overall power consumption of the system is superior to an equivalent GPP, a reasonable specification laptop for example. For comparison, the Intel i7-6700K CPU has a thermal design power of 91 W, and, must be combined with other powered components bringing the total power draw to likely exceed 300 W. Moreover, the thermal loss of the FPGA board is significantly less than an equivalent GPP which require cooling systems to prevent overheating.

5.6 Conclusions

In this chapter, the concept of simultaneous operation of multiple feature extraction algorithms is pioneered using HDL implementation on FPGA devices. This enables continuous real-time DSP of acoustic measurements from a consumer-grade microphone, delivering real-time fault diagnostics of an electrically-based fault from a BLDC motor drive system. The system is realised through the design and production of a bespoke PCB Arduino Microphone Shield, the development of an FPGA system wrapper containing HDL IP blocks of EMD and several WPD algorithms. System programming to the PYNQ-Z2 FPGA SoC realised experimental system testing and validation on the electrical fault condition. Experimental trials stream acoustic measurements through the PCB shield to be processed by several implementations of WPD simultaneously in continuous real-time with results obtained from the ILA. Hardware simulation results validates the HDL implementations of the feature extraction are successful. Furthermore, experimental results demonstrate accurate DSP from multiple feature extraction algorithms operating simultaneously and continuously in real-time, enabling accurate fault diagnostics. This marks a significant advancement from previous systems that typically match and tailor a single feature extraction method. The use of the parallel processing of FPGAs not only permits multiple algorithms to run concurrently, but also delivers efficient real-time DSP, where conventional GPPs would either lag, or require significant capital cost, high power consumption and thermal cooling to maintain the processing speed required. The FPGA devices are particularly suited to DSP for fault diagnostics owing to their relatively low-cost, low power consumption, reconfigurability, and fast parallel processing. Additionally, this chapter has proposed the use of advanced machine learning techniques for system training, feature extraction control and continuous algorithm tuning and adaptation. Specifically, two modes of operation are defined; training and monitoring. In training mode, the machine learning analyses the multiple extracted feature signals to determine the optimum feature extraction method, or combination thereof. In monitoring mode, the machine learning periodically and continuously adjusts the configuration parameters of the optimum feature extraction stream. This ensures the system delivers maximum diagnostic performance and is continuously adapting to changing operational and environmental characteristics. In summary, this

chapter has presented a concept all-in-one acoustic diagnostic system, and has provided the framework for its development. The system development has made significant steps towards achieving this goal, advancing the current state of acoustic fault diagnostic systems.

Chapter 6

Conclusions

This research project presents a comprehensive investigation into the use of acoustic measurements for fault diagnostics and condition monitoring of industrial systems. In Chapter 1 an in-depth review of the current state-of-the-art is presented with focus on three key areas viz. considerations for diagnostic systems in Section 2.1, and faults originating from mechanical fault modes in Section 2.2, and then electrical fault modes in Section 2.3. Based on the literature studied, outstanding problems concerning the industrial adoption of acoustic measurements for diagnostics and monitoring are defined in Section 1.1 and appropriate research objectives are given in Section 1.2. The subsequent chapters in this research project address the problems defined, and aim to meet the research objectives.

Chapter 3 considered the diagnostic performance of two consumer-grade acoustic sensors (a USB microphone and a smartphone), along with a vibration accelerometer, when applied to the diagnosis of six different Roller Element Bearing (REB) conditions. This suitability study into the use of consumer-grade acoustic sensors for rapid industrial roll-out is the most comprehensive of its kind. The processing and memory capabilities of the smartphone remain restrictive for complex signal processing and large training databases; nevertheless the method presented in this chapter can be readily implemented entirely on a smartphone device enabling on-site diagnostics given a suitable acoustic environment. As a minimum these highly accessible devices can be used for data acquisition and transmission. The experimental results unequivocally demonstrate that consumer-grade acoustic sensors are well-suited to diagnose and monitor fault modes that produce an audible frequency signature. These sensors outperformed the vibration sensor in all cases, particularly where the vibration information was unable to produce reasonable results at lower rotational speeds and lower radial load. Overall, the vibration measurements produced a classification

accuracy of 75 %, where the smartphone and microphone achieved 95 % and 100 % respectively. This is particularly salient owing to the feature extraction and classification operating without bias toward a particular measurement, working by automatically extracting a signature for each REB with no *a priori* input. This is also one of the contributions of this chapter, as training a single system that exhibits multiple classifiers for specific input conditions, has not been performed before. This approach is reasonable as in nearly all rotating machinery the speed and load are closely monitored for information and safety purposes. Prior investigations have experienced difficulty accounting for dynamic operating conditions but this method, expanded to include simple interpolation, now provides a viable solution. This marks a different and novel approach to solving the problems of diminished diagnostic accuracy when including dynamic operating conditions.

Chapter 4 continues the investigation into the use of consumer-grade acoustic sensors. The acoustic sensors are easily transferred to monitor a different application, where the vibration accelerometer could not be moved and reinstalled without major work and risk of damage. This experiment corroborates and adds to the findings from Chapter 3, demonstrating that these sensors are suitable for electrical origin fault modes in addition to mechanical. Furthermore, that these sensors can be used for continuous real-time processing, a necessary step for an industry-ready system.

The main contribution of this chapter is the acoustic diagnostics of electrical origin fault modes. The transient current instability reported has not been documented before and represents a novel and previously unstudied fault condition. Acoustic measurements are used for low-cost real-time detection of an acute electrical origin fault mode that manifests sporadically under well-bound operating conditions on a BrushLess Direct Current (BLDC) motor drive system. The fault is a transient current instability that arises in the motor supply from the controller due to the non-linear interaction of the Pulse Width Modulation (PWM)-controller parameters, parasitic components and digital controller realisation. This example fault is explored in this chapter as a representative case for diagnostics of a wider variety of electrical origin fault modes. In agreement with Chapter 3, the USB microphone performed marginally better due to the larger and more accessible diaphragm. However, the smartphone offers the potential to become an all-in-one future diagnostic tool given the obvious advantages of being established, easily

accessible, relative low-cost, self-powering, remote from the system, and with internet and other communication built in. This research may provide the stimulus for the widespread adoption of consumer-grade sensors and smartphone technology for fault detection and monitoring of both mechanical and electrical systems and fault modes. This chapter also makes an additional step towards an industry-ready diagnostic system through the demonstration of continuous real-time signal processing. The current instability fault manifests sporadically and unpredictably without any form of triggering or artificial damage which makes it an ideal candidate for continuous real-time monitoring. This is achieved but only for a relatively short time duration. To achieve practical monitoring, i.e. continuous real-time, and lower operational costs, further development is required and is given in Chapter 5.

Chapter 5 further extends the research from Chapters 3 and 4 through the implementation of time-frequency feature extraction Digital Signal Processing (DSP), realised in continuous real-time through programmable Field-Programmable Gate Array (FPGA) hardware. There are two primary contributions stemming from this chapter. First, the realisation of multiple continuous real-time feature extraction algorithms operating concurrently in parallel. The Wavelet Packet Decomposition (WPD) and Empirical Mode Decomposition (EMD) algorithms are designed for Hardware Description Language (HDL) implementation, and several variations of WPD (using different mother wavelets) and EMD are programmed for simultaneous operation on an FPGA device. Results from experimental trials, demonstrating two different WPD algorithms running together, validate the implementation on programmable hardware. This is the first known instance of multiple feature extraction algorithms running simultaneously in real-time. Second, the proposed concept of developing an 'all-in-one' acoustic diagnostic system capable of training and adapting to new faults and changing operational characteristics. Specifically, the use of advanced machine learning for system training, feature extraction control and continuous algorithm tuning and adaptation. In training mode, machine learning examines multiple extracted feature signals, determining the optimum feature extraction pathway or combination thereof. In monitoring mode, the machine learning periodically and continuously adjusts the configuration parameters of the optimum feature extraction stream. Presently, a system of this level of sophistication has not been proposed in the literature. If realised, it would be capable of training on

multiple fault modes and industrial systems, providing excellent diagnostic accuracy with no additional input required to match or tailor the feature extraction process. Further, it would be adaptable to changing operational and environmental characteristics, ensuring maximum diagnostic accuracy. This chapter has provided a substantial leap towards this end goal.

An additional contribution is that the implementation has been performed on a newly released FPGA development board (the PYNQ-Z2). This work may provide the stimulus for further development through FPGA implementation and also serve as a guide for others looking to employ similar FPGA development boards.

6.1 Project Contributions & Main Findings

The main contributions to knowledge and the main findings from this research are summarised below.

1. The use of acoustic measurements for fault diagnostics and condition monitoring of industrial systems has the potential to vastly improve the performance and cost to benefit ratio of established systems by either augmentation or replacement. Acoustic measurements can provide advantages including; earlier and more accurate detection of emerging changes, significantly improved cost to benefit performance, readily available and easy to use sensors, simpler setup and operation, and no detrimental impact on nominal system integrity by employing remote sensors. This is demonstrated experimentally in Chapters 3 and 4.

2. Consumer-grade acoustic sensors such as those found in smartphones or other voice recording microphones are ideally suited for diagnostics and monitoring for fault modes where the signature produced is in the audible frequency range. These sensor types can provide excellent diagnostic accuracy at early stages of fault formation and propagation. They are also remote from the system and can be easily transferred to other applications or replaced if damaged. This is demonstrated experimentally in Chapters 3 and 4. The processing and memory capabilities of smartphones remain restrictive for complex signal processing and large training databases, nevertheless smartphone type devices could be rapidly rolled-out for rapid on-site diagnostics or as a minimum for data acquisition and transmission.

3. The multi-Support Vector Machine (SVM) classification system presented in Chapter 3 represents a novel solution to the problem of degraded diagnostic performance for systems monitoring across dynamic operational parameters and conditions. The solution is reasonable as the operating parameters must be known and closely monitored values. Although a simple solution at this stage, it could be easily expanded to include interpolation allowing for accurate performance across all conditions as required.

4. The implementation of complex feature extraction and machine learning algorithms requires programmable hardware in order to achieve continuous real-time processing at reasonable costs and power consumption. FPGAs are best suited to this task and Chapter 5 has demonstrated low-cost continuous real-time acoustic diagnostics of an electrical fault mode using time-frequency feature extraction algorithms.

5. The enormous parallelism available in most FPGAs allows multiple feature extraction algorithms to be programmed to operate concurrently in continuous real-time. Chapter 5 provides the first known instance of this using a newly released FPGA development board (PYNQ-Z2). This work is able to serve as a guide for future researchers.

6. The proposed 'all-in-one' solution, describes a highly sophisticated system that utilises advanced machine learning for system training, feature extraction control and continuous algorithm tuning and adaptation. The foundation to develop this system is provided in Chapter 5. This approach solves problems including; single application design, improper feature extraction configuration, and system multi-application monitoring. The novelty here is two-fold. The approach of programming multiple feature extraction algorithms to solve multiple applications has not been proposed in the literature studied. Combining with advanced machine learning, this is the first attempt to develop an 'all in one' diagnostic solution.

In addition, research publications [1]–[3] have resulted from this project. These are included at the end of this document.

6.2 Project Evaluation

A project evaluation now examines how the original research objectives from Section 1.2 have been fulfilled and whether the problems, Section 1.1, have been sufficiently addressed.

6.2.1 Objectives

Objective 1

> *Investigate the potential simplicity of an acoustic diagnostic system for a mechanical fault mode - with a focus on the suitability of consumer-grade sensors for industrial adoption in the field.*

Chapter 3 achieves this objective, corroborated by Chapter 4. A very simple acoustic system that employs consumer-grade sensors provides very accurate diagnostics on a typical mechanical fault mode. The sensors are robust and easily transferable to other applications, remote from the system, achieve a very high benefit to cost ratio, and provide earlier and more accurate diagnostics than the established counterpart. Therefore these sensors are well-suited for adoption by industry.

Objective 2

> *Investigate the application of acoustic diagnostic methods to electrical fault modes.*

Chapter 4 looks specifically at a newly documented electrical origin fault mode. Acoustic sensors setup to perform an experiment to evaluate their effectiveness in diagnosing this fault. The results demonstrated that this type of fault is easily diagnosed using acoustic methods, even with consumer-grade sensors and with real-time processing. However, further research into other electrical fault modes is required to reinforce the results presented here.

Objective 3

> *Demonstrate real-time fault diagnostics for a naturally occurring fault that does not require human intervention to trigger or for the system to be shutdown.*

Chapter 4 achieves this through an experiment to diagnose an electrical current instability arising in the digital PWM controller of a BLDC motor

drive system. The current instability is transient and manifests sporadically and unpredictably with no human intervention under bound operating conditions.

Objective 4

> *Investigate the potential scope of reprogrammable hardware for use in the field of acoustic diagnostics and condition monitoring.*

Chapter 5 provides information on an example fault diagnostic system realised through FPGA. It is clear that FPGA hardware represents an obvious choice for a viable real-time processing solution. The potential for FPGA devices to expand DSP capabilities vastly increases the opportunities to exploit bigger and better feature extraction and decision making techniques, leading to a marked improvement in diagnostic accuracy and a wider variety of monitoring capabilities.

6.2.2 Problems

Problem 1

> *The vast majority of investigations into acoustic fault diagnostics and condition monitoring employ specialist research-grade piezoelectric transducers that are surface mounted to the component under test and monitor Acoustic Emission (AE) frequencies. Whilst laudable and of interest, in many cases consumer-grade sensors would be capable of providing comparable diagnostic performance. Further, these consumer-grade systems do not require complex pre-amplification, specialist cabling and Analogue to Digital Converter (ADC) equipment, and they provide a significantly improved cost to benefit ratio. Although some examples using consumer-grade sensors are available, there is still much development to prove the suitability of these sensors for a wide variety of monitoring applications.*

The work presented in Chapters 3 and 4 demonstrates the use of consumer-grade acoustic sensors on two different fault mode types. In particular, Chapter 3 shows how even very simple diagnostic systems can provide excellent performance. The publications [1]–[3] have contributed this research to the wider audience and thus this problem has been largely solved.

Problem 2

> *In nearly all reported experiments into acoustic fault diagnostics, the fault is artificially created through human intervention as a research exercise. The fault is nearly always created by intentionally causing physical damage to the mechanical integrity of the component. This provides data sets in the extreme healthy and damaged states, with no data for natural fault formation or propagation. It also has the added disadvantage of preventing continuous real-time diagnostics as the system must be shutdown, disassembled and reassembled with the damaged component. The delay and reassembly of the system may induce unintended changes within the data that could unintentionally skew the results.*

The experiment undertaken in Chapter 4, combined with publications [2], [3] demonstrates acoustic diagnostics of a fault mode that manifests without human triggering and with no artificial intervention or system damage whilst the system is in operation. Unfortunately, in this case the fault does not develop or propagate due to the electrical nature of the current instability. Nevertheless, this fault mode is an ideal candidate to demonstrate continuous real-time monitoring. For these reasons this problem is solved, although further work on a fault mode that develops over a long time period would further add to this case.

Problem 3

> *There have been very few examples of continuous real-time processing for acoustic condition monitoring and this is a critical success factor for an industry-ready system.*

The continuous real-time diagnostics demonstrated in Chapters 4 and 5, combined with publications [2], [3] clearly shows how real-time processing can be easily implemented using both General Purpose Processors (GPPs) and FPGA.

Problem 4

> *Continuous real-time processing of more complex feature extraction and machine learning algorithms is difficult and extremely costly to achieve on GPPs. The costs of implementing a continuous processing system on GPPs not only include very high specification and costly components but also high operational costs from high power consumption and cooling requirements.*

The work in Chapter 5 presents a low-cost and low-power solution with complex feature extraction implemented for real-time processing on a PYNQ-Z2 FPGA development board. This problem is therefore solved.

Problem 5

> *Achieving excellent diagnostic performance for most applications requires expert setup with appropriate selection and configuration of feature extraction and decision making algorithms. A diagnostic system is typically designed for a specific application with performance demonstrated in a single environment.*

The work in Chapter 5 presents a novel solution in the form of a highly adaptive system that can be used to diagnose and monitor a wide range of applications in different environments. Although this system remains in its infancy and requires further development, the concept demonstrated solves this problem.

Problem 6

> *The adoption of FPGA to implement the complex feature extraction and machine learning algorithms is very small. Although there are some examples where a single feature extraction algorithm has been implemented, there is very little in the field of acoustic condition monitoring and nothing regarding multiple concurrent algorithms.*

Once again, Chapter 5 presents the complete implementation of multiple feature extraction on FPGA, thus this problem has been addressed.

Problem 7

> *There remains much debate over the 'best' feature extraction and machine learning algorithms suitable for acoustic condition monitoring and fault diagnostics. Investigations into algorithm performance should be based*

> *on simulated data, and those based on experimental data (particularly where the data set is not publicly available) should not be given too much credence. In addition, the choice of the analysing domain, inherent algorithm and algorithm configuration should be tailored to the application.*

The theory presented in Section 2.1 contains a lot of information for appropriate selection of the analysing domain and feature extraction algorithm. Although further debate and research will always continue on this topic, ever advancing the field, it is hoped that the work presented aids in understanding and enables better choices to be made by others in the future.

Problem 8

> *To date, there is little to no literature addressing fault diagnostics for electrical fault modes, particularly when considering the use of acoustic measurements. Further, the majority of the electrically-based diagnostic techniques require specialist expertise to setup, are difficult to add to established systems, and the results can be difficult to interpret without expert knowledge.*

The definitions and theory presented in Chapter 1 hopefully provides clarity on the differences between mechanical and electrical fault modes in this work. The experiment presented in Chapter 4 combined with publications [2], [3] represent the first documented diagnostics of an electrical fault mode of this type. The acoustic sensors used do not require any specialist setup and the results are easily interpreted. Therefore, it is reasonable to state that this problem has been solved.

6.3 Recommendations & Further Investigation

The work in this project highlights a number of recommendations that if implemented can have a positive impact in the field of industrial fault diagnostics and condition monitoring.

1. Rapid adoption and roll-out of acoustic diagnostics for audible fault modes using consumer-grade devices such as smartphones and USB microphones. Permanent microphones can be easily installed nearby and smartphones can, as a minimum, be used to record and upload data and

receive the diagnostic result, for rapid on-site diagnostics.

2. Utilise FPGAs to implement more complex signal processing in real-time and thus have a more industry ready system.

3. Employ machine learning techniques for more advanced problems and ensure that these are robust across a range of acoustic environments.

Throughout this project a number of areas for further development and research have become apparent. These are listed below.

1. The multi-application diagnostic system developed through FPGA implementation requires further development to incorporate a wider variety of feature extraction algorithms and the autonomous machine learning techniques that focus on novelty detection and control.

2. Although many machine learning algorithms exist, the development of current and new machine learning techniques will deliver the greatest performance benefits to diagnostic systems.

3. More work studying the formation of many mechanical faults is warranted. The use of AE sensors to detect mechanical fault formation, rather than early formed stages, is a critical step to diagnosing faults at the earliest possible stage.

4. Additional long-term experimentation into the propagation and development of faults is also recommended. Many works have only focused on extreme healthy and unhealthy conditions and data is lacking for the formation and early development of the fault.

5. Experimental investigations into other electrical fault modes will support the results presented in Chapter 4. For example, an investigation into a power electronics fault causing issues with supply power to an electric motor drive system.

References

[1] J. Grebenik, Y. Zhang, C. Bingham, and S. Srivastava, "Roller element bearing acoustic fault detection using smartphone and consumer microphones - comparing with vibration techniques," in *Proceedings of the 17th International Conference on Mechatronics - Mechatronika (ME)*, IEEE, Prague, Czech Republic: IEEE, 2016, pp. 1–7.

[2] J. Grebenik, C. Bingham, and S. Srivastava, "Continuous acoustic monitoring of electrical machines; processing signals from USB microphone & mobile smartphone sensors detecting DC motor controller fault," in *Proceedings of the 5th International Conference on Control, Decision & Information Technologies (CoDIT)*, IEEE, Thessaloniki, Greece: IEEE, 2018, pp. 677–682.

[3] J. Grebenik, C. Bingham, and S. Srivastava, "Acoustic diagnostics of electrical origin fault modes with readily available consumer-grade sensors," *IET Electric Power Applications*, 2019. [Online]. Available: https://doi.org/10.1049/iet-epa.2019.0232.

[4] M. Destrade and G. Saccomandi, "Linear elastodynamics and waves," *Continuum Mechanics*, vol. 2, pp. 1–31, 2012.

[5] J. Willett. (2003). The technology of RF condensor microphones, Sennheiser UK, [Online]. Available: http://www.ips.org.uk/files/09_Technology_of_RF_Condenser_Mics.pdf (Accessed: 2017-11-06).

[6] P. White. (1998). Capacitor microphones explained, Sound On Sound, [Online]. Available: http://www.soundonsound.com/sos/feb98/articles/capacitor.html (Accessed: 2018-11-06).

[7] I. Ladabaum, X. Jin, H. T. Soh, A. Atalar, and B. T. Khuri-Yakub, "Surface micromachined capacitive ultrasonic transducers," *IEEE Transactions on Ultrasonics, Ferroelectrics, and Frequency Control*, vol. 45, pp. 678–690, 3 1998. [Online]. Available: https://doi.org/10.1109/58.677612.

[8] (2018). Microphones: polar pattern / directionality, Shure, [Online]. Available: http://www.shure.eu/support_download/educational_content/microphones-basics/microphone_polar_patterns (Accessed: 2018-11-06).

[9] K. Farrar, "Soundfield microphone - design and development of microphone and control unit," *Wireless World*, pp. 48–50, 1979.

[10] K. Farrar, "Soundfield microphone 2 - detailed functioning of control unit," *Wireless World*, pp. 99–103, 1979.

[11] C. M. Chorpening, "Contact microphone," pat., 1955.

[12] P.-C. Eccardt, K. Niederer, and B. Fischer, "Micromachined transducers for ultrasound applications," in *Proceedings of the International Ultrasonics Symposium*, IEEE, vol. 2, Toronto, Ontario, Canada: IEEE, 1997, pp. 1609–1618.

[13] Mistras - Physical Acoustics Corporation. (2018). S9208 - 20-1000 kHz miniture high fidelity displacement sensor, Mistras - Physical Acoustics Corporation, [Online]. Available: https : / / www . physicalacoustics . com / by - product / sensors / S9208 - 20 - 1000 - kHz - Miniature - High - Fidelity - Displacement - AE - Sensor (Accessed: 2018-11-07).

[14] O. Kroymann, "The optical microphone - introduction of a new technology," The Liverpool Institue of Performing Arts, 2005.

[15] Z. Du, L. Lu, W. Zhang, B. Yang, S. Wu, Y. Zhao, F. Xu, Z. Wang, H. Gui, J. Liu, and B. Yu, "High accuracy fiber optical microphone in a DBR fiber laser based on a nanothick silver diaphragm by self mixing technique," *Optics Express*, vol. 21, pp. 30 580–30 590, 25 2013. [Online]. Available: https://doi.org/10.1364/OE.21.030580.

[16] J. a. G. V. Teixeira, I. T. Leite, S. Silva, and O. Frazão, "Advanced fiber-optic acoustic sensors," *Photonic Sensors*, vol. 4, no. 3, pp. 198–208, 2014. [Online]. Available: https : / / doi . org / 10 . 1007 / s13320-014-0148-5.

[17] T. J. Holroyd, "The application of AE in condition monitoring," in *Proceedings of the British Institute of Non-Destructive Testing Conference on Condition Monitoring (BINDT CM2005)*, British Institute of Non-Destructive Testing (BINDT), vol. 47, Cambridge, United Kingdom: Holroyd Instruments Ltd., 2005, pp. 481–485.

[18] A. Graps, "An introduction to wavelets," *IEEE Computational Science and Engineering*, vol. 2, pp. 50–61, 2 1995. [Online]. Available: https: //doi.org/10.1109/99.388960.

[19] M. Entezami, E. Stewart, J. Tutcher, W. Driscoll, R. Ellis, G. Yeo, Z. Zhang, C. Roberts, T. Kono, and S. Bayram, "Acoustic analysis techniques for condition monitoring of roller bearings," in *Proceedings of the 6th Railway Condition Monitoring Conference*, IET, Birmingham, United Kingdom: IET, 2014, pp. 1–8.

[20] V. K. Rai and A. R. Mohanty, "Bearing fault diagnosis using FFT of intrinsic mode functions in hilbert-huang transform," *Mechanical Systems and Signal Processing*, vol. 21, pp. 2607–2615, 6 2007. [Online]. Available: https://doi.org/10.1016/j.ymssp.2006.12.004.

[21] N. G. Nikolaou and I. A. Antoniadis, "Rolling element bearing fault diagnosis using wavelet packets," *NDT&E International*, vol. 35, pp. 197–205, 3 2002. [Online]. Available: https://doi.org/10.1016/S0963-8695(01)00044-5.

[22] D. Mba and R. B. K. N. Rao, "Development of acoustic emission technology for condition monitoring and diagnosis of rotating machines; bearings, pumps, gearboxes, engines and rotating structures," *The Shock and Vibration Digest*, vol. 38, pp. 3–16, 1 2006. [Online]. Available: https://doi.org/10.1177/0583102405059054.

[23] W. He, Z.-N. Jiang, and K. Feng, "Bearing fault detection based on optimal wavelet filter and sparse code shrinkage," *Measurement*, vol. 42, pp. 1092–1102, 7 2009. [Online]. Available: https://doi.org/10.1016/j.measurement.2009.04.001.

[24] K. Feng, Z. Jiang, W. He, and Q. Qin, "Rolling element bearing fault detection based on optimal antisymmetric real laplace wavelet," *Measurement*, vol. 44, pp. 1582–1591, 9 2011. [Online]. Available: https://doi.org/10.1016/j.measurement.2011.06.011.

[25] P. K. Kankar, S. C. Sharma, and S. P. Harsha, "Rolling element bearing fault diagnosis using wavelet transform," *Neurocomputing*, vol. 74, pp. 1638–1645, 10 2011. [Online]. Available: https://doi.org/10.1016/j.neucom.2011.01.021.

[26] M. Amarnath and I. R. P. Krishna, "Empirical mode decomposition of acoustic signals for diagnosis of faults in gears and rolling element bearings," *IET Science, Measurement and Technology*, vol. 6, pp. 279–287, 4 2011. [Online]. Available: https://doi.org/10.1049/iet-smt.2011.0082.

[27] P. Konar and P. Chattopadhyay, "Bearing fault detection of induction motor using wavelet and support vector machines (SVMs)," *Applied Soft Computing*, vol. 11, pp. 4203–4211, 6 2011. [Online]. Available: https://doi.org/10.1016/j.asoc.2011.03.014.

[28] G. F. Bin, J. J. Gao, X. J. Li, and B. S. Dhillon, "Early fault diagnosis of rotating machinery based on wavelet packets - empirical mode decomposition feature extraction and neural network," *Mechanical Systems and Signal Processing*, vol. 27, pp. 696–711, 2012. [Online]. Available: https://doi.org/10.1016/j.ymssp.2011.08.002.

[29] Y. Lei, J. Lin, Z. He, and M. J. Zuo, "A review on empirical mode decomposition in fault diagnosis of rotating machinery," *Mechanical Systems and Signal Processing*, vol. 35, pp. 108–126, 1-2 2013. [Online]. Available: https://doi.org/10.1016/j.ymssp.2012.09.015.

[30] M. A. F. Pimentel, D. A. Clifton, L. Clifton, and L. Tarassenko, "A review of novelty detection," *Signal Processing*, vol. 99, pp. 215–249, 2014. [Online]. Available: https://doi.org/10.1016/j.sigpro.2013.12.026.

[31] M. M. M. H. Da Costa Cesar; Kashiwagi, "Rotor failure detection of induction motors by wavelet transform and fourier transform in non-stationary condition," *Case Studies in Mechanical Systems and Signal Processing*, vol. 1, pp. 15–26, 2015. [Online]. Available: https://doi.org/10.1016/j.csmssp.2015.05.001.

[32] P. A. Delgado-Arredondo, A. Garcia-Perez, D. Morinigo-Sotelo, R. A. Osornio-Rios, J. G. Avina-Cervantes, H. Rostro-Gonzalez, and R. d. J. Romero-Troncoso, "Comparative study of time-frequency decomposition techniques for fault detection in induction motors using vibration analysis during startup transient," *Shock and Vibration*, vol. 2015, 2015. [Online]. Available: https://doi.org/10.1155/2015/708034.

[33] A. Rai and S. H. Upadhyay, "A review on signal processing techniques utilized in the fault diagnosis of rolling element bearings," *Tribology International*, vol. 96, pp. 289–306, 2016. [Online]. Available: https://doi.org/10.1016/j.triboint.2015.12.037.

[34] F. Hemmati, W. Orfali, and M. S. Gadala, "Roller bearing acoustic signature extraction by wavelet packet transform, applications in fault detection and size estimation," *Applied Acoustics*, vol. 104, pp. 101–118, 2016. [Online]. Available: https://doi.org/10.1016/j.apacoust.2015.11.003.

[35] R. Yan, R. X. Gao, and X. Chen, "Wavelets for fault diagnosis of rotary machines - a review with applications," *Signal Processing*, vol. 96, Part A, pp. 1–15, 2014. [Online]. Available: https://doi.org/10.1016/j.sigpro.2013.04.015.

[36] P. G. Kulkarni and A. D. Sahasrabudhe, "Investigations on mother wavelet selection for health assessment of lathe bearings," *The International Journal of Advanced Manufacturing Technology*, vol. 90, 9-12 2017. [Online]. Available: https://doi.org/10.1007/s00170-016-9664-3.

[37] R. Yan, "Wavelet selection criteria for non-stationary vibration analysis in bearing health diagnosis," University of Massachusetts, 2007.

[38] N. E. Huang, Z. Shen, S. R. Long, M. C. Wu, H. H. Shih, Q. Zheng, N.-C. Yen, C. C. Tung, and H. H. Liu, "The empirical mode decomposition and the hilbert spectrum for nonlinear and non-stationary time series analysis," in *The Royal Society A* -

Mathematical, Physical and Engineering Sciences, The Royal Society, vol. 454, The Royal Society, 1998, pp. 903–995.

[39] Z. Wu and N. E. Huang, "Ensemble empirical mode decomposition - a noise assisted data analysis method," *Advances in Adaptive Data Analysis*, vol. 1, no. 1, pp. 1–41, 2009. [Online]. Available: https://doi.org/10.1142/S1793536909000047.

[40] R. Calif, F. G. Schmitt, and Y. Huang, "Multifractal description of wind power using arbitrary order hilbert spectral analysis," *Physica A - Statistical Mechanics and its Applications*, vol. 392, pp. 4106–4120, 18 2013. [Online]. Available: https://doi.org/10.1016/j.physa.2013.04.038.

[41] S. Zhang, S. Zhangz, B. Wang, and T. G. Habetler, "Machine learning and deep learning algorithms for bearing fault diagnostics - a comprehensive review," 2019.

[42] B. Samanta, K. R. Al-Balushi, and S. A. Al-Araimi, "Artificial neural networks and support vector machines with genetic algorithm for bearing fault detection," *Engineering Applications of Artificial Intelligence*, vol. 16, pp. 657–665, 7-8 2003. [Online]. Available: https://doi.org/10.1016/j.engappai.2003.09.006.

[43] I. T. Jolliffe, *Principal component analysis*, 2nd. New York, United States of America: Springer, 1986.

[44] R. Zhao, R. Yan, Z. Chen, K. Mao, P. Wang, and R. X. Gao, "Deep learning and its applications to machine health monitoring," *Mechanical Systems and Signal Processing*, vol. 115, pp. 213–237, 2019. [Online]. Available: https://doi.org/10.1016/j.ymssp.2018.05.050.

[45] Y. Yang, D. Yu, and J. Cheng, "A fault diagnosis approach for roller bearing based on IMF envelope spectrum and SVM," *Measurement*, vol. 40, no. 9 - 10, pp. 943–950, 2007.

[46] R. Tessier and W. Burleson, "Reconfigurable computing for digital signal processing - a survey," *Journal of VLSI Signal Processing*, vol. 28, no. 1, pp. 7–27, 2001. [Online]. Available: https://doi.org/10.1023/A:1008155020711.

[47] N. Kehtarnavaz and S. Mahotra, "FPGA implementation made easy for applied digital signal processing courses," in *Proceedings of the International Conference on Acoustics, Speech and Signal Processing (ICASSP)*, IEEE, Prague, Czech Republic, 2011, pp. 2892–2895.

[48] J. Misra and I. Saha, "Artificial neural networks in hardware - a survey of two decades of progress," *Neurocomputing*, vol. 74, pp. 239–255, 1-3 2010. [Online]. Available: https://doi.org/10.1016/j.neucom.2010.03.021.

[49] A. Ordaz-Moreno, R. d. J. Romero-Troncoso, J. A. Vite-Frias, J. R. Rivera-Gillen, and A. Garcia-Perez, "Automatic online diagnosis algorithm for broken-bar detection on induction motors based on discrete wavelet transform for FPGA implementation," *IEEE Transactions On Industrial Electronics*, vol. 55, pp. 2193–2202, 5 2008. [Online]. Available: https://doi.org/10.1109/TIE.2008.918613.

[50] D. Camarena-Martinez, M. Valtierra-Rodriguez, A. Garcia-Perez, R. A. Osornio-Rios, and R. d. J. Romero-Troncoso, "Empirical mode decomposition and neural networks on FPGA for fault diagnosis in induction motors," *The Scientific World Journal*, vol. 2014, pp. 1–17, 2014. [Online]. Available: https://doi.org/10.1155/2014/908140.

[51] M. Kashiwagi, C. Da Costa, and M. H. Mathias, "Digital systems design based on DSP algorithms in FPGA for fault identification in rotary machines," *Journal of Mechanics & Industry Research*, vol. 2, no. 1, pp. 1–5, 2014. [Online]. Available: https://doi.org/10.12966/jmir.03.01.2014.

[52] M. Kang, J. Kim, and J.-M. Kim, "An FPGA-based multicore system for real-time bearing fault diagnosis using ultrasampling rate AE signals," *IEEE Transactions on Industrial Electronics*, vol. 62, pp. 2319–2329, 4 2015. [Online]. Available: https://doi.org/10.1109/TIE.2014.2361317.

[53] S. F. Wirtz, A. P. A. Cunha, M. Labusch, G. Marzun, S. Barcikowski, and D. S¨offker, "Development of a low-cost FPGA-based measurement system for real-time processing of acoustic emission data - proof of concept using control of pulsed laser ablation in liquids," *Sensors*, vol. 18, 6 2018. [Online]. Available: https://doi.org/10.3390/s18061775.

[54] Y. Lu, I. S. Ahn, and R. Smith, "FPGA-based ultrasonic signal processing platform," in *Proceeedings of the International Conference on Electro Information Technology (EIT)*, IEEE, Grand Forks, North Dakota, United States of America: IEEE, 2016, pp. 0610–0611.

[55] S.-J. Huang, T.-M. Yang, and J.-T. Huang, "FPGA realization of wavelet transform for detection of electric power system disturbances," *IEEE Transactions on Power Delivery*, vol. 17, pp. 388–394, 2 2002. [Online]. Available: https://doi.org/10.1109/61.997905.

[56] M. Bahoura and H. Ezzaidi, "FPGA-implementation of wavelet-based denoising technique to remove power-line interference from ECG signal," in *Proceedings of the 10th International Conference on Information Technology and Applications in Biomedicine (ITAB)*, IEEE, Corfu, Greece: IEEE, 2010, pp. 1–4.

[57] M. B. Shinde and M. Sharma, "FPGA implementation of HHT for feature extraction of signals," *International Journal of Science Technology & Engineering*, vol. 3, pp. 314–318, 1 2016.

[58] C. S. Avinash and J. S. Rani Alex, "FPGA implementation of discrete wavelet transform using distributed arithmetic architecture," in *Proceedings of the International Conference on Smart Technologies and Management for Computing, Communication, Controls, Energy and Materials (ICSTM)*, IEEE, Chennai, India: IEEE, 2015, pp. 326–330.

[59] M.-H. Lee, K.-K. Shyu, P.-L. Lee, C.-M. Huang, and Y.-J. Chiu, "Hardware implementation of EMD using DSP and FPGA for online signal processing," *IEEE Transactions on Industrial Electronics*, vol. 58, pp. 2473–2481, 6 2011. [Online]. Available: https://doi.org/10.1109/TIE.2010.2060454.

[60] O. Boujelben and M. Bahoura, "Efficient FPGA-based architecture of an automatic wheeze detector using a combination of MFCC and SVM algorithms," *Journal of Systems Architecture*, vol. 88, pp. 54–64, 2018. [Online]. Available: https://doi.org/10.1016/j.sysarc.2018.05.010.

[61] M. Bahoura, "FPGA implementation of an automatic wheezing detection system," *Biomedical Signal Processing and Control*, vol. 46, pp. 76–85, 2018. [Online]. Available: https://doi.org/10.1016/j.bspc.2018.05.017.

[62] M. D. K. Das and M. Priyanka, "FPGA implementation of acoustic source localization algorithm," in *Proceedings of the International Conference on Wireless Communications, Signal Processing and Networking (WiSPNET)*, IEEE, Chennai, India: IEEE, 2016, pp. 146–150.

[63] V. Yaremenko, M. R. Azimi-Sadjadi, and J. Zacher, "Unattended acoustic sensor systems for source detection, classification, and tracking," *IEEE Transactions on Instrumentation and Measurement*, vol. 68, pp. 344–354, 2 2019. [Online]. Available: https://doi.org/10.1109/TIM.2018.2849458.

[64] J. McAllister, "FPGA-based DSP," in *Handbook Of Signal Processing Systems*, Institute of Electronics, Communications and Information Technology, Queen's Universtiy Belfast, Northern Ireland: Springer, 2010, pp. 363–392.

[65] Y.-Y. Hong and Y.-Q. Bao, "FPGA implementation for real-time empirical mode decomposition," *IEEE Transactions on Instrumentation and Measurement*, vol. 61, pp. 3175–3184, 12 2012. [Online]. Available: https://doi.org/10.1109/TIM.2012.2211460.

[66] M. A. Farahani, F. Mirzaei, and H. A. Farahani, "Implementation of a reconfigurable architecture of discrete wavelet packet transform with three types of multipliers on FPGA," in *Proceedings of the 24th Canadian Conference on Electrical and Computer Engineering (CCECE)*, IEEE, Niagara Falls, Ontario, Canada: IEEE, 2011, pp. 1459–1462.

[67] Z. German-Sallo, "Signal processing using FPGA structures," in *Proceedings of the 7th International Conference Interdisciplinarity in Engineering (INTER-ENG 2013)*, Petru Maior University of Tirgu-Mures and Romanian Academy of Technical Sciences, Tirgu Mures, Romania, 2013, pp. 112–118.

[68] Y. Yuan, K. Virupakshappa, Y. Jiang, and E. Oruklu, "Comparison of GPU and FPGA based hardware platforms for ultrasonic flaw detection using support vector machines," in *Proceedings of the International Ultrasonics Symposium (IUS)*, IEEE, Washington, District of Columbia, United States of America: IEEE, 2017.

[69] R. Herrero, A. Carpeño, S. Esquembri, M. Ruiz, and E. Barrera, "FPGA-based solutions for analog data acquisition and processing integrated in area detector using FlexRIO technology," *IEEE Transactions on Nuclear Science*, vol. 65, pp. 781–787, 2 2018. [Online]. Available: https://doi.org/10.1109/TNS.2017.2782827.

[70] M. Žvokelj, S. Zupan, and I. Prebil, "Multivariate and multiscale monitoring of large-size low-speed bearings using ensemble empirical mode decomposition method combined with principal component analysis," *Mechanical Systems and Signal Processing*, vol. 24, no. 4, pp. 1049–1067, 2010.

[71] M. Van and H.-J. Kang, "Bearing defect classification based on individual wavelet local fisher discriminant analysis with particle swarm optimization," *IEEE Transactions On Industrial Infomatics*, vol. 12, pp. 124–135, 1 2016. [Online]. Available: https://doi.org/10.1109/TII.2015.2500098.

[72] N. Tandon and A. Choudhury, "A review of vibration and acoustic measurement methods for the detection of defects in rolling element bearings," *Tribology International*, vol. 32, pp. 469–480, 8 1999. [Online]. Available: https://doi.org/10.1016/S0301-679X(99)00077-8.

[73] S. A. McInerny and Y. Dai, "Basic vibration signal processing for bearing fault detection," *IEEE Transactions On Education*, vol. 46, pp. 149–156, 1 2003. [Online]. Available: https://doi.org/10.1109/TE.2002.808234.

[74] W. Zhou, T. G. Habetler, and R. G. Harley, "Bearing condition monitoring methods for electric machines - a general review," in *Proceedings of the International Symposium on Diagnostics for Electric Machines, Power Electronics and Drives*, IEEE, Kraków, Poland: IEEE, 2007, pp. 3–6.

[75] A. Widodo, E. Y. Kim, J.-D. Son, B.-S. Yang, A. C. C. Tan, D.-S. Gu, B.-K. Choi, and J. Mathew, "Fault diagnosis of low speed bearing based on relevance vector machine and support vector machine," *Expert Systems with Applications*, vol. 36, pp. 7252–7261, 3 2009. [Online]. Available: https://doi.org/10.1016/j.eswa.2008.09.033.

[76] H. Qiu, J. Lee, J. Lin, and G. Yu, "Wavelet filter-based weak signature detection method and its application on rolling element bearing prognostics," *Journal of Sound and Vibration*, vol. 289, pp. 1066–1090, 4-5 2006. [Online]. Available: https://doi.org/10.1016/j.jsv.2005.03.007.

[77] J. Altmann and J. Mathew, "Multiple band-pass autoregressive demodulation for rolling-element bearing fault diagnosis," *Mechanical Systems and Signal Processing*, vol. 15, pp. 963–977, 5 2001. [Online]. Available: https://doi.org/10.1006/mssp.2001.1410.

[78] H. Li, F. Xu, H. Liu, and X. Zhang, "Incipient fault information determination for rolling element bearing based on synchronous averaging reassigned wavelet scalogram," *Measurement*, vol. 65, pp. 1–10, 2015. [Online]. Available: https://doi.org/10.1016/j.measurement.2014.12.032.

[79] Y. Yu, Y. Dejie, and C. Junsheng, "A roller bearing fault diagnosis based on EMD energy entropy and ANN," *Journal of Sound and Vibration*, vol. 294, no. 1 - 2, pp. 269–277, 2006.

[80] J. B. Ali, N. Fnaiech, L. Saidi, B. Chebel-Morello, and F. Fnaiech, "Application of empirical mode decomposition and artificial neural network for automatic bearing fault diagnosis based on vibration signals," *Applied Acoustics*, vol. 89, pp. 16–27, 2015. [Online]. Available: https://doi.org/10.1016/j.apacoust.2014.08.016.

[81] M. a. Z. a. B. a. G. Li Wei and Qiu, "Bearing fault diagnosis based on spectrum images of vibration signals," *Measurement Science and Technology*, vol. 27, pp. 1–10, 2016. [Online]. Available: https://doi.org/10.1088/0957-0233/27/3/035005.

[82] J. Shiroishi, Y. Li, S. Liang, T. Kurfess, and S. Danyluk, "Bearing condition diagnostics via vibration and acoustic emission measurements," *Mechanical Systems and Signal Processing*, vol. 11, pp. 693–705, 5 1997. [Online]. Available: https://doi.org/10.1006/mssp.1997.0113.

[83] A. M. Al-Ghamd and D. Mba, "A comparative experimental study on the use of acoustic emission and vibration analysis for bearing defect identification and estimation of defect size," *Mechanical Systems and Signal Processing*, vol. 20, pp. 1537–1571, 7 2006. [Online]. Available: https://doi.org/10.1016/j.ymssp.2004.10.013.

[84] S. Al-Dossary, R. I. Raja Hamzah, and D. Mba, "Observations of changes in acoustic emission waveform for varying seeded defect sizes in a rolling element bearing," *Applied Acoustics*, vol. 70, pp. 58–81, 1 2009. [Online]. Available: https://doi.org/10.1016/j.apacoust.2008.01.005.

[85] B. Eftekharnejad, M. R. Carrasco, B. Charnley, and D. Mba, "The application of spectral kurtosis on acoustic emission and vibrations from a defective bearing," *Mechanical Systems and Signal Processing*, vol. 25, pp. 266–284, 1 2011. [Online]. Available: https://doi.org/10.1016/j.ymssp.2010.06.010.

[86] M. Elforjani and D. Mba, "Accelerated natural fault diagnosis in slow speed bearings with acoustic emission," *Engineering Fracture Mechanics*, vol. 77, pp. 112–127, 1 2010. [Online]. Available: https://doi.org/10.1016/j.engfracmech.2009.09.016.

[87] B. Van Hecke, J. Yoon, and D. He, "Low speed bearing fault diagnosis using acoustic emission sensors," *Applied Acoustics*, vol. 105, pp. 35–44, 2016. [Online]. Available: https://doi.org/10.1016/j.apacoust.2015.10.028.

[88] Z. Mo, J. Wang, H. Zhang, X. Zeng, H. Liu, and Q. Miao, "Vibration and acoustics emission based methods in low-speed bearing condition monitoring," in *Proceedings of the Prognostics and System Health Management Conference*, IEEE, Chongqing, China: IEEE, 2018, pp. 871–875.

[89] C. James Li and S. Y. Li, "Acoustic emission analysis for bearing condition monitoring," *Wear*, vol. 185, pp. 67–74, 1-2 1995. [Online]. Available: https://doi.org/10.1016/0043-1648(95)06591-1.

[90] K. R. Al-Balushi, A. Addali, B. Charnley, and D. Mba, "Energy index technique for detection of acoustic emissions associated with incipient bearing failures," *Applied Acoustics*, vol. 71, pp. 812–821, 9 2010. [Online]. Available: https://doi.org/10.1016/j.apacoust.2010.04.006.

[91] B. Kilundu, X. Chiementin, J. Duez, and D. Mba, "Cyclostationarity of acoustic emissions (AE) for monitoring bearing defects," *Mechanical Systems and Signal Processing*, vol. 25, pp. 2061–2072, 6 2011. [Online]. Available: https://doi.org/10.1016/j.ymssp.2011.01.020.

[92] D. H. Pandya, S. H. Upadhyay, and S. P. Harsha, "Fault diagnosis of rolling element bearing with intrinsic mode function of acoustic emission data using APF-KNN," *Expert Systems with Applications*, vol. 40, pp. 4137–4145, 10 2013. [Online]. Available: https://doi.org/10.1016/j.eswa.2013.01.033.

[93] W. Li and C. K. Mechefske, "Detection of induction motor faults - a comparison of stator current, vibration and acoustic methods," *Journal of Vibration and Control*, vol. 12, pp. 165–188, 2 2006. [Online]. Available: https://doi.org/10.1177/1077546306062097.

[94] M. A. A. Elmaleeh, N. Saad, and M. Awan, "Condition monitoring of industrial process plant using acoustic emission techniques," in *Proceedings of the 3rd International Conference on Intelligent and Advanced Systems (ICIAS)*, IEEE, Manila, Philippines: IEEE, 2010, pp. 1–6.

[95] A. Glowacz, "Diagnostics of DC and induction motors based on the analysis of acoustic signals," *Measurement Science Review*, vol. 14, no. 5, pp. 257–262, 2014. [Online]. Available: https://doi.org/10.2478/msr-2014-0035.

[96] A. Glowacz, "Diagnostics of synchronous motor based on analysis of acoustic signals with the use of line spectral frequencies and k-nearest neighbor classifier," *Archives of Acoustics*, vol. 39, no. 2, pp. 189–194, 2014. [Online]. Available: https://doi.org/10.2478/aoa-2014-0022.

[97] J.-K. Park and J. Hur, "Detection of inter-turn and dynamic eccentricity faults using stator current frequency pattern in IPM-type BLDC motors," *IEEE Transactions On Industrial Electronics*, vol. 63, pp. 1771–1780, 3 2016. [Online]. Available: https://doi.org/10.1109/TIE.2015.2499162.

[98] A. Glowacz, W. Glowacz, Z. Glowacz, and J. Kozik, "Early fault diagnosis of bearing and stator faults of the single-phase induction motor using acoustic signals," *Measurement*, vol. 113, pp. 1–9, 2018. [Online]. Available: https://doi.org/10.1016/j.measurement.2017.08.036.

[99] A. Glowacz, "Fault diagnosis of single-phase induction motor based on acoustic signals," *Mechanical Systems and Signal Processing*, vol. 117, pp. 65–80, 2019. [Online]. Available: https://doi.org/10.1016/j.ymssp.2018.07.044.

[100] B. P. Sangeetha and S. Hemamalini, "Rational-dilation wavelet transform based torque estimation from acoustic signals for fault diagnosis in a three phase induction motor," *IEEE Transactions on Industrial Informatics (Early Access)*, vol. 15, pp. 3492–3501, 6 2019. [Online]. Available: https://doi.org/10.1109/TII.2018.2874463.

[101] J. L. Contreras-Hernandez, D. L. Almanza-Ojeda, S. Ledesma-Orozco, A. Garcia-Perez, R. J. Romero-Troncoso, and M. A. Ibarra-Manzano, "Quaternion signal analysis algorithm for induction motor fault detection," *IEEE Transaction on Industrial Electronics (Early Access)*, vol. 66, pp. 8843–8850, 11 2019. [Online]. Available: https://doi.org/10.1109/TIE.2019.2891468.

[102] A. Siddique, G. S. Yadava, and B. Singh, "A review of stator fault monitoring techniques of induction motors," *IEEE Transactions On Energy Conversion*, vol. 20, pp. 106–114, 1 2005. [Online]. Available: https://doi.org/10.1109/TEC.2004.837304.

[103] S. Nandi, H. A. Toliyat, and X. Li, "Condition monitoring and fault diagnosis of electrical motors - a review," *IEEE Transactions On Energy Conversion*, vol. 20, pp. 719–729, 4 2005. [Online]. Available: https://doi.org/10.1109/TEC.2005.847955.

[104] Y. Liu and A. M. Bazzi, "A review and comparison of fault detection and diagnosis methods for squirrel-cage induction motors - state of the art," *ISA Transactions*, vol. 70, pp. 400–409, 2017. [Online]. Available: https://doi.org/10.1016/j.isatra.2017.06.001.

[105] O. E. Hassan, M. Amer, A. K. Abdelsalam, and B. W. Williams, "Induction motor broken rotor bar fault detection techniques based on fault signature analysis – a review," *IET Electric Power Applications*, vol. 12, pp. 895–907, 7 2018. [Online]. Available: https://doi.org/10.1049/iet-epa.2018.0054.

[106] J. Pons-Llinares, V. Climente-Alarcón, R. Puche-Panadero, and J. A. Antonino-Daviu, "Bar breakage detection on squirrel cage induction motors via transient motor current signal analysis based on the wavelet transform, a review," Departamento de Ingeniería Eléctrica, Universidad Politécnica de Valencia, España, 2017.

[107] Y. Tian, D. Guo, K. Zhang, L. Jia, H. Qiao, and H. Tang, "A review of fault diagnosis for traction induction motor," in *Proceedings of the 37th Chinese Control Conference (CCC)*, Wuhan, China, 2018, pp. 5763–5768.

[108] N. Baydar and A. Ball, "A comparative study of acoustic and vibration signals in detection of gear failures using wigner-ville distribution," *Mechanical Systems and Signal Processing*, vol. 15, pp. 1091–1107, 6 2001. [Online]. Available: https://doi.org/10.1006/mssp.2000.1338.

[109] N. Baydar and A. Ball, "Detection of gear failures via vibration and acoustic signals using wavelet transform," *Mechanical Systems and Signal Processing*, vol. 17, pp. 787–804, 4 2003. [Online]. Available: https://doi.org/10.1006/mssp.2001.1435.

[110] B. Eftekharnejad and D. Mba, "Seeded fault detection on helical gears with acoustic emission," *Applied Acoustics*, vol. 70, pp. 547–555, 4 2009. [Online]. Available: https://doi.org/10.1016/j.apacoust.2008.07.006.

[111] T. H. Loutas, G. Sotiriades, I. Kalaitzoglou, and V. Kostopoulos, "Condition monitoring of a single-stage gearbox with artificially induced gear cracks utilizing on-line vibration and acoustic emission measurements," *Applied Acoustics*, vol. 70, pp. 1148–1159, 9 2009. [Online]. Available: https://doi.org/10.1016/j.apacoust.2009.04.007.

[112] R. Li and D. He, "Rotational machine health monitoring and fault detection using EMD-based acoustic emission feature quantification," *IEEE Transactions on Instrumentation and Measurement*, vol. 61, pp. 990–1001, 4 2012. [Online]. Available: https://doi.org/10.1109/TIM.2011.2179819.

[113] B. M. Fazenda and D. Comboni, "Acoustic condition monitoring of wind turbines - tip faults," in *Proceedings of the 9th International Conference on Condition Monitoring and Machinery Failure Prevention Technologies*, London, United Kingdom, 2012, pp. 1–15.

[114] I. Marinescu and D. A. Axinte, "A critical analysis of effectiveness of acoustic emission signals to detect tool and workpiece malfunctions in milling operations," *International Journal of Machine Tools and Manufacture*, vol. 48, pp. 1148–1160, 10 2008. [Online]. Available: https://doi.org/10.1016/j.ijmachtools.2008.01.011.

[115] D. Baccar and D. Söffker, "Wear detection by means of wavelet-based acoustic emission analysis," *Mechanical Systems and Signal Processing*, vol. 60 - 61, pp. 198–207, 2015. [Online]. Available: https://doi.org/10.1016/j.ymssp.2015.02.012.

[116] N. K. Verma, J. V. Singh, M. Gupta, S. Dixit, R. K. Sevakula, and A. Salour, "Smartphone application for fault recognition," in *Proceedings of the 6th International Conference on Sensing Technology (ICST)*, IEEE, Kolkata, India: IEEE, 2012, pp. 629–634.

[117] N. K. Verma, S. Sarkar, S. Dixit, R. K. Sevakula, and A. Salour, "Android app for intelligent CBM," in *Proceedings of the International Symposium on Industrial Electronics (ISIE)*, IEEE, Taipei, Taiwan: IEEE, 2013, pp. 1–6.

[118] N. K. Verma, J. V. Singh, M. Gupta, S. Dixit, R. K. Sevakula, and A. Salour, "Windows mobile and tablet app for acoustic signature based machine health monitoring," in *Proceedings of the 9th International Conference on Industrial and Information Systems (ICIIS)*, IEEE, Gwalior, India: IEEE, 2014, pp. 1–6.

[119] M. Ahadi and M. S. Bakhtiar, "Leak detection in water-filled plastic pipes through the application of tuned wavelet transforms to acoustic emission signals," *Applied Acoustics*, vol. 71, pp. 634–639, 7 2010. [Online]. Available: https://doi.org/10.1016/j.apacoust.2010.02.006.

[120] M. S. Sadooghi and S. E. Khadem, "A new performance evaluation scheme for jet engine vibration signal denoising," *Mechanical Systems and Signal Processing*, vol. 76 - 77, pp. 201–212, 2016. [Online]. Available: https://doi.org/10.1016/j.ymssp.2016.01.019.

[121] M. Elforjani and D. Mba, "Detecting natural crack initiation and growth in slow speed shafts with the acoustic emission technology," *Engineering Failure Analysis*, vol. 16, pp. 2121–2129, 7 2009. [Online]. Available: https://doi.org/10.1016/j.engfailanal.2009.02.005.

[122] Mistras - Physical Acoustics Corporation, "Acoustic combustion turbine monitoring system product bulletin," *Mistras*, 2012.

[123] T. Oraczewski, W. J. Staszewski, and T. Uhl, "Nonlinear acoustics for structural health monitoring using mobile, wireless and smartphone-based transducer platform," *Journal of Intelligent Material Systems and Structures*, vol. 27, pp. 786–796, 6 2016. [Online]. Available: https://doi.org/10.1177/1045389X15585902.

[124] A. A. Jaber and R. Bicker, "The state of the art in research into the condition monitoring of industrial machinery," *International Journal of Current Engineering and Technology*, vol. 4, no. 3, pp. 1986–2001, 2014.

[125] M. Riera-Guasp, J. A. Antonino-Daviu, and G.-A. Capolino, "Advances in electrical machine, power electronic, and drive condition monitoring and fault detection: state of the art," *IEEE Transactions On Industrial Electronics*, vol. 62, pp. 1746–1759, 3 2015. [Online]. Available: https://doi.org/10.1109/TIE.2014.2375853.

[126] S. Singh, A. Kumar, and N. Kumar, "Motor current signature analysis for bearing fault detection in mechanical systems," in *Proceedings of the 3rd International Conference on Materials Processing and Characterisation (ICMPC)*, vol. 6, Hyderabad, India: Elsevier, 2014, pp. 171–177.

[127] Y. Cekic and L. Eren, "Broken rotor bar detection via four-band wavelet packet decomposition of motor current," *Electrical Engineering*, vol. 100, pp. 1957–1962, 3 2018. [Online]. Available: https://doi.org/10.1007/s00202-017-0674-4.

[128] N. Leboeuf, T. Boileau, B. Nahid-Mobarakeh, N. Takorabet, F. Meibody-Tabar, and G. Clerc, "Effects of imperfect manufacturing process on electromagnetic performance and online interturn fault detection in PMSMs," *IEEE Transactions On Industrial Electronics*, vol. 62, pp. 3388–3398, 6 2015. [Online]. Available: https://doi.org/10.1109/TIE.2014.2387338.

[129] J. Arellano-Padilla, M. Sumner, and C. Gerada, "Winding condition monitoring scheme for a permanent magnet machine using high-frequency injection," *IET Electric Power Applications*, vol. 5, pp. 89–99, 1 2011. [Online]. Available: https://doi.org/10.1049/iet-epa.2009.0264.

[130] F. Immovilli, C. Bianchini, E. Lorenzani, A. Bellini, and E. Fornasiero, "Evaluation of combined reference frame transformation for interturn fault detection in permanent-magnet multiphase machines," *IEEE Transactions On Industrial Electronics*, vol. 62, pp. 1912–1920, 3 2015. [Online]. Available: https://doi.org/10.1109/TIE.2014.2348945.

[131] B. Sen and J. Wang, "Stator interturn fault detection in permanent-magnet machines using PWM ripple current measurement," *IEEE Transactions On Industrial Electronics*, vol. 63, pp. 3148–3157, 5 2016. [Online]. Available: https://doi.org/10.1109/TIE.2016.2515560.

[132] S. Hauck and A. DeHon, *Reconfigurable computing - the theory and practice of FPGA-based computation*. Burlington, Massachusetts, United States of America: Elsevier, 2010.

[133] Tul Corporation. (2018). PYNQ-Z2 schematics, [Online]. Available: http://www.tul.com.tw/download/TUL_PYNQ%20Schematic_R12.pdf (Accessed: 2019-06-04).

Roller element bearing acoustic fault detection using smartphone and consumer microphones

Comparing with vibration techniques

Jarek Grebenik*, Yu Zhang, Chris Bingham and Saket Srivastava

* The University of Lincoln, School of Engineering, Brayford Pool, Lincoln, LN6 7TS, UK
e-mail: {jgrebenik, yzhang, cbingham, ssrivastava}@lincoln.ac.uk

***Abstract*—Roller element bearings are a common component and crucial to most rotating machinery; their failure makes up around half of the total machine failures, each with the potential to cause extreme damage, injury and downtime. Fault detection through condition monitoring is of significant importance. This paper demonstrates bearing fault detection using widely accessible consumer audio tools. Audio measurements from a smartphone and a standard USB microphone, and vibration measurements from an accelerometer are collected during tests on an electrical induction machine exhibiting a variety of mechanical bearing anomalies. A peak finding method along with use of trained Support Vector Machines (SVMs) classify the faults. It is shown that the classification rate from both the smartphone and the USB microphone was 95 and 100%, respectively, with the direct physically detected vibration results achieving only 75% classification accuracy. This work opens up the opportunity of using readily affordable and accessible acoustic diagnosis and prognosis for early mechanical anomalies on rotating machines.**

Keywords – roller element bearing; acoustic; fault; defect; detection; diagnosis; smartphone; consumer; microphone; vibration; motor; comparison; machine learning; support vector machine; SVM

Abbreviations: AE – Acoustic Emission, ANN – Artificial Neural Network, SVM – Support Vector Machine

I. INTRODUCTION

All rotating machines employ a method of supporting and reducing friction on the rotating shaft. The vast majority use roller element bearings due to their excellent operational performance. As a component vital to smooth operation, their failure can cause extreme damage to other machine components, prolonged downtime, heavy repair costs and potential for fatality. Approximately half of all rotating machine failures are due to issues with the roller bearings making early detection of defects a high priority [1]. Bearing damage can also lead to performance degradation, excessive vibration, noise and damage to other components if left unchecked. This makes online condition monitoring highly desirable so potential issues can be detected and rectified during scheduled maintenance. Common defects include galling, spalling, brinelling, peeling, wear, fatigue, overloading, particle ingress and lack of lubrication [2, 3]. Depending on where the defect occurs it can excite one of the four characteristic fault frequencies: ball pass frequency outer (BPFO), ball pass frequency inner (BPFI), ball spin frequency (BSF) and fundamental train frequency (FTF) [1, 4]. Determined by the bearing geometry and rotational speed, these frequencies, described in Equations (1) – (4), manifest in both vibration and acoustic signals, detectable with appropriate processing techniques, albeit in different frequency ranges.

$$BPFO = \frac{nf_r}{2}\left[1 - \frac{d}{D}\cos\Phi\right] \quad (1)$$

$$BPFI = \frac{nf_r}{2}\left[1 + \frac{d}{D}\cos\Phi\right] \quad (2)$$

$$BSF = f_r\frac{D}{2d}\left[1 - \left(\frac{d}{D}\cos\Phi\right)^2\right] \quad (3)$$

$$FTF = \frac{f_r}{2}\left[1 - \frac{d}{D}\cos\Phi\right] \quad (4)$$

where f_r is the shaft speed, n is the number of rollers, Φ is the angle of load from the radial plane, d is the ball diameter, and D is the pitch diameter - under conditions of no slippage.

The frequency and amplitude of such defects provides an indication of the presence and severity of the defect with harmonics indicating the defect origin [1]. It is important to recognise that in the case of a point defect, such frequencies are related to how often there is a defect impact and characteristics will manifest at different frequencies in the audio and vibration frequency spectrums.

For bearing fault classification, physical vibration sensing methods are well established, but advances in computational technology and signal processing techniques have allowed acoustic methods to be developed, with associated advantages viz. being remote to the equipment means acoustic sensors can be setup more easily, quickly and safely and are not prone to the same issues of vibration or heat damage as with surface mounted sensors; acoustic measurements are able to detect faults at an earlier stage in their emergence; the acoustic signal is likely to contain more defect information such as size and position and should give greater accuracy than vibration measurements [1, 2, 5, 6, 7].

Acoustics have been well established as promising for fault detection and condition monitoring with research being active for at least 2 decades [1, 2]. However, only relatively recently have significant advancements been made compared to earlier studies through use of advanced computational hardware, signal processing tools and machine learning techniques [2, 6, 8]. Furthermore, the uptake of acoustic techniques has been slow due to a historic knowledge, confidence in, and reliance on, direct vibration sensing systems; with acoustic techniques remaining in their relative infancy with regard to widespread

familiarity and industry expertise [2, 6]. This paper aims to demonstrate the potential simplicity of using acoustic technology whilst showing that low-cost and readily available devices are able to be employed. Therefore, this paper presents an investigation into the use of smartphones and consumer-grade microphones for acoustically detecting faults on roller element bearings using Fourier transform feature extraction and multi-SVM classification.

A. *Traditional Acoustic Fault Detection Methods*

In [7], experimental results from acoustic and vibration signals for seeded defects on the outer race of roller bearings are compared in an effort to identify the defect type and estimate its size. The test facility employed a piezoelectric Physical Acoustic WD sensor (100 – 1000 kHz) and a resonant accelerometer (flat frequency response between 0.01 – 8 kHz – Model 236 Isobase); sampling rates ranged between 2 – 10 MHz. Despite not performing any pre-processing, they were able to detect and estimate the size of protrusions on the outer race. Results from vibration measurements were unable to detect early defects or discern any further information. Another study, [9], investigated low speed bearing fault diagnosis using both vibration and acoustic signals and comparing the performance of a relevance vector machine and a SVM. For data collection, a micro-DSP system was created using PCI board with 18-bit, 10 MHz A/D conversion and onboard processing sampling at 500 kHz. The signal was supplied by a Physical Acoustics R3a AE sensor with a frequency range of 25 – 530 kHz. Pre-processing was by independent component analysis using the top five components as input features. Again, the authors found the acoustic signal to give superior classification accuracy to the vibration sensor measurements, more so when using the relevance vector machine over the SVM. The authors of [10] present a hybrid signal processing technique combining ensemble empirical mode decomposition with multiscale principal component analysis for detecting incipient faults in large-size low-speed roller bearings. Four specialised Valpey-Fisher VP-1093 pinducers with a frequency response of 0.001 – 10 MHz were used – these are designed for shock wave applications. This method is general in nature allowing it to be applied to a wide range of problems; it demonstrated its efficacy using both acoustic and vibration measurements, particularly with non-stationary signals. The work presented in [11] employs a wavelet packet transform on an acoustic signal for fault detection and size estimation in roller bearings. The AE frequency range for faults were identified as 100 kHz to 1 MHz and a Nano-30 Physical Acoustic sensor (good frequency response from 125 – 750 kHz) was used being sampled at 2 MHz for 5 seconds. Plackett-Burman Experimental Design determined the most sensitive parameter from ring down counts, peak value, rms, kurtosis, burst duration, crest factor and skewness. Wavelet coefficients were calculated utilizing DMeyer, Daubechies, Symlets, and Coiflets orthogonal mother wavelet families to investigate which wavelet function maximizes its Kurtosis to Shannon Entropy ratio. Using the continuous wavelet transform and Kurtosis to Shannon Entropy ratio as quantitative measurements the optimal mother wavelets for signal decomposition were chosen. After applying the wavelet packet transform, the signal envelope in different frequency bands was calculated using the Hilbert-transform. This method delivers excellent fault detection, specialising in extracting weak impulse-like fault features heavily masked by noise. In [12], acoustic signals were analysed using Hilbert-Huang transform for feature extraction and an asymmetric proximity function and k - nearest neighbour hybrid classification algorithm. The authors of [13] looked at acoustic and vibration signals, processing using an adaptive line enhancer and high-frequency resonance technique. They used a Physical Acoustics R15 sensor with a frequency response of 150 kHz connected directly to an ALM8 processor which outputs a demodulated version similar to that processed with high-frequency resonance. The work of [14] used a Physical Acoustics D9201A sensor with a 20 – 90 kHz band-pass filter and 8-bit 200 kHz A/D conversion. Signal processing was by high frequency resonance, finding better performance using a short-time overlapping energy technique – similar to the method to be used in this paper. Several studies [9, 10], have identified the limitations of acoustic techniques; requiring high frequency (over 100 kHz) response and data acquisition using specialised hardware; sampling between 1 and 5 MHz. Low speed applications require longer recording durations to capture the mechanical defect frequencies giving high data storage and processing demands. Consequently, acoustic data is often analysed in the hit-based or continuous time spectrum and rarely in the frequency spectrum.

This work uses readily accessible equipment sensitive in the audible frequency range with much lower sampling rates to record acoustic fingerprints of different bearing faults; investigating the suitability for fault diagnosis.

B. *Classification & Machine Learning Algorithms*

The performance of any classification algorithm is highly dependent on the differentiating features presented for training. Several studies [15, 16, 17], have compared the performance of SVMs and ANNs for bearing fault classification and concluded that SVMs outperform their counterpart with regard to accuracy, training time and computational efficiency. The authors of [15] compared SVMs with ANNs, optimising their parameters using genetic algorithms and finding the ANN to require significantly more training time. Both systems were capable of 100% accuracy, but the SVM was significantly quicker. In [16], results from two classification methods are compared; a radial basis kernel SVM optimised for the cost and gamma parameters to use the minimum number of support vectors, and a three-layer feed-forward artificial neural network trained using supervised back propagation. Results indicated that the SVM is more readily implemented, and gave better results. SVMs tends to perform better than ANNs for this application, but only for smaller datasets [17]. Note that implementation on real industrial machines would require a much larger and more sophisticated data set in which case ANNs would likely give better performance. Based on these findings, in this study a multi-SVM classification learner is employed; negating the effects of different operating conditions by training a new SVM for each operational regime.

II. METHODOLOGY

In this section, details of the experimental setup used to capture runtime data are given followed by the signal processing and machine learning techniques used to analyse the data.

A. Experimental Setup & Data Acquisition

A Gunt PT501 bearing fault simulator consists of an electric drive motor, shaft with laser tachometer, and bearing housing with interchangeable bearings. The bearing housing vibration is monitored using a built in single-axis accelerometer mounted vertically. The housing is horizontally loaded by winding a micrometre screw onto a rubber compression spring mounted to the housing edge. A control unit provides power to the motor for a user defined speed setting. The vibration accelerometer is connected to a OWON VDS3102 USB oscilloscope allowing remote sampling using a laptop. Microphone audio measurements are sampled using two Audio-Technica AT2020 USB+ condenser cardioid microphones. These are setup in stereo equidistant from and facing the bearing housing. The experimental setup is shown in Fig. 1. The seeded bearing defects under study are shown in Fig. 2. Smartphone audio is sampled using a Samsung Galaxy S7 Edge placed ≈ 20 cm away with the microphone facing the bearing. This is an intuitively sensible positon based on operational ease and optimum sound pressure level; closer causes overload of the sensor during louder operating regimes and further away permits greater signal attenuation. The smartphone position was not fixed in keeping with real-world practical operation.

Table I summarises the experimental setup and equipment used. Data is recorded for each combination of speed, load and bearing resulting in 24 different operating conditions ($6\ speeds \times 4\ loads$) and 144 different setups ($24\ operating\ conditions \times 6\ bearings$). The speed setting correlates linearly with the actual shaft rpm and are listed at no load (as loading the bearing reduces the rpm by approximately 1 to 2 rpm per mm). The load also correlates linearly, with load being applied from approximately 3.8 mm, with settings 4, 5 and 6 mm corresponding approximately to 5, 18 and 32 N respectively.

B. Signal Processing & Classification

Fig. 3 gives an overview of the signal processing methodology. For each setup, measurements are imported into Matlab and the time signal extracted. The data is divided into training and testing datasets for the SVM; using the first 4 datasets for training and a fifth for testing. The smartphone dataset signals are divided into two 4-second signals; one for training and one for testing. The audio signals are clipped to 8 seconds from the middle removing unwanted artefacts from the beginning and end of the recording. To create a sufficient number of observations each signal is divided into ten 1-second overlapping observations. Although it is possible to increase the classification accuracy by increasing the number of observations, it impacts computational time. Fig. 4 shows a time plot of the smartphone audio for one of the observations. Frequency responses are calculated for each observation sample using a Fast Fourier Transform. Fig. 5 shows example frequency responses for the same observation. It can be seen that the energy content of the signal is primarily contained in the 0 – 5,000 Hz range for the acoustic data and 0 – 16,000 Hz for the vibration data (not shown). Within these ranges, peaks above a set threshold are extracted. The threshold is calculated for each operating condition based on bearing A as the mean plus the standard deviation (1σ was found to be optimal). The frequency ranges specified above are then divided into bins and the peaks in each bin obtained. Fig. 6 shows the peaks above the threshold, the bin edges and the mean of the frequency plot.

Three features are calculated for the SVM: the total number of peaks above the threshold within the specified frequency range, the number of peaks in each bin and the product of the amplitude of the peaks in each bin. The frequency range for each bin is fixed at 100 Hz, giving 50 bins for the acoustic frequency range and 160 for the vibration. This gives a total number of SVM input features as 101 (total number of peaks, count of peaks in each bin and product of peaks in each bin) for acoustic and 321 for the vibration. The data is then rearranged for input into the SVM, with features representing columns and observations representing rows in the input table.

For each operating condition (speed and load combination) a quadratic SVM (2^{nd} order polynomial kernel function) is trained using a box constraint of 1, and without standardisation of the data. By using a different SVM for each operating condition, inaccuracies due to changes of the speed and load are eliminated allowing the SVM to differentiate exclusively between the bearings. This is reasonable for real-world machinery as operating settings will be known. Evaluation of SVM accuracy is by k-fold cross-validation using 5 non-overlapping folds; this splits the observations into folds and trains with the out-of-fold observations and validates using the in-fold observations and then calculates the average error over all folds. Note that the cross-validation is only performed on the training dataset for the purpose of preventing under and over fitting and increasing SVM robustness.

For system testing, the exact same processing is carried out on the testing data. The respective SVM for each operating condition is used with the associated test data input. Finally, modal recombination recombines the observations into an overall response for each input signal. As there are 10 observations per signal, a majority of 6 identical responses is required.

There are a number of limitations to this methodology. The signals used in this case are all under steady-state conditions – real world applications will exhibit both transients and dynamic stability. However, this method could be easily expanded to include dynamic signals, alternatively a larger dataset would allow accurate interpolation between the support vectors which should provide a reasonable response. This method does not address online condition monitoring, the aim being to detect faults as they form and monitor their growth allowing maximum use before planned maintenance is required. Moreover, only a limited number and type of defect are used.

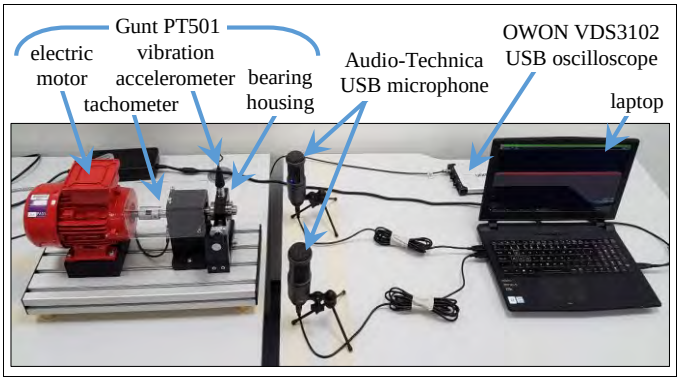

Fig. 1. Experimental setup showing; the Gunt PT501, two USB microphones, the OWON oscilloscope, and the laptop. The smartphone position is not shown as it varied, however, it was placed roughly between the two microphones at about the same height as the bearing.

Fig. 2. Damaged bearings from left to right; bearing C showing the inner race defect, bearing E showing the roller defect and bearing F showing wear. Note there was only a single defect on the inner race of bearing E compared to the two defects seen above on bearing C.

TABLE I. EXPERIMENTAL PROCEDURE

Setting		Description		
Bearings NU 204 E TVP2; 12 rollers at 7.5 mm diameter & 34 mm pitch diameter	**A**	New bearing with no damage (reference bearing)		
	B	Damage to outer race		
	C	Damage to inner race		
	D	Damage to roller element		
	E	Damage to outer race, inner race and roller element		
	F	Heavily worn bearing		
Speed Setting & Equivalent Speed		Setting: 0 → 298 rpm		
		Setting: 2 → 829 rpm		
		Setting: 4 → 1341 rpm		
		Setting: 6 → 1865 rpm		
		Setting: 8 → 2428 rpm		
		Setting: 10 → 3050 rpm		
Load Settings		3, 4, 5 and 6 mm		
		Smartphone	**Microphone**	**Vibration**
Sampling software & format		Android Voice Recorder: mp3 @160 kbps	Matlab: Matlab file	OWON VDS_S2: text file
Sampling rate		44,100 Hz	48,000 Hz	100,000 Hz
A/D resolution		8-bit	16-bit	8-bit
Sensor frequency response		Unknown	20 to 20,000 Hz	1 to 10,000 Hz
Sensitivity		Unknown	-19dB ± 4 (audio circuit)	100 mV/g & 1V/division
Repeats		1	5	5
All recordings were single channel and of 10 second duration.				

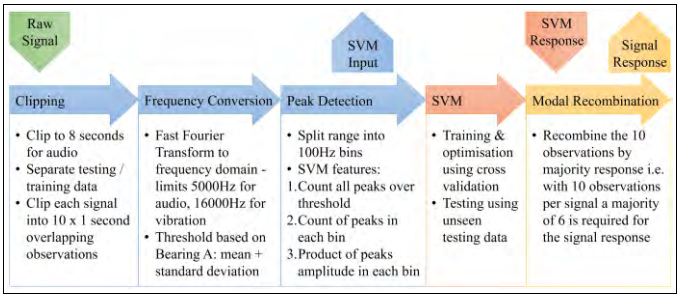

Fig. 3. Signal processing methodology.

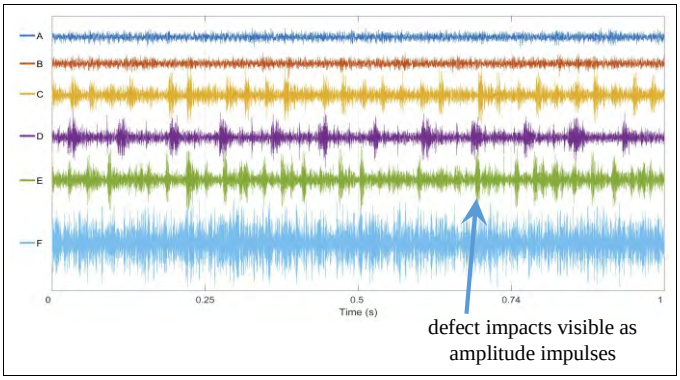

Fig. 4. Smartphone audio one second time plot for all bearings at speed 6 and load 5. Note the clearly visible audio spikes visible for bearings C and D; inner race and roller defects respectively.

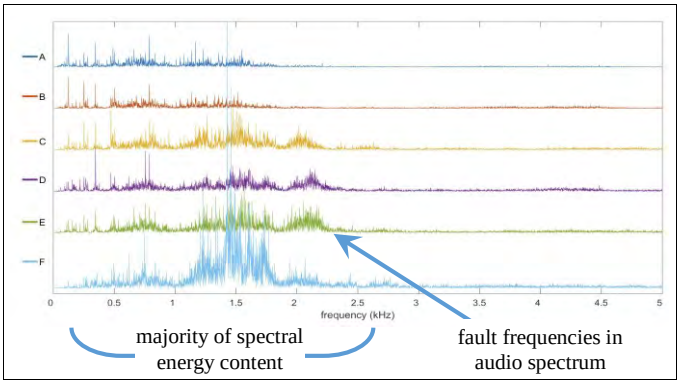

Fig. 5. Smartphone frequency plot for all bearings at speed 6 and load 5. Note the differences from that of bearing A are primarily related to the defects present and characterise the fault frequencies in the audio frequency spectrum. However, there will also be small differences caused by tiny changes in operating conditions, setup, etc.

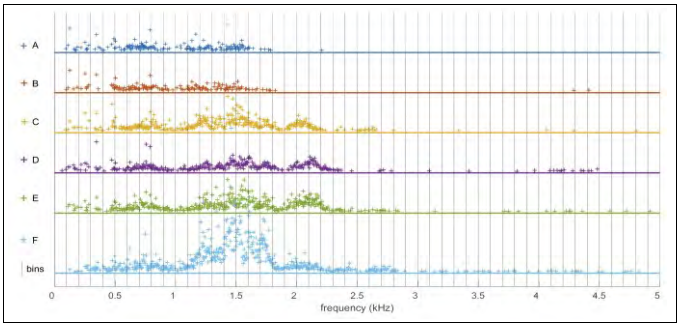

Fig. 6. Smartphone peaks plot for all bearings at speed 6 and load 5. Vertical lines represent bin boundaries, and the horizontal line shows the mean of each signal. Note the cut off threshold was the mean plus one standard deviation.

III. Experimental Results

Table II shows the cross validation classification accuracy from the training data averaged across all operating conditions, it is clear the system performs very well. Table III shows the classification accuracy from the testing data categorised by bearing, speed and load. The values are a percentage of correct classification across all the observations. Table IV shows the count of the misclassified signals after all the observations have been regrouped using modal recombination. It can be seen that with modal recombination the accuracy is increased further. Furthermore, it highlights where misclassifications occur most. For the smartphone data this is at low loads with a total of 6 misclassifications out of 144 inputs; 4 and 2 of those at load settings 3 and 4 mm respectively.

For the microphone data, regrouping the observations gives perfect classification, but examining the signal majorities revealed that the performance is only just good enough to achieve this. Whilst the vibration accuracy has increased to 75% it still exhibits some misclassifications, particularly between bearings A and B. This is likely due to the outer race fault not producing sufficiently strong vibrations to allow differentiation. At a load setting of 6 mm the vibrations are sufficient to significantly increase the classification accuracy.

The results clearly show significantly greater classification accuracy of the acoustic signals compared with the vibration measurements. Fig. 7 shows that as the speed increases the classification accuracy is better for both acoustic and vibration signals. It is notable that the sound level indicator displayed during recording with the smartphone was at its maximum value for speed settings 8 and 10 when load was applied. This might be a cause for the degradation in accuracy for the smartphone results compared to the microphone, and if so could be rectified by positioning the smartphone further away reducing the sound pressure to within its most sensitive range. Fig. 8 shows greater classification accuracy as the load increases. The acoustic performance is increasingly better than vibration at low loads and speeds. Fig. 9 shows that bearing E was the most difficult to classify. This is expected as it exhibits the combined faults of bearings B, C and D. Examining the misclassifications reveals they are usually attributed to bearings B, C, or D i.e. a fault is still detected as it not misclassified as a healthy bearing. Clearly the most important differentiation is between a healthy and unhealthy bearing state; bearing A and the other five bearings. This is where the acoustic method outperformed the vibration with no misclassifications; compared to the vibration with 7 unhealthy signals classified as healthy and 9 healthy signals classified as unhealthy (out of 144 inputs).

There is sufficient information in the acoustic signals to detect the faults under all operating conditions, particularly at low load and speed, where the vibration only started to achieve reasonable performance at high load. Moreover, there are no misclassifications between healthy and unhealthy bearings with the acoustic signals, whereas approximately 5% of vibration signals are misclassified as healthy.

TABLE II. Multi-SVM Training Data Cross Validation Accuracy

	Smartphone	Microphone	Vibration
Mean Accuracy (%)	99.97	99.97	99.75
Standard Deviation	0.02	0.03	0.01

TABLE III. Observation Classification Results (%)

		Smartphone	Microphone	Vibration
Bearing	**A**	96.25	95.83	63.75
	B	95.83	96.25	57.08
	C	87.50	95.83	82.08
	D	97.08	93.75	72.50
	E	90.83	95.00	68.33
	F	95.42	99.58	85.83
Speed Setting	**0**	90.42	90.83	50.42
	2	93.75	97.08	75.00
	4	93.75	97.08	72.92
	6	97.92	95.42	81.25
	8	91.67	97.08	75.42
	10	95.42	98.75	74.58
Load Setting (mm)	**3**	86.67	92.78	65.00
	4	94.17	95.28	68.89
	5	97.22	97.78	69.72
	6	97.22	98.33	82.78
Overall Accuracy (%)		**93.82**	**96.04**	**71.60**

TABLE IV. Grouped Signal Error Count

		Smartphone	Microphone	Vibration
Bearing	**A**	0	0	7
	B	0	0	10
	C	2	0	4
	D	0	0	6
	E	2	0	5
	F	2	0	3
Speed Setting	**0**	1	0	11
	2	1	0	3
	4	1	0	7
	6	0	0	3
	8	2	0	4
	10	1	0	7
Load Setting (mm)	**3**	4	0	10
	4	2	0	13
	5	0	0	9
	6	0	0	3
Total Misclassified		6	0	35
Overall Accuracy (%)		**95.83**	**100**	**75.69**

TABLE V. Motor Control Classification Results

	Smartphone	Microphone
Overall Accuracy (%)	**97.50**	**100**

The ability of the smartphone and microphone to outperform the vibration signal not only demonstrates the efficacy of acoustics but also the suitability of this type of consumer equipment for bearing fault diagnosis and similar applications. Whilst for real applications the training database and processing requirements exceed the capabilities of smartphones, these devices are suitable for data acquisition which can then be uploaded for processing to then deliver the classification result.

The use of multi-SVM classification based on the operating conditions lead to a significant increase in the classification accuracy and was just as easy to program. This method of programming can be easily expanded to allow interpolation for dynamic signals. When classifying between bearings, the ability to differentiate exclusively between them without inaccuracies caused by different operating conditions is one of the main contributing factors to the high classification accuracies achieved.

IV. Extension to Motor Control System Diagnostics

The case studies have been extended to include consideration of current controller dynamics. Unstable current dynamics in brushless pulse modulation machines, for instance, is a relatively common issue under widely varying operational conditions or when commissioning controllers. In the most severe circumstances, inappropriately controlled currents can lead to permanent demagnetisation of the motor as well as damage of the power electronics. A brushless dc motor is setup, controlled using a digital PWM current controller with a 10kHz PWM frequency. The current controller is known to exhibit transient instability under some operating conditions creating high frequency torque transients. The smartphone and audio microphones are used to sample audio under two operating conditions both healthy and unhealthy states. The smartphone records 3 samples of 10 seconds, and the microphones record 5 samples of 3 seconds. The signals are processed exactly as previously discussed. Table V shows the results – with only a single observation misclassification with the smartphone (based on 40 observation inputs. Fig. 10 shows a current instability captured using an oscilloscope. The acoustic setup was easily transferred to a different machine for this investigation, whereas the vibration probe could not be transferred to a different machine without considerable work and high risk of damage.

V. Conclusion

This paper set out to demonstrate the potential simplicity of acoustic bearing fault detection compared with previous works and compare results with vibration measurements. The setup and method is proven to deliver extremely good classification accuracy with easy to setup independent sensors and reduced computational demands. The multi-SVM approach was shown to be extremely effective for allowing differentiation exclusively between the bearings. The method also shows great applicability to motor control system diagnostics. The suitability of consumer audio recording tools opens up bearing fault diagnosis to a much wider audience with improved cost/benefit performance.

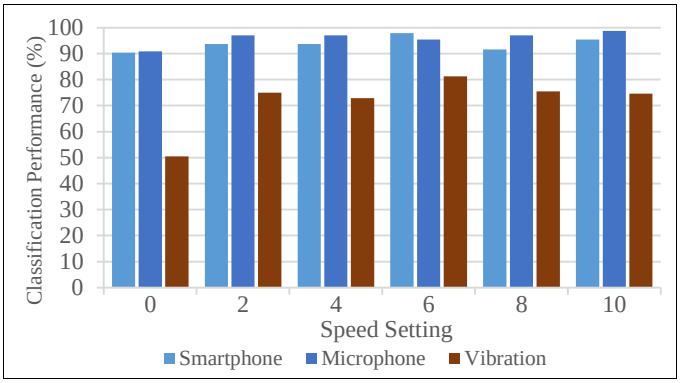

Fig. 7. Speed setting classification performance based on Table III.

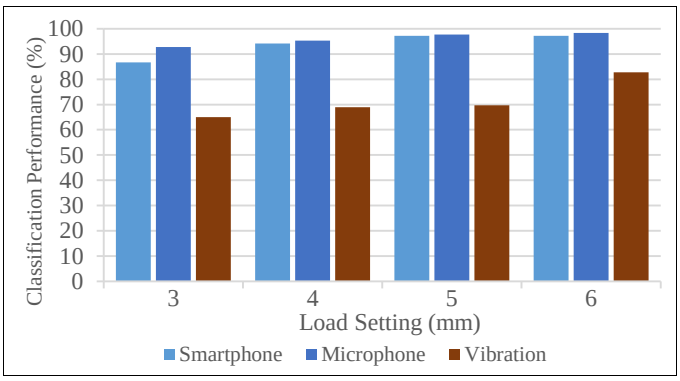

Fig. 8. Load setting classification performance based on Table III.

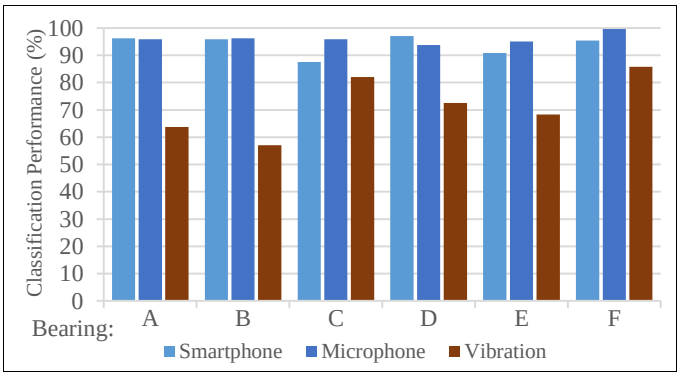

Fig. 9. Bearing classification performance based on Table III.

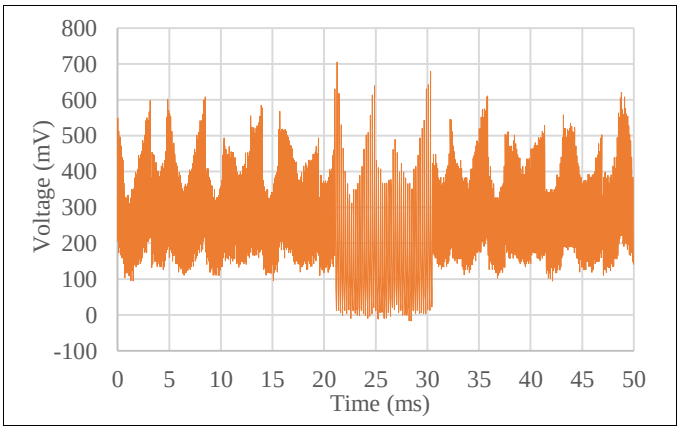

Fig. 10. Oscilloscope save showing motor PWM current – instability visible between 21 and 31 milliseconds.

ACKNOWLEDGMENTS

The author would like to thank Damiano Rossetti who assisted with the SVM coding, and Pierre Francq who assisted in the optimisation of the system.

REFERENCES

[1] A. Rai and S. H. Upadhyay, "A review on signal processing techniques utilized in the fault diagnosis of rolling element bearings," *Tribology International*, vol. 96, pp. 289-306, 2016.

[2] N. Tandon and A. Choudhury, "A review of vibration and acoustic measurement methods for the detection of defects in rolling element bearings," *Tribology International*, vol. 32, no. 8, p. 469–480, 1999.

[3] M. Entezami, E. Stewart, J. Tutcher, W. Driscoll, R. Ellis, G. Yeo, Z. Zhang, C. Roberts, T. Kono and S. Bayram, "Acoustic analysis techniques for condition monitoring of roller bearings," *Railway Condition Monitoring, 6th Conference 2014*, pp. 1-8, 2014.

[4] S. A. McInerny and Y. Dai, "Basic vibration signal processing for bearing fault detection," *IEEE Transactions On Education*, vol. 46, no. 1, pp. 149-156, 2003.

[5] H. Li, F. Xu, H. Liu and X. Zhang, "Incipient fault information determination for rolling element bearing based on synchronous averaging reassigned wavelet scalogram," *Measurement*, vol. 65, pp. 1 - 10, 2015.

[6] D. Mba and R. B. K. N. Rao, "Development of acoustic emission technology for condition monitoring and diagnosis of rotating machines; bearings, pumps, gearboxes, engines and rotating structures," *The Shock and Vibration Digest*, vol. 38, no. 1, pp. 3 - 16, 2006.

[7] A. M. Al-Ghamd and D. Mba, "A comparative experimental study on the use of acoustic emission and vibration analysis for bearing defect identification and estimation of defect size," *Mechanical Systems and Signal Processing*, vol. 20, no. 7, p. 1537–1571, 2006.

[8] X. Lou and K. A. Loparo, "Bearing fault diagnosis based on wavelet transform and fuzzy inference," *Mechanical Systems and Signal Processing*, vol. 18, no. 5, pp. 1077 - 1095, 2004.

[9] A. Widodoa, E. Y. Kimb, J.-D. Sonc, B.-S. Yangc, A. C. C. Tanb, D.-S. Gud, B.-K. Choid and J. Mathewb, "Fault diagnosis of low speed bearing based on relevance vector machine and support vector machine," *Expert Systems with Applications*, vol. 36, no. 3, pp. 7252 - 7261, 2009.

[10] M. Žvokelj, S. Zupan and I. Prebil, "Multivariate and multiscale monitoring of large-size low-speed bearings using ensemble empirical mode decomposition method combined with principal component analysis," *Mechanical Systems and Signal Processing*, vol. 24, no. 4, pp. 1049 - 1067, 2010.

[11] F. Hemmati, W. Orfali and M. S. Gadala, "Roller bearing acoustic signature extraction by wavelet packet transform, applications in fault detection and size estimation," *Applied Acoustics*, vol. 104, p. 101–118, 2016.

[12] D. H. Pandya, S. H. Upadhyay and S. P. Harsha, "Fault diagnosis of rolling element bearing with intrinsic mode function of acoustic emission data using APF-KNN," *Expert Systems with Applications*, vol. 40, no. 10, pp. 4137 - 4145, 2013.

[13] J. Shiroishi, Y. Li, S. Liang, T. Kurfess and S. Danyluk, "Bearing condition diagnostics via vibration and acoustic emission measurements," *Mechanical Systems and Signal Processing*, vol. 11, no. 5, pp. 693 - 705, 1997.

[14] C. James Li and S. Y. Li, "Acoustic emission analysis for bearing condition monitoring," *Wear*, vol. 185, no. 1 - 2, pp. 67 - 74, 1995.

[15] B. Samanta, K. R. Al-Balushi and S. A. Al-Araimi, "Artificial neural networks and support vector machines with genetic algorithm for bearing fault detection," *Engineering Applications of Artificial Intelligence*, vol. 16, no. 7 - 8, pp. 657 - 665, 2003.

[16] P. Konar and P. Chattopadhyay, "Bearing fault detection of induction motor using wavelet and support vector machines (SVMs)," *Applied Soft Computing*, vol. 11, no. 6, pp. 4203-4211, 2011.

[17] Y. Yang, D. Yu and J. Cheng, "A fault diagnosis approach for roller bearing based on IMF envelope spectrum and SVM," *Measurement*, vol. 40, no. 9 - 10, pp. 943 - 950, 2007.

[18] K. Feng, Z. Jiang, W. He and Q. Qin, "Rolling element bearing fault detection based on optimal antisymmetric real Laplace wavelet," *Measurement*, vol. 44, no. 9, pp. 1582-1591, 2011.

[19] W. He, Z.-N. Jiang and K. Feng, "Bearing fault detection based on optimal wavelet filter and sparse code shrinkage," *Measurement*, vol. 42, no. 7, pp. 1092 - 1102, 2009.

Continuous Acoustic Monitoring of Electrical Machines; Processing Signals from USB Microphone & Mobile Smartphone Sensors Detecting DC Motor Controller Fault

Jarek Grebenik*, Chris Bingham and Saket Srivastava
* The University of Lincoln, School of Engineering, Brayford Pool, Lincoln, LN6 7TS, UK
e-mail: {jgrebenik, cbingham, ssrivastava}@lincoln.ac.uk

***Abstract*— Transient current instability is one of the most common faults evident in Pulse Width Modulation (PWM) controlled brushless DC motors. This paper explores the under-developed field of real-time acoustic diagnostics for electrically based faults using consumer grade sensors. Current instabilities produce an audible torque transient on the motor, easily detectable using consumer acoustic sensors; a USB microphone and smartphone in this case. Two time-frequency signal processing techniques, Wavelet Packet Transform (WPT) and Empirical Mode Decomposition (EMD), are used to isolate information pertaining to the fault and are assessed for computational performance. This gives four processed signals to search for instabilities using a peak finding technique. We then compare the performance of each method. With the USB microphone WPT signal correlating the best results (93%), a simplistic logarithmic predictive model is used to estimate the durations for the next experimental run, in real-time. The results prove that readily accessible and affordable consumer acoustic sensors can be used for real-time fault diagnostics with a high degree of accuracy.**

Keywords: acoustic; electric; electrical; fault; detection; diagnosis; smartphone; consumer; microphone; motor; real-time; online; signal processing; wavelet packet transform; WPT; empirical mode decomposition; EMD; time-frequency analysis

Abbreviations: AE – Acoustic Emission, EEMD – Ensemble Empirical Mode Decomposition, EMD – Empirical Mode Decomposition, IMF – Intrinsic Mode Function, PWM – Pulse Width Modulation, WPT – Wavelet Packet Transform

I. Introduction

Acoustic supervision and monitoring is an attractive prospect for many industrial applications with proven advantages over many established systems including; earlier and more accurate detection, non-invasive and readily accessible sensors and better cost-benefit performance [1]. Research in this field is highly active with the majority focussed on seeded mechanical impact based faults, detecting the acoustic shockwave.

Acoustic Emission (AE) energy indexing/analysis has been used to detect seeded mechanical defects on roller element bearings [2, 3]. Similar case study is also explored in [4, 5, 6] using wavelet analysis. A good example of vibration analysis for bearing fault detection using wavelet transform is [7]. Another study investigates seeded mechanical defects on roller element bearings and gears using EMD of acoustic signals [8]. The work in [9] uses wavelet signal processing of vibration and acoustic signals to detect a simulated cracked tooth in a gear box. Another study mentions the requirement for real-time condition monitoring in industry and looks at motor fault diagnosis. However, it is unclear whether the experiment demonstrates real-time detection, and this is an area that is highly underdeveloped in this field [10]. All prior works discussed use specialised, research grade AE sensors, not easily accessible, that require mounting to the component to deliver sufficient signal to noise ratio. A review of condition monitoring and fault diagnostics for electrical motors is given in [11]. However, all the faults in this work are seeded and there is little mention of acoustic techniques. There is very little literature on acoustic diagnostics for electrically-based faults nor for real-time processing.

As opposed to seeded mechanical faults, it is far more difficult to detect and model transient current instabilities arising in PWM-based DC motors. Electronically commutated motors require a closed-loop power controller to convert the DC supply to AC for each phase; synchronising the motor. The design and operation of each controller will vary depending on the supply, type of motor and application. Often, controllers under commissioning, motor tuning, or operating in widely varying conditions, can result in transient current instabilities delivered to the motor. These instabilities could potentially cause damage to the controller or demagnetisation of the motor [12]. Detection could allow intervention to prevent further damage, and diagnostics could help assess maintenance requirements.

We present a novel application of acoustic monitoring to detect electro-mechanical instabilities on a brushless DC electric motor. Our work explores aspects previously unaddressed in the literature, namely; real-time processing and expansion to include electrically based faults. Consumer sensors (which are easily accessible) are used to highlight the under-usage of these types of sensor in both research and industry. Acoustic signals are processed in real-time to reveal the instability time-frequency information. This is done using two signal processing techniques, WPT and EMD, which are analysed for computational performance and ability to deliver information pertaining to the fault.

Our proposed solution uses a bespoke PWM power control system that delivers intermittent transient current instabilities with increasing frequency for higher voltages. At the end of the previous PWM cycle, the controller calculates the new duty from the demand. When the sampled current is already too high, the next cycle is switched off. This can resolve or continue to the end of the commutation period. A detailed view of the instability is given in Figure 1. This fault is native to this particular setup and is used here as an example of the potential electro-mechanical faults requiring diagnostic information.

Acoustics are well suited to this application due to the audible torque transient caused by the current instabilities; hence an electro-mechanical fault. In this case, the frequency

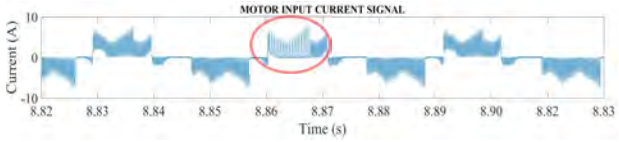

Figure 1: Motor current signal showing instability #4 at the centre.

information is almost entirely in the audible range of a human ear. This permits the use of consumer sensors which are more accessible and can be remote from the workpiece. Should faults deliver ultrasonic frequencies then contact based sensors would likely be required.

In the next section, we describe the experimental setup and signal processing techniques employed. Detail is given on the design of WPT and EMD as used in the experiment, complete with an explanation on the real-time processing for this work. The experimental results are discussed with focus on; the diagnostic performance of the acoustic sensors and signal processing techniques, and real-time computational processing efficiency. The main findings, their impact and significance are conferred in the conclusions.

II. Methodology

This section describes and justifies the research approach; providing information regarding the experimental setup, data acquisition and signal processing. Two experimental runs are undertaken; the preliminary run gathers initial data allowing design of a predictive diagnostic model. This model is used to estimate instability duration throughout the primary run, in which processing is undertaken in real-time. The experimental setup for both runs is identical; the only minor improvements made to the preliminary run was the addition of real-time processing for predictive diagnostics.

A. Experimental Setup & Data Acquisition

The experimental setup is given in Figure 2. A Unite MY1020 1600 W, 36 V brushless DC motor is controlled using a custom Arduino-based digital PWM controller; consisting of two boards (low and high power). These are powered by a Keysight E3631A triple output DC PSU, set to deliver a voltage range of −15 to +15 V and a Voltcraft PS-1302D 0 − 30 V, 2 A PSU. The controller setup delivers a 10 kHz current to drive the motor; speed is controlled by adjusting the supply voltage. High voltages or rapid voltage ramp up delivers intermittent transient instabilities. A USB microphone (Audio-Technica AT2020 USB+) and a smartphone (Samsung Galaxy S7 using WO Mic) are USB connected to a laptop; sampled by Matlab at 48 kHz with 16 bit resolution. Both sensors are placed approximately 10 cm away with their sensitive planes aimed toward the motor. A single phase of the motor input current from a Hall-effect sensor control feedback loop is sampled at 250 kHz with 16 bit resolution using a Tektronix DPO 7054C oscilloscope.

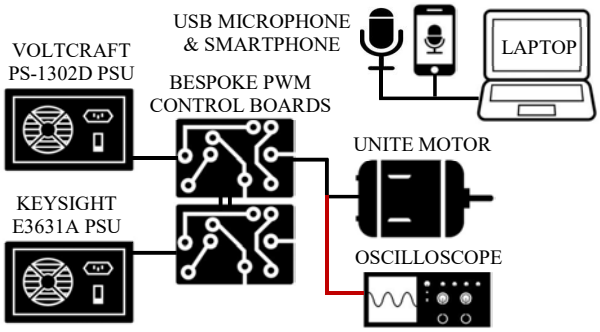

Figure 2: Diagram of the experimental setup.

The practical operation of the sampling is complex; both the audio and current sampling must be triggered manually. The smartphone audio signal lags the USB microphone signal by approximately 0.5 s due to the smartphone audio streaming software. To capture sufficient instabilities a sampling duration of 20 s is chosen based on previous experience. The oscilloscope is set to sample for 20 s. To accommodate for the time delay from manual triggering and the smartphone lag, the audio sampling duration is set to 25 s. The audio is triggered first, followed by the oscilloscope within the 5 s window. This allows for the audio and current signals to be synchronised in post processing. The Voltcraft control voltage for each run was slightly different (approximately 21 V for the first run and 23 V for the second run), as creating the conditions for instabilities to manifest is difficult to control.

B. Signal Processing & Analysis

For the preliminary run, all data streams are synchronised manually in the time-domain. This is repeated for analysis purposes in post for the primary run. Figure 3 shows the raw unprocessed signals from the oscilloscope current, and microphone and smartphone audio.

The aim of signal processing is to extract and separate the fault information from the background noise as much as possible. The instability can be detected by finding a spike in the audio signal indicating the louder ticking sound of the torque transient. However, the time domain information is noisy, meaning a peak finding technique could either miss instabilities due to insufficient amplitude, or have erroneous detection due to background noise. By analysing the time-frequency domain, much of the background noise can be removed with complex filtering. A filtered signal can then be analysed for spikes indicative of instabilities.

The preliminary run audio signals are used to design the WPT and EMD signal processing parameters, the peak finding detection method and some simplistic diagnostics. This design is performed through post-analysis, not in real-time. The designed method is then implemented for the main run in real-time. WPT and EMD [5, 13] are selected for testing

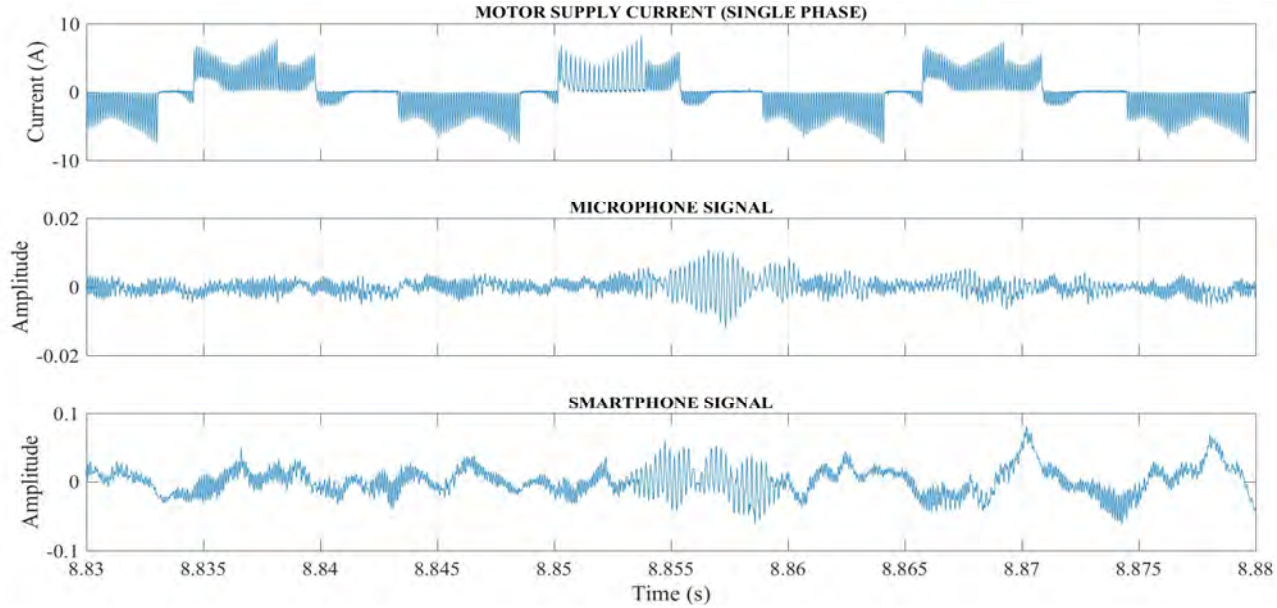

Figure 3: Plot of the synchronised raw signals showing instability #6. Note the units of the audio signal are vacillating as only the relative changes in amplitude that are of interest.

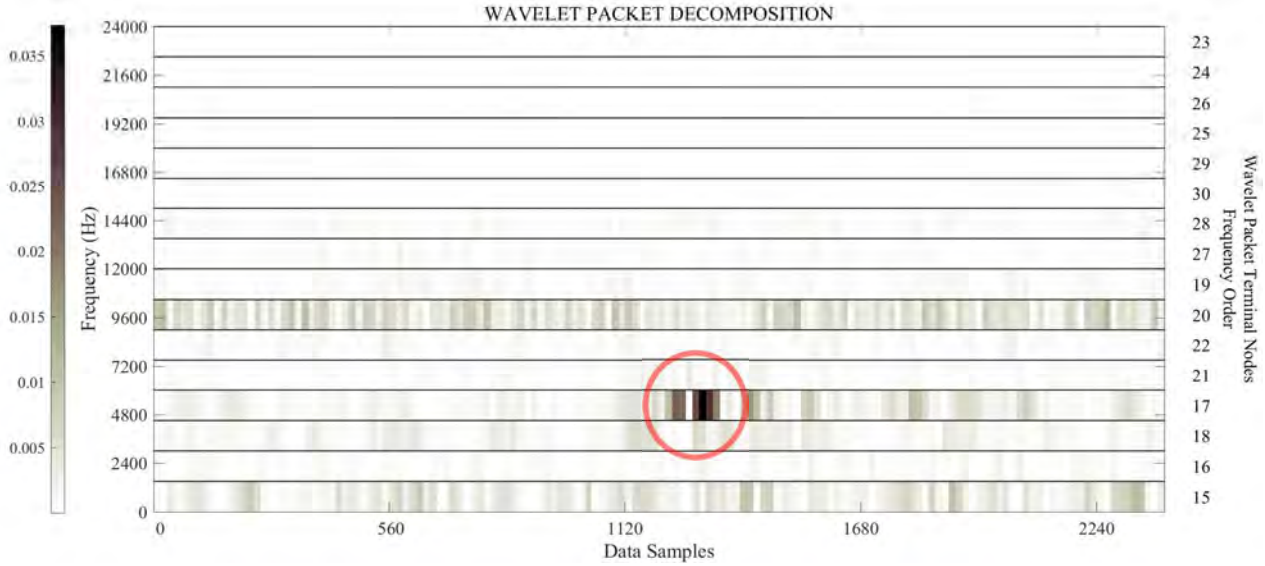

Figure 4: WPT dmey level 4 frequency ordered terminal node coefficients clearly showing the instability information in node 17.

as they are prominent time-frequency techniques in acoustic diagnostic literature. WPT allows for complex filtering to accurately reconstruct the fault information whilst leaving out unwanted noise [4, 5, 6]. EMD decomposes a signal by sifting the mean of the upper and lower envelopes into IMFs. This technique is more akin to an empirical algorithm rather than a theoretical transform; however, this makes it especially good with non-stationary and non-linear signals; an ideal candidate for fault detection [8, 13]. EEMD [14] is not required as audio is highly oscillatory by nature. Furthermore, the additional processing is highly computationally intensive and unsuitable for real-time processing.

1) Wavelet Packet Transform Design

The parameters that require selection and optimisation are; the selection of the mother wavelet, the number of levels of decomposition and, selection of the reconstruction node. The mother wavelet is chosen based on the maximum signal energy to Shannon-entropy ratio as detailed in [15]. 60 different mother wavelets from the Haar, Daubechies, Symlets, Coiflets, Biorthogonal, Reverse-Biorthogonal, Discrete approximation of Meyer (dmey) and Fejer-Korovkin families are analysed. The dmey wavelet gave very high performance; isolating nearly all the fault information into a single terminal node. The wavelet analyser is used to determine the required level of decomposition using the terminal node coefficients (Figure 4); aiming to maximise

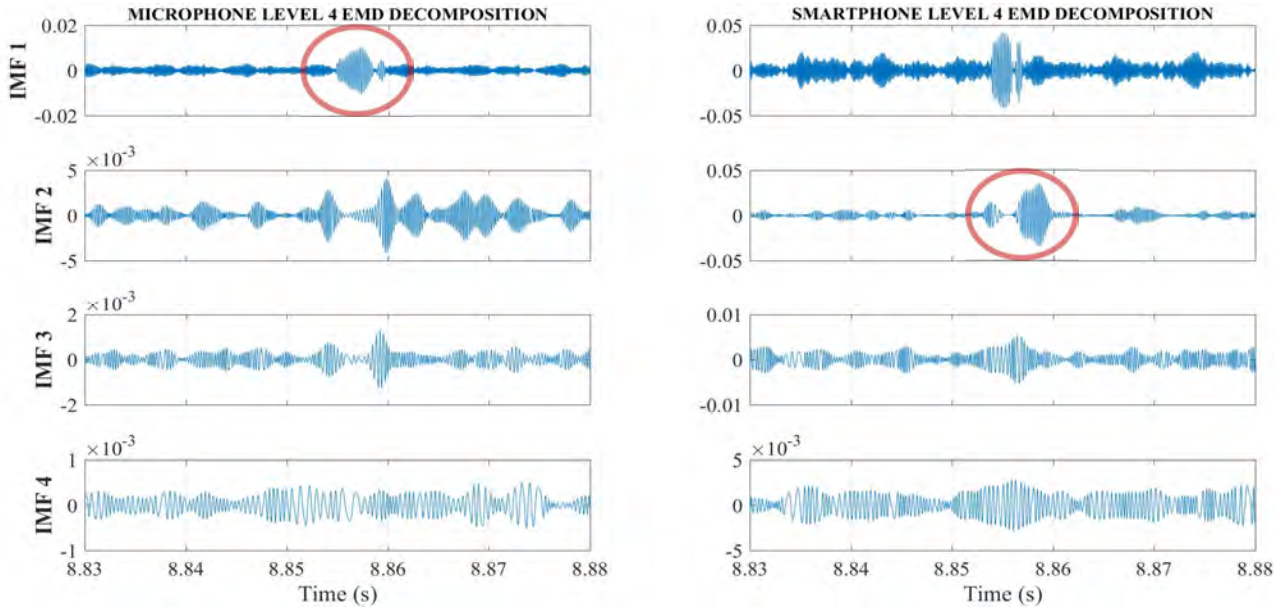

Figure 5: EMD level 4 decomposition of both the microphone (left) and smartphone (right) test signals.

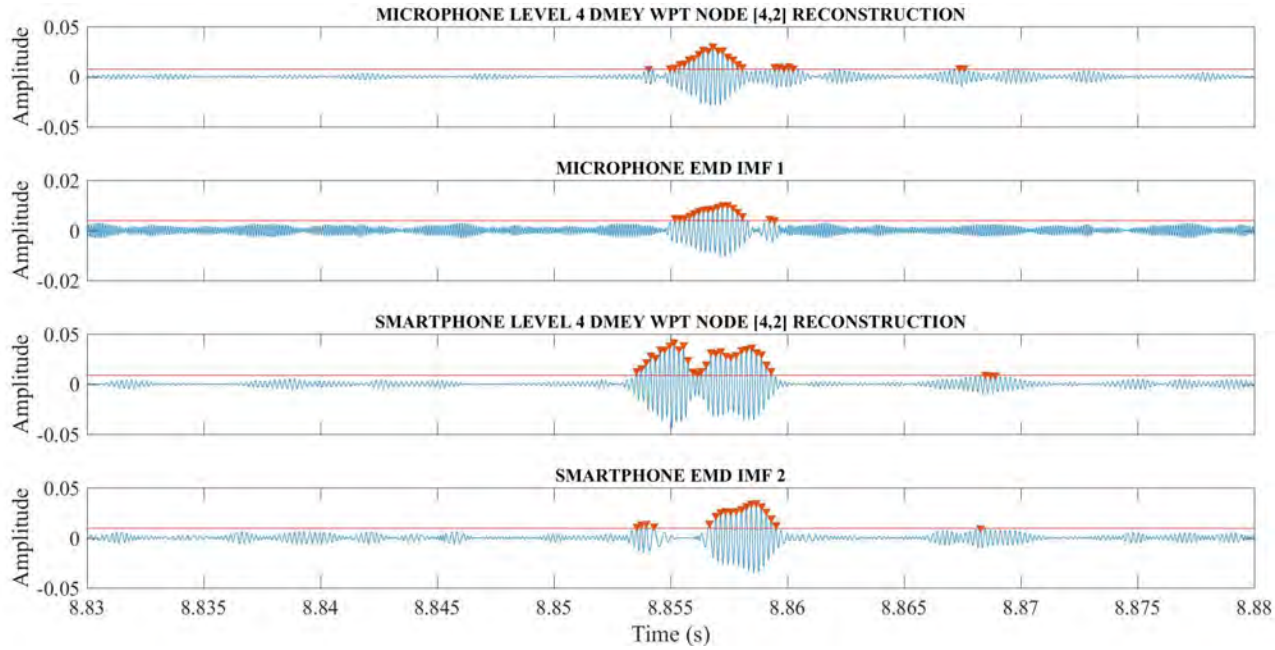

Figure 6: Microphone and smartphone signals processed by WPT and EMD. Threshold and the representative peaks are highlighted.

isolation of the fault information into the minimum number of nodes. This is clearly visible in node 17 as shown. The node's coefficients are used to reconstruct the signal; preserving the fault information and filtering out most of the unwanted noise.

2) Empirical Mode Decomposition Design

To determine the required level of decomposition the audio signals are initially decomposed to give 4 IMFs, shown in Figure 5. For the microphone and smartphone, IMF 1 and IMF 2 are selected respectively for further processing. This is based on visual analysis showing the best separation of the fault information away from background noise.

3) Instability Detection Design

To summarise, the original microphone and smartphone signals (Figure 3), are processed through WPT and EMD to give 2 × 2 signals (shown in Figure 6):

- microphone WPT
- smartphone WPT
- microphone EMD IMF 1
- smartphone EMD IMF 2.

The fault information signal to noise ratio is significantly improved. A standard peak finding algorithm detects the instability spikes in each processed signal. A standard deviation based amplitude threshold, is set for each signal such that only instability spikes protrude above. The key to diagnostic tuning is setting the threshold such that sufficient

width is detected to estimate the duration. Windowing discretises between separate instabilities (requiring a minimum separation of 0.02 s). This value is chosen based on observation to be sufficient to distinguish between different instabilities but, not so long as to class two separate instabilities together. Figure 6 shows the threshold line and separate instabilities highlighted.

4) Diagnostics Design

Basic diagnostics are performed to illustrate the potential for acoustics for similar applications. For each processed signal (Figure 6), the duration between the first and last peak found for a single instability is correlated against the actual duration (derived from the current signal) according to Eq. 1.

$$\rho_{X,Y} = \frac{\sum(x-\bar{x})(x-\bar{y})}{\sqrt{\sum(x-\bar{x})^2 \sum(x-\bar{y})^2}} \quad \text{Eq. 1}$$

A simplistic logarithmic model is developed, based on the best performing correlation results (in this case microphone WPT), to predict the instability duration in real-time throughout the primary run.

5) Real-Time Processing

To bound the problem, the purpose of real-time processing is to detect faults quickly enough to either shutdown the motor or provide a warning to the operator. Real-time processing can either be achieved using analog or digital techniques. Analog processing by nature performs much faster than digital, but this is beyond the scope of this work. Digital processing relies on splitting the data into discretised time segments. The previous segment can be searched for faults whilst the next is recorded. For continuous operation, this relies on the processing time being shorter than the time duration of each segment. The segment duration determines the refresh rate and detection response time of the system.

In this case, the refresh rate is set to 0.2 s, fast enough for all intended purposes and appearing real-time to the user. As the next segment is recorded the previous one is searched for instabilities as per the methods described above. The primary run current signal and audio are synchronised and processed identically to the preliminary run. The diagnostic results are analysed for accuracy against the actual instabilities and their durations. The results are presented in the next section.

III. Results & Discussion

This work set out to push the boundary of acoustic monitoring into diagnosing electrically-based faults; this case uses a transient current instability on an electric motor by way of example. By using consumer sensors, the practical uses these devices can deliver are highlighted. The diagnostic and computational performance of real-time WPT and EMD signal processing is examined.

A. Acoustics & Sensors Diagnostic Performance

The preliminary run first to last peak durations are given in Table I. For the 10 instabilities that occurred, all were detected by each processed signal. Table II gives the same results from the primary run where 82 instabilities occurred; some have been omitted for brevity. The greater number of instabilities is due to the higher control voltage. All instabilities were detected by each processed signal; with a single exception of microphone EMD instability 44, one of the shortest that occurred. There were no erroneous detections in either run. This issue has been partially addressed through complex time-frequency filtering, but minimising false alarms is beyond the scope of this work.

TABLE I: THE FIRST TO LAST PEAK DURATION OF EACH PEAK CLUSTER FROM THE PROCESSED AUDIO SIGNALS CORRELATED AGAINST THE ACTUAL INSTABILITY DURATION DERIVED FROM THE CURRENT SIGNAL ANALYSIS.

RUN 1 FIRST TO LAST PEAK DURATIONS (SECONDS)					
Instability Number	*Current*	*Microphone*		*Smartphone*	
		WPT	*EMD*	*WPT*	*EMD*
1	0.003	0.014	0.003	0.024	0.019
2	0.003	0.014	0.003	0.019	0.015
3	0.003	0.007	0.003	0.009	0.009
4	0.002	0.002	0.000	0.008	0.007
5	0.003	0.013	0.003	0.017	0.018
6	0.003	0.014	0.004	0.015	0.015
7	0.003	0.014	0.003	0.028	0.019
8	0.003	0.014	0.003	0.019	0.019
9	0.001	0.002	0.001	0.008	0.007
10	0.001	0.001	0.001	0.006	0.009
Correlation (%)		**93.38**	**75.31**	**81.70**	**82.25**

TABLE II: SUMMATIVE TABLE OF THE FIRST TO LAST PEAK DURATION FROM THE SECOND REAL-TIME RUN.

RUN 2 FIRST TO LAST PEAK DURATIONS (SECONDS)						*LOGARITHMIC ESTIMATION ERROR (%)*
Instability Number	*Current*	*Microphone*		*Smartphone*		
		WPT	*EMD*	*WPT*	*EMD*	
1	0.003	0.005	0.004	0.014	0.013	-12.957
2	0.003	0.005	0.004	0.013	0.014	-11.814
3	0.003	0.004	0.004	0.013	0.009	-22.268
4	0.003	0.005	0.004	0.018	0.013	-12.957
5	0.003	0.005	0.004	0.013	0.011	-14.548
11	0.003	0.005	0.003	0.009	0.009	-14.412
44	0.001	0.002	-	0.009	0.009	48.877
60	0.001	0.008	0.008	0.024	0.007	376.768
81	0.003	0.005	0.004	0.009	0.009	-12.957
82	0.003	0.005	0.004	0.014	0.009	-14.548
Min	**0.001**	**0.002**	**0.003**	**0.006**	**0.001**	**-25.692**
Max	**0.003**	**0.008**	**0.008**	**0.025**	**0.021**	**376.768**
Mean	**0.003**	**0.005**	**0.004**	**0.012**	**0.010**	**-1.209**
Std. Dev.	**0.001**	**0.001**	**0.001**	**0.004**	**0.003**	**64.941**

With almost perfect detection rates for all processed signals, the consumer sensors and time-frequency signal processing techniques are ideally suited for remote monitoring of electrical machines. To expand on this achievement, additional information, providing a diagnostic element, can be extracted from the acoustic signals. Estimating the instability duration from the acoustic signal can indicate whether preventative or corrective intervention is required. By way of example, Table II also gives the logarithmic model (based on the microphone WPT signal) estimation error. Demonstrating that, despite its simplicity; based on a small preliminary data set with no validation, still accurately predicted the durations with only -1.2% mean error. However, due to the limitations of the model and training data the spread is quite high. Nevertheless, it still illustrates that acoustics has huge potential for diagnostic capabilities.

TABLE III: FIRST TO LAST PEAK DURATION CORRELATIONS.

(%)	WPT	EMD	Average
Microphone	93.38	75.31	84.35
Smartphone	81.70	82.25	81.97
Average	87.54	78.78	83.16

TABLE IV: AVERAGE FRAME PROCESSING TIMES ACROSS ALL FRAMES AND FOR EACH SIGNAL PROCESSING METHOD.

	FRAME PROCESSING TIME (SECONDS)			
	MEAN	***STD DEV***	***MAX***	***MIN***
WPT	0.2034	0.0454	0.6205	0.1460
EMD	0.2037	0.0495	0.6554	0.1189
DIFFERENCE	-0.0003	-0.0042	-0.0349	0.0271

Table III gives the correlation results from the preliminary data showing that the microphone sensor and WPT processing performed the best with 84.4% and 87.5% correlations respectively. The best overall correlation of 93.4%, naturally comes from the microphone signal processed using WPT.

The smartphone performance compared to the microphone is particularly impressive considering the aperture and diaphragm are considerably smaller. The technology currently present in smartphones prevents them from becoming an all-in-one diagnostic tool, although this is likely to change as processing and memory improves. Comparing to analysing the current signal, these methods provide a simple and cost-effective solution. Although current analysis would provide better accuracy, due to the high sampling rates and specialist knowledge required it is significantly more difficult.

B. *Real-Time Acoustic Fault Diagnosis – EMD & WPT Performance Comparison*

WPT outperformed EMD both diagnostically and computationally. WPT isolated almost all the fault information within a single terminal node, delivering a well-filtered signal and improved performance. EMD split some information between the IMFs due to the nature of sifting. The computation required for EMD is greater than WPT, despite the inclusion of the duration prediction. Table IV gives the processing times that indicate which is more computationally intensive. Despite a minute time difference of -3.42×10^{-4} s, this represents a significant cost saving over long periods. Note that the processing time for each frame is slightly longer than the recording time meaning this system will only run up to the limits of the computer memory. For a continuous system, faster processing would be required so the frame processing time is smaller than the recording time.

IV. CONCLUSION

Real-time acoustic fault diagnosis, of an electrically-based fault, using consumer sensors, is demonstrated on a transient current instability for a PWM controlled brushless DC motor. 100% of the instabilities were detected with the microphone sensor and WPT processing proving the strongest candidates. This broadens the horizon for acoustic monitoring, previously limited to seeded mechanical faults, to include electrically-based faults. Acoustic processing in real-time, seriously under-developed in the literature, is performed digitally. This aspect is crucial for industry adoption of acoustic measurements for monitoring and supervision purposes. Here, accessible laptop hardware is used, easily achieving real-time processing. The consumer sensors show that research grade costly sensors are not required until fault information is contained in ultrasonic frequencies. These sensors have added advantages; being remote from the workpiece, able to monitor components with limited or no access, excellent accuracy and diagnostic capabilities as well cost-benefit performance. The historic knowledge, confidence and reliance surrounding established condition monitoring techniques such as vibration has resulted in the uptake of acoustics by industry to be very slow. The methods demonstrated are applicable to almost any fault with an acoustic signature. It is hoped that this work could open opportunities for future development of this field.

V. REFERENCES

[1] D. Mba and R. Rao, "Development of acoustic emission technology for condition monitoring and diagnosis of rotating machines; bearings, pumps, gearboxes, engines and rotating structures," *The Shock and Vibration Digest,* vol. 38, no. 1, pp. 3 - 16, 2006.

[2] K. Al-Balushi, A. Addali, B. Charnley and D. Mba, "Energy Index technique for detection of Acoustic Emissions associated with incipient bearing failures," *Applied Acoustics,* vol. 71, no. 9, pp. 812 - 821, 2010.

[3] S. Al-Dossarya, R. Raja Hamzahb and D. Mba, "Observations of changes in acoustic emission waveform for varying seeded defect sizes in a rolling element bearing," *Applied Acoustics,* vol. 70, no. 1, pp. 58 - 81, 2009.

[4] P. Konar and P. Chattopadhyay, "Bearing fault detection of induction motor using wavelet and support vector machines (SVMs)," *Applied Soft Computing,* vol. 11, no. 6, pp. 4203 - 4211, 2011.

[5] N. Nikolaou and I. Antoniadis, "Rolling element bearing fault diagnosis using wavelet packets," *NDT&E International,* vol. 35, no. 3, pp. 197 - 205, 2002.

[6] F. Hemmati, W. Orfali and M. Gadala, "Roller bearing acoustic signature extraction by wavelet packet transform, applications in fault detection and size estimation," *Applied Acoustics,* vol. 104, pp. 101 - 118, 2016.

[7] P. Kankar, S. C. Sharma and S. Harsha, "Rolling element bearing fault diagnosis using wavelet transform," *Neurocomputing,* vol. 74, no. 10, pp. 1638 - 1645, 2011.

[8] M. Amarnath and I. R. P. Krishna, "Empirical mode decomposition of acoustic signals for diagnosis of faults in gears and rolling element bearings," *IET Science, Measurement and Technology,* vol. 6, no. 4, pp. 279 - 287, 2011.

[9] T. Loutas, G. Sotiriades, I. Kalaitzoglou and V. Kostopoulos, "Condition monitoring of a single-stage gearbox with artificially induced gear cracks utilizing on-line vibration and acoustic emission measurements," *Applied Acoustics,* vol. 70, no. 9, pp. 1148 - 1159, 2009.

[10] M. Elmaleeh, N. Saad and M. Awan, "Condition monitoring of industrial process plant using acoustic emission techniques," in *2010 International Conference on Intelligent and Advanced Systems (ICIAS)*, Kuala Lumpur, 2010.

[11] S. Nandi, H. A. Toliyat and X. Li, "Condition Monitoring and Fault Diagnosis of Electrical Motors - A Review," *IEEE Transactions On Energy Conversion,* vol. 20, no. 4, pp. 719 - 729, 2005.

[12] M. Riera-Guasp, J. A. Antonino-Daviu and G.-A. Capolino, "Advances in electrical machine, power electronic, and drive condition monitoring and fault detection: state of the art," *IEEE Transactions On Industrial Electronics,* vol. 62, no. 3, pp. 1746 - 1759, 2015.

[13] N. Huang, Z. Shen, S. Long, M. Wu, H. Shih, Q. Zheng, N.-C. Yen, C. C. Tung and H. Liu, "The empirical mode decomposition and the Hilbert spectrum for nonlinear and non-stationary time series analysis," *The Royal Society Proceedings A - Mathematical, Physical and Engineering Sciences,* vol. 454, pp. 903 - 995, 1998.

[14] Z. Wu and N. Huang, "Ensemble Empirical Mode Decomposition - A Noise Assisted Data Analysis Method," *Advances in Adaptive Data Analysis,* vol. 1, no. 1, pp. 1 - 41, 2009.

[15] R. Yan, "Wavelet selection criteria for non-stationary vibration analysis in bearing health diagnosis," *University of Massachusetts,* 2007.

IET Journals
The Institution of Engineering and Technology

Acoustic Diagnostics of Electrical Origin Fault Modes with Readily Available Consumer-Grade Sensors

ISSN 1751-8644
doi: 0000000000
www.ietdl.org

Jarek Grebenik[1*], *Chris Bingham*[2], *Saket Srivastava*[3]

[1,2,3] *School of Engineering, The University of Lincoln, Brayford Pool, Lincoln, LN6 7TS, United Kingdom*
** E-mail: jgrebenik@lincoln.ac.uk*

Abstract: Acoustic diagnostics, traditionally associated with mechanical fault modes, can potentially solve a wider range of monitoring applications. Typically, fault modes are induced purposefully by the researcher through physical component damage whilst the system is shutdown. This paper presents low-cost real-time fault diagnostics of a previously unreported acute electrical origin fault that manifests sporadically during system operation with no triggering intervention. A suitability study into acoustic measurements from readily available consumer-grade sensors for low-cost real-time diagnostics of audible faults, and a brief overview of the theory and configuration of the wavelet packet transform (including optimal wavelet selection methods) and empirical mode decomposition processing algorithms is also included. The example electrical origin fault studied here is an unpredictable current instability arising with the PWM-controller of a BrushLess DC motor. Experimental trials positively detect 99.9 % of the 1160 resultant high-bandwidth torque transients using acoustic measurements from a USB microphone and a smartphone. While the use of acoustic techniques for detecting emerging electrical origin faults remains largely unexplored, the techniques demonstrated here can be readily adopted for the prevention of catastrophic failure of drive and power electronic components.

1 Introduction

Acoustic condition monitoring is well reported for the assessment of operational integrity in many mechanically-based industrial applications with proven advantages over established techniques, e.g. vibration monitoring. Acoustic measurements can offer earlier and more accurate detection of emerging changes in system characteristics, improved cost-benefit trade-off, readily accessible transducers, ease of setup and operation, and no detrimental impact on nominal system integrity by virtue of employing remote sensors. Nevertheless, established confidence and reliance on traditional vibration-based techniques has largely impeded the uptake of acoustic-based counterparts for industrial system monitoring, despite their advantages [1]–[11]. Moreover, much of the published research employing acoustic methods focus on detecting mechanically-seeded, impact-based faults, usually identifying the initial acoustic front with specialist Acoustic Emission (AE) sensors [1]–[4], [11]–[14]. Roller Element Bearing (REB) faults are particularly prevalent due to their proportionally high failure rate and the breakdown of vibration-based methods at slow rotational speeds [15], [16].

Several authors [1]–[3], [11], [14], compare acoustic and vibration measurements experimentally and all largely agree on the relative advantages: the responsiveness to early-stage defects and greater diagnostic accuracy. A distinctive feature of AE detection is the traditional use of specialist transducers that require surface mounting to the component to detect ultrasonic frequencies which would otherwise rapidly attenuate through an air medium.

To-date consumer-grade sensors have been used largely for urban noise mapping and voice monitoring for medical and speech recognition purposes, although extensions to system monitoring have been previously reported by [17] where a mobile smartphone and tablet is used to detect air leakage from an industrial air compressor by differentiating healthy and leaking states through audio feature classification. A prior investigation in [18] diagnoses six common faults in REBs using very similar sensors to those given here. In laboratory conditions, the sensors achieved 100 % and 95 % accurate detection from the USB microphone and smartphone, respectively. The investigation demonstrated the suitability of such consumer-grade sensors for identifying mechanical faults. Nevertheless, the computational and memory technology present in mobile smartphones and tablets remains restrictive for complex real-time signal processing, currently preventing a black-box all-in-one solution.

Most reported fault detection techniques concerning induction motors focus on broken rotor bars, shorted windings or bearing defects, where the damage is often intentionally induced by the researcher as a laboratory exercise, whilst the system is offline. From a measurement perspective this provides data only in the extreme healthy and unhealthy states, whereas in real-world systems damage often emerges slowly as the components damage over a protracted period. Reviews of many such faults are given in [19]–[24] with notable comparisons of different methods. For instance, [25] diagnoses shorted stator coils using acoustic measurements analysed using a line spectrum frequency technique. A set of feature vectors are then calculated to be classified using a k-nearest neighbour algorithm that clusters similar vectors based on their Minkowski distance, allowing separation between healthy and fault condition classifications. More recently in [26], [27] differential diagnoses between several REB defects and a number of seeded physical structure changes that cause electrical faults, including shorted coils of auxiliary and main windings, shorted coils of auxiliary windings, broken rotor bars, and broken squirrel-cage ring on a single-phase induction motor using acoustics. Feature extraction is based on frequency vectors that help form a feature vector of between 1 and 22 frequency components. Training data allows a nearest neighbour classifier to then match new data to known values. The microphone used is inexpensive and readily available but the faults are identified offline and require relevant training data to provide correct diagnoses. [28] distinguish between broken rotor bars and several REB defects under various operating conditions by analysing a smoothed-pseudo Vigner-Ville distribution, and in [29] an interesting method to estimate three-phase induction motor torque from acoustic signals is presented. The authors utilise a six-level relational-dilation wavelet transform to preserve frequency resolution in the lower bands. During diagnostics of REB cage faults, broken rotor bars and single phasing faults, the authors show that the estimated torque from the acoustic signals is very close to the measured torque. A different approach to detect imbalance and bearing damage on an

induction motor is presented in [30] where triple-axis vibration measurements are analysed using a quaternion-based algorithm. This method is very computationally efficient using basic mathematical operations and not requiring space transformations which are commonplace when considering most other techniques. [31] detect a broken rotor bar with a Field-Programmable Gate Array (FPGA) implementation for faster, real-time processing of the motor current signal, while [32] diagnose stator inter-turn, dynamic eccentricity, and a combination of both using a finite element system model and frequency analysis from an oscilloscope. These latter investigations [31], [32], demonstrate the commercial requirement for fault detection in real-time, delivering near instant operator feedback, where all previously discussed literature reports post-trial analysis. Real-time detection allows timely intervention, possibly during the commissioning process, to ameliorate costly on-site operational faults and prevent catastrophic failure.

Despite the electrical basis of the above fault research, the failure mechanism continues to be a physical change from human intervention whilst the system is shutdown. In contrast, electrically-seeded faults, which are often transient and with unpredictable recurrence characteristics, are typically detected using three broad methods, viz. quantitative detection [33], high-frequency injection [34], [35], and Motor Current Signature Analysis (MCSA) [33], [36]. High-frequency injection operates on the same principle as sensorless motor control, where the saliency is used to estimate rotor position by superimposing a low-magnitude, high-frequency sinusoidal signal on the excitation voltage and measuring the high-frequency modulation changes. By profiling these to healthy and unhealthy states these signatures can be used to detect faults in the windings or elsewhere in the electromagnetic circuit [34], [36]. MCSA is a well-established technique that can be used to detect a wide-range of motor faults. However, it remains computationally intensive, requiring frequency analysis to determine harmonic components and fault signatures. This makes it unsuitable to detect transient characteristics [19], [20], [34], [36]. Nevertheless, this problem has been partially addressed in [23] where the authors detect bar breakage through transient MCSA realised through Continuous Wavelet Transform (CWT) and Discrete Wavelet Transform (DWT). Another example is given in [37] where stator currents are analysed using a four-level Wavelet Packet Transform (WPT) to detect broken rotor bar fault. However, the accuracy of fault detection deteriorates under light or no-load conditions. These electrically-based fault detection techniques, whilst effective and widely adopted, require specialist expertise, equipment, access to system components and can be difficult to install on established systems.

Building on previous research in [38], this paper demonstrates the suitability of acoustic measurements from consumer-grade sensors for the real-time detection of sporadic, unpredictable and transient current instabilities of electrical origin. Specifically, as an example case study, a permanent magnet BLDC motor drive system that exhibits sporadic current instabilities which only occur during well-bounded operating regimes (at relatively high rotor speeds under light load conditions) is considered in this instance. It is notable that a 25 % change in the proportional gain element of the current controller negates the unstable operation thereby indicating that the instability is controller induced, and a result of the non-linear interaction of the motor electrical parameters, parasitic components and digital controller realisation. By way of example, Fig. 1 shows each phase current supplied to the BLDC motor under no-load operation (hence the voltage overhead is insufficient to produce classical 'flat-topped' current waveforms). In this case, four discrete periods of unstable controller induced current oscillations that remain for the commutation period can be seen. These unstable events have the potential to propagate to drive system failure, poor performance or possible demagnetisation of the motor (if the commutation sequence is disrupted). Although a single significant event could initiate these failure modes, a more likely scenario is that multiple minor events would occur over a prolonged period, causing long-term damage that would otherwise remain undetected. The current instabilities induce an audible, mechanical torque transient within the motor, producing an acoustic signature in the audible range (20 Hz to 20 kHz) commensurate with typical PWM frequencies and AC sources, and making consumer-grade acoustic transducers appropriate. This differs from prior investigations that typically employ vibration sensors or specialised piezoelectric transducers, surface mounted for higher-frequency pickup (typically 100 kHz to 1 MHz). Such sensor systems are of comparatively high-cost, require complex specialist setup and operation (low-noise transmission and amplification, and fast data acquisition), are more susceptible to operational damage, and are intrusive to the system under test. Electrical origin fault modes are traditionally diagnosed electrically with techniques such as MCSA. Furthermore, to date, research has focussed on detecting faults caused by mechanical changes to the system. The method presented here is widely applicable to both mechanical and electrically-seeded faults that result in an audible signature. The particular case considered in this paper represents one practical example. The key contributions of this paper are:

- the diagnosis of electrical origin faults where the failure mode is unseeded (i.e. not by human intervention) and manifests sporadically during continuous system operation,
- the proposed use of consumer-grade acoustic sensors that are readily available for low-cost continuous real-time monitoring,
- a brief comparison of methods for optimal selection of the mother wavelet when using wavelet transformations.

2 Underlying Principles

2.1 Acoustic Transducers

Consumer-grade acoustic transducers are designed to measure longitudinal pressure waves in air within the audible frequency range (consistent with the music and telephonic industries). These integrated sensor systems are highly-developed and mass produced, and are therefore widely available, low-cost and easy to use. Four main acoustic sensor categories exist; capacitive, inductive, piezoelectric and optical. Most surface mounted 'research-grade' sensors are piezoelectric, whereas consumer-grade sensors usually operate on capacitive principles as follows. Typically, a thin gold-coated mylar diaphragm forms a flexible capacitor plate that moves with respect to the other plate in response to acoustic pressure waves, Fig. 2. This changes the capacitance, usually in the region of 10

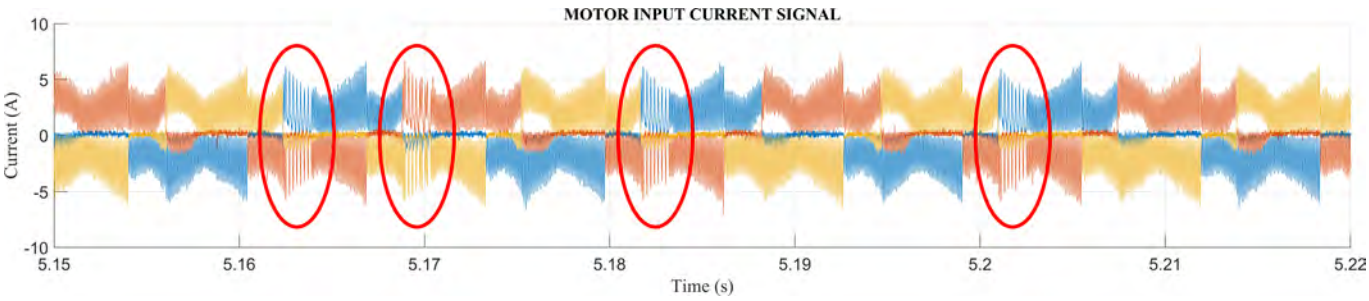

Fig. 1: Three-phase BLDC motor currents with four distinct current instabilities circled.

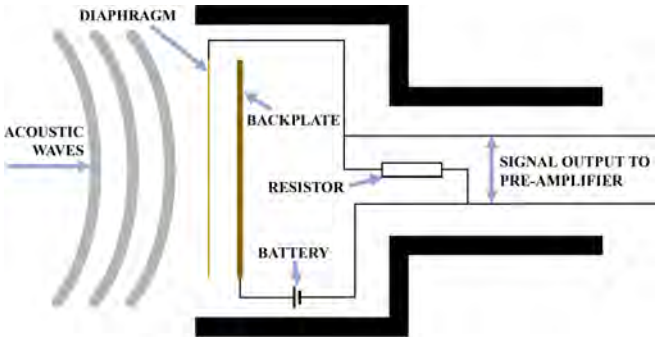

Fig. 2: Diagram of a simple capacitive microphone circuit.

to 50 pF. A phantom power source provides a DC voltage (usually 48 V) that pulls the diaphragm taut. As the capacitance changes, the small voltage fluctuations across a high load resistor are amplified and measured as the audio signal. These remote sensors commonly exhibit directional sensitivity that are depicted as polar patterns of four primary types: omni-direction, bi-directional, cardioid or super-cardioid. The cardioid pattern is most suitable in this case and for condition monitoring since it is most sensitive at the front with reduced lateral and minimal rear pick-up [39].

Unlike surface-mounted counterparts these consumer-grade sensors suffer from signal attenuation through the air which is more pronounced at higher frequencies. They are also prone to superimposed noise from a variety of external sources, and careful selection of the feature extraction algorithm is therefore necessary.

2.2 *Fault Signature Extraction*

Separating the acoustic fault signature from unwanted noise can prove challenging in a real-world environment. Noise from the surrounding environment and auxiliary electrical sources, combined with signal attenuation through medium transmission, sensor imperfections, and analogue to digital conversion, can result in the fault signatures becoming buried. The goal of feature extraction is to isolate as much fault information as possible with minimal computation overhead.

Mathematically, there are three primary domains in which signals are traditionally analysed. Firstly is the time domain with a plethora of mathematical techniques and algorithms available, ranging in complexity from basic mathematical operations such as multiplication through to composite sequential operations forming algorithmic analysis. Secondly, the Fourier transform or variations thereof, which converts a time or spatial domain signal to a frequency representation. In signal processing the Fast Fourier Transform (FFT) is commonly utilised to determine underlying frequency content. The third domain, known as the time-frequency domain, allows the study of both time and frequency information simultaneously. However, there is a trade-off in resolution between time and frequency domains. Fig. 3 illustrates the concept of how these different domains can trade-off resolution. Although excellent resolution can be achieved in both time and frequency using techniques such as Short-Time Fourier Transform (STFT), a significantly disproportionate amount of computation is required, making this technique unsuitable for low-cost real-time continuous processing and for larger datasets. An advantage of so-called wavelet transforms is in the configuration of the domain resolutions, making the algorithm significantly more efficient whilst still achieving the required resolution performance.

Fault detection algorithms can be broadly categorised into those that can detect continuous (e.g. a mechanically worn component or a pressurised leak) or transient (e.g. a mechanical impact such as damage to the race of a roller bearing) faults. Identifying a continuous fault is relatively straightforward as marked differences between healthy and unhealthy states would usually be evident in the frequency spectrum. Equally in the time domain a change from a healthy to an unhealthy state may also be evident. However, transient

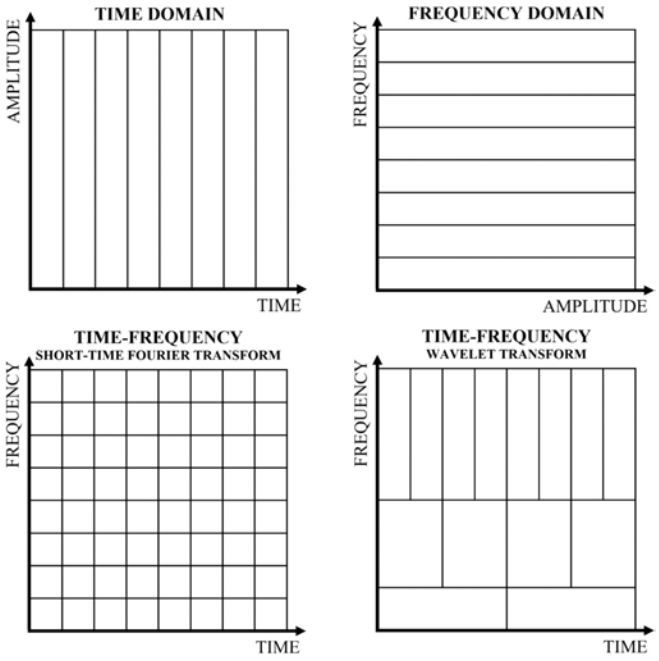

Fig. 3: Diagram illustrating the resolution differences between time, frequency, and time-frequency domains.

fault types can prove more challenging as the fault signature is often hidden in the time domain and may only result in very low-level changes in the frequency domain. A time-frequency algorithm can then be used to better identify such conditions. When considering different feature extraction methods, it is critical that the nature of the fault features are well-understood. In this case, as is common with transient fault detection, the signature is of high frequency and short time duration. Therefore, an optimal detection algorithm would seek to reveal frequency changes with respect to time, as corroborated in [3], [5]–[10], [12], [40]–[45].

There are many well-known time-frequency techniques such as the STFT, spectrogram analysis, wavelet transform, Wigner distribution, Wigner-Ville, Choi-Williams, and Hilbert-Huang Transform (HHT), from which many variations are derived. For this work, two feature extraction algorithms, WPT and Empirical Mode Decomposition (EMD), are chosen for comparative purposes. These techniques are prominent in the field and their suitability and excellent performance for such applications are well-documented. Aiming to demonstrate the suitability of real-time acoustic signal processing for previously unexplored fault types (of electrical origin and with no physical change to nominal system integrity), it is desirable to use WPT and EMD as they are commonly used and well-understood in the wider industry to provide an initial investigation into this novel application sector [44]. An overview of both techniques is now provided along with some insight on why these specific variations are particularly suited to this application.

2.2.1 Wavelet Theory: The wavelet transform can be considered a dynamic extension to the classical Fourier transform which uses the sum of complex exponentials, but instead employs a dyadic dilation of a scaling function and translation of a mother wavelet function (example given in Fig. 4). The CWT of a finite energy signal $x(t)$ is the result of convolving that signal with a dyadic scaling and translation of a mother wavelet $\Psi(t)$ of the form:

$$W_{(\alpha,b)} = \alpha^{\frac{1}{2}} \int_{-\infty}^{\infty} x(t)\Psi * \left(\frac{t-b}{\alpha}\right) dt \qquad (1)$$

where $W_{(\alpha,b)}$ is the wavelet coefficient, α is the dyadic scaling, b is the dyadic translation and Ψ is the mother wavelet.

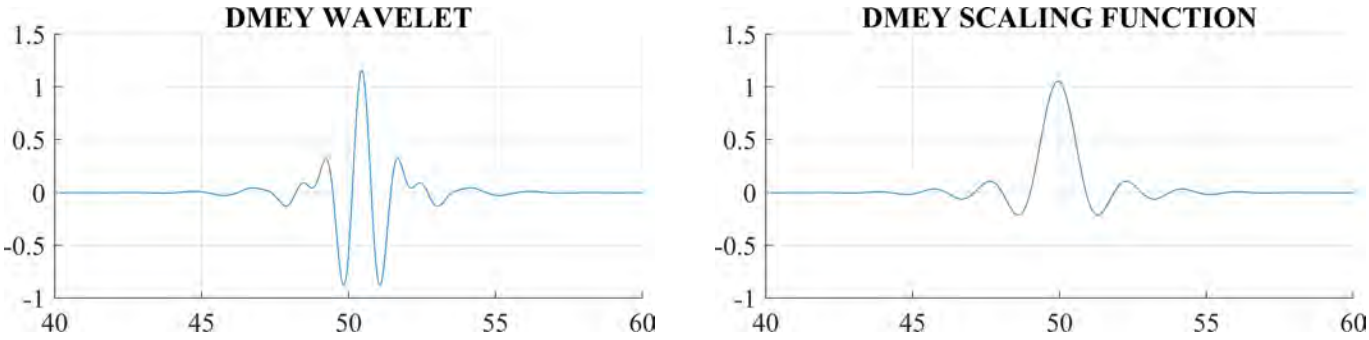

Fig. 4: The dmey mother wavelet and scaling function. Axes units not relevant here.

A true CWT requires an infinite number of functions that generate an infinite number of coefficients, which is impossible to realise practically. Letting $\alpha = 2^m$ and $b = n2^m$ (where m and n are integers), the CWT becomes discrete and forms an orthonormal basis set;

$$\Psi_{(m,n)}(t) = 2^{-\frac{m}{2}}\Psi(2^{-m}t - n) \tag{2}$$

allowing realisable calculation overhead. The base scale is usually a fractional power of 2 in the form $2^{j/v}$, where j represents the number of scales and v represents the fidelity of each scale (sometimes known as the number of 'voices per octave'). The resulting number of coefficients remains very high - an M by N matrix, where N is the input signal length and M is the number of scales.

The DWT discretises the scale to $2^{j/1}$ with only a single 'voice per octave' and base scale of 2. This results in the number of coefficients being equal to an $L + 1$ by N matrix, where L is the decomposition level. The DWT convolves the original signal with a low pass filter $h(n)$ and high pass filter, $g(n)$, and downsamples by a factor of 2. $h(n)$ and $g(n)$ are a coarse discretisation of the dyadic scaling and wavelet function, and take the form:

$$h(n) = \frac{1}{\sqrt{2}}\langle\varphi(t), \varphi(2t - n)\rangle \tag{3}$$

$$g(n) = \frac{1}{\sqrt{2}}\langle\Psi(t), \Psi(2t - n)\rangle = (-1^n)h(1 - n) \tag{4}$$

where $\varphi(t)$ is the dyadic scaling function.

This results in approximate coefficients cA_1 and detail coefficients cD_1. The process can be repeated on the approximation coefficients to give a multi-level decomposition, as depicted in Fig. 5. Reconstruction of the signal involves upsampling by two and convolving the approximation and detail coefficients with low and high pass reconstruction filters respectively, giving the real approximation and detail that are then summed [7], [44].

The WPT follows the same principle but additionally decomposes the 'detail path' and the 'approximation path' at each level. This

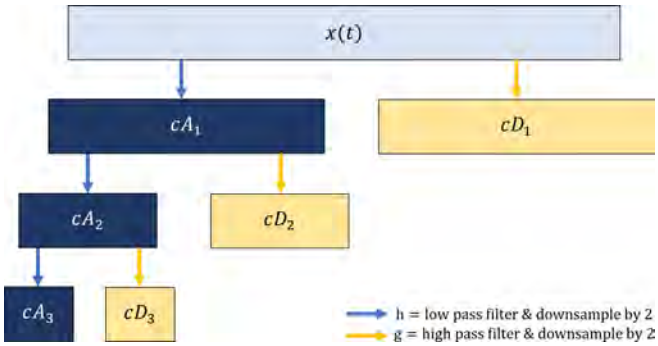

Fig. 5: Example three level DWT. Original time domain signal is $x(t)$, and signal reconstruction uses cA_3 and cD_1 to cD_3.

results in an even wavelet packet tree shown in Fig. 6. Frequency folding which occurs with WPT results in low pass filtered signals containing information on the high frequency content. Consequently, the reconstruction order is aligned to the frequency order by inverting the position of each right-hand branch (illustrated by the red swap arrows and text). For example, at the third level the natural order is 0, 1, 2, 3, 4, 5, 6, 7 but the frequency order becomes 0, 1, 3, 2, 7, 6, 4, 5 [7], [44].

Although the CWT offers high-fidelity, it is excessive for this purpose and the computational resources required are generally too large for low-cost real-time continuous processing. The DWT or WPT offers a sparse representation of the signal providing compression, but also reconstruction of the original signal from the approximation and detail coefficients. The additional terminal nodes of WPT over DWT allows deeper analysis of the different frequencies and the complex reconstruction can use specific terminal nodes facilitating unparalleled isolation of fault information, revealing the abrupt changes in hidden frequencies [3], [6], [7], [44].

2.2.2 Empirical Mode Decomposition Theory: EMD forms the first part of the Hilbert-Huang Transform [46] and is a time domain signal decomposition method particularly suited to analysing non-linear and non-stationary systems and signals. Each decomposition level begins with a sifting operation where smooth upper and lower envelopes of the signal based on local maxima and minima (using cubic spline interpolation) are generated. The mean of the two envelopes m_1 is then subtracted from the original signal to give the first sifted component, $h_1 = x(t) - m_1$. The second sifting iteration treats h_1 as the input and m_{11} is the mean of the new input upper and lower envelopes giving $h_{11} = h_1 - m_{11}$. This process is repeated k times, $h_{1k} = h_{1(k-1)} - m_{1k}$ until a termination criterion is reached. This forms the first Intrinsic Mode Function (IMF), $c_1 = h_{1k}$ which is subtracted from the original signal to give the first residue $r_1 = x(t) - c_1$. The residue is then treated as the input and the sifting process repeats j times until the stoppage criterion, $r_j = r_{(j-1)} - c_j$ is reached. Various stoppage criteria can be used, such as a standard deviation match, a predefined threshold, energy difference tracking or S-number (the number of consecutive sifting iterations where the number of zero crossings and extrema are the same or differ by one). The IMFs are oscillatory functions with higher IMF decomposition levels revealing subsequently lower frequencies. All the IMFs are the same length as the original signal and they must satisfy the two criteria below such that their superposition will reconstruct the original signal:

- the number of IMF extrema (the sum of the maxima and minima) and the number of zero crossings must either be equal or differ at most by one;
- at any point of an IMF the mean value of the envelope defined by the local maxima and the envelope defined by the local minima shall be zero.

It is well known that EMD is prone to mode mixing and aliasing issues with more intermittent signals, resulting in IMFs that are devoid of physical meaning. EMD also degrades when multiple concurrent data points form a flat or non-oscillatory part of the signal

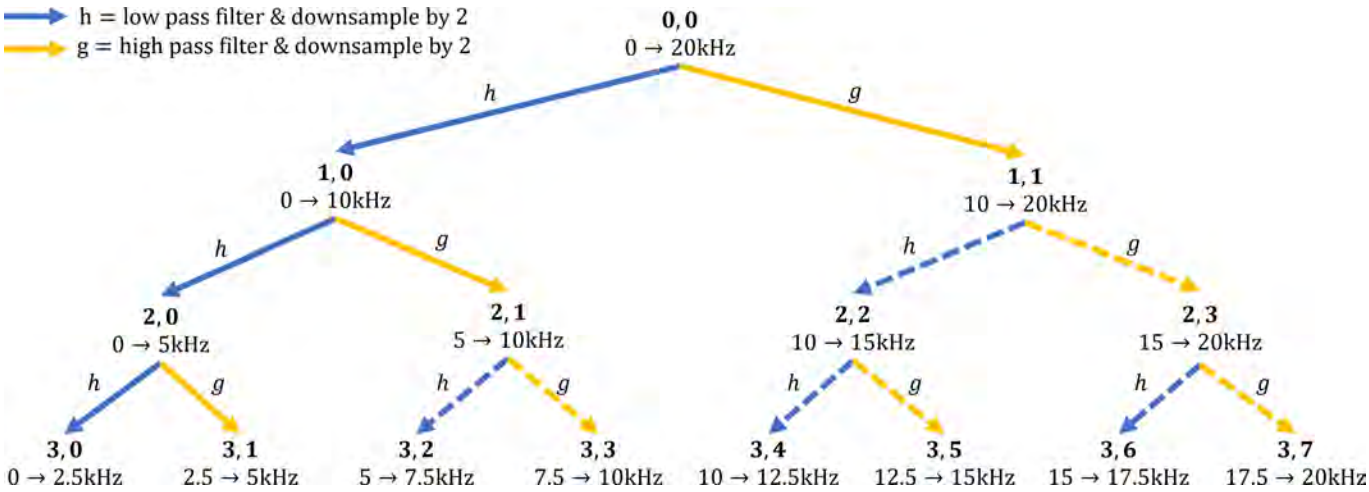

Fig. 6: Example three level WPT tree showing the frequency range corresponding to each node coordinate. Dashed lines show the additional branches of WPT compared to DWT.

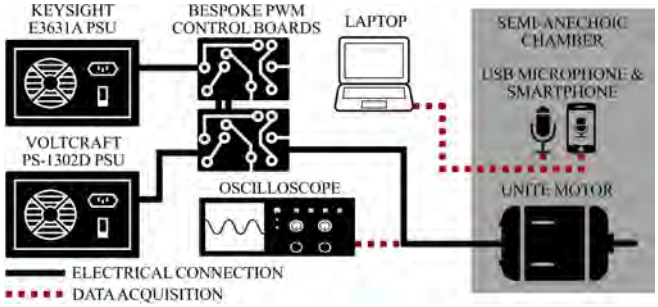

Fig. 7: Experimental setup diagram.

e.g. a square wave. To counter these disadvantages Ensemble Empirical Mode Decomposition (EEMD) [47] adds white noise to the input signal and then takes the ensemble mean of multiple outputs to form a single IMF. Accuracy is increased by using more ensembles, cancelling the white noise. However, this is computationally intensive and makes EEMD unsuitable for low-cost real-time processing. Further, since acoustic signals are highly-oscillatory EEMD would not provide any significant advantage over conventional EMD. Although EMD remains a time domain algorithm, it does provide an analysis of pseudo-time-frequency information. However, the result is devoid of physical meaning and the IMFs are not precisely orthogonal. For the acoustic signals analysed here, EMD can imprecisely reveal the short-time transient frequency changes with excellent detection accuracy providing isolation of an empirically-derived fault signature.

3 Experimental Setup

A three-phase BLDC 36 V 1600 W Unite MY1020 motor is powered through a bespoke digital current controller. Internal Hall-effect sensors are used to facilitate commutation. Consumer-grade acoustic transducers, specifically an Audio-Technica AT2020 USB+ microphone and a Samsung Galaxy S7 smartphone using WO Mic, are both positioned $\approx$10 cm from the motor with their sensitive planes directed toward the motor. A setup diagram is given in Fig. 7. Both acoustic sensors have their own inbuilt analogue to digital converter and connect digitally for continuous real-time sampling at 48 kHz with 16-*bit* resolution using Matlab. In parallel with the sampling, Matlab discretises the data into packets and processes each one using the feature extraction techniques, delivering real-time analysis every 0.2 s. A posteriori knowledge of the instability duration (approximately 1.5 ms) is used to define the system refresh rate of 5 Hz; sufficiently long to capture entire instability periods but fast enough to prevent damage to the motor drive. The three motor phase currents are measured using three isolated high-bandwidth Hall-effect current sensors, sampled at 250 kHz with 16-*bit* resolution on an oscilloscope. The high sampling rate allows inter-PWM current characteristics to be captured. The motor and acoustic sensors are sited in a semi-anechoic chamber, ensuring minimal background noise. Nevertheless, signal processing is still required to adequately separate the fault information from unwanted motor noise.

3.1 Wavelet Packet Transform Configuration

Optimal selection of the mother wavelet is critical to the performance of the WPT and is dictated by the similarity of the wavelet shape to the signal of signature through dilation and translation. In other words, through dilation and translation how well can the wavelet match the signal or signature. There is no defined method to determine this, and researchers have devised various quantitative measures, all fundamentally based on experimentation and a posteriori knowledge of relevant signatures. Typically, a selection of different wavelets are tested for various quantitative performance factors such as maximum energy, minimum entropy, minimum reconstruction error, cross-correlation to name a few. In [48], five attributes (energy, Shannon-entropy, signal power to noise power ratio, mean square error, and maximum absolute squared deviation) are evaluated for twenty-six different wavelets. Three separate weighting schemes are applied to the attributes using the analytic hierarchy process (based on pairwise comparison matrix of the attributes). Each weighting scheme revealed a performance ranking order of the wavelets analysed where the highest-ranking wavelet is deemed to deliver the best performance for the given application. A slightly simpler approach is given in [49], where the maximum energy to Shannon-entropy ratio is used as a measure of wavelet performance. This method is undertaken for the investigation in this paper, as the acoustic fault signature is known to be of a transient nature within the normal operational characteristics of the motor. Although for certain applications it may be necessary to undertake a further comparative study of information measures (joint entropy, conditional entropy, mutual informal, relative entropy and comparative information entropy for example), it is unnecessary in this case due to the transient nature of the fault signature. Therefore, the best maximum energy to Shannon-entropy ratio is used to select the wavelet. Sixty different wavelet types from the Haar, Daubechies, Symlets, Coiflets, Biorthogonal, Reverse-Biorthogonal, Discrete approximation of Meyer (dmey) and Fejer-Korovkin families are analysed; revealing the dmey wavelet (from Fig. 4) to be most suitable for these signals.

The required number of decomposition levels is visually determined through inspection of the terminal node coefficients using the Matlab wavelet analyser; aiming to maximise the isolation of the fault signature from unwanted noise. This analysis, Fig. 8 shows

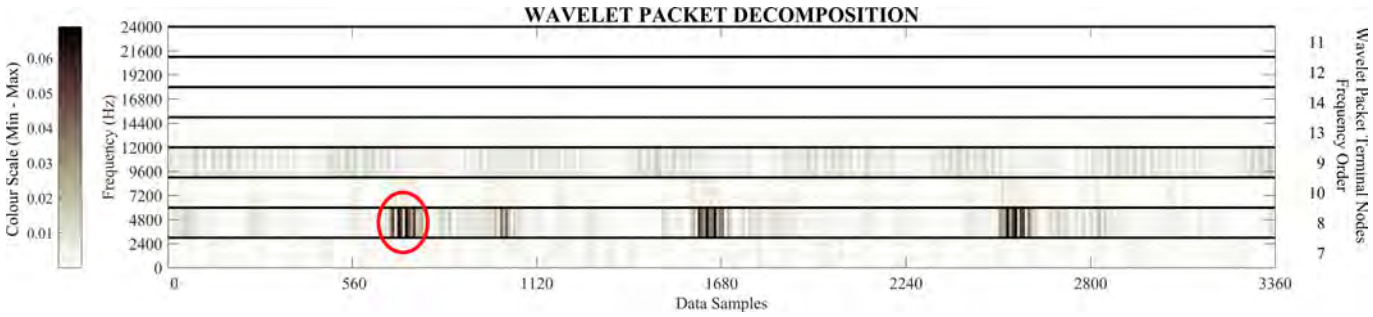

Fig. 8: Microphone data dmey 3-level WPT terminal node coefficients. The instability information from Fig. 1 can be seen as dark patches in terminal node [3,1] or 8. First one circled for clarity.

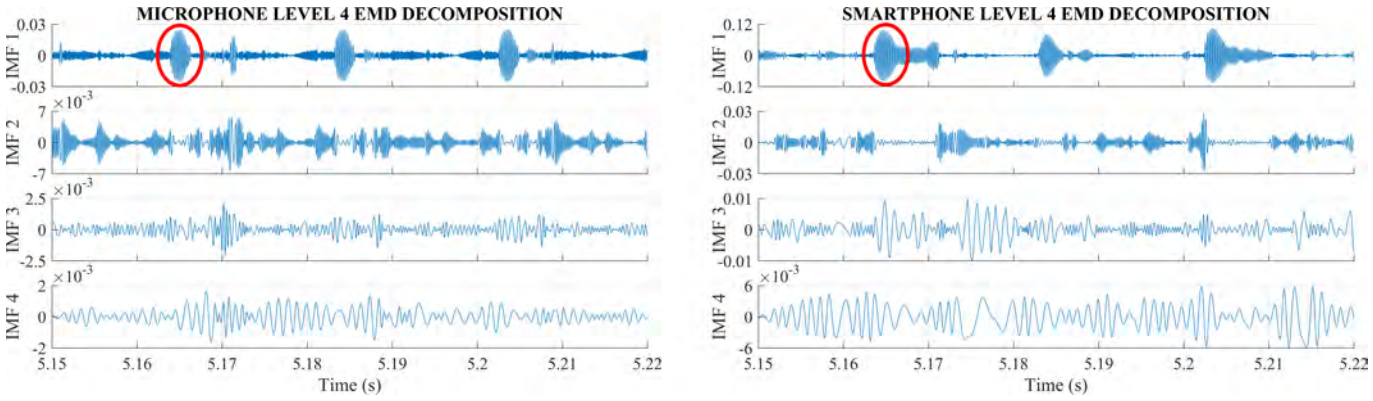

Fig. 9: EMD 4-levels with microphone data on the left, and smartphone data on the right. Only relative amplitude are significant on the IMFs (in descending order), with the red circle marking the first of four instabilities.

excellent fault signature isolation into terminal node $[3, 1]$ or 8. The higher coefficient values are colour mapped darker. The original signal is reconstructed from these coefficients thus excluding most of the unwanted noise and erroneous frequencies and delivering the fault information signature. Reconstruction is realised through upsampling by two and convolving the approximation and detail coefficients with low and high pass reconstruction filters respectively which gives the real approximation and detail that is summed together.

3.2 Empirical Mode Decomposition Configuration

An empirical approach is used to establish the required number of decomposition levels. Both microphone and smartphone measurements are initially decomposed into four levels giving the four IMFs shown in Fig. 9. As the fault information is expected to be high-frequency it would likely be contained in the early IMFs. The default stopping criterion is based on standard deviation matching and a maximum of 2000 sifting iterations allow normal operation of the sifting process.

The results, Fig. 9, shows the majority of the fault information is preserved in IMF 1. Hence, only a 2-level decomposition is necessary; providing the first IMF for further analysis and a residue signal containing everything else i.e. the remaining noise. Interestingly, there is no apparent information relating to the instabilities in any of the remaining IMFs indicating only higher-frequency fault information.

3.3 Fault Diagnostic Method

In summary, the acoustic measurements from the USB microphone and smartphone sensors are pre-processed using the WPT and EMD algorithms described above delivering four sensor / algorithm combinations, Fig. 10. A standard peak finding approach is the final step to detect the instabilities in each pre-processed signal. Detection is qualified using an amplitude threshold based on the standard deviation of each processed signal (data from a preliminary test run). Windowing discretises individual instabilities using a lower limit separation of $0.02\,\mathrm{s}$ (sufficiently long to distinguish between instability periods, but short enough to not class two separate instabilities together as a single entity). Fig. 10 shows the detection threshold line along with the identified instability start and end points.

4 Experimental Results

The results from three experimental trials are now presented with analysis of the sensor and feature extraction algorithm relative performance, and detection rates of the electrically-seeded instabilities.

4.1 Consumer Transducer Performance

Firstly, the number of unstable periods for each trial are counted from the motor phase current measurements, and are compared in Table 1 against the four sensor and algorithm combinations (top row of each trial). The bottom row of each trial is a percentage of the sensor/algorithm detection rate against the actual occurrences. The green values show that the microphone/WPT combination provided $100\,\%$ accuracy in detecting the fault periods during trials 1 and 2, with only a single missed instability period during trial 3. This excellent performance is further highlighted in Table 2, where the mean percentage of correct detection across all three trials reveals the performance of the sensors, algorithms and combinations. The USB microphone marginally outperforms the smartphone by $1.7\,\%$, achieving an overall detection rate of $99.9\,\%$. This is attributable to its larger, open diaphragm, compared to the smartphone which has a water-resistant microphone within a small aperture. Nevertheless, the smartphone performance remains impressive considering the relative disadvantages. The semi-anechoic environment minimises

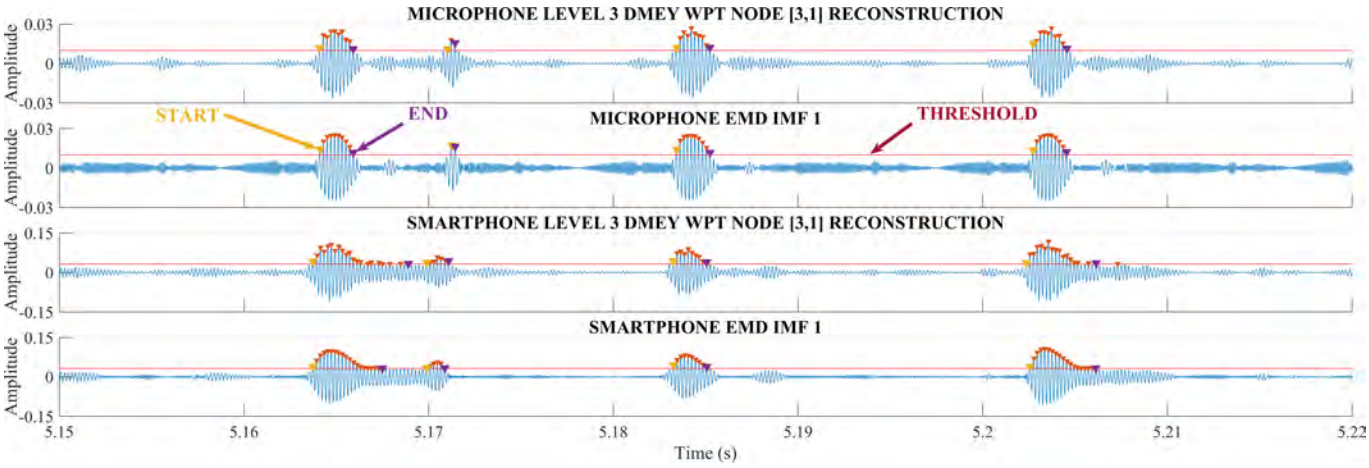

Fig. 10: Processed signals showing almost exclusively fault information. The peak detection threshold is shown by the horizontal red line with detected peaks marked in red, and the start and end of each discrete instability in yellow and purple respectively.

Table 1 The total number of unstable features found for each trial using the phase current measurements as a reference for the acoustically detected faults. Blue indicates that some unstable periods were missed, orange indicates false positive detections (which also result in percentages over 100 %), and green shows the best performance.

TRIAL	INSTABILITY PERIODS DURING TRIAL	ACOUSTIC DETECTOR PERFORMANCE			
		MICROPHONE		SMARTPHONE	
		WPT	EMD	WPT	EMD
1	327	327	326	309	290
		100.0%	99.7%	94.5%	88.7%
2	690	690	658	685	668
		100.0%	95.4%	99.3%	96.8%
3	143	142	142	147	145
		99.3%	99.3%	102.8%	101.4%
TOTAL	1160	1159	1126	1141	1103
		99.9%	97.1%	98.4%	95.1%

background noise and is partially responsible for the high detection rates achieved. Even so, the results do demonstrate the potential benefits of the proposed methodology.

4.2 Fault Signature Extraction Algorithm Performance

Results in Tables 1 and 2 show that the WPT algorithm outperforms EMD in detection performance by isolating the fault signature entirely into one terminal node. In some cases, EMD failed to separate events that occurred in close proximity, resulting in multiple instabilities being classed as one by the detection algorithm.

Regarding real-time processing, the mean data packet processing times provide an indication of computational efficiency for the feature extraction algorithms as given in Table 3. The times are normalised to the system refresh rate (0.2 s) for clarity. Processing times are seen to be very close to the system refresh rate. A slower processing rate is not suitable for real-time systems as the time lag will continue to increase and the system will run out of memory. Both feature extraction algorithms performed well overall, with EMD exhibiting the slowest and fastest processing. However, WPT proved to be consistently faster, delivering the fastest mean processing time.

Table 2 Correct detection percentage across all three trials.

	WPT	EMD	MEAN
MICROPHONE	99.9%	97.1%	98.5%
SMARTPHONE	98.4%	95.1%	96.1%
MEAN	99.1%	96.1%	

Table 3 Mean processing times across all trials normalised to the system refresh rate.

TRIAL	WPT	EMD
1	-0.31	1.69
2	-0.55	-2.37
3	-0.52	-0.18
MEAN	-0.46	-0.28

5 Conclusion

This paper presents the use of acoustic measurements for low-cost real-time detection of an acute electrical origin fault mode that manifests sporadically under well-bound operating conditions on a BrushLess Direct Current (BLDC) motor drive system. The example fault mechanism investigated is a transient current instability that arises in the motor supply from the controller due to the non-linear interaction of the PWM-controller parameters, parasitic components and digital controller realisation. This case study

verifies that acoustic measurements are capable of detecting electrical origin faults. Low-cost continuous real-time acoustic monitoring is realised through the readily available consumer-grade sensors employed, specifically a USB microphone and portable smartphone. These sensor types can be easily and readily adopted to solve a wide variety of real-world condition monitoring and fault detection requirements in both mechanical and electrical systems and of both mechanical and electrical origin fault modes. Across the three experimental trials undertaken, 1160 discrete unstable controller induced current oscillations were present. An investigation into the suitability of consumer-grade sensors and feature extraction algorithm performance, (specifically combinations of a USB microphone and smartphone acoustic transducers with Wavelet Packet Transform (WPT) or Empirical Mode Decomposition (EMD) feature extraction) revealed that all combinations delivered excellent performance. However, it was the USB microphone and WPT feature extraction that performed best - correctly identifying 1159 (99.9 %) of the instabilities. This is attributed to the larger diaphragm of the USB microphone and optimal selection of the analysing wavelet by the highest energy to Shannon-entropy ratio method. Although the USB microphone performed marginally better, the smartphone offers the potential to become an all-in-one future diagnostic tool given the obvious advantages of being established, easily accessible, relative low-cost, self-powering, remote from the system, and with internet and other communication built in. This research may provide the stimulus for the widespread adoption of consumer-grade sensors and smartphone technology for fault detection and monitoring of both mechanical and electrical systems and fault modes.

References

[1] T. H. Loutas, G. Sotiriades, I. Kalaitzoglou, *et al.*, "Condition monitoring of a single-stage gearbox with artificially induced gear cracks utilizing on-line vibration and acoustic emission measurements," *Applied Acoustics*, vol. 70, no. 9, pp. 1148 –1159, 2009.

[2] B. Eftekharnejad, M. R. Carrasco, B. Charnley, *et al.*, "The application of spectral kurtosis on acoustic emission and vibrations from a defective bearing," *Mechanical Systems and Signal Processing*, vol. 25, no. 1, pp. 266 –284, 2011.

[3] F. Hemmati, W. Orfali, and M. S. Gadala, "Roller bearing acoustic signature extraction by wavelet packet transform, applications in fault detection and size estimation," *Applied Acoustics*, vol. 104, pp. 101 –118, 2016.

[4] H. Li, F. Xu, H. Liu, *et al.*, "Incipient fault information determination for rolling element bearing based on synchronous averaging reassigned wavelet scalogram," *Measurement*, vol. 65, pp. 1 –10, 2015.

[5] M. Amarnath and I. R. P. Krishna, "Empirical mode decomposition of acoustic signals for diagnosis of faults in gears and rolling element bearings," *IET Science, Measurement and Technology*, vol. 6, no. 4, pp. 279 –287, 2011.

[6] P. Konar and P. Chattopadhyay, "Bearing fault detection of induction motor using wavelet and support vector machines (svms)," *Applied Soft Computing*, vol. 11, no. 6, pp. 4203 –4211, 2011.

[7] N. G. Nikolaou and I. A. Antoniadis, "Rolling element bearing fault diagnosis using wavelet packets," *NDT&E International*, vol. 35, no. 3, pp. 197 –205, 2002.

[8] K. Feng, Z. Jiang, W. He, *et al.*, "Rolling element bearing fault detection based on optimal antisymmetric real laplace wavelet," *Measurement*, vol. 44, no. 9, pp. 1582 –1591, 2011.

[9] W. He, Z.-N. Jiang, and K. Feng, "Bearing fault detection based on optimal wavelet filter and sparse code shrinkage," *Measurement*, vol. 42, no. 7, pp. 1092 –1102, 2009.

[10] P. K. Kankar, S. C. Sharma, and S. P. Harsha, "Rolling element bearing fault diagnosis using wavelet transform," *Neurocomputing*, vol. 74, no. 10, pp. 1638 –1645, 2011.

[11] K. R. Al-Balushi, A. Addali, B. Charnley, *et al.*, "Energy index technique for detection of acoustic emissions associated with incipient bearing failures," *Applied Acoustics*, vol. 71, no. 9, pp. 812 –821, 2010.

[12] D. Mba and R. B. K. N. Rao, "Development of acoustic emission technology for condition monitoring and diagnosis of rotating machines; bearings, pumps, gearboxes, engines and rotating structures," *The Shock and Vibration Digest*, vol. 38, no. 1, pp. 3 –16, 2006.

[13] T. J. Holroyd, "The application of ae in condition monitoring," *Insight - Non-Destructive Testing and Condition Monitoring*, vol. 47, no. 8, pp. 481 –485, 2005.

[14] A. M. Al-Ghamd and D. Mba, "A comparative experimental study on the use of acoustic emission and vibration analysis for bearing defect identification and estimation of defect size," *Mechanical Systems and Signal Processing*, vol. 20, no. 7, pp. 1537 –1571, 2006.

[15] Z. Mo, J. Wang, H. Zhang, *et al.*, "Vibration and acoustics emission based methods in low-speed bearing condition monitoring," in *Proceedings of the Prognostics and System Health Management Conference*, Chongqing, China, 2018.

[16] B. Van Hecke, J. Yoon, and D. He, "Low speed bearing fault diagnosis using acoustic emission sensors," *Applied Acoustics*, vol. 105, pp. 35 –44, 2016.

[17] N. K. Verma, J. V. Singh, M. Gupta, *et al.*, "Windows mobile and tablet app for acoustic signature based machine health monitoring," in *Proceedings of the 9th International Conference on Industrial and Information Systems (ICIIS)*, IEEE, Gwalior, India, 2014, pp. 1 –6.

[18] J. Grebenik, Y. Zhang, C. Bingham, *et al.*, "Roller element bearing acoustic fault detection using smartphone and consumer microphones - comparing with vibration techniques," in *Proceedings of the 17th International Conference on Mechatronics - Mechatronika (ME)*, IEEE, Prague, Czech Republic, 2016.

[19] A. Siddique, G. S. Yadava, and B. Singh, "A review of stator fault monitoring techniques of induction motors," *IEEE Transactions On Energy Conversion*, vol. 20, no. 1, pp. 106 –114, 2005.

[20] S. Nandi, H. A. Toliyat, and X. Li, "Condition monitoring and fault diagnosis of electrical motors - a review," *IEEE Transactions On Energy Conversion*, vol. 20, no. 4, pp. 719 –729, 2005.

[21] Y. Liu and A. M. Bazzi, "A review and comparison of fault detection and diagnosis methods for squirrel-cage induction motors - state of the art," *ISA Transactions*, vol. 70, pp. 400 –409, 2017.

[22] O. E. Hassan, M. Amer, A. K. Abdelsalam, *et al.*, "Induction motor broken rotor bar fault detection techniques based on fault signature analysis – a review," *IET Electric Power Applications*, vol. 12, pp. 895 –907, 7 2018.

[23] J. Pons-Llinares, V. Climente-Alarcón, R. Puche-Panadero, *et al.*, "Bar breakage detection on squirrel cage induction motors via transient motor current signal analysis based on the wavelet transform, a review," Departamento de Ingeniería Eléctrica, Universidad Politécnica de Valencia, España, 2017.

[24] Y. Tian, D. Guo, K. Zhang, *et al.*, "A review of fault diagnosis for traction induction motor," in *Proceedings of the 37th Chinese Control Conference (CCC)*, Wuhan, China, 2018, pp. 5763 –5768.

[25] A. Glowacz, "Diagnostics of synchronous motor based on analysis of acoustic signals with the use of line spectral frequencies and k-nearest neighbor classifier," *Archives of Acoustics*, vol. 39, no. 2, pp. 189 –194, 2014.

[26] A. Glowacz, W. Glowacz, Z. Glowacz, *et al.*, "Early fault diagnosis of bearing and stator faults of the single-phase induction motor using acoustic signals," *Measurement*, vol. 113, pp. 1 –9, 2018.

[27] A. Glowacz, "Fault diagnosis of single-phase induction motor based on acoustic signals," *Mechanical Systems and Signal Processing*, vol. 117, pp. 65 –80, 2019.

[28] W. Li and C. K. Mechefske, "Detection of induction motor faults - a comparison of stator current, vibration and acoustic methods," *Journal of Vibration and Control*, vol. 12, no. 2, pp. 165 –188, 2006.

[29] B. P. Sangeetha and S. Hemamalini, "Rational-dilation wavelet transform based torque estimation from acoustic signals for fault diagnosis in a three phase induction motor," *IEEE Transactions on Industrial Informatics*, 2018.

[30] J. L. Contreras-Hernandez, D. L. Almanza-Ojeda, S. Ledesma-Orozco, *et al.*, "Quaternion signal analysis algorithm for induction motor fault detection," *IEEE Transaction on Industrial Electronics*, 2019.

[31] A. Ordaz-Moreno, R. d. J. Romero-Troncoso, J. A. Vite-Frias, *et al.*, "Automatic online diagnosis algorithm for broken-bar detection on induction motors based on discrete wavelet transform for fpga implementation," *IEEE Transactions On Industrial Electronics*, vol. 55, no. 5, pp. 2193 –2202, 2008.

[32] J.-K. Park and J. Hur, "Detection of inter-turn and dynamic eccentricity faults using stator current frequency pattern in ipm-type bldc motors," *IEEE Transactions On Industrial Electronics*, vol. 63, no. 3, pp. 1771 –1780, 2016.

[33] M. Riera-Guasp, J. A. Antonino-Daviu, and G.-A. Capolino, "Advances in electrical machine, power electronic, and drive condition monitoring and fault detection: State of the art," *IEEE Transactions On Industrial Electronics*, vol. 62, no. 3, pp. 1746 –1759, 2015.

[34] F. Immovilli, C. Bianchini, E. Lorenzani, *et al.*, "Evaluation of combined reference frame transformation for interturn fault detection in permanent-magnet multiphase machines," *IEEE Transactions On Industrial Electronics*, vol. 62, no. 3, pp. 1912 –1920, 2015.

[35] J. Arellano-Padilla, M. Sumner, and C. Gerada, "Winding condition monitoring scheme for a permanent magnet machine using high-frequency injection," *IET Electric Power Applications*, vol. 5, no. 1, pp. 89 –99, 2011.

[36] B. Sen and J. Wang, "Stator interturn fault detection in permanent-magnet machines using pwm ripple current measurement," *IEEE Transactions On Industrial Electronics*, vol. 63, no. 5, pp. 3148 –3157, 2016.

[37] Y. Cekic and L. Eren, "Broken rotor bar detection via four-band wavelet packet decomposition of motor current," *Electrical Engineering*, vol. 100, pp. 1957 –1962, 3 2018.

[38] J. Grebenik, C. Bingham, and S. Srivastava, "Continuous acoustic monitoring of electrical machines; processing signals from usb microphone & mobile smartphone sensors detecting dc motor controller fault," in *Proceedings of the 5th International Conference on Control, Decision & Information Technologies (CoDIT)*, IEEE, Thessaloniki, Greece, 2018.

[39] K. Farrar, "Soundfield microphone - design and development of microphone and control unit," *Wireless World*, pp. 48 –50, 1979.

[40] M. A. F. Pimentel, D. A. Clifton, L. Clifton, *et al.*, "A review of novelty detection," *Signal Processing*, vol. 99, pp. 215 –249, 2014.

[41] A. Rai and S. H. Upadhyay, "A review on signal processing techniques utilized in the fault diagnosis of rolling element bearings," *Tribology International*, vol. 96, pp. 289 –306, 2016.

[42] G. F. Bin, J. J. Gao, X. J. Li, *et al.*, "Early fault diagnosis of rotating machinery based on wavelet packets - empirical mode decomposition feature extraction and neural network," *Mechanical Systems and Signal Processing*, vol. 27, pp. 696 – 711, 2012.

[43] Y. Lei, J. Lin, Z. He, *et al.*, "A review on empirical mode decomposition in fault diagnosis of rotating machinery," *Mechanical Systems and Signal Processing*, vol. 35, pp. 108 –126, 2013.

[44] M. M. M. H. Da Costa Cesar; Kashiwagi, "Rotor failure detection of induction motors by wavelet transform and fourier transform in non-stationary condition," *Case Studies in Mechanical Systems and Signal Processing*, vol. 1, pp. 15 –26, 2015.

[45] P. A. Delgado-Arredondo, A. Garcia-Perez, D. Morinigo-Sotelo, *et al.*, "Comparative study of time-frequency decomposition techniques for fault detection in induction motors using vibration analysis during startup transient," *Shock and Vibration*, 2015.

[46] N. E. Huang, Z. Shen, S. R. Long, *et al.*, "The empirical mode decomposition and the hilbert spectrum for nonlinear and non-stationary time series analysis," in *The Royal Society A - Mathematical, Physical and Engineering Sciences*, The Royal Society, vol. 454, 1998, pp. 903 –995.

[47] Z. Wu and N. E. Huang, "Ensemble empirical mode decomposition - a noise assisted data analysis method," *Advances in Adaptive Data Analysis*, vol. 1, no. 1, pp. 1 –41, 2009.

[48] P. G. Kulkarni and A. D. Sahasrabudhe, "Investigations on mother wavelet selection for health assessment of lathe bearings," *The International Journal of Advanced Manufacturing Technology*, vol. 90, 9 - 12 2017.

[49] R. Yan, "Wavelet selection criteria for non-stationary vibration analysis in bearing health diagnosis," University of Massachusetts, 2007.